

DEVELOPMENT AND VALIDATION OF AN ANALYTICAL METHOD FOR CONDENSED TANNIN EXTRACTS OBTAINED FROM THE BARK OF FOUR TREE SPECIES USING HPLC

FAUSTINO RUIZ-AQUINO¹, ROSSY FERIA-REYES², JOSÉ GUADALUPE RUTIAGA-QUIÑONES³,
WENCESLAO SANTIAGO-GARCÍA¹, MARIO ERNESTO SUÁREZ-MOTA¹,
HÉCTOR HUGO ESQUIVEL-REYES¹

¹ UNIVERSIDAD DE LA SIERRA JUÁREZ
MÉXICO

² UNIVERSIDAD DE GUANAJUATO
MÉXICO

³ UNIVERSIDAD MICHOACANA DE SAN NICOLÁS DE HIDALGO
MÉXICO

(RECEIVED JUNE 2020)

ABSTRACT

Herein, we evaluated the content of condensed tannins present in the bark of four tree species that are *Quercus laurina* Humb. & Bonpl., *Quercus crassifolia* Humb. & Bonpl., *Arbutus xalapensis* Kunth, and *Prunus serotina* Ehrn. An analytical method using high-performance liquid chromatography (HPLC) for condensed tannin extracts was developed and validated. Also, the aqueous extracts were analyzed by Fourier transform infrared spectroscopy (FTIR). Based on the Stiasny number, *A. xalapensis*, and *Q. laurina* represent an important source of condensed tannins, which may be subject to exploitation. Using infrared spectroscopy, it was observed that tannins do not show an important signal of carbonyl groups (aromatic esters) with respect to high purity catechin. Furthermore, the band of the hydroxyl group is less pronounced in tannins, because various hydroxyl are interacting with each other. However, it can be seen that the method of extraction of wood tannins developed in this work, presents satisfactory results.

KEYWORDS: Stiasny number, infrared spectroscopy, liquid chromatography.

INTRODUCTION

In the forests of the Sierra Juárez, Oaxaca, Mexico, stands with structural dominance of *Quercus laurina* Humb & Bonpl., and *Quercus crassifolia* Humb. & Bonpl. have been found, species that cohabit with *Arbutus xalapensis* Kunth, and *Prunus serotina* Ehrn, among

others (Ruiz-Aquino et al. 2015). The wood of these species is used in rustic constructions (Ruiz-Aquino et al. 2016, 2019), and the elaboration of charcoal for fuel, and for its bark there are no reports on its use. The bark of the trees is considered a waste product, if the debarking is carried out in the industry it becomes a pollutant, while in the debarking in the field the bark is integrated as nutrients into the soil (Giménez et al. 2008). The bark is an important source of resins, latex, tannins, and substances that protect the tree from fungi and insects (Cuttler et al. 2007). In the bark of forest species of the families Clusiaceae, Cupressaceae, Ebenaceae, Fabaceae, Fagaceae, Sapotaceae, Pinaceae, among others, some authors have shown that condensed tannins are both chemically and economically interesting for the preparation of adhesives and resins destined to the production of particleboards and that they could be successfully used as substitutes for phenol in the production of phenol–formaldehyde resins (Tondi et al. 2010, Naima et al. 2015). Plant tannins or polyphenols are secondary metabolites distributed in sectors of the plant kingdom (Isaza 2007), can represent 2 to 40% of the dry bark mass of various forest species (Paes et al. 2006). They are chemically classified into hydrolyzable and condensed. Hydrolyzables are glucose polyesters, whereas condensates are made of catechin monomers and are known as flavonoids (Pizzi 1983).

Currently tannin compounds extraction is diverse, for example Bosso et al. (2016) analyzed the extracting effectiveness tannins grapes in some solvents (water, ethanol, acetone, ethyl acetate), used as pure or in binary and ternary mixtures. But, the polyphenolic compounds of tannins are molecules belonging to classes different from one another for the degree of polarity. The extraction method to be employed is influenced by the chemical nature of the substance, sample particle size, and also by the presence of interfering substances. Extraction time, temperature, solvent-to-feed ratio, the number of repeated extractions of the sample, as well as the choice of extraction solvents are the crucial parameters affecting the extraction yield. Solubility is influenced by both extraction time and temperature. A higher temperature simultaneously increases solubility and mass transfer velocities as well as decreases viscosity and surface tension of solvents contributing to a higher extraction rate (Mojzer et al. 2016).

This study evaluates the purity potential of tannin extraction in the bark of four tree species that are *Q. laurina* Humb. & Bonpl., *Q. crassifolia* Humb. & Bonpl., *Arbutus xalapensis* Kunth, and *Prunus serotina* Ehrn., and an analytical method is developed by HPLC, for the characterization of functional groups, Fourier transform infrared spectroscopy (FT-IR) is used.

MATERIAL AND METHODS

Study area

The study was conducted in the Ixtlán de Juárez forest, Oaxaca, Mexico, which is located 170° 18' 16" – 170° 34' 00" N and 96° 31' 38" – 96° 20' 00" O, the climate is temperate humid and subhumid with rains in summer (Castellanos-Bolanos et al. 2008). The forest harvesting area is located at an altitude of 2,156 to 2,458 m.

Material collection

Part of the bark of the standing trees was removed, trying not to damage the entire circumference of the stems to ensure the transport of nutrients and photoassimilates in the trees. The bark samples were oven dried at 103°C for 48 hours (Paes et al. 2006). Subsequently, they were crushed using a Wiley® mill and sieved with a mesh with an opening size of 1 mm (Aguilar-López et al. 2012).

Tannin extraction

Tannin extraction was carried out with 5.0 g of ground bark and 75.0 mL of distilled water, 100 μ l of glacial acetic acid is added to the aqueous medium in a 250 mL Erlenmeyer flask, in a water bath at 87°C. The addition of acetic acid is to prevent oxidation of tannin extracts. Subsequently, the cold extract was filtered using 11 micron porosity Whatman brand filter paper and the filtrate was adjusted to 100 mL (Pedraza-Bucio and Rutiaga-Quiñones 2011).

Total extract

For the quantification of condensed tannins, the remaining volume (50mL) was used; 5.0 mL of formaldehyde and 2.5 mL of HCl were added to this solution using a Soxhlet system for 30 min. It was subsequently filtered and the filtrate was dried at 105°C for 24 hours. The Stiasny number is calculated using equation Eq. 1 (Paes et al. 2006):

$$NS = \frac{W_1}{W_2} \times 100 \quad (1)$$

where: NS = Stiasny number; W1 = solid mass (g) in 100 mL of extract; W2 = precipitate mass (g) in formaldehyde.

With the Stiasny number and the total extract amount, the amount of condensed tannins

$$TC = \frac{NS \times ET}{100} \quad (2)$$

where: TC = condensed tannins (%); NS = Stiasny number; ET = total extract (%).

All extractions were performed in triplicate.

Liquid chromatographic system

All reagents used were HPLC grade, catechin HPLC grade, methanol, phosphoric acid (sigma Aldrich), Milli-Q water of 18.0 μ S. The analysis was carried out in a CC5-BAS liquid chromatograph equipped with a quaternary pump, with an UV-116 BAS detector. Thermo Scientific Hypersil BDS C₁₈ reverse phase column of 250 mm \times 4.6 mm and 5.0 μ m particle size was used for this study. The peaks corresponding to catechin were detected at λ = 280 nm at elution time of t = 2.57 min using a mobile phase methanol water 60:40 (v/v%) nm, flow of 1.0 mL \cdot min⁻¹ in isocratic system.

Analysis of tannin extracts by infrared spectroscopy with Fourier transforms

For the identification of the functional groups present the tannin extracts a Spectrum 100 FT-IR Spectrometer was used in a wave number range between 500 - 4500 cm⁻¹.

Method development for identification of tannin

For the analysis by liquid chromatography a standard of high purity catechin was used, the detection method was optimized to identify the tannins of the wood extracts. From a solution of 2000 mg \cdot L⁻¹ of catechin HPLC grade dissolved in a 3.0 mM., solution of H₃PO₄. Solutions of 300.0, 250.0, 180.0, 130.0, 80.0, 40.0, 25.0, 10.0 mg \cdot L⁻¹ were prepared and diluted with a 3.0 mM, solution of H₃PO₄. The addition of phosphoric acid in the samples is to prevent oxidation

and to obtain a better chromatographic signal from the tannin. For this study a mobile phase of MeOH/ H₂O (60:40 v/v%) was used at $\lambda=280$ nm, flow 1.0 ml·min⁻¹, the system flow was isocratic, 1980 psi pressure and $\approx 32^\circ\text{C}$, 20 μL of the sample was injected into the chromatographic column, all samples were made in triplicate. Linear regression of each of the areas under the curve of the chromatograms checked the linearity of the same; the results represented the average of three curves performed.

Linearity, precision, accuracy, detection and quantification limits

The method linearity, recovery, precision (repeatability and intermediary precision), detection and quantification limits were evaluated according to Borman and Elder (2017). The linearity of the curves was estimated by regression using the last square method. The slope, intercept (with respective confidence intervals) and coefficient of determination (R^2) were calculated and evaluated. Each test catechin standard and tannin extractive solution of tree selective was injected in triplicate and the repeatability was evaluated for peak areas and retention times of tannin through the relative standard deviation (RSD) (%).

RESULTS AND DISCUSSION

In Tab. 1 the average content of total extract, Stiasny number and condensed tannins of the four tree species under study is presented. The amount of total extract of *Q. crassifolia* y *A. xalapensis* is higher than that reported for the heartwood of *Haematoxylon brasiletto* Karst (7.6%) (Pedraza-Bucio y Rutiaga-quiñones 2011), and also higher than the maximum reported for the bark of eight pine species from the Durango state Mexico (2.36 - 10.61%) (Rosales and Gonzalez 2003). The differences found are attributed to two factors, the first is the extraction conditions and the second is the specific characteristics of each species, related to the chemical composition, site conditions and age of the tree species (Paes et al. 2006).

Tab. 1: Total extract, number of Stiasny, and condensed tannins in the bark of four tree species.

Content	Bark of tree species (%)			
	<i>Prunus serotina</i>	<i>Quercus crassifolia</i>	<i>Arbutus xalapensis</i>	<i>Quercus laurina</i>
Total extract	2.84 (0.23)	13.74 (0.78)	10.70 (0.44)	6.35 (0.13)
Stiasny number	24.21(2.62)	36.37 (5.03)	53.73 (6.27)	66.79 (0.90)
Condensed tannins	0.68 (0.02)	4.97 (0.41)	5.73 (0.43)	4.24 (0.14)

(RSD) (%) - the values in parenthesis represent the standard deviation.

A higher percentage of Stiasny was found in the bark of *Q. laurina* (66.79%), this value is slightly lower than that reported by Rosales and González (2003) for *Pinus ayacabuite* (69%) and *Pinus durangensis* (69.3%). Stiasny values greater than 65 represent an important source of condensed tannins (Rosales et al. 2002). The amount of condensed tannins is within the range (0.41% – 13.67%), reported for the bark of eleven wood species from Costa Rica (Aguilar-Lopez et al. 2012), the values are lower than those reported for the bark of four species of pine in Brazil (7.85% – 13.82%) (Da Silva et al. 2012). Condensed tannins have applications in formulating wood adhesives (Aguilar-López et al. 2012), in leather tanning (Colín-Urieta et al. 2013), the use of condensed tannins in ruminants has shown beneficial effects (Márquez and Suárez 2008) among others. High performance liquid chromatography

was used to verify the purity of the tannins obtained with the extraction method implemented.

The optimized liquid chromatography conditions were achieved after preliminary assays, where different combination of methanol, water and a mixture phosphoric acid 3.0 mM were tested, the results is show following.

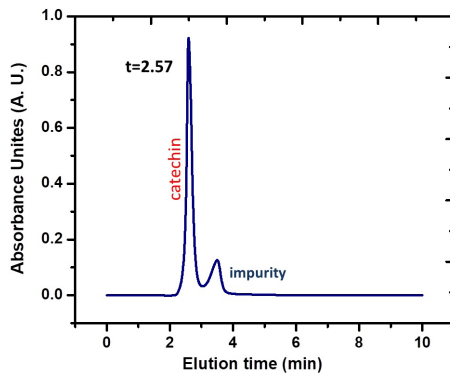


Fig.1: Chromatogram of 300 mg.L⁻¹ catechin standard with isocratic flow rate conditions 1.0 mL.min⁻¹, mobile phase of MeOH / H₂O (60:40 v/v%) $\lambda=280$ nm, 1980 psi of pressure system and $\approx 32^{\circ}\text{C}$, 20 μL sample injection and Thermo Scientific Hypersil BDS C18 reverse phase column of 250 mm \times 4.6 mm and 5.0 μm particle size was using.

The Fig. 1 shows a chromatogram good defined of 300 mg.m⁻¹ catechin standard at elution time of $t = 2.54$ min, posteriorly at time = 3.5 min we observed a signal of impurity of standard, the flow of system was isocratic. Fig. 2 shows the chromatograms corresponding to calibration curves of 300 to 10 mg.m⁻¹ catechin standard, we can observe that a good linearity proportional at concentration analyzed. The linearity was evaluated for each standard substance. The calibration curves were obtained by plotting peak areas upon concentrations using eight standard solutions.

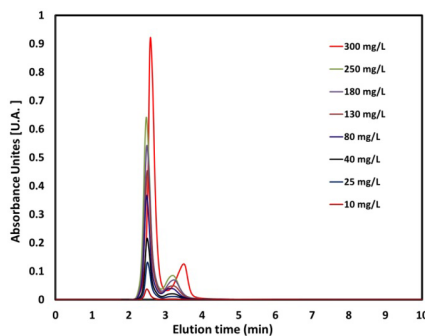


Fig. 2: Chromatograms of 300, 250, 180, 130, 80, 40, 25, 10 mg.L⁻¹ catechin standard with isocratic flow rate conditions 1.0 mL.min⁻¹, mobile phase of MeOH / H₂O (60 : 40 v/v%) $\lambda=280$ nm, 1980 psi of pressure system and $\approx 32^{\circ}\text{C}$, 20 μL sample injection and Thermo Scientific Hypersil BDS C18 reverse phase column of 250 mm \times 4.6 mm and 5.0 μm particle size was using.

The R^2 values were greater than 0.997, showing that the calculated regression curves could explain significantly the experimental variance (Fig.3). Thus, the calculated straight line could explain more than 99% of the experimental data. The confidence intervals for both intercept points included zero.

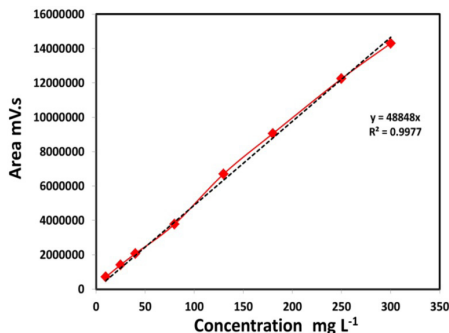


Fig. 3: Calibration curves of catechin standard.

Therefore, the result confirms the absence of constant systematic errors in the analytical method. The detection, and quantification limits were estimated from the calibration curve slopes. The limits of detection were $10 \text{ mg}\cdot\text{L}^{-1}$ of catechin. With the standardized chromatographic method, the quantification of tannin extracts from the bark of the four wood species was carried out and analyzed.

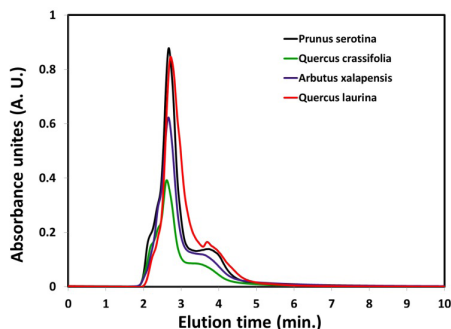


Fig. 4: Chromatograms of $40 \text{ mg}\cdot\text{L}^{-1}$ of tannin extract from the bark of four tree species using isocratic flow rate conditions $1.0 \text{ mL}\cdot\text{min}^{-1}$, mobile phase of $\text{MeOH}/\text{H}_2\text{O}$ (60:40 v/v%) $\lambda=280 \text{ nm}$, 2280 psi of pressure system, and $\approx 32^\circ\text{C}$, $20 \mu\text{L}$ sample injection and Thermo Scientific Hypersil BDS C18 reverse phase column of $250 \text{ mm} \times 4.6 \text{ mm}$, and $5.0 \mu\text{m}$ particle size was using.

Fig. 4 shows the chromatograms corresponding to the tannin extracts from the bark of the four species under study obtained with the extraction method implemented. The signal shows that the elution times of the extracted tannins are, the elution time of the tannin is $t = 2.78 \text{ min}$, and it is observed that at $t = 3.2 \text{ min}$ is the signal corresponding to the impurity of the tannin extracted is observed for each of the barks of the species under study. This shift in the retention time of the tannin is due to the presence of carboxylic groups present in the wood

tannin extract that exert a greater pressure on the chromatographic column, and this causes the slight displacement of the sample with respect to when you have the high purity standard.

Thus, the amount of total tannins obtained for each of the bark species are: *Prunus serotina* 290 mg L⁻¹, *Quercus crassifolia* 130 mg L⁻¹, *Arbutus xalapensi* 250 mg L⁻¹, and *Quercus laurina* 275 mg L⁻¹. In the extraction of tannins it is important the polarity of solvent depends on its dielectric constant (ϵ), which affects the capacity of the solvent to solubilize molecules tannin compounds with different degree of polarity. Where the water dielectric constant is $\epsilon = 80.1$, and $\epsilon = 6.2$ acid acetic (Naima et al. 2015). In this work, the use of acetic acid acts as a protic solvent in the extraction medium with water. The acid present in the extraction process prevents the oxidation of tannins in an aqueous medium, which is reflected in the chromatographic analysis.

The tannins present in the wood extracts are condensable, of which there are three structured groups of tannins that are; hydrolyzed tannins, condensable tannins, and phlorotannins, which are produced through three different biosynthetic pathways. Hydrolyzable tannins are produced by a shikimic acid pathway that leads to the production of gallic acid (the fundamental monomer unit). Phlorotannins are derived from the Malonyl-CoA pathway produced by the phloroglucinol building block while condensed tannins are derived by mixed biosynthesis from the above two pathways that produce Flavan-3,4-diol (monomer units) which are then polymerized by condensation (Stafford 1983).

Spectroscopy FTIR

Fig. 5 shows the infrared spectrum that corresponds to the catechin standard and that is used to compare with the tannin extracts under study. In the spectrum it is observed that the main signals correspond to slight displacements according to what was reported by Silverstein and Bassler (1962), which is probably related to the presence of different types of phenols.

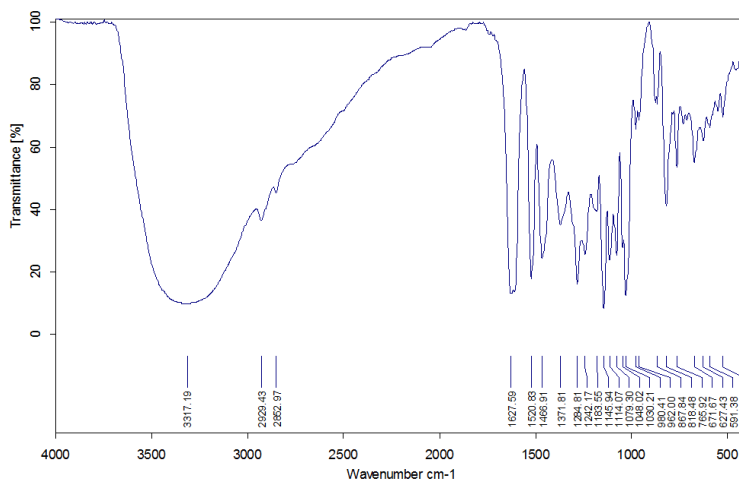


Fig. 5: Infrared spectroscopy of catechin standard.

The spectrum of catechin where it can find a strong absorption around 3600, and 3000 cm⁻¹ with a wide and strong band centered at 3317.9 cm⁻¹ respectively. These bands are assigned to the hydroxyl groups (OH) stretching vibrations and due to the wide variety of hydrogen bonding

between OH. In this spectrum it can notice a sharp peak at 2929.43 cm^{-1} associated with the symmetric and antisymmetric C-H stretching vibrations of CH_2 and CH_3 groups respectively. Also it does not appear signals of free water molecules due there is no evidence of bands at 2150 cm^{-1} and 1650 cm^{-1} (H-O-H bending vibrations), and at about 700 cm^{-1} . The deformation vibration of the carbon-carbon bonds in the phenolic groups absorbs in the region of $1600\text{-}1475\text{ cm}^{-1}$. At 750 cm^{-1} shows the result distortion vibration of C=C in benzene rings. Around 1460 cm^{-1} stretching vibrations of $\text{-C-C}_{\text{aromatic}}$ groups appear (Socrates 2001). Tab. 2 shows details of the peaks found by FTIR of the catechin standard.

Tab. 2: Main FTIR signals of the catechin standard and its comparison with those of the literature (Socrates 2001).

Frequency (cm^{-1}) (Catechin stand.)	Signal type	Chemical bond type	Assignment
3317.19	Elongation	O-H y N-H	Hydroxyls and amines
2929.43	Asymmetric elongation	C-H	CH_2 saturation groups
2852.97	Asymmetric elongation	C-H	Hydrocarbons
1627.59	Symmetrical bending vibration	C=O	Flavonoid, lipids and amino acids
1520.83	Elongation	Aromatic compounds	Flavonoids and aromatic rings
1371.81	Bending vibration	C-H	Flavonoid group CH_3
1284.81	Bending vibration (O-H) and asymmetric flexion (C-CO)	O-H and C-CO	Hydrocarbons
1242.17	bending vibration (O-H) and asymmetric flexion (C-CO)	C-H	Flavonoid group CH_3
1183.55 – 1079.30	Elongation vibration (C-C) and flexion (C-OH)	C-C and C-OH	Flavonoids and secondary alcohol groups
1048.02	Elongation (=C-O-C), Elongation (C-C) and flexion (C-OH)	=C-O-C, C-C and C-OH	Primary alcohols group
1030.21	Elongation vibration (C-C) and flexion (C-OH)	C-C and C-OH	Flavonoids and second. alcohol groups
867.84	Symmetric stretching vibration	C-C-O	Primary and secondary alcohols
818.48 – 525.94	Symmetric stretching vibration (C-H)	Aromatic compounds	Primary and secondary alcohols outside the flexion plane

Fig. 6 shows the infrared spectra of tannins extracted with water from the bark of the four timber species. An in-depth analysis by infrared micro spectroscopy indicates that the main tannin-related bands are found in 1727 , 1612 , and 1513 cm^{-1} , in these wave number ranges: (i) Region carbonyl region $1800\text{-}1480\text{ cm}^{-1}$; including: carbonyl groups (ester, ketone, aldehyde, amide I), amide II, carboxylate groups and aromatic groups, (ii) Region carbohydrate region $1190 - 850\text{ cm}^{-1}$; including all bands of carbohydrates n (C-O-C) (Silverstein and Bassler 1962).

The spectra obtained here are found in the region 650–4000 cm^{-1} , recorded by L. Chupin et al. (2013), for the bark of *Pinus pinaster* extracted with different conditions, where the band at 3300 cm^{-1} is assigned as OH stretch vibration in phenolic and aliphatic structures, in the same way, Jablonski et al. (2015), assigned to the hydroxyl group stretching vibration a broad band at $\sim 3300 \text{ cm}^{-1}$.

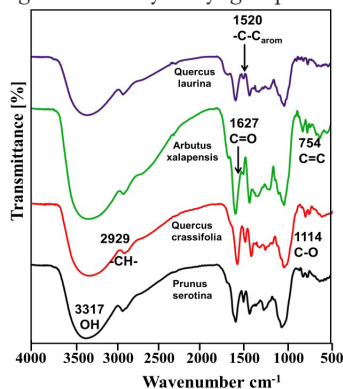


Fig. 6: Infrared spectroscopy of the four types of bark.

Detailed information is listed in Tab. 3; these results are similar to those reported in the literature for polyphenolic compounds as tannins, and tannic acid (Hillis 1964).

Tab. 3: Wave range limits and corresponding absorption bands for standardized integration method applied to all FPA and synchrotron IR maps.

Integration region No.	Mapped bands
i) 1705 -1570 cm^{-1}	ν (C=O); amide
	$\nu_{as}(\text{COO}^-)$;
	ν (C=C); aromatic quadrant ring stretch
ii) 1530 -1480 cm^{-1}	ν (C=C); aromatic semicircle ring stretch
iii) 1260-1210 cm^{-1}	ν (C-C), ν (C-O) (lignin)
iv) 1180-950 cm^{-1}	ν (C-O-C) (carbohydrates)

CONCLUSIONS

Of the tree barks evaluated in this work and based on the Stiasny number, the *Arbutus xalapensis* and *Quercus laurina* species contain a significant amount of condensed tannins of 10.7% and 6.3%, respectively which can be exploited. Using infrared spectroscopy, it was observed that the tannins do not show an important signal of the carbonyl groups (aromatic esters) with respect to the high purity catechin. The band of the hydroxyl group in tannins is less pronounced, because several hydroxyls are bonded. With the extraction method used and the analytical method developed for the quantification of tannins from the bark of trees, they show that the tannins of the tree species *Prunus serotina* and *Quercus crassifolia* are around 83% approximately and these extracts show a high purity with respect to the Catequina standard.

These results compared with the different extraction methods for tannins show a similar performance in terms of extraction yields and amount of tannins extracted; the use of solvents is low and economically feasible for future work.

REFERENCES

1. Aguilar-López, J., Jaén-Jiménez, J.C., Vargas-Abarca, A.S., Jiménez-Bonilla, P., Vega-Guzmán, I., Herrera-Núñez, J., Borbón-Alpizar, H., Soto-Fallas, R.M., 2012: Extraction and evaluation of condensed tannins from the bark of eleven timber species from Costa Rica. *Revista Tecnología en Marcha* 25(4): 15-22.
2. Beltrán-Rodríguez, L., Maldonado-Almanza, B., Blancas, J., Sierra-Huelz, A., Cristians, S., Bye, R., 2018: Barks as non-timber forest products in Mexico: national analysis and recommendations for their sustainable use. CONACyT, México, 52 p.
3. Borman, P., Elder, D., 2017: Q2(R1) validation of analytical procedures. In: ICH Quality Guidelines: An Implementation Guide (ed. Teasdale A., Elder D., Nims RW). Pp 127-166, John Wiley & Sons. USA.
4. Bosso, A., Guaita M., Petrozziello, M., 2016: Influence of solvents on the composition of condensed tannins in grape pomace seed extracts. *Food Chemistry* 207: 162-169.
5. Castellanos-Bolaños, J.F., Treviño-Garza, E.J., Aguirre-Calderón, O.A., Jiménez-Pérez, J., Musalem-Santiago, M., López-Aguillón, R., 2008: Forest structure of managed Patula pine in Ixtlán de Juárez, Oaxaca, Mexico. *Madera y Bosques* 14(2): 51-63.
6. Colín-Urieta, S., Ochoa-Ruiz, H.G., Rutiaga-Quiñones, J.G., 2013: Tannin content in the bark of two species of paracata (*Erythroxylon compactum* Rose and *Senna skinneri* Benth. Irwin & Barneby). *Revista Chapingo serie ciencias forestales y del ambiente* 19(1): 115-124.
7. Cutler, D., Botha, T., Stevenson, D., 2007: *Plant anatomy: An applied approach*. Wiley-Blackwell. England, 312 p.
8. Da Silva, F.E., Costa, L.R.C., Oliveira, B.E., Nascimento, A.M., Da Silva, M.L., 2012: Tannin contents in the bark of four pinus species. *Floresta e Ambiente* 16(2): 30-39.
9. Gimenez, A.M., Moglia, J.G., Hernandez, P., Gerez, R., 2008: The feasibility of increasing the Chaco forests value by exploiting the forest bark. *Quebracho-Revista de Ciencias Forestales* (15): 9-14.
10. Hillis, W., 1964: The formation of polyphenols in trees. 2. The polyphenols of *Eucalyptus sieberiana* Kino. *Biochemical Journal* 92: 516-521.
11. Isaza, J.H., 2007: Vegetable tannins or polyphenols. *Scientia et Technica* 1(33): 13-18.
12. Jablonsky, M., Vernarecová, M., Ház, A., Dubinyová, L., Skulcova, A., Sladková, A., Surina, I., 2015: Extraction of phenolic and lipophilic compounds from spruce (*Picea abies*) bark using accelerated solvent extraction by ethanol. *Wood Research* 60(4): 583-590.
13. L, Chupin, Motillon, C., Charrier-El Bouhtoury, F., Pizzi, A., Charrier, B., 2013: Characterisation of maritime pine (*Pinus pinaster*) bark tannins extracted under different conditions by spectroscopic methods, FTIR and HPLC. *Industrial Crops and Products* 49: 897-903.
14. Marquez Lara, D., Suarez Londoño, Á., 2008: The use of condensed tannins as a nutritional and sanitary alternative in ruminants. *Revista de Medicina Veterinaria* 1(16): 87-109.
15. Mojzer, E., Hrnčič, M., Škerget, M., Knez, Ž., Bren, U., 2016: Polyphenols: Extraction methods, antioxidative action, bioavailability and anticarcinogenic effects. *Molecules* 21(7): 1-38.
16. Naima, R., Oumam, M., Hannache, H., Sesbou, A., Charrier, B., Pizzi, A., Charrier-El Bouhtoury, F., 2015: Comparison of the impact of different extraction methods on polyphenols yields and tannins extracted from Moroccan *Acacia mollissima* barks. *Industrial Crops and Products* 70: 245-252.
17. Paes, J.B., Diniz, C.E.F., Marinho, I.V., de Lima, C.R., 2006: Tannin potencial evaluation of six forest species of Brazilian semi-arid region. *Cerne* 12(3): 232-238.

18. Pedraza-Bucio, F.E., Rutiaga-Quiñones, J.G., 2011: Tannic extract of Brazilian Palo wood. *Revista Conciencia Tecnológica* 42: 36-41.
19. Pizzi, A., 1983: Tanin-based adhesives. In: *Wood adhesives: chemistry and technology.* (ed. M. Dekker). Pp 177-246, New York.
20. Rosales, C.M., Gonzales, L.R.F., 2003: Comparison of the content of phenolic compound in the bark of eight pine species. *Madera y Bosques* 9(2): 41-49.
21. Rosales, M., Galindo, A., González, R.F., 2002: Tannins condensed in the bark of *Pinus chihuahuana* and *Pinus durangensis*. *Información Tecnológica* 13(1): 39-42.
22. Ruiz-Aquino, F., González-Peña, M.M., Valdez-Hernández, J.I., Romero-Manzanares, A., 2016: Anatomical structure of the wood of two oaks from Oaxaca. *Madera y bosques* 22(1): 177-189.
23. Ruiz-Aquino, F., Ruiz-Ángel, S., Santiago-García, W., Fuente-Carrasco, M.E., Sotomayor-Castellanos, J.R., Morelia, M., Carrillo-Parra, M.A., 2019: Energy characteristics of wood and charcoal of selected tree species in Mexico. *Wood Research* 64(1): 71-82.
24. Ruiz-Aquino, F., Valdez-Hernández, J.I., Romero-Manzanares, A., Manzano-Méndez, F., Fuentes-López, M.E., 2015: Spatial distribution of two oak species and ecological attributes of pine-oak woodlands from Ixtlán de Juárez, Oaxaca. *Revista Chapingo. Serie Ciencias Forestales y del Ambiente* 21(1): 67-80.
25. Silverstein, R.M., Bassler, G.C., 1962: Spectrometric identification of organic compounds. *Journal of Chemical Education* 39(11): 546-553
26. Socrates, G., 2001: Infrared and Raman characteristics group frequencies, tables and chart. 3a. ed., John Wiley & Sons, Inc., USA, 118 p.
27. Stafford, H.A., 1983: Enzymic regulation of procyanidin biosynthesis; lack of a flav-3-en-3-ol intermediate. *Phytochemistry* 22(12): 2643-2646.
28. Tondi, G., Pizzi, A., Delmotte, L., Parmentier, J., Gadiou, R., 2010. Chemical activation of tannin-furanic carbon foams. *Industrial Crops and Products* 31 (2): 327-334.

FAUSTINO RUIZ-AQUINO*, WENCESLAO SANTIAGO-GARCÍA,
MARIO ERNESTO SUÁREZ-MOTA, HÉCTOR HUGO ESQUIVEL-REYES
UNIVERSIDAD DE LA SIERRA JUÁREZ
INSTITUTE OF ENVIRONMENTAL STUDIES
AVENIDA UNIVERSIDAD S/N
68725, IXTLÁN DE JUÁREZ
OAXACA
MÉXICO

*Corresponding author: ruiz.aquino@unsij.edu.mx

ROSSY FERIA-REYES
UNIVERSIDAD DE GUANAJUATO
CHEMISTRY DEPARTMENT
DIVISION OF NATURAL AND EXACT SCIENCES
CERRO DE LA VENADA S/N, PUEBLITO DE ROCHA
36040, GUANAJUATO
MÉXICO

JOSÉ GUADALUPE
RUTIAGA-QUIÑONES,
UNIVERSIDAD MICHOACANA DE SAN NICOLÁS DE HIDALGO
FACULTY OF WOOD TECHNOLOGY ENGINEERING
AV. FCO. J. MÚJICA, S/N, COLONIA FELICITAS DEL RÍO
58040, MORELIA, MICHOACÁN
MÉXICO

TENSILE PROPERTIES OF SURFACE MODIFIED BAMBOO SLICES COATED WITH EPOXY RESIN CONSIDERING THE CORROSION OF ACID AND ALKALI ENVIRONMENT

QIANG MA, ZHAO LIU, HENGLIN XIAO, ZHI CHEN
HUBEI UNIVERSITY OF TECHNOLOGY
CHINA

(RECEIVED APRIL 2020)

ABSTRACT

This paper presents an anticorrosive method to protect bamboo from the corrosion induced by coating a layer of epoxy resin on the surface of bamboo slices. Four surface modifications including heat treatment, alkali treatment, coupling treatment and acetylation treatment are applied to bamboo slices. The results indicate that the ultimate tension of bamboo slices decreases when corroded in solutions with different pH for different time, while epoxy resin protects the bamboo slices from corrosion to maintain the tensile properties by coated on its surface. The surface morphology indicates that four modifications have different degrees of influence on the surface and material of bamboo slices, which can reduce the ultimate tension of bamboo slices, but improve the interfacial combination between the surface of bamboo slices and epoxy resin. Acetylation treatment was the most effective modification analysed by Fourier-transform infrared spectroscopy (FT-IR) among them.

KEYWORDS: Bamboo slices, epoxy resin, corrosion, tensile properties, surface modifications, interfacial combination.

INTRODUCTION

With the continuous deepening of the concept of green economy and sustainable development, the application of ecological building materials, especially those used as reinforcement in construction technology for reinforced soil, has been increasingly attended. Some natural plant materials with high strength and favorable toughness, such as bamboo root, palm fiber and wheat straw, when be used as reinforcement, can effectively improve the mechanical properties of the reinforced soil (Hegde and Sitharam 2015, Li et al. 2012). Moreover, the tensile properties

of the reinforcement are the most basic technical indicators for reinforced soil structural design, which can directly affect the mechanical properties and service life of the reinforced soil (Shinoda and Bathurst 2004, Wesseloo et al. 2004, Subaida et al. 2008). For example, slope soil maintains its slope stability when reinforced with plant roots, and the tension of plant roots plays a leading role in the stability of soil, which has been proved by the tensile test and the direct shear test on roots-reinforced soil (McIvor et al. 2008, Ghestem et al. 2011, Ma et al. 2018). Compared with some synthetic materials, natural plant materials provide better reinforcement in construction technology for reinforced soil. More importantly, they are degradable and environmentally friendly, which have better economic and ecological benefits as traditional geopolymer replacement for reinforcement engineering.

The recent progress of green building materials presents a great opportunity for the application of bamboo in the reinforced soil. As a kind of natural reinforcement, bamboo is recognized as a viable, sustainable and engineering alternative to other materials in many areas worldwide (Ahmad and Kamke 2005, Yan et al. 2017). It possesses various applications in the engineering field for its strong adaptability, regeneration and reproduction ability, and can play a better role than other natural plant material in the reinforcement process (Khalil et al. 2012, Luo et al. 2014, Trujillo et al. 2014). At present, there are many researches on the mechanical properties of bamboo and its application in practical engineering. Tensile strength of single bamboo fiber isolated chemically is 47.6% higher than that of isolated mechanically, and the tensile strength and modulus of bamboo strips made from the outer portion of the bamboo are higher than that of inner portion (Chen et al. 2015). The shear strength of soil can be improved by reinforcing with bamboo slices, and the peak shear strength of bamboo root reinforced soil increases with increasing soil-root volume ratio (Ma'arif 2012).

However, the degradability of natural plants makes them prone to corrosion in acid and alkali environment, which may affect their mechanical properties and makes them difficult to chronically exert their reinforcing effect (Hsu et al. 2010). Notably, due to the influence of civil engineering environment, the natural bamboo material will be corroded when be applied as reinforcement in the soil (Qin et al. 2015), which will decrease the mechanical properties of the reinforced soil. Therefore, to extend the service life of bamboo and maintain the mechanical properties of reinforced soil, it is particularly important to conduct corrosion prevention on bamboo (Shafizadeh and Kavanagh 2005). The anticorrosion of bamboo mainly include physical and chemical methods. However, The validity of physical methods is short, and such as heat treatment will decrease the mechanical properties of bamboo (Yun et al. 2016, Zhao et al. 2019). Chemical method is to use preservatives to kill fungi and pests in bamboo, which will easily pollute the environment and has been pointed out that preservatives are not evenly distributed in bamboo (Qin et al. 2015). An effective and economic anti-corrosion method is to coat the material with epoxy resin, a kind of polymer with good physical properties, corrosion resistance, abrasion resistance, stability and low cost (Yang et al. 2014). However, the poor adsorbability towards polymers, induced by the hydrophilicity of nature plant, makes adhesion between the nature plant and polymer inadequate (Luft 1961, Antov et al. 2020). On the basis of maintaining the form and strength of natural plant, the surface modification of natural plant by physical or chemical methods can improve the interfacial compatibility between the surface of natural plant and epoxy resin (Bledzki et al. 1996). Although there are many research articles concerning the tensile properties of bamboo, the focus is seldom concentrated upon the bamboo corrosion that occurs during application in the recent literature. And there are few studies on the regularities of mechanical properties of bamboo slices under corrosion, the anticorrosion effect of epoxy resin on bamboo slices, and the influences of surface modification in improving the interfacial combination between epoxy resin and bamboo slices.

To solve the above problems, in this paper, the mechanical properties of Moso bamboo slices under different pH and corrosion time were studied, and the anti-corrosion effect of epoxy resin on bamboo slices was investigated. And four surface modification treatments (heat treatment, alkali treatment, coupling treatment and acetylation treatment) were conducted on the bamboo slices. The regularities of mechanical properties of bamboo slices were illustrated by tensile tests and surface morphology analysis of modified bamboo slices, and the surface modification effects of different modification methods were characterized by Fourier-transform infrared spectroscopy (FT-IR). The research can provide scientific guidance for the utilization of bamboo in civil engineering and the epoxy resin in the anti-corrosion of natural plant

MATERIAL AND METHODS

According to the test methods for physical and mechanical properties of bamboo used in building (Chen et al. 2015), five-year-old Moso bamboos obtained from Enshi, Hubei Province in China were selected as objective materials. All pristine samples were selected from the outer portion of the bamboo and the location between 4 - 5 m measured from the bottom of the bamboo trunk, and were processed into slices with a uniform dimension of 200 mm (L) × 5 mm (W) × 1 mm (T). The physical and mechanical parameters of Moso bamboo are listed in Tab. 1 according to relevant studies (Lakkad and Patel 1981, Jin et al. 2014).

Tab.1: Physical and mechanical parameters of Moso bamboo.

Parameter	Value range
Density ($\text{g}\cdot\text{cm}^{-3}$)	0.6 ~ 1.1
Tensile strength (MPa)	140 ~ 800
Elastic modulus (GPa)	11 ~ 32
Ultimate elongation (%)	2.5 ~ 3.7
Acid and alkali resistance	weak

Corrosion test

In order to study the influence of pH and corrosion time on the tensile properties of bamboo slices, as well as the anticorrosion property of epoxy resin on bamboo slices, solutions with different pH were prepared with a concentration of 35% HCl reagent and a concentration of 5% NaOH reagent, and the coated samples were prepared by applying a layer of epoxy resin adhesive (E7730) evenly on the surface of the pristine sample followed by curing at room temperature for 24 h. Correspondingly, one set of pristine samples and coated samples were marinated in the solutions with different pH in range 2 - 13 for 15 days, and the other set of pristine samples and coated samples were impregnated in the solution of pH 4.0 and pH 10.0 for different time (1, 3, 5, 7, 15, 28 days), respectively. The mass lose induced by corrosion were measured after soaked samples were washed with distilled water and followed by being stored under laboratory temperature ($20 \pm 2^\circ\text{C}$) and relative humidity ($65 \pm 15\%$) for 2 days. Afterwards, their tensile properties were measured.

Surface modification treatment of bamboo slices

The surface modification of bamboo slices consisted of following two physical methods: heat treatment and alkali treatment, and two chemical methods: silane coupling and acetylation coating: (1) *Heat treated bamboo slices (HTBS)*. Bamboo slices were heated

in a high-temperature test chamber (H/GDWJ-500L) at 120°C for 4 h. When the slices were cooled to room temperature, the mass loss rate was measured. (2) *Alkali treated bamboo slices (ATBS)*. Bamboo slices were immersed in a solution of 5% NaOH for 2 h at room temperature. After being taken out, they were washed repeatedly with dilute acid solution until the washing solution became neutral measured by pH meter, then they were dried in a high-temperature test chamber at 80°C for 4 h. (3) *Coupling agent treated bamboo slices (CTBS)*. Bamboo slices were immersed in mixture solutions (six part 95% ethanol solution and four part 0.6% A-174 silane coupling agent) with pH 4.0 adjusted by 50% acetic acid for 2 h, then removed and dried in a high-temperature test chamber at 80°C for 4 h. (4) *Acetylated bamboo slices (ALBS)*. Neutralize the alkali-treated bamboo slices with dilute acid, then immersed them in 50% acetic acid for 2 h. After being taken out, they were washed with distilled water and dried in a high-temperature test chamber at 80°C for 4 h.

After the modification, the surface morphology of all samples were observed by high-power microscope. Meanwhile, to characterize the influence of modification on chemical functional groups of the samples surface, Fourier transform infrared (FT-IR) spectra were measured by infrared spectroscopy (Thermo Nicolet 6700). Afterwards, applying a layer of epoxy resin (E7730) evenly on the surface of the modified samples. When the epoxy resin adhesive was completed cured by stored at room temperature for 24 h, the ultimate tension of coated and uncoated samples was measured

Tensile tests

The preparation and test method of the tensile properties of bamboo slices was in accordance with the procedure described in testing methods for physical and mechanical properties of bamboo used in building (Chen et al. 2015). The laboratory Max Test universal testing machine (WDW-10E) was adopted for the tensile tests. A slice of polyethylene plastic with 10 mm length are glued by epoxy resin adhesive on each end of the testing sample to be fixed into the fixtures without splitting. When loading, the tensile direction of the testing machine should follow the longitudinal length direction of the bamboo slice. Only when the fracture location is at least 10 mm away from the fixture, can experimental results be judged as valid data. The test was terminated upon the sample was broken. The loading speed is uniformly 0.1 mm.min⁻¹, and five effective replicates were conducted for each sample type

RESULTS AND DISCUSSION

Tensile tests

Effect of pH on ultimate tension of samples during laboratory

Fig. 1a shows that in the acidic environment, when UTBS were corroded in the solution with pH 6.0 and pH 2.0 for 15 days, respectively, the mass loss rate increased from 2.5% to 5.2%, and the corresponding ultimate tension decreased from 0.525 kN to 0.453 kN, which decreased by 24.1% and 34.5% respectively compared with that of uncorroded UTBS (0.692 kN). Notably, because the pH of bamboo was between 5.1 and 6.6 (Lo et al. 2012), the bamboo slices corroded and the ultimate tension decreased by 0.163 kN (23.6%) even under the neutral environment of pH 7.0 for 15 days. In alkaline environment of pH 8.0 and pH 13.0, the mass loss rate increased from 1.34% to 5.3%, and the corresponding ultimate tension decreased by 16.4% (0.114 kN) and 55.6% (0.385 kN) compared with that of uncorroded UTBS, respectively. However, as shown in Fig. 1b, when corroded for 15 days in both acidic and alkaline environments, the mass loss rate of the ERBS was negative and changed only slightly (the maximum was -0.24% in pH 13),

which was attributed to the water absorption of epoxy resin adhesive (Popineau et al. 2005). Meanwhile, the ultimate tension of corroded ERBS only decreased slightly compared with that of ERBS without corrosion (0.677 kN), and the maximum decrease was by 0.04% (0.027 kN) when corroded at pH 12.0 for 15 days. It can be inferred that under the condition of constant corrosion time, the tensile properties of bamboo slices decrease with the increase of corrosion solution concentration, whereas epoxy resin can protect the tensile properties of bamboo slices from the influence of pH

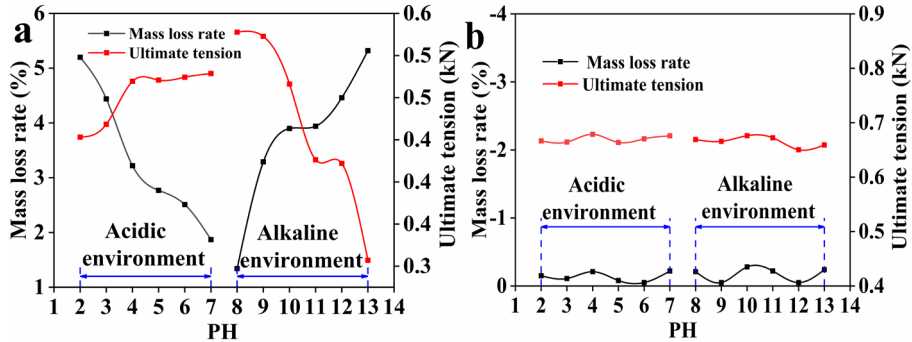


Fig. 1: Regularities of mass loss rate and ultimate tension of (a) pristine samples (UTBS) and (b) samples coated by epoxy resin adhesive (ERBS) under different pH.

Effect of corrosion time on ultimate tension of samples

As can be seen in Fig. 2a, with the increase of corrosion time, the mass loss rate of UTBS increases and the ultimate tension decreases under the condition of constant pH. When UTBS were corroded in the solution with pH 4.0 for 1 day and 28 days, respectively, the mass loss rate increased from 1.9% to 3.4%, and the corresponding ultimate tension decreased from 0.678 kN to 0.490 kN, which decreased by 2.0% and 29.2% respectively compared with that of uncorroded UTBS (0.692 kN). The alkaline environment of pH 10.0 had a greater impact on the ultimate tension of UTBS, which decreased by 9.0% (0.064kN) and 38.6% (0.243 kN) when be corroded for 1 day and 28 days, respectively. As shown in Fig. 2b, the ultimate tension of corroded ERBS only decreased slightly compared with that of uncorroded ERBS (0.677 kN), and the maximum decrease was by 0.08% (0.046 kN) when corroded at pH 4.0 for 5 days, which means that corrosion time had slightly effect on the ultimate tension of ERBS.

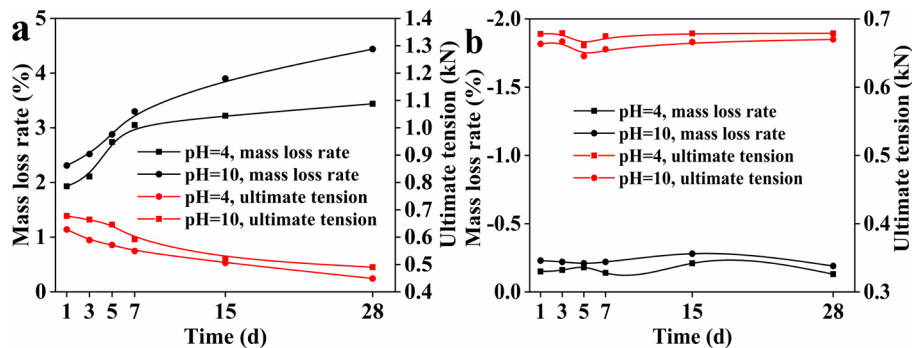


Fig. 2: Regularities of mass loss rate and ultimate tension of (a) UTBS and (b) ERBS under different corrosion time.

The chemical composition of bamboo slices is mainly composed of cellulose, hemicellulose and lignin (Chen et al. 2011). Cellulose mainly determines the longitudinal tensile properties of plant cell walls, and the higher the cellulose content, the better the longitudinal tensile properties of cells (Li and Shen 2011). Hemicellulose is closely related to cellulose and lignin in the cell wall and mainly acts as an adhesive (Vanholme et al. 2010). Lignin has the ability to increase the mechanical strength of cell walls, and to resist microbial erosion (Boerjan et al. 2003). The HCl and the NaOH are capable of degrade the cellulose, hemicellulose and lignin in the bamboo slices (Silverstein et al. 2007), which will further affect the tensile properties of bamboo slices. Consequently, with the increase of concentration of HCl and NaOH solution and corrosion time, the UTBS were prone to be affected by corrosion and tensile properties significantly decreased. However, the epoxy resin adhesive with good anti-corrosion performance, can work as a protective layer to protect the bamboo slices from corrosion induced by contacting with HCl and NaOH solution, so as to maintain rather than improve the excellent tensile mechanical properties of the bamboo slices. Therefore, the changes of pH and corrosion time have little effect in the tensile properties of ERBS.

Tensile properties of surface modified bamboo slices

Surface modification can cause different degrees of damage to the bamboo slices. Only when the improvement of the interface adhesion between the bamboo slices and the epoxy resin exceeds the reduction in the strength of the bamboo slices, the surface modification is meaningful (Liu et al. 2010).

Tab. 2: Ultimate tension of Moso bamboo slices treated with different surface modification.

Samples of bamboo slices	Ultimate tension (kN)	
	Uncoated	Coated
UTBS	0.692	0.677
HTBS	0.538	0.805
ATBS	0.456	0.789
CTBS	0.369	0.693
ALBS	0.402	0.847

Tab. 2 shows that surface modification reduced the ultimate tension of bamboo slices, among which the maximal reduction is 0.323 kN (46.6%) of CTBS, and the minimum reduction is 0.154 kN (22.3%) of HTBS. Due to the small amount of water contained in the epoxy resin adhesive and the poor interface compatibility between the epoxy resin adhesive and the surface of bamboo slices (Zheng et al. 2018), the epoxy resin cannot improve the tensile properties of the bamboo slice when be coated on the surface of bamboo slice, and the ultimate tension of coated UTBS (0.677 kN) is 0.015 kN (1.4%) less than that of uncoated UTBS (0.692 kN). Moreover, compared with uncoated modified samples, the ultimate tension of coated modified samples has been increased to different degrees. The maximal increase is 0.445 kN (110.7%) of ALBS, the minimum increase is 0.267 kN (38.6%) of HTBS. And compared with coated UTBS, the maximal increase of ultimate tension is by 0.170 kN (25.1%) of ALBS. Owing to the damage of coupling agent treatment to the tensile properties of bamboo slices, the minimum increase of ultimate tension is only by 0.016 kN (2.3%) of CTBS. Which indicates that the four modifications improved the interfacial compatibility between the surface of bamboo slices and the epoxy resin adhesive, the treatment of coupling agent in terms) of improving the tensile properties of bamboo slices is not obvious, and the treatment of acetylation is the most effective method among them.

Surface morphology analysis of bamboo slices

The surface of UTBS (Fig. 3a) is relatively smooth and flat, with a few impurity particles. In comparison, the surface of the physically modified bamboo slices (HTBS and ATBS) has become rough and uneven to varying degrees, which can improve the interfacial combination between the surface of bamboo slices and the epoxy resin adhesive. It can be clearly observed that the surface of HTBS (Fig. 3b) is rougher, with many uneven potholes and the color becomes darker. This is because the heat treatment removed the impurities on the surface of bamboo slices, and made part of cellulose and hemicellulose in the bamboo thermal degradation and carbonization (Kartal et al. 2008). Besides, the surface of ATBS (Fig. 3c) becomes rough which can be attributed to the removal of impurities and the dissolution of some lignin and hemicellulose in bamboo slices by alkali treatment (Zhang et al. 1994). The surfaces of chemically modified CTBS (Fig. 3d) and ALBS (Fig. 3e) do not become evidently rough, but the materials become relatively soft. And the improvement of interfacial compatibility between the surface of bamboo slices and the epoxy resin adhesive, can be reasonably explained by the fact that silane coupling agent can reduce the content of hydroxyl group, and acetyl group can replace the hydroxyl group on the cell wall of the bamboo slices, as shown in Fig. 4. Both chemical modifications reduced the water absorption of bamboo slices and made them malleable.

The interface layer which exists between epoxy resin and the bamboo slice plays a decisive role in the mechanical properties of the epoxy resin-coated bamboo slice (Rong et al. 2001). All the four modification methods can change the surface morphology of the bamboo slices, and improve the interfacial combination between the surface of bamboo slices and the epoxy resin adhesive, which confirms the conclusion that the ultimate tension of coated samples can be enhanced by modification before the epoxy resin is coated

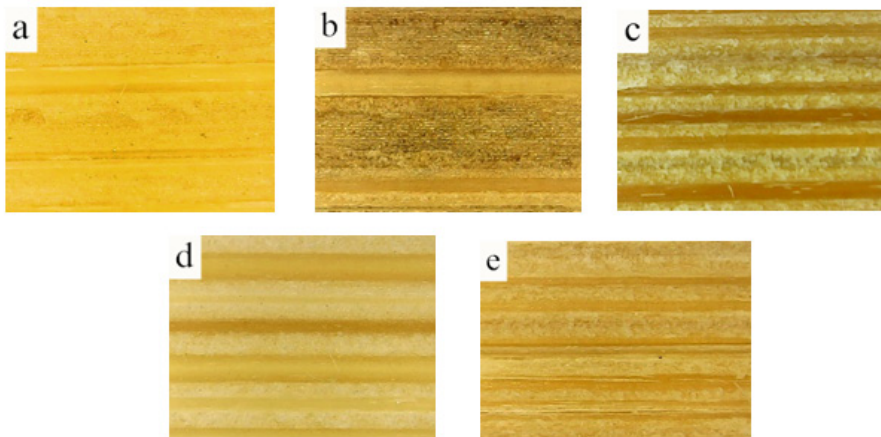


Fig. 3: Surface micrographs of (a) UTBS, (b) HTBS, (c) ATBS, (d) CTBS and (e) ALBS.

Infrared spectroscopic analysis

FT-IR can be used to qualitatively analyze the change of surface functional groups of bamboo slices caused by modification. As can be seen in Fig. 4, due to the dissolution of hemicellulose in bamboo slices after acetylation treatment, the carbonyl functional group (C=O) at 1720 cm^{-1} of ALBS corresponding to hemicellulose disappeared. Which confirmed the conclusion that the treatment of acetylation is the most effective method for improving the interfacial compatibility between the surface of bamboo slices and the epoxy resin adhesive. Besides, the FT-IR of the other three modified bamboo slices are almost the same with the untreated bamboo slice

(UTBS), which can be attributed to the fact that the physical modification method does not cause chemical changes on the surface of bamboo slices. Although silane coupling agent can reduce the content of hydroxyl groups on the surface of bamboo fibers, the effect is not obvious.

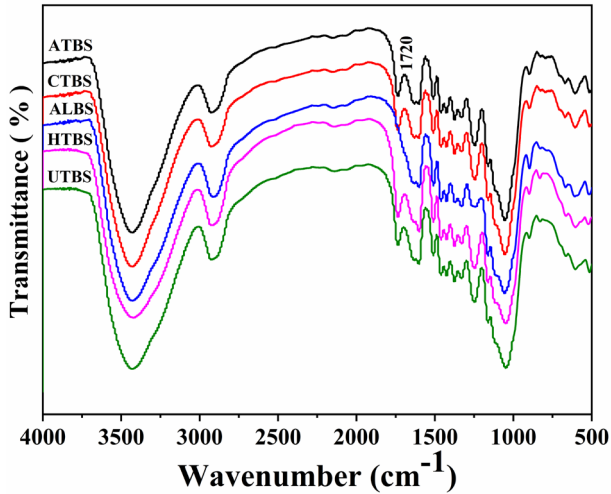


Fig. 4: FT-IR spectra of bamboo slices treated by different modifications.

CONCLUSIONS

(1) As an elastic material, Moso Bamboo has poor corrosion resistance, the acid and alkali environment will cause corrosion to bamboo slices and affect their tensile properties. Moreover, with the increase of acid and alkali solution concentration and marinating time, the ultimate tension of bamboo slices gradually decreases. The maximum reduction is 0.385 kN (55.6%) when be corroded in solution with pH 13.0 for 15 days, and 0.243 kN (38.6%) when be corroded in solution with pH 10.0 for 28 days. Therefore, anticorrosive treatment or other protective measures can be taken to protect the tensile properties and extend the service life of Moso bamboo. (2) Coating the surface of bamboo slices with epoxy resin adhesive can protect them from corrosion by acid and alkali environment. However, due to the poor interfacial compatibility between the surface of bamboo slice and the epoxy resin adhesive, the epoxy resin adhesive can only maintain but not improve the tensile mechanical properties of bamboo. Reasonable surface modification can be taken to improve their interfacial compatibility. (3) Surface modification will reduce the ultimate tension of bamboo slices. Among which the maximal reduction is 0.323 kN (46.6%) of bamboo slices treated by coupling agent, and the minimum reduction is 0.154 kN (22.3%) of bamboo slices treated by heating. The surface morphology indicates that modification can make the surface of bamboo slices become rough or the material become relatively soft, which can improve the interfacial compatibility between the surface of bamboo slice and the epoxy resin adhesive. Compared with the unmodified coated bamboo slice, the treatment of coupling agent in terms of improving the tensile properties of bamboo slices is not obvious, only increases by 0.016 kN (2.3%), and the treatment of acetylation is the most effective modification by reacting with the carbonyl group, which ultimate tension has been increased by 25.1% (0.170 kN).

ACKNOWLEDGMENT

The authors are very grateful that this research was financially supported by grants from National Key R&D Program of China (No. 2016YFC0502208), National Natural Science Foundation of China (NSFC) (No. 51678223), Hubei Provincial Education Department Key Project (No. D20171402), and Green Industrial Project of Hubei University of Technology (No. YXQN2017001).

REFERENCES

1. Ahmad, M., Kamke, F., 2005: Analysis of Calcutta bamboo for structural composite materials: physical and mechanical properties. *Wood Science and Technology* 39(6): 448-459.
2. Antov, P., Savov, V., Neykov, N., 2020: Sustainable bio-based adhesives for eco-friendly wood composites. A review. *Wood Research* 65(1): 51-62.
3. Bledzki, A.K., Reihmane, S., Gassan, J., 1996: Properties and modification methods for vegetable fibers for natural fiber composites. *Journal of Applied Polymer Science* 59(8): 1329-1336.
4. Boerjan, W., Ralph, J., Baucher, M., 2003: Lignin biosynthesis. *Annual Review of Plant Biology* 54(1): 519-546.
5. Chen, H., Cheng, H.T., Wang, G., Yu, Z.X., Shi, S.Q., 2015: Tensile properties of bamboo in different sizes. *Journal of Wood Science* 61(6): 552-561.
6. Chen, W.S., Yu, H.P., Liu, Y.X., Hai, Y.F., Zhang, M.X., Chen, P., 2011: Isolation and characterization of cellulose nanofibers from four plant cellulose fibers using a chemical-ultrasonic process. *Cellulose* 18(2): 433-442.
7. Ghestem, M., Sidle, R.C., Stokes, A., 2011: The influence of plant root systems on subsurface flow: implications for slope stability. *Bioscience* 61(11): 869-879.
8. Hegde, A., Sitharam, T.G., 2015: Use of bamboo in soft-ground engineering and its performance comparison with geosynthetics: experimental studies. *Journal of Materials in Civil Engineering* 27(9): 04014256.
9. Hsu, T.C., Guo, G.L., Chen, W.H., Hwang, W.S., 2010: Effect of dilute acid pretreatment of rice straw on structural properties and enzymatic hydrolysis. *Bioresource Technology* 101(13): 4907-4913.
10. Jin, C., Li, J., Han, S., Wang, J., Sun, Q., 2014: A durable, superhydrophobic, superoleophobic and corrosion-resistant coating with rose-like ZnO nanoflowers on a bamboo surface. *Applied Surface Science* 320: 322-327.
11. Kartal, S.N., Hwang, W.J., Imamura, Y.J., 2008: Combined effect of boron compounds and heat treatments on wood properties: Chemical and strength properties of wood. *Journal of Materials Processing Technology* 198(1-3): 234-240.
12. Khalil, H.P.S.A., Bhat, I.U.H., Jawaid, M., Zaidon, A., Hermawan, D., Hadid, Y.S., 2012: Bamboo fibre reinforced biocomposites: a review. *Materials and Design* 42: 353-368.
13. Lakkad, S., Patel, J., 1981: Mechanical properties of bamboo, a natural composite. *Fibre Science and Technology* 14(4): 319-322.
14. Li, H., Shen, S., 2011: The mechanical properties of bamboo and vascular bundles. *Journal of Materials Research* 26(21): 2749-2756.
15. Li, M., Chai, S.X., Zhang, H.Y., Du, H.P., Wei, L., 2012: Feasibility of saline soil

- reinforced with treated wheat straw and lime. *Soils and Foundations* 52(2): 228-238.
16. Liu, T.M., Zheng, Y.S., Hu, J., 2010: Surface modification of aramid fibers with new chemical method for improving interfacial bonding strength with epoxy resin. *Journal of Applied Polymer Science* 118(5): 2541-2552.
 17. Lo, S.F., Wang, S.Y., Tsai, M.J., Lin, L.D., 2012: Adsorption capacity and removal efficiency of heavy metal ions by Moso and Ma bamboo activated carbons. *Chemical Engineering Research and Design* 90(9): 1397-1406.
 18. Luft, J.H., 1961: Improvements in epoxy resin embedding methods. *Journal of Cell Biology* 9(2): 409-414.
 19. Luo, H., Yue, L., Wang, N., Zhang, H., Lu, X., 2014: Manufacture of binderless fiberboard made from bamboo processing residues by steam explosion pretreatment. *Wood research* 59(5): 861-870.
 20. Ma, Q., Yang, Y., Xiao, H., Xing, W., 2018: Studying shear performance of flax fiber-reinforced clay by triaxial test. *Advances in Civil Engineering* 2018: 1-8.
 21. Ma'ruf, M.F., 2012: Shear strength of Apus bamboo root reinforced soil. *Ecological Engineering* 41: 84-86.
 22. McIvor, I.R., Douglas, G.B., Hurst, S.E., Hussain, Z., Foote, A.G., 2008: Structural root growth of young Veronese poplars on erodible slopes in the southern North Island, New Zealand. *Agroforestry Systems* 72(1): 75-86.
 23. Popineau, S., Rondeau-Mouro, C., Sulpice-Gaillet, C., Shanahan, M.E., 2005: Free/bound water absorption in an epoxy adhesive. *Polymer* 46(24): 10733-10740.
 24. Qin, D., Ren, H., Zhang, L., Li, Z., 2015: Enhancing enzymatic digestibility of bamboo by fungal pretreatment. *Wood Research* 60(1): 25-32.
 25. Rong, M.Z., Zhang, M.Q., Liu, Y., Yang, G.C., Zeng, H.M., 2001: The effect of fiber treatment on the mechanical properties of unidirectional sisal-reinforced epoxy composites. *Composites Science and Technology* 61(10): 1437-1447
 26. Shafizadeh, S., Kavanagh, J.A., 2005: Pathogenicity of *Phytophthora spp.* species and *Pythium undulatum* isolated from *Abies procera* Christmas trees in Ireland. *Forest Pathology* 35(6): 444 - 450.
 27. Shinoda, M., Bathurst, R.J., 2004: Lateral and axial deformation of PP, HDPE and PET geogrids under tensile load. *Geotextiles and Geomembranes* 22(4): 205-222.
 28. Silverstein, R.A., Chen, Y., Sharma Shivappa, R.R., Boyette, M.D., Osborne, J., 2007: A comparison of chemical pretreatment methods for improving saccharification of cotton stalks. *Bioresource Technology* 98(16): 3000-3011.
 29. Subaida, E., Chandrakaran, S., Sankar, N., 2008: Experimental investigations on tensile and pullout behaviour of woven coir geotextiles. *Geotextiles and Geomembranes* 26(5): 384-392.
 30. Trujillo, E., Moesen, M., Osorio, L., Vuure, A.W.V., Ivens, J., Verpoest, I., 2014: Bamboo fibres for reinforcement in composite materials: strength Weibull analysis. *Composites Part A: Applied Science and Manufacturing* 61: 115-125.
 31. Vanholme, R., Demedts, B., Morreel, K., Ralph, J., Boerjan, W., 2010: Lignin biosynthesis and structure. *Plant Physiology* 153(3): 895-905.
 32. Wesseloo, J., Visser, A.T., Rust, E., 2004: A mathematical model for the strain-rate dependent stress-strain response of HDPE geomembranes. *Geotextiles and Geomembranes* 22(4): 273-295.
 33. Yan, W., Zhou, J., Zhang, B., Fu, W., Chen, Z., 2017: Development design and mechanical properties of arc bamboo. *Wood Research* 62(3): 365-372.

34. Yang, W.J., Neoh, K.G., Kang, E.T., Teo, S.L.M., Rittschof, D., 2014: Polymer brush coatings for combating marine biofouling. *Progress in Polymer Science* 39(5): 1017-1042.
35. Yun, H., Li, K., Tu, D., Hu, C., South, G.C., 2016: Effect of heat treatment on bamboo fiber morphology crystallinity and mechanical properties. *Wood Research* 61(2): 227-233
36. Zhang, M.Q., Zhu, S.P., Zeng, H.M., Lu, Y., 1994: A biomaterial based carbon fiber. *Die Angewandte Makromolekulare Chemie: Applied Macromolecular Chemistry and Physics* 222(1): 147-163.
37. Zhao, X., Tu, D., Chen, C., Zhou, Q., 2019: Prediction of the mechanical properties of thermally-modified rubber wood on the basic of its surface characteristic. *Wood Research* 64(1): 25-34.
38. Zheng, K.K., Gao, C.H., He, F.S., Lin, Y.X., Liu, M., Lin, J., 2018: Study on the interfacial functionary mechanism of rare-earth-solution-modified bamboo-fiber-reinforced resin matrix composites. *Materials* 11(7): 1190-1205.

QIANG MA, ZHAO LIU, HENGLIN XIAO, ZHI CHEN*
HUBEI UNIVERSITY OF TECHNOLOGY
SCHOOL OF CIVIL ENGINEERING AND ARCHITECTURE
WUHAN 430068
CHINA

*Corresponding author: chenzhi1988420@126.com

COMPARATIVE ANALYSIS OF STATIC AND DYNAMIC MOE OF PANNÓNIA POPLAR TIMBER FROM DIFFERENT PLANTATIONS

ANTAL KÁNNÁR, CSILLA CSIHA
UNIVERSITY OF SOPRON
HUNGARY

(RECEIVED SEPTEMBER 2020)

ABSTRACT

The aim of this study has been to investigate the suitability of Pannónia poplar (*Populus × euramericana* cv. Pannónia) timber for structural purposes. Static and dynamic modulus of elasticity (MOE) has been determined on samples of 4 different Hungarian plantation origins. The results of the dynamic test showed the same range as the static test, showing a good correlation of the two measurements. As result it can be stated that the domestic Hungarian Pannónia poplar species have in average 11000 N·mm⁻² modulus of elasticity. This exceeds considerably the threshold limit value (7000 N·mm⁻²) necessary for structural applications according to Eurocode 5. Therefore Pannonia poplar is suitable for structural applications, and are a good alternative of the widely used coniferous species in construction sector.

KEYWORDS: Pannónia poplar, modulus of elasticity (MOE), bending strength.

INTRODUCTION

The territory of Hungary is populated roughly in 10% by hybrid poplar species. Around half of the hybrid poplar species consists of Pannónia poplar, which is planted on large areas, as result of good cultivation experiences, high resistance against diseases, good radication vein and favorable shape developed. In spite of these good properties, poplar is mostly used for paper and stillage production in Hungary. Hungary needs to import coniferous species for the purpose of wooden structural element production, whilst large stocks of straight, branch free, 30 year old, 50-70 cm diameter poplar trunks are available (Papp and Horváth 2016). The aim of this study is to investigate the suitability of the Pannónia polar for construction purposes, first of all for glulam production. This prime material supply, with its annual 1 million m³ exploitation may contribute to the reduction of the imported stocks (Rábai et al. 2020). In our study we put the accent on the modulus of elasticity measured both with dynamic and static method, in order to define the category of the EN 338 met by the values of the 4 sample groups, representing different

territories of origin. In the past years other investigations of poplar hybrids also have been performed. Pásztor et al. (2017) investigated the development of physico-mechanical properties of young Pannónia poplar during dry thermal treatment. According to these measurements based on three point bending tests, the average modulus of elasticity of small size samples ($20 \times 20 \times 300$ mm) didn't reached $8000 \text{ N}\cdot\text{mm}^{-2}$. International publications also point out the remarkable properties of the poplar species (Beery et al. 1983, Bodig 1979, Pellicane and Bodig 1981, Zhou 1989, Zhou 1989, Kruger and Wagenfuer 2020). The poplar mechanical properties are very similar to coniferous wood species (Schniewind 1968, Schniewind 1972, Hoffmeyer and Davidson 1989, Martins et al. 2019). Hodusek et al. (2017) investigated MOR of Mexican cedar and Canadian poplar *Populus × canadensis*) with static and dynamic method. Testing 60 pieces of 80×80 mm poplar samples, they have found $10000 \text{ N}\cdot\text{mm}^{-2}$ MOR, what considerably exceeds $7000 \text{ N}\cdot\text{mm}^{-2}$, required for structural applications. They also stated, that the MOR values in case of poplar, obtained with 4 point bending test respectively with vibration, dynamic method differed from each other only in 1-2%. Castro and Fragnelli (2006) stated as conclusion, that poplar wood is suitable for load bearing purposes, especially for LVL (laminated veneer lumber) beam production. Zhou (1990) had been successful with poplar in OSB production. Basterra et al. (2012) investigated poplar wood material similar to Pannónia poplar. The MOR values measured by him showed an average of $7700 \text{ N}\cdot\text{mm}^{-2}$, whilst the average bending strength used to be $67 \text{ N}\cdot\text{mm}^{-2}$, thus the poplar wood tested, was found to be suitable for load bearing purposes. These values could be raised with 50% by combining the boards with fiber reinforcement. Mirzaei et al. (2018) tested glulam beams manufactured from hydrothermally treated poplar lamellas and stated that both the MOE and the bending strength increased due to the treatment. Cheng and Hu (2011) investigated the effect of carbon fiber reinforcement on the static and dynamic MOE of polar samples. Their defect free samples showed $11500 \text{ N}\cdot\text{mm}^{-2}$ MOE, whilst with the model set up by them the effect of fiber reinforcement could be clearly shown. Castro and Paganini (2003) investigated mechanical properties of poplar and eucalypt wood with the purpose of glulam production. The investigated poplar samples showed an average MOE of $9600 \text{ N}\cdot\text{mm}^{-2}$, and bending strength of $44 \text{ N}\cdot\text{mm}^{-2}$, complying thus with the requirements set for structural use of the material. They were successful in combining the eucalypt and poplar lamellas in order to improve with 50% the MOE of the beam solely composed by polar lamellas. Roohnia et al. (2010) searched for a typical parameter by vibration analysis, in order to enable the evaluation of the end cracking of beams. They stated that the measure of cracking is associated with the difference between the GL_R and GL_T . In case of defect free beams these two values are mostly the same. The poplar samples tested by them showed a MOE of $10000 \text{ N}\cdot\text{mm}^{-2}$. Based on these results we can state that poplar may be suitable for structural purposes, or as massive wood, or as glulam, or as LVL, or as other materials like OSB.

In the followings we search for an answer whether the strength values of the Hungarian Pannónia poplar wood material reach the level suitable for structural application, as large stocks of this material are available. Furthermore also needs to be investigated whether is there a relevant influence of the territory of origin on the properties of the wood material growing on different sites.

MATERIAL AND METHODS

Four groups of samples have been prepared for investigation, each being collected on representative Hungarian sites Győr, Kapuvár, Solt and Újrónafő (Tab. 1). From the trunks

collected on four different plantation sites. The 25 mm thick boards have been prepared, kiln dried, planed, cut to size 2200 × 70 × 20 mm (grain × tangential × radial) and conditioned at 20°C and 65% relative humidity (RH). The moisture content of the sample batches has been determined as average of 3 measurements per lamella. The equilibrium moisture content (MC) has been 12% ± 1%. A total of 146 knot free samples have been investigated.

Tab. 1: The characteristics of the plantation sites and wood samples according to the forest registry.

Plantation site	Height above sea level (m)	Character of the site	Age of trees (years)	Average height of trees (m)	Average diameter BH (cm)
Győr 540B	≤ 150 m	lowland not flood basin	25	26	27
Kapuvár 35A	≤ 150 m	lowland not flood basin	28	30	36
Solt 3A	≤ 150 m	lowland flood basin	28	20	24
Újrónafő 11G	≤ 150 m	lowland not flood basin	25	27	32

When deciding on the length of samples, a second phase of investigation has been taken into consideration, where 5 layer glued laminated beams are foreseen to be tested. Choosing this length the ratio of length/cross section meets the requirements of the standard, being 18–20. This value makes possible the effect of the shear strength to be ignored at bending tests and in the same time when measuring the static MOE of the lamellas, this ratio allowed a 400 mm span. The distance between the two upper crossheads has been 120 mm, during the four point bending test. The length of lamellas made possible three measurements to be performed, on three different portions of the sample, on one lamella. As consequence, the MOE of each lamella is calculated as average of three measurements. Beside the mechanical tests reported here, other complex material science investigations are in progress at the University of Sopron, regarding these hybrids. In the frame of those investigations the density of these samples originating from three different plantations of the KAEG Ltd has been measured and reported: Kapuvár 35A, Győr 540B and Újrónafő 11G showed 409.6 kg·m⁻³, 420.3 kg·m⁻³, and 459.6 kg·m⁻³ (Farkas and Horváth 2018). Based on these values can be stated, that even the lowest average densities reach the value of 410 kg·m⁻³, typical for class C22, and are far higher than the value of 350 kg·m⁻³, typical for C14, being the lowest density class allowed for structural uses. MOE of samples originating from different plantations has been determined with two different methods: on one side by sound velocity measurements performed with the Fakopp-PLG nondestructive timber grading instrument (Divos and Tanaka 1997), and on the other side by static four point bending tests as per EN 408. After the measurements the results of the static and the dynamic tests have been compared in order to check the reliability of the dynamic tester when measuring Pannónia poplar timber also, as those measurements are easy to be performed even on site. For bending strength measurements 18 samples from each plantation have been collected, according to EN 408.

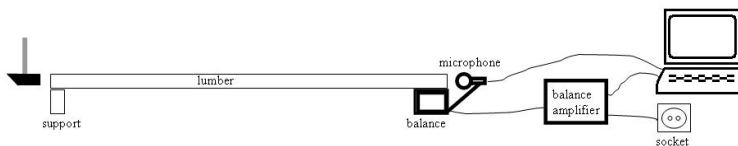


Fig. 1: Fakopp-PLG measuring instrument.

Fakopp-PLG is a dynamic MOE measuring instrument which provides data on the bending strength upon calculation. The measuring principle of the instrument is based on the detection with a microphone of the longitudinal sound frequency emitted by a hammer (Fig. 1).

During the measurement, the investigated sample was placed on a balance and its weight was measured. Based on a length measurement, performed with laser distance meter and the size of the cross section, the software calculated the density of the sample using Eq. 1 taking into account the difference in MC at the time of measurement and in the laboratory:

$$\rho = \frac{m}{l \cdot w \cdot h \cdot \left(1 + \frac{u}{100}\right)} \quad (1)$$

where: m – mass (kg), l – length (m), w – width (m), h – thickness, u (%) – difference in MC between at the time of measurement and in the laboratory.

The measuring method defines the dynamic MOE based on equation Eq 2:

$$MOE_{mean} = \frac{m}{l \cdot w \cdot h} \cdot (2lf)^2 \cdot 0,92 \cdot (1 + U/50) \quad (2)$$

where: f – the frequency of the longitudinal wave.

The instrument provides the characteristic value of the sample based on the determined average MOE, and associates the strength class (Divos and Tanaka 2000), taking into account the values of Eurocode 5.

RESULTS AND DISCUSSION

The average static and dynamic MOE values of the different plantations are shown on Fig. 2. Comparing the results of the static tests to the dynamic ones, we can state that in case of samples from Győr, Kapuvár and Solt the dynamic measurements resulted 1%, 6% and 7% higher values than the static measurements, respectively.

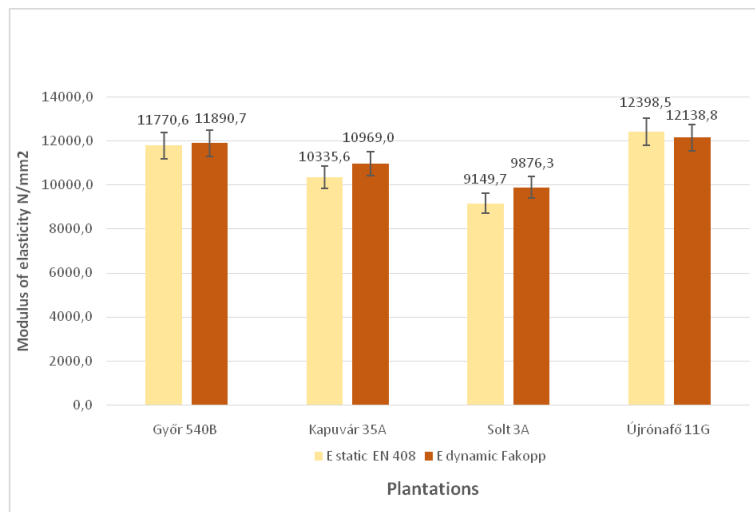


Fig. 2: Comparison of the static and dynamic MOE.

In case of samples from Újrónafő, the dynamic tests resulted 2% lower values relative to the static test values. The samples from Győr and Újrónafő originated from younger trunks than the two others, and whilst they showed mostly similar MOE, compared to the samples from the other plantations their modulus of elasticity used to be significantly higher. Comparing the absolute value of the averages measured/calculated with the two different methods, 4% difference has been found, thus the much faster dynamic method is considered a suitable method for the approximation of the expected modulus of elasticity in practice. The main parameters of the samples are shown in Tab. 2.

Tab. 2: Static and dynamic MOE of Pannónia poplar samples from four different sites.

Plantation ID	Number of samples Stat/Dyn	MOE stat EN408 (N·mm ⁻²)	Std (N/mm ²)	MOE dyn Fakopp (N·mm ⁻²)	Std (N·mm ⁻²)	Difference (%) Dyn/Stat
Győr 540B	135/45	11770.6	1288.7 (11%)	11890.7	977.4 (8%)	1.01
Kapuvár 35A	165/55	10335.6	1267.5 (12%)	10969.0	1166.7 (11%)	5.77
Solt 3A	114/38	9149.7	1248.5 (14%)	9876.3	1353.5 (14%)	7.36
Újrónafő 11G	24/8	12398.5	768.8 (6%)	12138.8	919.7 (8%)	-2.14

* Values in brackets are the standard deviation (%).

The difference between the number of samples of the static and dynamic tests is due to the measuring techniques, as during the dynamic measurements the boards have been measured once, whilst during the static test the length of the board allowed three measurements per board. This way the static MOE of each board has been calculated as average of three measurements.

The lowest average MOE has been measured in case of Solt3A samples, whilst the highest in case of Újrónafő 11G samples, and the difference between these two has been 26% in case of static tests, whilst 17% in case of dynamic tests. The samples originating from flood basins (Solt3A) resulted the lowest MOE, showing that the soil conditions are with negative influence not only on the mass increase/diameter of the trunk, but on the mechanical properties also, such as the MOE. As Tab. 2 shows, the standard deviations both in case of static and dynamic tests approximate 10%, which can be considered a conveniently low value, taking into account that remains under 20%, which is typical to wood, as biological material (Kánnár 2014, Kánnár et. all. 2019, Galuppi and Royer 2014, Yue et al. 2019, Lang et al. 2003). Considering all the tested samples the static MOE has been calculated 10 914 N·mm⁻², whilst the dynamic MOE has been 11 219 N·mm⁻², which means that in average the results of the dynamic tests have been 2.8% higher, and this has been considered a good correlation. The differences between static and dynamic MOE values are shown in the last column of Tab. 3. Based on these results can be stated that the dynamic tests result in general about 4% higher values than the static test. The only exception are the values measured in case of Újrónafő samples, in this case the static measurements resulted higher values than the dynamic ones, but has to be mentioned, that in this case the number of tested samples has been significantly lower, which may be the reason of the deviation. The relatively small difference between the two measuring technics leads to the conclusion, that the dynamic method is also suitable for the calculation and prediction of the MOE. In order to authenticate the measurements, 18 randomly chosen samples have been selected for bending strength tests, according to EN 408. Result are shown in Tab. 3.

Tab. 3: Static and dynamic strength of Pannónia poplar samples of different origin.

Plantation ID	Number of samples Dyn/Stat	Strength class according EN 338 estimated by Fakopp-PLG	Average static bending strength (N·mm ²)
Győr 540B	45/3	C30	67.22
Kapuvár 35A	55/3	C27	76.61
Solt 3A	38/11	C22	68.12
Újrónafő 11G	8/3	C30	87.54

The reason of the relative small number of samples and the random test used to be, that after being tested for bending strength, the boards/lamellas went for further processing: 5 layer glued, laminated beams have been produced and tested.

The third column of Tab. 3 shows the average estimated bending strength class, the value of which is characteristic, meaning that its 5% quantile's value gives the value of the expected bending strength in N·mm⁻². Thus the strength class gives the expected value of the bending strength with high reliability, from 100 cases only 5 case it can be expected to get lower values. The values recorded by measurement exceed considerably the estimated bending strength values, thus suit with high reliability to the design values calculated from the strength class.

We would like to mention in the same time, that the tested samples have been all defect and knot free, thus probably manifested somewhat higher bending strength than unselected, common boards would show. As conclusion can be stated that the investigated Pannónia poplar populations possess in average 11 000 N·mm⁻² MOE. The expected strength associated with this elasticity characteristic not only reaches, but exceeds the threshold limit value 7 000 N·mm⁻² prescribed for structural applications, respectively the 14 N·mm⁻² bending strength of class C14. Based upon these data can be confirmed that the investigated plantation sites provide Pannónia poplar timber suitable for structural applications, and can replace the widely used coniferous species in construction sector.

CONCLUSIONS

In frame of this research the main question used to be the suitability of the harvestable, mature, 0.5 m³ Pannónia poplar timber of different Hungarian plantations, for structural applications. Four plantation sites have been involved in the research, a total of 146 samples of 2240 x 70 x 20 mm dimension have been tested both by static and dynamic MOE test. Beside performing static measurements according to EN 408 in the laboratory, the suitability of the Fakopp instrument, which measures dynamic MOE has been also evaluated and compared to the static measurement. However it is more efficient applicable in industrial environment and makes possible even on site measurement and adjudication of the MOE. Comparing the average MOE of the different sites, they showed a maximum of 26% deviation in case of static measurements, whilst only 17% in case of dynamic measurements, which means that the conditions of the different sites have a major influence on the modulus of elasticity of the wood material. The most unfavorable results have been measured in case of flood area samples. The standard deviation of both static and dynamic measurements remained under 10%, which is much lower than the 20%, considered minor for wood as inhomogeneous biological material. The static MOE in average of all tested samples resulted 10 914 N·mm⁻², whilst the dynamic one 11 219 N·mm⁻². Considering all samples, the dynamic tests MOE have been 2.8% higher than the one measured by static method, which means that the dynamic one

is also suitable for MOE testing. In conclusion can be stated that that the investigated plantation sites provide Pannónia poplar timber with average MOE of 11 000 N-mm⁻². This exceeds considerably the threshold limit value necessary for structural applications. Therefore poplars of these sites are suitable for structural applications, and are a good alternative of the widely used coniferous species in construction sector.

ACKNOWLEDGMENTS

This research was sponsored by the OTKA K116216 “Complex analysis of the physico-mechanical and surface physical properties of wood with low density” project. The financial supports are gratefully acknowledged.

REFERENCES

1. Basterra, L.A., Acuna, L., Casado, M., López, G., Bueno, A., 2012: Strength testing of poplar duo beams, *Populus x euramericana* (Dode) Guinier cv. I-214, with fibre reinforcement. *Construction and Building Materials* 36: 90-96.
2. Beery, W.H., Ifju, G., Mclain, T.E., 1983: Quantitative wood anatomy - relating anatomy to transverse tensile strength. *Wood and Fiber Science* 5(4): 395-407.
3. Bodig, J., 1979: Load-carrying efficiency of homogeneous wood composites. *Wood and Fiber* 10(3): 188-199.
4. Castro, G., Paganini, F., 2003: Mixed glued laminated timber of poplar and *Eucalyptus grandis* clones. *Holz als Roh- und Werkstoff* 60: 291-298.
5. Castro, G., Fragnelli, G., 2006: New technologies and alternative uses for poplar wood. *Universidad de Huelva* 2: 27-36.
6. Cheng, F., Hu, Y., 2011: Nondestructive test and prediction of MOE of FRP reinforced fast-growing poplar glulam. *Composite Science and Technology* 71: 1163-1170.
7. Divos, F., Tanaka, T., 1997: Lumber strength estimation by multiple regression. *Holzforschung* 51(5): 467-471.
8. Divos, F., Tanaka, T., 2000: Effects of creep on modulus of elasticity determination of wood. *Journal of Vibration and Acoustics* 122(1): 89-92.
9. Galuppi, L., Royer-Carfagni, G., 2014: Localized contacts, stress concentrations and transient states in bent lamination with viscoelastic adhesion. An analytical study. *International Journal of Mechanical Sciences* 103: 275-287.
10. Hodousek, M., Dias, A.M.P.G., Martins, C., Marques, A.F.S., Böhm, M., 2017: Comparison of non-destructive methods based on natural frequency for determining the modulus of elasticity of *Cupressus lusitanica* and *Populus x Canadensis*. *Bio Resources* 12: 270-282.
11. Hoffmeyer, P., Davidson, R.W., 1989: Mechano-sorptive creep mechanism of wood in compression and bending. *Wood Science and Technology* 23: 215-227.
12. Kánnár, A., 2014: Evaluation of glulam beams' performance in special environmental conditions. *Wood Research* 59: 803-812.
13. Kánnár, A., Karácsonyi, Zs., Andor, K., Csóka, L., 2019: Analysis of glued-laminated timber structure during five years of outdoor operation. *Construction and Building Materials* 205: 31-38.
14. Krueger, R., Waegenfuer, A., 2020: Comparison of methods of determining shear modulus of wood. *European Journal of Wood and Wood Products* 78(6): 1087-1094.

15. Martins, C., Cruz, H., Dias, A.M.P.G., 2019: Using non-destructive testing to predict the mechanical properties of glued laminated poplar. *Proceedings of the Institution of Civil Engineers: Structures and Buildings* 172(9): 661-670.
16. Mirzaie, G., Mohebbi, B., Ebrahimi, G., 2018: Technological properties of glulam beams made from hydrothermally treated poplar wood. *Wood Material Science and Engineering* 13(1): 36-44.
17. Lang, E.M., Bejo, L., Divos, F., Kovacs, Z., Anderson, R.B., 2003: Orthotropic strength and elasticity of hardwoods in relation to composite manufacture. Part III: Orthotropic elasticity of structural veneers. *Wood and Fiber Science* 35(2): 308-320.
18. Papp É., Horváth N., 2016: Nyár faanyagok anyagtudományi vizsgálataihoz szükséges hazai szakirodalom áttekintése, értékelése (An overview and evaluation of Hungarian publications required for material science examinations of poplar wood species). *Faipar* 64(2): 22-28.
19. Pásztory, Z., Horváth, N., Börcsök, Z., 2017: Effect of heat treatment duration on the thermal conductivity of spruce and poplar wood. *European Journal of Wood and Wood Products* 75(5): 843-845.
20. Pellicane, P.J., Bodig, J., 1981: Sampling error in the bending strength distribution of dimension lumber. *Wood Science and Technology* 15(3): 211-225.
21. Rábai, L., Horváth, N., Kánnár, A., Csiha, Cs., 2020: Study on the wettability of Pannónia poplar (*P. x euramericana* Pannónia) from two Hungarian plantations: Győr and Solt. *European Journal of Wood and Wood Products* 78(5): 1057-1060.
22. Roohnia, M., Yavari, A., Tajdini, A., 2010: Elastic parameters of poplar wood with end-cracks. *Annals of Forest Science* 67(4): 409.
23. Schniewind, A.P., 1968: Recent progress in the study of the rheology of wood. *Wood Science and Technology* 2(3): 188-206.
24. Schniewind, A.P., 1972: Wood as a linear orthotropic viscoelastic material. *Wood Science and Technology* 6(1): 43-57.
25. Yue, K., Wang, L., Xia, J., Zhang, Y., Chen, Z., Liu, W., 2019: Experimental research on mechanical properties of laminated poplar wood veneer/plastic sheet composites. *Wood and Fiber Science* 51(3): 320-331.
26. Zhou, D., 1989: A study of oriented structural board made from hybrid poplar-effects of some factors of mechanical forming installation for orientation effectiveness. *Holz als Roh- und Werkstoff* 47(10): 405-407.
27. Zhou, D., 1990: A study of oriented structural board made from hybrid poplar. Physical and mechanical-properties of OSB. *Holz als Roh- und Werkstoff* 48(7-8): 293-296.

ANTAL KÁNNÁR*
UNIVERSITY OF SOPRON
INSTITUTE FOR APPLIED MECHANICS AND STRUCTURES
BAJCSY Zs. 4.
H-9400 SOPRON, HUNGARY
*Corresponding author:antal.kannar@skk.nyme.hu

CSILLA CSIHA
UNIVERSITY OF SOPRON
INSTITUTE FOR WOODBASED PRODUCT AND TECHNOLOGY
BAJCSY ZS. 4.
H-9400 SOPRON, HUNGARY

INFLUENCE OF THE ENVIRONMENTAL POLLUTION ON THE DISTRIBUTION AND POLYMERIZATION DEGREE OF CELLULOSE IN BARK AND WOOD FROM SCOTS PINE (*PINUS SYLVESTRIS* L.) STEM

DONATA KRUTUL, ANDRZEJ RADOMSKI, ANDRZEJ ANT CZAK, MICHAŁ DROŹDŹEK
TERESA KŁOSIŃSKA, DOMINIKA SZADKOWSKA, JANUSZ ZAWADZKI
WARSAW UNIVERSITY OF LIFE SCIENCES
POLAND

(RECEIVED JUNE 2020)

ABSTRACT

The pine stems were cut from three different polluted environments – Ist trees degradation degree (weak pollution), IInd trees degradation degree (strong pollution) and IIIrd trees degradation degree (connected with very strong pollution). On the basis of obtained results it was stated that environmental pollution caused changes in late wood participation, as well as distribution of cellulose on the stem cross- and longitudinal section. It also changed cellulose content in bark from the butt-end section, which was about 26% regardless the degradation degree. The environmental pollution caused also an increase of viscometric average polymerization degree of cellulose in heartwood in relation to heartwood adjacent sapwood and sapwood from butt-end section. Regardless the degradation degree, cellulose polymerization degree in heartwood adjacent sapwood from the middle part of the stem was higher in comparison to sapwood and heartwood. Moreover, the environmental pollution caused the increase of viscometric average polymerization degree of cellulose in bark. The polymerization degree of cellulose in bark from the butt-end section of IIIrd degradation degree stems was 22% and 23% higher in comparison to the Ist and IInd degradation degree.

KEYWORDS: Pine, sapwood, sapwood adjacent heartwood, cellulose, polymerization degree.

INTRODUCTION

Trees are a good archive of changes in the ecosystem in which they are grown. They are exposed to climate change and pollution. Changes in the ecosystem can affect the chemical structure of the wood (Sensuła et al. 2015, Waliszewska et al. 2019). Pine wood is the basic raw material for pulp production and more, that is why the studies of holocellulose, α -cellulose

and cellulose on the cross- and longitudinal section of pine stem is an important factor studied by many researchers (Harwood 1971, Uprichard 1971, Krutul 1994, Fengel and Wegener 2003, Willför et al. 2005, Waliszewska et al. 2015, Antczak et al. 2016, Zawadzki et al. 2016, Funda et al. 2020). According to Krutul (1994), cellulose content in 110-year-old pine stems increases from pith perimeter, regardless the stem height. Differences in cellulose content between sapwood and heartwood are the most significant in butt-end section and up to the height of 20 m. Whereas, at higher level these contents differ only by about 15%.

Depending on environmental pollution degree, higher or lower changes in content and distribution of mineral substances and extractives may be observed, as well as structural components on the cross- and longitudinal section. Changes caused by the environmental pollution are related to decrease of annual increments width and the increase of late wood participation in comparison to unpolluted wood (Sensula et al. 2017, Cindoruk et al. 2020). According to Krutul (1994), in 110-year-old pine wood, gained from the unpolluted environment, higher correlation coefficient between cellulose content and late wood participation may be found for samples from cross-sections from the height of 6 and 10 m (correspondingly 0.8466 and 0.9130) in relation to samples gained from 2 m height (0.5874). The dependence between cellulose content and late wood participation along the stem occurs in the group of annual increments 1st – 10th (from the perimeter), with the correlation coefficient of 0.81 (Krutul 1994).

Krutul et al. (2006) performed studies on the influence of the heat and power plant on the cellulose content in wood, branches, roots and bark of Scots pine. Samples for the analysis were collected 1 and 21 km far from the emission source. It was stated that cellulose content is lower in pith adjacent wood in relation to sapwood both in butt-end and middle section, as well as in the top of the stem. Such a distribution was also denoted in former paper of Krutul (1994), concerning pine trees growing in the environment unpolluted with any industrial emissions. According to Krutul et al. (2006) cellulose content in bark from trees growing in the distance of 1 and 21 km from the heat and power plant equals 21.9% and 23.0% correspondingly, and does not much differ from the literature data (23.1% - Fengel and Wegener 2003, 22.2% - Räsänen and Athanassiadis 2013, 20.2% - Rowell 2005). Industrial emissions caused by heat and power plants also did not influence the cellulose content in pine wood in relation to results obtained for samples obtained from unpolluted environment (Krutul et al. 2006).

Polymerization degree is the important parameter of cellulose and it may be examined with different methods including viscometry. According to Zawadzki et al. (2006), viscometric average polymerization degree of cellulose isolated from Scots pine sapwood is in the range of 549-553 (isolated with Cross-Bevan method), 497-502 (Kürschner-Hoffer method) and 471-482 (Seifert method). It means that isolation with Seifert method causes higher degree degradation in comparison to other methods. That is why viscometric average polymerization degree of cellulose may be the indicator testifying of its degradation under the influence of physical, chemical and mechanical factors. The highest percent difference in the viscometric average polymerization degree was denoted for sapwood adjacent heartwood and in sapwood in relation to the pith adjacent sapwood. It equals correspondingly 27% to 45% and 35% to 48% (Krutul 1988). However, it must be emphasized that viscometric average polymerization degree may be the best parameter for comparisons.

The aim of this paper is to examine the influence of the pollution caused by “Kędzierzyn” Nitrogen Industrial Plant on the cellulose content and its viscometric average polymerization degree on the cross- and longitudinal section of Scots pine stems. Nitrogen Industrial Plant “Kędzierzyn” has performed production of ammonia, nitric acid and nitrogenous fertilizers since 1954. Phthalic acid anhydride waxes and fatty acids were additional products. Heat and power station was also built in the area. Since the beginning of 80's, condition of the environment has

begun to improve because of eco-policy. For example, the emission of the ammonia in Nitrogen Industrial Plant in 1991 was 4000 tons and in 2005 about 500 tons.

MATERIAL AND METHODS

The research material of Scots pine stems were collected from Vth Silesian region in December. Three about 80-year-old trees were cut from each environments – characterized with IIIrd trees degradation degree (connected with very strong pollution), IInd trees degradation degree (strong pollution) and Ist trees degradation degree (weak pollution). The degree of trees degradation in studied zones was defined and related to the distance between the trees and the Nitrogen Industrial Plant “Kędzierzyn”. Trees from the Ist zone were within 25 km of the Nitrogen Industrial Plant, from the IInd zone were within 15 km of the Nitrogen Industrial Plant and trees from the IIIrd zone were within 1 km of the Nitrogen Industrial Plant.

The 300 mm thick disks were cut from each analyzed stem (from butt-end section, half-height and top part). Following zones were distinguished on disks cross-section: sapwood, heartwood adjacent sapwood and heartwood. In the top part of the disk diameter only sapwood and heartwood were distinguished. In butt-end and middle sections bark was collected too. Width measurement of the annual rings and the proportion of late wood were made according to the standard PN-55/D-04110. Samples were extracted before further analysis in the ethanol-benzene mixture (1:1) in the Soxhlet apparatus. Cellulose was isolated by Kürschner-Hoffer method (Saeman et al. 1954, Krutul 2002).

Viscometric average polymerization degree of the Kürschner-Hoffer cellulose was determined with Ubbelohde method (Zawadzki et al. 2006). Viscometer with the capillary no. I was used, CuEN (cupriethylendiamine hydroxide) was applied as the cellulose solvent. The value of the viscometric average polymerization degree was calculated on the basis of Immergut equation $P_v^{0.905} = 0.75[\eta]$. Experiments were performed at the temperature of 25°C. The Viscoclock timer was used for time measurements. Three experiments of each sample were done and standard deviation were calculated.

RESULTS AND DISCUSSION

The rings width showed large fluctuations depending on the habitat and growth conditions of the tree (Matulewski et al. 2019). The annual rings width is a criterion that allows assessment of the wood technical properties. It is assumed that wood with an annual ring width less than 3 mm is narrow-grained. In high-quality wood, the annual rings narrow gradually and evenly from the pith to the bark of the trunk. Based on the data presented in Figs. 1a,b,c, it can be concluded that the tested pine wood was narrow-grained. The width of annual rings did not exceed 3 mm, regardless of the environmental contamination. Sapwood and sapwood adjacent heartwood was characterized by narrower annual rings than heartwood, regardless of the environmental contamination and the height. Sapwood annual rings in Scots pine from very strong polluted area were from 40% to 60% narrower than sapwood annual rings in Scots pine from strong and weak polluted areas. Annual rings in sapwood adjacent heartwood from middle section were characterized from 40% to 60% smaller width than annual rings in sapwood and about two time smaller than annual rings in heartwood. Heartwood from the top section of the Scots pine trunks were characterized from 40% to 90% wider annual rings than sapwood from the same trunk section, regardless of the environmental contamination (Fig. 1).

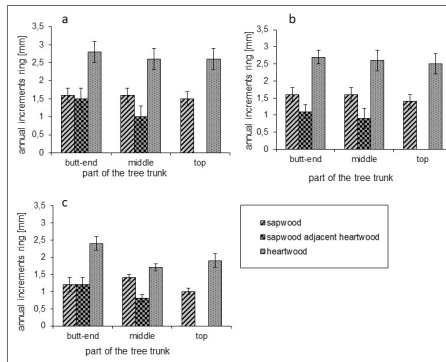


Fig.1: Annual increments participation in analyzed samples of Scots pine wood (*Pinus sylvestris* L.); a- Ist degradation degree (weak pollution), b- IInd degradation degree (strong pollution), c- IIIrd degradation degree (very strong pollution).

Wood density as well as compression strength and other strength parameters are proportionally related with the participation of late wood. As it arises from data presented in the Fig. 2, late wood participation in the butt-end section of the stem of IIIrd degradation degree was 35% and 30% higher in sapwood to correspondingly Ist and IInd degradation degree stems. This value in the heartwood adjacent sapwood and heartwood from middle stem section was lower in IIIrd degradation degree stems in comparison to Ist and IInd degradation degree stems. Late wood participation was similar for all degradation degrees in the top part of the stem. The results obtained are consistent with the data of Krutul (1994). According to these literature data, in 110-year-old pine trees, late wood participation increases from pith to bark. The largest proportion of late wood was characterized by wood at a height of 2 m from the base of the trunk. In sapwood from the Scots pine trunks from weak and strong polluted areas late wood participation was similar in the all height zones. Whereas, in the Scots pine trunks from very strong polluted areas, sapwood was characterized about 20% less late wood participation in top part of trunk compared to butt-end and middle part of trunk. The heartwood from top part of trunks was characterized less late wood participation than in the middle and butt-end parts of trunk, regardless of the environmental contamination (Fig. 2).

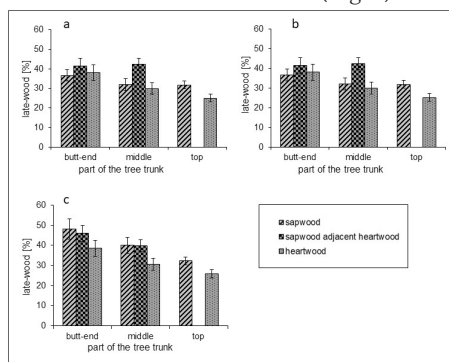


Fig.2: Late wood participation in analyzed samples of Scott pine wood (*Pinus sylvestris* L.); a- Ist degradation degree (weak pollution), b - IInd degradation degree (strong pollution), c- IIIrd degradation degree (very strong pollution).

Fig. 3 presents cellulose content in analyzed samples of wood and bark. Cellulose content in sapwood was higher than in heartwood, regardless the height and degradation degree. Cellulose content in sapwood from the butt-end section was 5% higher in relation to heartwood (Ist degradation degree) or 6% higher (IInd and IIIrd degradation degree). Butt-end section from IIIrd degradation degree stem contained more cellulose and late wood in relation to Ist and IInd degradation degree samples. Sapwood from the middle part of the IIIrd degradation degree stem contained more late wood and about 20% more cellulose in relation to samples of Ist degradation degree. Moreover sapwood from the middle part of the IIIrd degradation degree stem contained almost similar to samples of IInd degradation degree late wood participation, but cellulose content was higher in comparison to other degradation degrees samples. Heartwood contained similar late wood and cellulose content regardless the degradation degree. Late wood participation from the sapwood from the top part of IInd degradation degree stem was similar and cellulose content was about 5% lower in relation to samples from Ist and IIIrd degradation degree. Heartwood, regardless the degradation degree, contained similar late wood and cellulose.

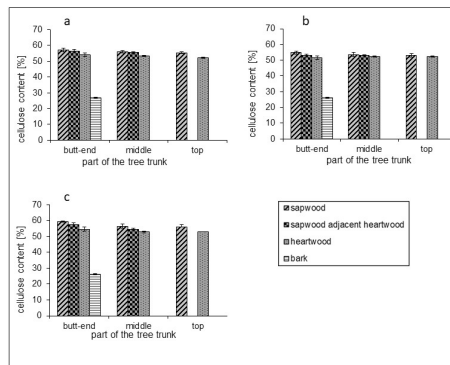


Fig.3: Cellulose content in wood and bark of analyzed samples of Scots pine stems (*Pinus sylvestris* L.); a- Ist degradation degree (weak pollution), b - IInd degradation degree (strong pollution), c- IIIrd degradation degree (very strong pollution).

Summarizing it may be stated that the environmental pollution did not influence the distribution of cellulose on the stem cross-section, what is consistent with Krutul (1994). It was denoted that cellulose content in 110-year-old Scots pine increased in the direction from the pith to perimeter, regardless the height. However, environmental pollution could influenced the content and distribution of cellulose on the longitudinal section and late wood participation. Cellulose content in bark from the butt-end section was similar regardless the degradation degree. It equals 26.8%, 26.0% and 26.2% for correspondingly Ist, IInd and IIIrd degradation degree. Cellulose content in bark was about 50% lower in relation to wood, regardless the environmental pollution. According to Krutul et al. (2006), cellulose content in Scots pine stems collected in the distance 1 and 21 km from the heat and power plant was on the level 21.8% and 23.0% respectively. Räisänen and Athanassiadis (2013) denoted that Scots pine bark contains 22.2% of cellulose, while Fengel and Wegener (2003) determined this value to be 23.1%. The environmental pollution could also influenced the cellulose content in bark which was about 15% higher in relation to Räisänen and Athanassiadis (2013) data and about 12% higher in comparison to values denoted by Fengel and Wegener (2003).

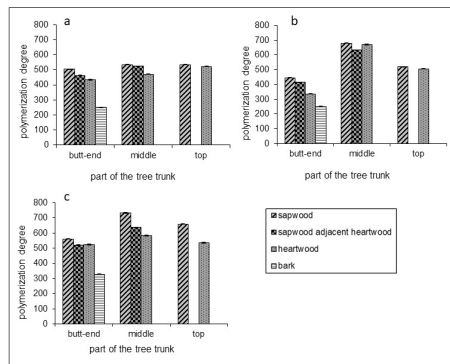


Fig. 4: Viscometric average polymerization degree of cellulose in analyzed pine stem zone; a- Ist degradation degree (weak pollution), b - IInd degradation degree (strong pollution), c- IIIrd degradation degree (very strong pollution).

Fig. 4 presents values of the cellulose polymerization degree in analyzed pine stem zones. This value for the cellulose from the IIIrd degradation degree wood collected from the butt-end section was higher in relation to other degradation degrees regardless the analyzed zone. In sapwood, heartwood adjacent sapwood and heartwood, the increase of cellulose average polymerization degree from the IIIrd degradation degree samples equaled 17.5%, 16.0% and 5.0% in relation to Ist degradation degree samples, and 30.0%, 19.0% and 16.0% in relation to IInd degradation degree samples, correspondingly. In butt-end section, heartwood, the environmental pollution probably caused the increase of the average polymerization degree in relation to heartwood adjacent sapwood and sapwood.

In the middle part of the stem, regardless the degradation degree, cellulose polymerization degree in heartwood adjacent sapwood was higher in comparison to sapwood and heartwood. In IInd degradation degree samples the cellulose polymerization degree was higher than value obtained for other degradation degrees. For the Ist and IIIrd degradation degree cellulose polymerization degree in heartwood was higher in relation to sapwood, while in IInd degradation degree samples values for heartwood and sapwood were similar. It must be stated, that environmental pollution probably influenced the viscometric average polymerization degree of cellulose on the wood cross-section. Average polymerization degree of cellulose in sapwood from the top part of the stem was from 2% to 7% higher in relation to heartwood in case of Ist and IIIrd degradation degree. These values for heartwood and sapwood from IInd degradation degree stem were similar again.

Polymerization degree of cellulose in bark collected from the butt-end section of IIIrd degradation degree stems was 22% and 23% higher in comparison to the Ist and IInd degradation degree, correspondingly (Fig. 4). It shows that the environmental pollution probably caused the increase of cellulose viscometric average polymerization degree in bark.

CONCLUSIONS

Obtained results lead to following statements: (1) The environmental pollution which originate from the Nitrogen Industrial Plant "Kędzierzyn" could caused changes of late wood

participation. The distribution of cellulose on the cross- and longitudinal section of stems was also could be dependent on the environmental pollution. It also probably caused an increase of viscometric average polymerization degree of cellulose in heartwood in relation to heartwood adjacent sapwood and sapwood from butt-end section. (2) Regardless the degradation degree, cellulose polymerization degree in heartwood adjacent sapwood from the middle part of the stem was higher in comparison to sapwood and heartwood. Also in bark, cellulose polymerization degree probably increased as the result of the environmental pollution.

REFERENCES

1. Antczak, A., Radomski, A., Drożdżek, M., Zawadzki, J., Zielenkiewicz, T., 2016: Thermal ageing of cellulose with natural and synthetic antioxidants under various conditions. *Drewno* 59(196): 139-152.
2. Cindoruk, S.S., Sakin, A.E., Tasdemir, Y., 2020: Levels of persistent organic pollutants in pine tree components and ambient air. *Environmental Pollution* 256: 113418.
3. Dupont, A.L., Mortha, G., 2004: Comparative evaluation of size-exclusion chromatography and viscometry for the characterization of cellulose. *Journal of Chromatography A* 1026 (1-2): 129-141.
4. Fengel, D., Wegener, G., 1984: *Wood (chemistry, ultrastructure, reaction)*. Walter de Gruyter Press, Berlin, New York, 613 pp.
5. Funda, T., Fundová, I., Fries, A., Wu, H.X., 2020: Genetic improvement of the chemical composition of Scots pine (*Pinus sylvestris* L.) juvenile wood for bioenergy production. *GCB Bioenergy* 12(10): 848-863.
6. Harwood, V.D., 1971: Variation in carbohydrate analyses in relation to wood age in *Pinus radiata*. *Holzforschung* 25(3): 73-77.
7. Krutul, D., 1988: Content of cellulose and some of its properties analyzed on the cross- and longitudinal sections of oak trunk. *Folia Forestalia Polonica Series B - Wood Science* 18: 41-56.
8. Krutul, D., 1994: Variation in cellulose content in the stem of pine wood (*Pinus sylvestris* L.). *Annals of Warsaw University-SGGW. Forestry and Wood Technology* 45: 43-49.
9. Krutul, D., 2002: Exercises in wood chemistry and selected issues in organic chemistry. WULS-SGGW Press, Warsaw, Pp 125-127.
10. Krutul, D., Makowski, T., Hrols, J., 2006: Influence of heating power station on the chemical composition of wood, bark, branches and main roots of Scotch pine (*Pinus sylvestris* L.). *Annals of Warsaw University-SGGW. Forestry and Wood Technology* 59: 16-23.
11. Krutul, D., Drożdżek, M., Zielenkiewicz, T., Radomski, A., Zawadzki, J., Antczak, A., 2009: Distribution and some properties of cellulose in the stem of oak wood (*Quercus petraea* Liebl.). *Annals of Warsaw University-SGGW. Forestry and Wood Technology* 68: 436-443.
12. Matulewski, P., Buchwal, A., Makohonienko, M., 2019: Higher climatic sensitivity of Scots pine (*Pinus sylvestris* L.) subjected to tourist pressure on a hiking trail in the Brodnica Lakeland, NE Poland. *Dendrochronologia* 54: 78-86.
13. PN-55/D-04110, 1955: Physical and mechanical properties of wood. Study on the percentage of early and late wood.
14. Räisänen, T., Athanassiadis, D., 2013: Basic chemical composition of the biomass components of pine, spruce and birch. *Forest Refine*. Finnish Forest Research Institute, 3 pp.

15. Rowell, R.M., Pettersen, R., Han, J.S., Rowell, J.S., Tshabalala, M.A., 2005: Cell wall chemistry. In: Handbook of wood chemistry and wood composites (ed. Rowell R.M.). CRC Press. Boca Raton, Pp 35-74.
16. Saeman, J.F., Moore, W.E., Mitchell, R.L., Millet, M.A., 1954: Techniques for the determination of pulp constituents by quantitative paper chromatography. TAPPI 37: 336-343.
17. Sensuła, B., Wilczyński, S., Monin, L., Allan, M., Pazdur, A., Fagel, N., 2017: Variations of tree ring width and chemical composition of wood of pine growing in the area nearby chemical factories. Geochronometria 44(1): 226-239.
18. Sensuła, B., Wilczyński S., Opała, M., 2015: Tree growth and climate relationship: dynamics of Scots pine (*Pinus sylvestris* L.). Growing in the near-source region of the combined heat and power plant during the development of the pro-ecological strategy in Poland. Water Air Soil Pollution 226 (7): 220-236.
19. Uprichard, J.M., 1971: Cellulose and lignin content in chemical composition, density and tracheid length. Holzforschung 25(4): 97-105.
20. Waliszewska, B., Mleczyk, M., Zborowska, M., Goliński, P., Rutkowski, P., Szentner, K., 2019: Changes in the chemical composition and the structure of cellulose and lignin in elm wood exposed to various forms of arsenic. Cellulose 26(10): 6303-6315.
21. Waliszewska, B., Prączyński, W., Zborowska, M., Stachowiak-Wencek, A., Waliszewska, H., Spek-Dźwigąła, A., 2015: The diversification of chemical composition of pine wood depending on the tree age. Annals of Warsaw University-SGGW. Forestry and Wood Technology 91: 182-187.
22. Willför, S., Sundberg, A., Hemming, J., Holmbom, B., 2005: Polysaccharides in some industrially important softwood species. Wood Science and Technology 39(4): 245-57.
23. Zawadzki, J., Gawron, J., Antczak, A., Kłosińska, T., Radomski, A., 2016: The influence of heat treatment on the physico-chemical properties of pinewood (*Pinus sylvestris* L.). Drewno 59(196): 49-57.
24. Zawadzki, J., Radomski, A., Antczak, A., Drożdżek, M., 2006: The influence of cellulose determination methods on viscometric degree of polymerization. Annals of Warsaw University-SGGW. Forestry and Wood Technology 59: 405-409.

DONATA KRUTUL, ANDRZEJ RADOMSKI, ANDRZEJ ANTCAK*, MICHAŁ DROŹDŹEK,
TERESA KŁOSIŃSKA, DOMINIKA SZADKOWSKA, JANUSZ ZAWADZKI
WARSAW UNIVERSITY OF LIFE SCIENCES
INSTITUTE OF WOOD SCIENCES AND FURNITURE
NOWOURSYNOWSKA 159
02-776 WARSAW
POLAND

*Corresponding author: andrzej_antczak@sggw.edu.pl

PREPARATION THE ROSE-LIKE HYDROPHOBIC SURFACE OF WOOD BASED MATERIALS BY SOFT LITHOGRAPHY

ZEYU ZHANG, BINGRU SHAO, FAPENG WANG, JIUYIN PANG, LING SU
BEIHUA UNIVERSITY
CHINA

(RECEIVED JUNE 2020)

ABSTRACT

To prepare hydrophobic wood with rose-like hydrophobic surface and avoid moisture damage to wood. In this paper, With polyvinyl alcohol (PVA) as the elastic mold, the microstructure of the rose petals was replicated on the wood surfaces by soft lithography. The soft lithography technique was used to modify the wood sur-face, transferring over it a rose-like topography, based on a micro/nano hierarchical structure using fresh rose as the template. The surface of poplar coated with polystyrene was reconstructed twice using 1, 3, 5, 8 and 10% PVA as templates, respectively. The results show that the average contact angle of poplar surface coated with polystyrene is more than 130°, that of fresh rose surface is about 140°, and that of untreated wood is about 60°. Therefore, the wood surface with polystyrene has obtained a similar structure to that of rose surface and has a certain hydrophobicity. In addition, the microstructures observed by means of SEM, showing rough surface structures with micro-nanopapillate hills on wood surfaces. Water droplets could easily roll down on such wood surfaces, exhibiting super-hydrophobic and low adhesion properties. The successful fabrication of rose-like wood provided a new direction for researches on the super-hydrophobic of wood, which could effectively prevent the damage of moisture to wood.

KEYWORDS: Hydrophobic wood, polyvinyl alcohol, polystyrene, soft lithography, rose petals.

INTRODUCTION

The surface of wood contains a large number of hydrophilic groups and pore structures, which will cause decay, cracking, and mildew in a long-term humid environment (Liu et al. 2015, Liu and Wang 2016, Lahtela and Karki 2015). The preparation of a hydrophobic wood can effectively avoid the damage of water to the wood (Ma 2018, Liu and Cao 2018), thereby increasing the service life of wood. The water droplets are not completely spread out on a smooth and flat ideal uniform solid surface but at a certain angle, as shown in Fig. 1a (Wang 2018).

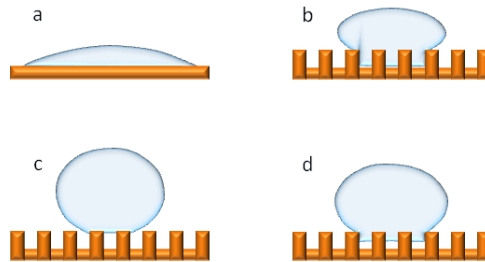


Fig. 1: The contact model of water drop on different rough surfaces.

But in fact, the surface has a certain roughness. The roughness affects the wettability of the material and determines the size of the contact angle. The wettability mainly depends on the surface energy and surface structure of the material (Wang et al. 2011, Jirous-Rajkovič et al. 2007, Kudela 2014). However, after hundreds of millions of years of evolution in nature, the special structure in the organism gives the living body a special function (Yang et al. 2016, Gao 2014), such as superhydrophobicity (Hou and Fang 2016, Wozniak et al. 2018), self-cleaning (Ma et al. 2013), hydrophilic (Wang et al. 2017a,b, Senarathna et al. 2020), low adhesion (Hou et al. 2019), etc. depending on the state of the water droplets on the superhydrophobic surface. The part where the droplet contacts the rough solid surface may be completely wetted, or it may contact the surface in a non-wetting mode with lower adhesion, or a transition state of the two, as shown in Figs. 1b-d. The rose surface is a surface with high adhesion and hydrophobicity (Ebert and Bhushan 2012). The petal surface has a dense micropapillary array with nano-folds. These regular micro-nano structures provide sufficient roughness for the hydrophobic effect (Zhang et al. 2018). According to the hydrophobic phenomenon existing in nature, it is bionic through chemical reagents to obtain a polymer film with multi-functional characteristics, which is covered on the surface of wood, so that the wood has a micro-nano surface with the same structure as rose petals, thus having the same as rose petal. The hydrophobic characteristics of the wood solve the defect of wood hydrophilicity, thus expanding the application range of wood.

Peng et al. (2013) adopted the template printing method, using fresh taro leaves as the mother board, so as to construct a structure with fine cavities on the surface, and then modified by dip coating method, and finally by poly-n-octadecylsiloxane. The modification and modification of the nanosheets proved that the experimental results obtained significantly improved the hydrophobic properties. Lee et al. (2004) used hot pressing method to press polystyrene into porous alumina and waited for cooling to remove the alumina template, thus obtaining a hydrophobic polystyrene surface. Zhao et al. (2019) used chemical vapor deposition to obtain a hydrophobic film, but the cost of this method is relatively high and cannot be widely used in production.

In this paper, the template printing method is used to prepare the micro-nano structure of the rose-like surface on the wood surface using polyvinyl alcohol and polystyrene (Feng and Dou 2015, Pu et al. 2010). PS itself can reduce the surface energy of the substance to achieve a better hydrophobic effect on the wood surface (Lin et al. 2013, Cheng et al. 2014). The results show that using water contact angle, chemical analysis and other analysis methods to determine

that the surface of the wood has the shape of a rose surface can effectively prevent moisture from entering the internal pores, thereby extending the service life of the wood and opening up new areas.

MATERIAL AND METHODS

Fresh rose petals, poplar specimens (purchased from Jilin City, Jilin Province, China), polyvinyl alcohol (PVA) reagents in different concentrations (the concentrations are 1, 3, 5, 8 and 10%), self-made polystyrene (PS) were used for the experiment. Vacuum drying box: DZ-1BC was used for obtain the negative form of rose petals. Scanning electron microscope (SEM) was used for detect the surface morphology of poplar. The contact angle meter was used to measure the contact angle of the wood surface; the Energy Spectrometer: X-MaxN was used for elemental analysis ;the electric heating constant temperature water bath was used to heat the reagent.

Preparation of polystyrene

Take modification of polyoxyethylene alkylphenol ether by succinic acid (OS) and sodium lauryl sulfate (SLS) and dissolve them in a three-necked bottle, then drop styrene to obtain emulsifier (PE). At the same time, the temperature of the water bath was controlled at 75°C, the PE that had already been prepared is added, and the potassium persulfate (APS) aqueous solution and Benzoyl peroxide (BPO) are added dropwise until the blue color disappeared, that is, PS emulsion is obtained.

Mass fractions of PVA configuration

The PVA powders of certain quality were separately taken into three bottles and placed in a water bath pot. The temperature was controlled between 88 and 95°C. The solution with 1, 3, 5, 8 and 10% mass fraction could be prepared by stirring until the PVA solution was clarified.

Poplar samples were prepared by PVA/PS on the surface of rose petals

First, trim the rose petals to a suitable size, and then stick them on the glass plate with milky glue, add the previously prepared PVA solution evenly on the surface of the rose flower, remove the air bubbles, and dry it in a vacuum drying oven at 60°C for about 2 hours (Fig.2) .

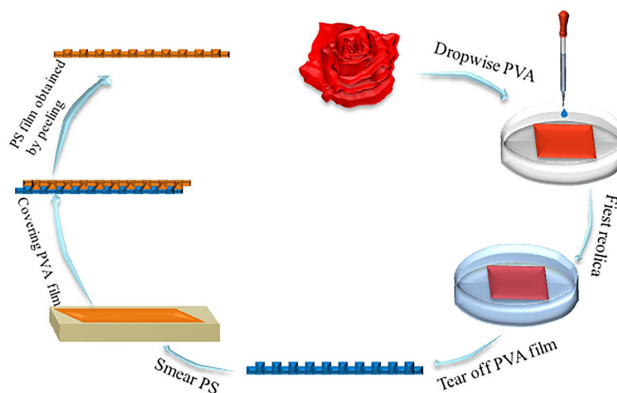


Fig. 2: The flow chart of the biomimetic preparation of rose structure surfaces.

Take out and gently tear off the PVA soft film to get the negative type of rose petals. Then, the prepared PS was evenly coated on the poplar veneer with a glass rod, and then the PVA soft film was pasted on the poplar sample under a certain pressure, and put it at room temperature for 12 hours, peel off the PVA soft film, that is to say. A positive shape of rose petals was obtained on the surface of the poplar. Finally, the contact angle of water droplets on the poplar surface was measured by the contact angle tester, and the surface morphology of poplar was detected by the scanning electron microscope.

In the experiment, PVA has good film-forming properties and the mechanical properties of the film are excellent. PVA is covered on the rose petals to make it form a film opposite to the micro-nano structure of rose petals. PS has good corrosion resistance, and its solution is white liquid. Coating polystyrene on wood can solve the problem of dyeing white wood.

Characterization of wood materials and treated wood surfaces

The surface morphology of wood material and treated wood was observed by scanning electron microscopy (SEM). The microscopic image of a sample was obtained by enlarging the observation at different locations. The wettability of wood and treated wood was measured by OCA20 contact angle meter (German Dataphysics) at room temperature. The average value of contact angle was calculated and the final contact angle was obtained.

RESULTS AND DISCUSSION

Morphology of water droplets on different sample surfaces

Fig. 3a is a macro photo of water droplets on the surface of rose petals. It can be clearly seen that the water droplets are in a spherical state on the surface of the rose flower, which can explain that the surface of the rose petals has extremely strong hydrophobic properties.

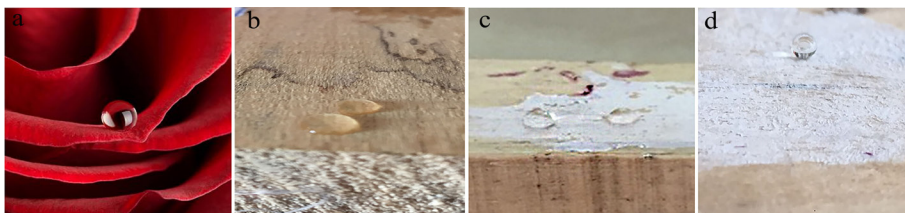


Fig. 3: Morphology of droplets on the surface of rose and wood specimen.

Fig. 3b is a macro picture of water beads on the wood surface. The water beads are obviously wetted on the wood surface, and the contact angle is about 15.7° , which fully reflects that the wood is a hydrophilic material with a large number of hydroxyl groups and its hydrophobic performance is poor. Fig. 3c is a macro photo of water beads on wood coated with polyvinyl alcohol (PVA). The water beads are infiltrated on the surface, and the contact angle is about 73.24° , showing strong hydrophilic properties. Fig. 3d is a picture of water drops on the surface of the bionic rose petals. The water drops are in a spherical state, and their contact angle is about 135.5° , which fully exhibits strong hydrophobic properties. It can be seen that after the wood is bionic, its contact angle has increased from 15.7° to 135.5° , indicating that the surface of the wood after bionics has hydrophobic properties similar to rose petals.

Effect of different concentration of PVA solution on contact angle

In Fig. 4a the contact angle of water droplets on the surface of wood material is only 15.7° , showing a hydrophilic state. In Fig. 4b the contact angle of water droplets on wood surface treated by template method with 1% PVA film as master plate is 121.5° . The hydrophobicity of water droplets is improved obviously, which shows that this method has certain effect on improving the hydrophobicity of wood surface. Figs. 4c-e show the contact angle of wood surface treated with the concentration of 3%, 5% and 8% of PVA film as water droplets. The contact angle shows a slow upward trend, but the difference is small, and the hydrophobic performance is relatively stable. Fig. 4f shows that the contact angle of the wood surface treated with 10% PVA as template is 135.5° . The water droplets are plump and round, showing super hydrophobicity and low adhesion, and the hydrophobicity is further improved. Fig. 4g shows that the contact angle of rose surface is 143.5° .

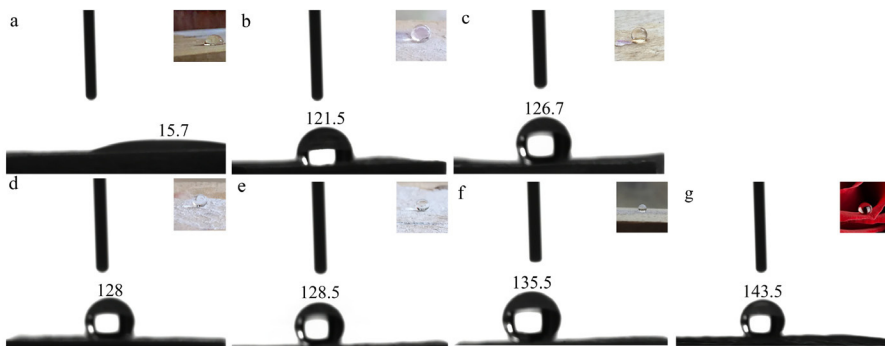


Fig. 4: Microscopic and macroscopic images of wood surface treated with water drops at different concentrations of PVA: (a) wood material surface, (b) 1% PVA film, (c) 3% PVA film, (d) 5% PVA film, (e) 8% PVA film, (f) 10% PVA film, (g) rose surface.

It is also obvious from Fig. 5 that the effectiveness of PVA addition, and with the increase of PVA concentration, the contact angle of PS-coated wood surface increases gradually, and the 10% PVA contact angle is closest to the rose surface, showing better hydrophobic effect.

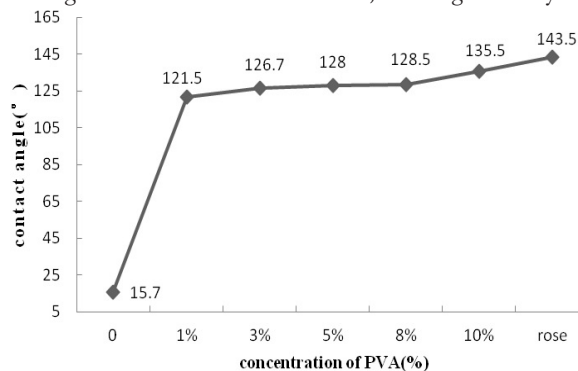


Fig. 5: Wood material, different concentrations of PVA film for the master treatment of wood and rose surface contact angle change trend.

It is proved that the template printing method using PVA as template has made the same kind on the wood surface coated with PS. The surface structure of rose has similar hydrophobic effect with that of rose. Effect of wood surface hydrophobization caused using soft lithography was also reported by Ebert and Bhushan (2012), and surfaces exhibiting the so-called “petal effect” (super hydrophobicity with high droplet adhesion). Results obtained indicated that the micro and nano structures on the surface of roses were prepared by ZnO nanoparticles. The results showed that different concentrations of nanoparticles had different contact angles of high and low adhesion states, which proved that the hydrophobic performance of the experimental results was significantly improved.

In Figs. 6a,b can be seen that there are many porous holes on the surface of wood. The cell wall is composed of microcrystals, microfibrils and fibrils. These microcrystals and microcrystals, microfibrils and microfibrils, fibrils and fibrils are connected with each other and form a microcapillary system. Their inner surface is huge, so they have strong water absorption. Fig. 6c is a micrograph of PVA film obtained by template printing for the first time. The surface of PVA film has regular micro-nanostructure, which is the reverse of rose surface. Fig. 6d is the result of secondary replica of the hydrophobic surface of rose-like wood. The surface is uneven, contrary to the PVA film, but it also has regular micro-nanostructure, which provides a certain roughness on the wood surface and improves the hydrophobic performance. However, compared with roses, the hydrophobicity of the surface similar to roses needs to be improved. This may be due to the partial relaxation of the applied stress in the PS film under a transient external load might also be responsible for some bit of smoothing of the replicated patterns.

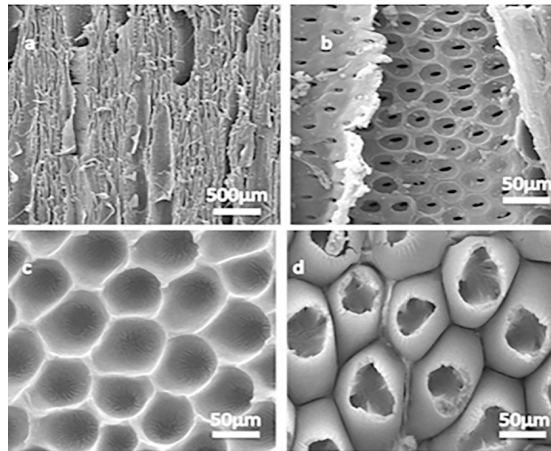


Fig. 6: SEM images of (a) and (b) wood surface, (c) PVA film, (d) a second replicated rose-like wood surface, (e) rose surface.

He et al. (2017) used soft printing technology to prepare the structural surface of similar Chinese rose on the surface of bamboo material. The bamboo material has relatively smooth surface microstructure, and the fiber texture is clearly visible. The bionic Chinese rose petal bamboo structure protruded outward, showing hemispherical shape, and arranged tightly with papillae of different sizes. The above evidence proves that biomimetic modification can improve the stability of bamboo, which also provides a reference for this paper.

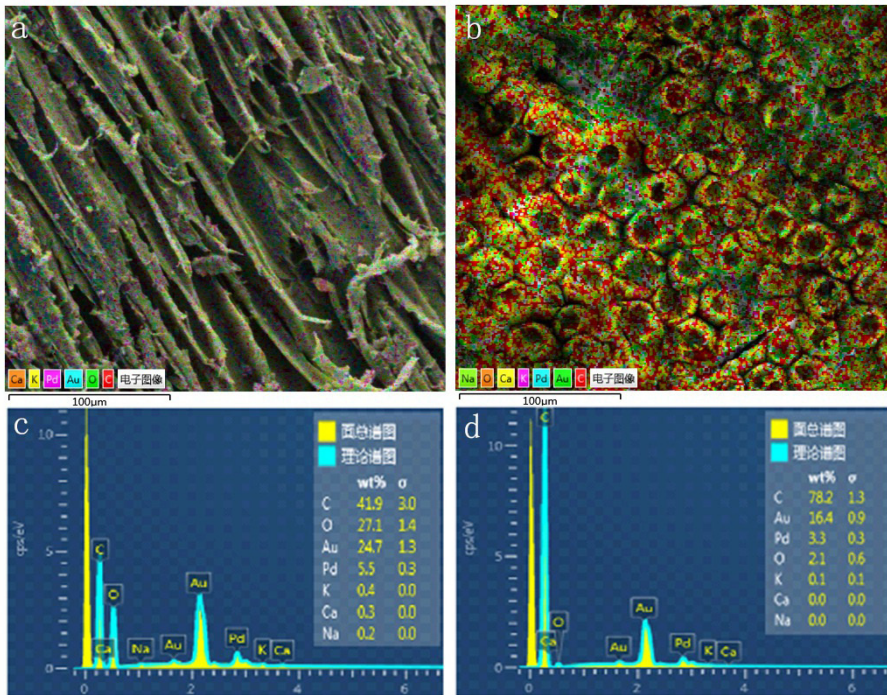


Fig. 7: The Energy dispersive spectrometer (EDS) spectrum of (a) wood surface, and (b) rose-like surface.

Figs. 7a,c are surface energy spectrum of wood. It can be seen that there are carbon, oxygen and a small amount of potassium, calcium and sodium on the surface of wood (gold and palladium come from coatings). The energy spectrum of the wood on the surface of rosette-like flowers in Figs. 7b,d show that there are only a large number of carbon and gold elements, a small amount of oxygen elements and no other elements, which indicates that the elements on the surface of rosette-like flowers come from wood and PS are not roses, confirming that the hydrophobic structure was effectively replicated on the rose-like wood surface.

CONCLUSIONS

Inspired by biology, this study successfully simulated the rough structure of rose surface on wood surface by template printing (soft printing technology) using rose as template and PVA of different concentration, which effectively prevented wood from damp damage. The study found that: (1) Two complex structures and their different surfaces can be observed by scanning electron microscopy (SEM). The first complex produces a structure opposite to that of a rose, while the second complex produces a rose-like structure on the surface of wood. (2) The water contact angle of the wood on the rose-like surface prepared by template printing is about 135.5° , very close to the contact angle of the rose surface. 1% PVA has very good hydrophobic effect. The contact angle of the wood surface is raised from 69° to 121.5° , and with the increase of PVA concentration, the contact angle is also increasing. The experimental results show

that 10% PVA has the best hydrophobic effect. Contact angle closest to rose surface. (3) EDS can prove that the elements of wood on the surface of rose-like flowers come from wood rather than roses. (4) The successful preparation of rose-like hydrophobic wood surface proves that the hydrophobic properties of wood surface and other hydrophilic materials can be achieved by nanotechnology, which provides a new research direction for hydrophobic modification. (5) This study not only deepens the understanding of the hydrophobic mechanism of plant leaves in nature, but also provides a new direction for the study of water resistance and anti-corrosion of wood surface. Successful preparation of biomimetic hydrophobic wood can prolong the service life of wood, and broaden the application fields and prospects of wood industry.

ACKNOWLEDGMENT

We would like to acknowledge support from the National Natural Science Foundation of China (31800480), and Project of Jilin Provincial Development and Reform Commission (2021C041-6).

REFERENCES

1. Cheng, X.L., Wang, S.T., Hong, B.S., Zhou, Q., 2014: Study on improving hygroscopicity of ammonium nitrate coated with polystyrene. *Adhesion* 35(04): 76-78+87.
2. Ebert, D., Bhushan, B., 2012: Wear-resistant rose petal-effect surfaces with superhydrophobicity and high droplet adhesion using hydrophobic and hydrophilic nanoparticles. *Journal of Colloid and Interface Science* 384(1): 182-188.
3. Feng, Y.Y., Dou, X.Q., 2015: Study on micro-nanostructure and antimicrobial adhesion of biomimetic rose petals. *Biotechnology World* 2: 181.
4. Gao, N., 2014: Construction and anti-fouling performance of stable bionic hydrophilic surface. Northwest University. Shan Xi, 90 pp.
5. He, X.W., Fu, S.Y., Dai, Y.P., Jin, C.D., Wang, F.P., 2017: Research on surface characteristics of bamboo with bionic super-hydrophobic Chinese rose/TiO₂. *World Bamboo and Rattan* 15(05): 11-15.
6. Hou, L.X., Fang, L., 2016: Progress in preparation and application of superhydrophobic surfaces. *Chemical Bulletin* 79(10): 897-904.
7. Hou, D., Li, T., Chen, X., He, S., Ren, Z.J., 2019: Hydrophobic nanostructured wood membrane for thermally efficient distillation. *Science Advances* 5(8): eaaw3203.
8. Jirouš-Rajkovič, V., Bogner, A., Mihulja, G., Vrsaljko, D., 2007: Coating adhesion and wettability of aged and preweathered fir wood and pine wood surfaces. *Wood Research* 52(2): 39-48.
9. Kudela, J., 2014: Wetting of wood surface by a liquids of a different polarity. *Wood Research* 59(1): 11-24.
10. Liu, M., Wu, Y.Q., Qing, Y., Tian, C.H., Jia, S.L., Rosa, Li, X.G., 2015: Advances in biomimetic superhydrophobic functional modification of wood. *Functional Materials* 46(14): 14012-14018.
11. Liu, F., Wang, C.Y., 2016: Biomimetic superhydrophobic functionalization of wood. *Science and Technology Report* 34(19): 389-396.
12. Lee, W., Jin, M.K., Yoo, W.C., Lee, J.K., 2004: Nano-structuring of a polymeric substrate with well-defined nanometer-scale topography and tailored surface wettability. *Langmuir* 20(18): 7665-7669.

13. Lin, G.Q., Li, P., Xiong, X.F., Lu, G.Q., Wang, X.H., Qiu, L.Z., 2013: Fabrication of high performance flexible thin film transistors by different surface modifications. *Journal of Luminescence* 34(10): 1392-1399.
14. Liu, Z., Cao, J.Z., 2018: Fabrication of superhydrophobic wood surface with a silica/silicone oil complex emulsion. *Wood Research* 63(2): 353-364.
15. Lahtela, V., Karki, T., 2015: Determination and comparison of some selected properties of modified wood. *Wood Research* 60(5): 763-772.
16. Ma, Y.Z., 2018: Preparation and multifunction of super-hydrophobic surface. *Contemporary Chemical Research* 8: 148-150.
17. Ma, R., Wei, Y., Guo, H., Yang, F., Qian, F., 2013: Preparation and characterization of a new bionic-recreation superhydrophobic surface. *Chinese Journal* 58(14): 1326.
18. Peng, P.P., Ke, Q., Zhou, G., Tang, T., 2013: Fabrication of microcavity-array superhydrophobic surfaces using an improved template method. *Journal of Colloid and Interface Science* 395: 326-328.
19. Pu, X., Ge, J.F., Chen, C.C., 2010: Research progress on biomimetic superhydrophobic surface with micro-nano hierarchical structure. *Guangdong Chemical Industry* 37(5): 25-28+40.
20. Senarathna, R.M.D.M., Wanniarachchi, W.K.I.L., Jayawardhana, S., 2020: Replication of the surface wettability of plant leaves with different surface morphologies using soft lithography. *International Journal of Nanoscience* 19(3): 1950018.
21. Wang, N., Zhao, Y., Jiang, L., 2011: Bioinspired multi-scale micro/nanostructured materials. *Journal of Chemistry of Colleges and Universities* 32(3): 421-428.
22. Wang, F.P., 2018: Biomimetic preparation of plant leaf micro-nano structure and its properties by bamboo surface deposition method. *Zhejiang A&F University*: Pp 8-11.
23. Wang, F.P., Li, S., Wang, L., 2017a: Fabrication of artificial super-hydrophobic lotus-leaf-like bamboo surfaces through soft lithography. *Colloids and Surfaces A: Physicochemical and Engineering Aspects* 513: 389-395.
24. Wang, F.P., Wang, L., Wu, H.P., Pang, J., Gu, D., Li, S., 2017b: A lotus-leaf-like SiO₂ superhydrophobic bamboo surface based on soft lithography. *Colloids and Surfaces A: Physicochemical and Engineering Aspects* 520: 834-840.
25. Wozniak, M., Ratajczak, I., Lis, B., Krystofiak, T., 2018: Hydrophobic properties of wood treated with propolis-silane formulations. *Wood Research* 63(3): 517-524.
26. Yang, W.L., Ji, X.B., Xu, J.L., 2016: Super hydrophilic surface from nature to bionics to practical application. *Chemical Progress* 28(6): 763-772.
27. Zhang, Y.W., Jingran, B., Wang, S.Q., Cao, Q.Q., Li, Y., Zhou, J.H., Zhu, B.W., 2018: Functional food packaging for reducing residual liquid food: thermo-resistant edible superhydrophobic coating from coffee and beeswax. *Journal of Colloid and Interface Science* S0021979718310762.
28. Zhao, Y., Song, B., Cui, X., Ren, Y., Yue, W., Wang, Y., 2019: High electrocatalytic reduction using ZnS micropolyhedron: Direct sulfuration of ZIF-8 film on conducting glass by chemical vapour deposition. *Materials Letters* 250: 193-196.

ZEYU ZHANG, BINGRU SHAO, FAPENG WANG, JIUYIN PANG*, LING SU*
BEIHUA UNIVERSITY
YIFU BUILDING, EAST CAMPUS OF NORTH CHINA UNIVERSITY
132013 JILIN
CHINA

*Corresponding authors: pangjiuyin@163.com and sulingling2007@163.com

ELIMINATION OF ADHESIVE IMPURITIES OF THE RECOVERED PAPER IN FLOTATION PROCESS

VLADIMÍR KUŇA, JOZEF BALBERČÁK, ŠTEFAN BOHÁČEK
PULP AND PAPER RESEARCH INSTITUTE
SLOVAKIA

VLADIMÍR IHNÁT
SLOVAK FOREST PRODUCTS RESEARCH INSTITUTE
SLOVAKIA

(RECEIVED MAY 2020)

ABSTRACT

The article presents results of the elimination of sticky impurities from recovered paper in laboratory flotation of three pulp suspensions with different whiteness, obtained directly from the production line before entering flotation. A combination of commercial agents releasing undesirable substances from recovered paper and means for regulation and stabilization of froth and modified micronized bentonit was used. In the flotation purification of pulp suspension with a whiteness of 53%, the combination of Prodeink Extra, Prodeink AS10 and Hydrocol OT reduced the macrostickies content by 58%, the ash content decreased from 18.5% to 4.5%, the whiteness increased from 53% to 56.4% and the residual color content was reduced from 385 ppm to 294 ppm. The pulp suspension with a whiteness of 64% showed a reduction in the content of macrostickies by 66%, a reduction in the ash content by 23.2%, an increase in whiteness by 1.4% and a reduction in the residual color content from 245 ppm to 194 ppm. The pulp suspension with a whiteness of 68.3% showed a decrease in the content of macrostickies by 58.1%, the ash content decreased from 35.7% to 6.3%, the whiteness increased by 1.1% and the content of residual color decreased from 157 ppm to 117 ppm.

KEYWORDS: Macrostickies, flotation, bentonit, whiteness, residual color, ash content, recovered paper, pulp suspension.

INTRODUCTION

New environmental challenges arise in paper industry in recent years and new solutions must be applied, as: retention systems (Kuřna et al. 2016, Mayr et al. 2017), decarbonization (Griffin 2018) and heat recovery systems (Pařitný et al. 2015, 2017), upgraded alkaline cooking processes (Balberćák et al. 2017, 2018), processing of wasted materials (Ihnát et al. 2020, Mařura et al. 2019), etc. The use of recycled fibers has been growing rapidly. Methods of their reuse are also developing (Russ et al. 2013) but they are difficult to put into practice.

In waste paper processing, handling processes of recycled fiber are more complex than the primary fiber processing because waste paper consists of a mixture of different types of fibers or types of paper. Another reason is the presence of pollutants and harmful substances that can contribute to the formation of sticky impurities (Pulz 2000). In order to meet the quality requirements, the pollutants must be removed. The term "purity" is commonly used with respect to optical, chemical, colloidal, microbiological and processing aspects (Holik 2000). Impurities and contaminants are gradually removed using various separation criteria, such as particle size, shape and deformability, density and surface properties of particles. Sequence of operations depends mainly on properties of the raw material and the required properties of the final product (Engstrand and Johansson 2009). In processing of recovered paper, there are two main ways of handling stickies: removal and/or elimination of stickies in the process of sorting, cleaning, flotation, and bleaching (Sarja et al. 2007, Kuřna et al. 2018) and prevention against deposit formation through dispersion, fixation and stickiness removal

Flotation

Flotation is one way of separating undesirable parts from waste paper. Numerous approaches which define usable flotation models are defined in the literature. *Mixed models* of the flotation process try to combine the ideas used in the so-called *chemical kinetic models* with *probabilistic models*. One generally accepted model describes the ability of a dye to float, as the change in a dye particle per unit time in a given volume. Such a change depends on the number of collisions between the particle and the bubble in a unit volume per unit time (represented by z_c , n_p , n_b , where z_c is the rate constant, and n_p and n_b are numbers of parts and bubbles), and on the already mentioned individual probabilities of interaction $P_{(C)}$, $P_{(A)}$, and $P_{(R)}$:

$$dn_p / dt = - z_c n_p n_b P_{(C)} P_{(A)} P_{(R)} \quad (-) \quad (1)$$

where: $P_{(C)}$ depends on particle and bubble size as well as on hydrodynamic conditions; $P_{(A)}$ depends on the ratio of colored particle and bubble size, hydrophobicity and contact time; and $P_{(R)}$ depends on particle weight, contact angle, consistency and flow hydrodynamics.

Efficiency of the flotation process is depended on the surface and colloidal chemistry of the system, as well as on the types of equipment used for air dispersion, mixing and foam separation.

Flotation in deinking process

In flotation, a large range of particles is distributed based on their surface properties (Amand 1997, Engstrand 2005). Flotation provides a high fiber yield but poor physical properties of the fiber due to the fines content of the fibers (Shammas 2010). During flotation, air is introduced into the low consistency pulp (0.8% -1.5%) and the hydrophobic particles

are brought to the top surface after connection to the air bubbles. The pigment-containing froth that has formed in the process is mechanically removed at the top of the flotation cell, by overflow or vacuum (Lassus 2000). As mentioned, flotation is based on the surface properties of the particles. It removes larger hydrophobic particles as opposed to washing, which removes hydrophilic particles.

Several partial surface chemical processes take place during flotation decolorization. The separation of the ink from the fibers, its agglomeration, flotation and foaming are the main steps. Re-bonding of the ink to the fiber is undesirable, but it occurs and is particularly a problem for water-based inks. Agglomeration of paint particles is necessary to achieve flotation because small particles do not bind to bubbles due to hydrodynamic forces. Ability of moving of the small particles is too low and these will follow the flow line around the bubble, while the larger particles collide with it and, under favorable conditions, interact and bond with each other. Collectors, often calcium fatty acid soaps, are used to achieve agglomeration and further improve the chemical interactions between the paint particles and the air bubbles (Engstrand 2005).

Theoretically, flotation should contribute to the efficient removal of micro stickies, due to their hydrophobicity, which facilitates the attachment of sticky particles to air bubbles in a manner similar to paint particles. In addition, unwanted particles are removed in the size range (10-100 μm) due to sorting (Engstrand 2005). Amount of 81% of the micro stickies are removed in the first flotation stage. Post-flotation is able to remove both macro and micro stickies (Lassus 2000, Delagoutte 2008).

Most micro stickies that have been introduced into the process in the sorting step after dispersion are removed in post-flotation (Delagoutte 2008). However, certain conditions during flotation may result in reduction of hydrophobicity of the adhesive particles, leading to lower separation efficiency. This may be due to the time dependence of the surface tension of the adhesive particles, which leads to a reduction of surface tension of the stickies after the addition of the chemicals used in the decolorization in the flotation stage. Another reason may be the adsorption of surfactants on the surface of stickies (Holik 2000). Poor removal of stickies in a favorable size range can also occur due to the disk structure of adherent particles that are not removed by air bubbles (Holik 2000).

MATERIAL AND METHODS

Three suspensions of pulp (VL5, VL1 and VL0) were prepared for combinations of three chemicals (Prodeink Extra, Prodeink AS10 a Hydrocol OT/Bentonit 4). Chemical charges ($\text{kg}\cdot\tau^{-1}$) are shown in Tabs. 1-3. Composition of recovered paper of the suspensions was: (1) VL5 suspension – 92.5% mix of newspapers and magazines + 7.5% broke from paper machine, (2) VL1 suspension – 13% mix of newspapers and magazines + 79.5% white office waste + 7.5% broke from paper machine, and (3) VL0 suspension – 2,5% mix of newspapers and magazines + 90% white office waste + 7,5% broke from paper machine. Two mixtures of surfactants and two types of bentonites were used for laboratory flotation as: (a) Prodeink Extra (Makokem d.o.o., Zagreb, Croatia) – a mixture of surfactants to release unwanted substances from the recovered paper, (b) Prodeink AS10 (Makokem d.o.o., Zagreb, Croatia) – a mixture of surfactants to control the froth during flotation, (c) Hydrocol OT (HOT) (Süd Chemie AG, Moosburg, Germany) – alkalinized micronized bentonit with an average particle size of 4 μm , and (d) Bentonit 4(B4) – alkalinized micronized bentonit with an average particle size of 6 μm .

Laboratory flotation

Laboratory flotation tests were performed in the flotation cell shown in Fig. 1, according to the procedure below. The basic suspensions, at a concentration of 1.2%, were homogenized by stirring for 1 min. Chemical 1 (Prodeink EXTRA) was added to the homogenized suspension. The sample was mixed and the chemical was allowed to act for 30 min. The required amount of chemical 2 (Prodeink AS10) was added. The sample was mixed again and the chemical was allowed to act for 10 min. The required amount of chemical 3 (Hydrocol OT) was added, after mixing the chemical was allowed to act for 10 min. A total of 2.6 liters of sample was taken and transferred to a flotation device. After starting the flotation device, in addition to mixing, the air supply was switched on. The amount of air was adjusted to bubble gently. The floated froth was removed continuously. After 10 min of flotation, both stirring and air supply were stopped. Laboratory sheets were made from the floated suspension, from which the required parameters were determined.

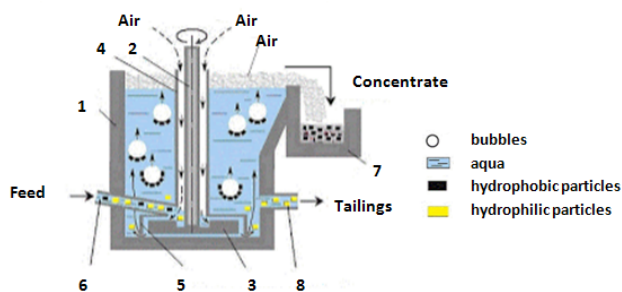


Fig. 1: Laboratory flotation machine (Petrovskaya 2007): (1) flotation machine, (2) support, (3) rotor, (4) air inlet, (5) stator, (6) feed inlet, (7) froth discharging area, (8) release of tailings.

Determination of stickies

For the determination of sticky impurities, a sample of 30 g was used, which was sorted in a laboratory sorter Sommerville on a 150 μm slice plate under constant rinsing. Sorting time was 20 min. The material captured on the sorting plate was quantitatively transferred using a Rapid-Kothen sheet-cutter to a filter paper of 220 mm diameter so that it is distributed evenly over its entire surface. Filter paper with the sorted substance was allowed to dry freely in the air. Sheets of sorted and dried material were placed between two clean filter sheets with a diameter of 220 mm. They were pressed in a press with heated plates at a temperature of 160°C and a pressure of 2.5 MPa for 4 min. After pressing and cooling, the sheets were separated from each other and impurities greater than 0.1 mm² are counted, which were compressed or bonded to the filter paper. Evaluation of the number of sticky impurities is given in pcs.kg⁻¹ substances.

Determination of ash content, whiteness and residual color in pulp suspensions

Whiteness and residual color were determined according to STN ISO 2470-1, ISO 3688, resp. Determination of ash content in pulp suspensions was performed according to ISO 1762.

RESULTS AND DISCUSSION

During laboratory tests of flotation cleaning of recovered paper we applied a combination of three types of chemicals in order to improve its paper forming properties. The agent for releasing undesirable substances from the recovered paper Prodeink Extra, the agent for agglomerating undesirable substances and improving the sorting efficiency of Hydrocol OT, bentonit B4 and the agent for regulating the froth during flotation Prodeink AS.

Laboratory tests were performed on three types of pulp suspensions: the suspension VL5 with whiteness of 53% prepared from dark types of recovered paper, the suspension VL1 with whiteness of 64% prepared from mix of dark and bright types of recovered paper and the suspension VL0 with whiteness of 68% prepared from bright types of recovered paper. In addition to determining the content of macrostickies, the ash content, whiteness and residual color in individual water bodies was determined as part of the evaluation of the quality of flotation procedures. The results of laboratory research, applications of flotation in the elimination of macrostickies, are presented in Tabs. 1-3 and in Figs. 2-5

Tab.1: The effect of flotation on the properties of VL5 suspension with whiteness 53%.

Sample	Pro Extra (kg.t ⁻¹)	Pro AS10 (kg.t ⁻¹)	Bentonit (kg.t ⁻¹)	Macrostickies (pc per kg)	Ash (%)	Whiteness ISO (%)	Residual color (ppm)
Primary*	0	0	0	450	18.5	53	385
F0	0	0	0	428	8.3	54.8	369
F1	2	0	0	412	5.1	55.2	351
F2	2	0.5	0	390	4.8	56	318
F3	2	1	0	316	4.6	56.1	306
F4	2	0.5	2	190	4.5	56.4	294
F5	1	0	0	420	5.6	54.8	369
F6	1	0.5	0	398	4.8	55.5	345
F7	1	1	0	326	4.6	56.3	307
F8	1	0.5	2	299	4.4	56	313
F9	1	0.5	4	230	4.6	56.5	287
F10	1	1	2	285	4.7	56.3	295
F11	1	1	4	224	5.2	55.8	321

* The sample without flotation.

Tab.2: The effect of flotation on the properties of VL1 suspension with whiteness 64%.

Sample	Pro Extra (kg.t ⁻¹)	Pro AS10 (kg.t ⁻¹)	Bentonit (kg.t ⁻¹)	Macrostickies (pcs per kg)	Ash(%)	Whiteness ISO (%)	Residual color (ppm)
Primary*	0	0	0	900	29.3	64.0	245
F0	1	0	0	860	7.9	64.1	242
F1	1	0.5	0	620	7.3	64.5	227
F2	1	1	0	550	6.9	64.6	225
F3	1	0.5	2HOT	445	6.1	64.6	223
F4	1	0.5	4HOT	500	6.2	65.3	225
F5	1	1	2HOT	305	6.1	65.2	194
F6	1	1	4HOT	319	6.2	65.2	197

F7	1	0.5	2B4	483	6.1	64.7	223
F8	1	0.5	4B4	480	6.4	64.7	224
F9	1	1	2B4	310	6.2	65.1	195
F10	1	1	4B4	318	6.3	65.0	198

* The sample without flotation.

Tab.3: The effect of flotation on the properties of VL0 suspension with whiteness 68.3%.

Sample	Pro Extra (kg.t ⁻¹)	Pro AS10 (kg.t ⁻¹)	Bentonit (kg.t ⁻¹)	Macrostickies (pcs per kg)	Ash (%)	Whiteness ISO (%)	Residual color (ppm)
Primary*	0	0	0	1230	35.7	68.3	157
F0	1	0	0	1180	8.5	68.5	153
F1	1	0.5	0	845	7.3	68.8	137
F2	1	1	0	720	6.9	69.0	132
F3	1	0.5	2HOT	680	6.3	69.3	127
F4	1	0.5	4HOT	680	6.2	69.3	130
F5	1	1	2HOT	520	6.3	69.5	117
F6	1	1	4HOT	515	6.3	69.4	117
F7	1	0.5	2B4	695	6.3	69.2	120
F8	1	0.5	4B4	680	6.4	69.2	121
F9	1	1	2B4	540	6.1	69.2	119
F10	1	1	4B4	530	6.2	69.2	120

* The sample without flotation.

The effect of flotation procedures on the content of macrostickies

The best results of the elimination of macrostickies on the VL5 suspension were obtained by the F4 flotation procedure (Tab. 1). By applying this procedure, the content of macrostickies was reduced from 450 to 190 pcs.kg⁻¹, which represents a decrease by 58%. For the VL1 suspension, the best results in the elimination of macrostickies were obtained by the F5 procedure (Tab. 2). With this combination of chemicals a reduction in the content of macrostickies by 66% (decrease from 900 pcs.kg⁻¹ to 305 pcs.kg⁻¹) was achieved. With the VL0 suspension, the best macrostickies elimination results were obtained with the F6 combination (Tab. 3). This combination of chemicals reduced the content of macrostickies by 58.1% (decrease from 1230 pcs.kg⁻¹ to 515 pcs.kg⁻¹). The results obtained are consistent with the results (Lassus 2000 and Delagoutte 2008), which achieved flotation efficiency of up to 81% in eliminating macrostickies.

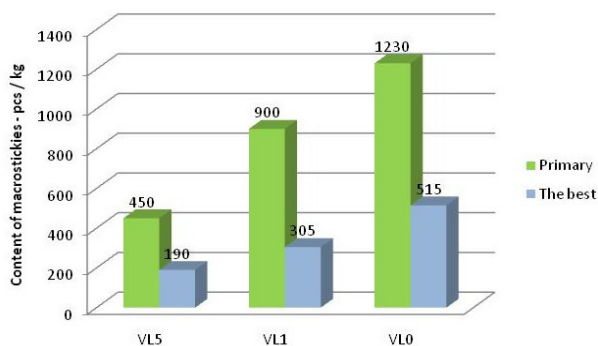


Fig. 2: The effect of flotation procedures on the content of macrostickies.

The effect of flotation procedures on whiteness

By applying the best working procedures for individual types of suspensions (Tabs. 1-3), an increase of whiteness by 3.4% was achieved for the VL5 suspension, by 1.3% for the VL1 suspension, and by 1.1% in the VL0 suspension, as stated and (Fig. 3). The optical properties (whiteness or yellowness) of recycled paper are the focus of several authors (Jurić et al. 2018, Tutuș et al. 2013). Bleaching agents are present in suspensions for this purpose.

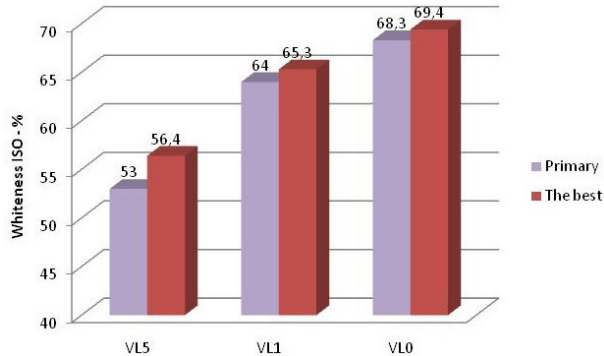


Fig. 3: Effect of flotation procedures on whiteness.

The effect of flotation procedures on ash content

The ash in pulp consists of several different components, which can be mineral substances from the wood raw material, metallic residues from pipes and machinery parts or residues from chemicals used in the pulping process. Often the ash content is related to the filler content (e.g. calcium carbonate, clay) in pulp (Kirilova and Lindberg 2012). The effect of flotation on ash content in the suspensions are shown in Fig. 4. Using the best working procedures according to Tabs.1-3, a reduction of the ash content was achieved for the VL5 suspension by 14.0%, for the VL1 suspension by 23.2%, and for the VL0 suspension by 29.4% (Fig. 4).

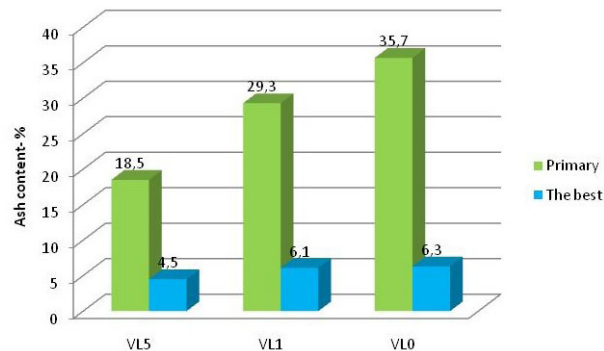


Fig. 4: The effect of flotation procedures on ash content.

The effect of flotation procedures on residual color content

The best working practices for individual suspensions (Tabs.1-3) allowed to reduce the residual color content from 385 ppm to 294 ppm for VL5 suspension, from 245 ppm to 194 ppm

for VL1 suspension and from 157 ppm to 117 ppm for VL0 suspension, as it is shown in (Fig. 5). According to some authors, it is possible to achieve up to 50% efficiency in flotation in reducing residual color (Xiansheng et al. 1998, Imamoglu et al. 2013).

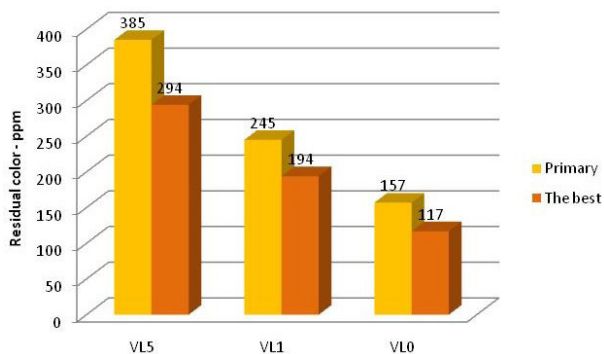


Fig. 5: The effect of flotation procedures on residual color content.

CONCLUSIONS

By a suitable combination of paper agents in the processing of recovered paper, it is possible to increase the efficiency of flotation while eliminating macrostickies. The combination of Prodeink Extra intended to improve the release of undesirable substances from recovered paper, Hydrocol OT intended for agglomeration of stickies and Prodeink AS10 intended for stabilization of flotation froth, a reduction of macrostickies contents in pulp suspensions VL5 by 58%, in VL1 by 66% and in VL0 by 58.1% was achieved. The application of suitable chemicals has increased the flotation efficiency in reducing the ash content, increasing the whiteness of pulp and reducing the residual color content, as well. Better quality of pulp suspension after flotation creates better conditions at its quality in a line of recovered paper processing which has a positive effect on paper production as a whole.

ACKNOWLEDGMENT

This work was supported by the Slovak Research and Development Agency under contract No. APVV-16-0409

REFERENCES

1. Amand, F.J.S., 1997: Hydrodynamics of flotation' experimental studies and theoretical analysis. TAPPI Recycling Symposium, TAPPI Press, Atlanta, GA, 219 pp.
2. Balbercak, J., Bohacek, S., Medo, P., Ihnat, V., Lubke, H., 2017: Chemical processing of waste wood based agglomerates Part I: Evaluation of properties of fluting liners made of semichemical pulp obtained by a mildly alkaline sulphur-free cooking process. Wood Research 62(5): 715-726.

3. Balbercak, J., Bohacek, S., Pazitny, A., Ihnat, V., Lubke, H., 2018: Chemical processing of waste wood based agglomerates part II: Evaluation of properties of fluting liners made of semichemical pulp obtained by an alkaline cooking process. *Wood Research* 63(1): 35-44.
4. Blanco, A., Miranda, R., Negro, C., Garcia-Suarez, C., Garcia-Prol, M., Sanchez, A., 2007: Full characterization of stickies in a newsprint mill: the need for a complementary approach. *Tappi Journal* 6(1):19-25.
5. Delagoutte, T., 2008: Stickies characterization along the deinking lines of the SCA tissue mills. Grenoble, 68 pp.
6. Engstrand, P., Johansson, B., 2009: Paper recycling. In: *Pulping Chemistry and Technology* (ed. Ek, M., Gellerstedt, G., Henriksson, G.), Walter de Gruyter, Berlin, Pp 391-427.
7. Griffin, P.W., Hammond, G.P., Norman, J.B., 2018: Industrial decarbonisation of the pulp and paper sector: A UK perspective. *Applied Thermal Engineering* 134: 152-162.
8. Holik, H., 2000: Unit operations and equipment in recycled fiber processing. In: *Recycled fiber and deinking* (ed. Götsching, L., Pakarinen, H.), Fapet Oy. Helsinki, Finland, Pp 91-201.
9. Ihnát, V., Lübke, H., Balberčák, J., Kuňa, V., 2020: Size reduction downcycling of waste wood. *Review. Wood Research* 65(2): 205-220.
10. Jurič, I., Novaković, D., Kašiković, N., Dedijer, S., Milić, N., Vasić, J., 2018: Influence of optical paper properties of recycled and non-recycled papers for digital printing on colour reproduction. In: *8th Conference on Information and Graphic Arts Technology, Slovenia, 7-8 June*, University of Ljubljana, Pp 207-213.
11. Kirilova, S., Lindberg, S., 2012: Sticky deposits in a tissue manufacturing process. Master of Science Thesis. Chalmers University of technology, Göteborg, 74 p.
12. Kuňa, V., Balberčák, J., Pažitný, A., Russ, A., Boháček, Š., 2018: Tackiness reducing of stickies surfaces by inorganic agents and organic polymers. *Wood Research* 63(6): 1013-1019.
13. Kuňa, V., Balberčák, Opálená, E., Pažitný, A., Russ, A., Schwartz, J., 2016: The effect of multi-component retention systems on the properties of the paper suspensions. *Wood Research* 61(5): 767-776.
14. Lassus, A., 2000: Recycled fiber and deinking. In: *Recycled fiber and deinking* (ed. Götsching, L., Pakarinen, H.). Pp 241-264, Fapet Oy. Helsinki, Finland.
15. Mayr, M., Eckhart, R., Winter, H., Bauer, W., 2017: A novel approach to determining the contribution of the fiber and fines fraction to the water retention value (WRV) of chemical and mechanical pulps. *Cellulose* 24: 3029-3036.
16. Mašura, V., Balberčák, J., Kuňa, V., Mikulášik, R., 2019: Reaction phases of the wood constituents' degradation during Kraft cooking of spruce chips. *Wood Research* 64(6): 975-985.
17. Petrovskaya, N., 2007: Fundamentals of the theory of flotation. Libro, 192 pp.
18. Pažitný, A., Boháček, Š., Medo, P., Balberčák, J., 2015: Application of innovative heat recovery unit in paper industry with potential utilization in wood-processing and furniture industry. *Wood Research* 60 (1): 101-112.
19. Pažitný, A., Boháček, Š., Medo, P., Balberčák, J., Schwartz, J., Kuňa, V., Ihnát, V., 2017: Possibilities of removing condensate from a heat recovery unit utilizable in paper industry. *Wood Research* 62 (2): 273-282.
20. Putz, J., 2000: Stickies in recycled fiber pulp. In: *Recycled fiber and deinking* (ed. Götsching, L., Pakarinen, H.), Fapet Oy. Helsinki, Finland, Pp 441-498.

21. Russ, A., Schwartz, J., Boháček, Š., Lübke, H., Ihnát, V., Pažitný, A., 2013: Reuse of old corrugated cardboard in constructional and thermal insulating boards. *Wood Research* 58(3): 505-510.
22. Shammas, N., Wang L.K., Selke, W.A., 2010: Completely closed water systems in paper mills. In: Volume 12. Flotation Technology (ed. Wang, L.K., Shammas, N.K., Selke, W.A., Aulenbach, D.B.), Humana Press. New York, Pp 401-427.
23. Sarja, T., 2007: Measurements, nature and removal of stickies from deinked pulp. Faculty of Technology of the University of Oulu, Finland, 82 pp.
24. Tutuş, A., Demir, N., Çiçekler, M., 2013: Evaluation of waste papers in producing newspaper. In: International Caucasian Forestry Symposium, Artvin, Turkey, 24-26 October. Pp 894-897, Artvin Coruh University.
25. Xiansheng, N, Miller, J.D., Yeboah, Y.D., 1998: The effect of ink types and printing processes on flotation deinking efficiency of wastepaper recycling. *Environmental Engineering and Policy* 1(1): 47-58.
26. Imamoglu, S., Karademir, A., Pesman, E., 2013: Effect of flotation deinking on the removal of main colors of oil-based inks from uncoated and coated office papers. *Bioresources* 8(1): 45-58.

VĽADIMÍR KUŇA*, JOZEF BALBERČÁK, ŠTEFAN BOHÁČEK
PULP AND PAPER RESEARCH INSTITUTE
DUBRAVSKA CESTA 14
84104 BRATISLAVA
SLOVAK REPUBLIC

*Corresponding author: kuna@vupc.sk

VĽADIMÍR IHNÁT
SLOVAK FOREST PRODUCTS RESEARCH INSTITUTE
DUBRAVSKA CESTA 14
84104 BRATISLAVA
SLOVAK REPUBLIC

MECHANICAL PROPERTIES OF POLISH-GROWN *PINUS SYLVESTRIS* L. STRUCTURAL SAWN TIMBER FROM THE BUTT, MIDDLE AND TOP LOGS

SŁAWOMIR KRZOSEK, MAREK GRZEŚKIEWICZ,
IZABELA BURAWSKA-KUPNIEWSKA, PIOTR MAŃKOWSKI
WARSAW UNIVERSITY OF LIFE SCIENCES – SGGW
POLAND

MAREK WIERUSZEWSKI
POZNAŃ UNIVERSITY OF LIFE SCIENCES
POLAND

(RECEIVED DECEMBER 2019)

ABSTRACT

The research consisted in testing Polish sawn timber dedicated for construction applications made of pines (*Pinus sylvestris* L.) that grew in the Silesian Forestry Region, taking into account three parts of the log: butt, middle and top. The boards had the same cross section, a nominal thickness of 40 mm and width of 138 mm, typical for Polish structural timber. The mean nominal length of the boards under research amounted to 3500 mm. Each set was composed of 70 boards. Before the tests, boards were dried in an industrial drier until reaching the moisture content of 12%, and they were planed on 4 sides. First of all, the sawn timber was graded into strength classes, and their dynamic modulus of elasticity (MOE_dyn) was tested with a non-destructive method, with the use of a portable MTG device. The next step consisted in a bending test with four points of support, according to the EN 408 standard, and with the use of the TiraTest 2300 machine, in order to determine the global modulus of elasticity (MOE_EN-408) and the static bending strength, also referred to as modulus of rupture (MOR). Finally, the average growth ring width was determined for each board (PN-D-94021), as well as wood density according to EN-408. The hereby paper presents the test results for all the tested sawn timber boards, taking into account the part of log that each board came from: butt, middle or top. The hereby paper presents the influence of density on the mechanical properties of wood, taking into account the location on the round timber. The analysis does not include the influence of the width of annual growth rings and the proportion of latewood on the wood properties under research.

KEYWORDS: MOE, MOR, pine sawn timber, butt, middle and top.

INTRODUCTION

In accordance with the requirements binding in the European Union, sawn timber dedicated to construction application has to be strength graded. There are two methods of strength grading of coniferous timber for construction applications: visual and machine-assisted strength grading. Strength grading based on visual inspection consists in examining every piece of timber carefully and classifying it within the appropriate strength class on the basis of visible defects of wood structure, shape and processing. As a result of strength grading based on visual inspection, the timber is classified into different grades. Most EU member state have their own, national standards for the visual strength grading of timber. The only common requirement that has to be fulfilled by the national standards of visual strength grading is that they have to comply with EN 14081-1.

Strength grading machines measure specific wood properties that can be verified in a non-destructive way and that are directly correlated with wood's bending strength. The higher the correlation between the property tested by the machine and the bending strength, the more reliable will be the results of strength grading performed by that machine. In Europe, many different kinds of devices were developed and introduced at an industrial scale, and have been described by many researchers (Glos 1982, Denzler et al. 2005, Krzosek 2005 and 2009, Karlsson 2009, Krzosek and Bacher 2011). Strength grading machines can be based on measuring the density and modulus of elasticity of the tested timber. The modulus of elasticity can be measured in bending (static modulus of elasticity) or with the use of ultrasounds or frequency of own vibrations (dynamic modulus of elasticity). The density of the tested timber can be determined with a stereometric method or with the use of X-rays (Bucur 2003).

Krzosek and Grzeškiewicz (2008) compared the results of visual and machine strength grading done for the same batch of timber with the use of MTG. As a result of the conducted tests, concluded that the use of the device causes a higher efficiency in better strength grades, comparing to the results of the visual strength grading method, with less pieces being rejected. Similar results have been obtained by Krzosek (2009), who tested a batch of pine timber (766 pieces). Comparative research was also conducted for the modulus of elasticity of pine timber from Lithuania (3006 x 90 x 35 mm). In this study, the result of static bending strength in four-point flexural test achieved with the use of a Metriguard device was slightly higher (modulus of elasticity in static bending 11323 MPa, dynamic modulus of elasticity 10351 MPa). Higher values of density of the wood under research went together with bigger differences between the MOE values obtained with different methods. The relation between MOR and MOE measured with different methods (MTG, using Metriguard machine by passing specimens flat-wise through it, flatwise bending test equipment Long Span) was similar (Mišeikyte et al. 2008, Baltrušaitis and Mišeikytė 2011).

A comparison of non-destructive and destructive tests of spruce (and oak) wood, with the use of the Fakopp ultrasound sensor, longitudinal vibration method and static bending test were presented by Oberhofnerová et al. (2016). The correlation between the modulus of elasticity determined with dynamic and static method in line with ČSN 49 0116 amounted to $R = 0.71$. The MOE determined with the dynamic method was by over 60% higher than the MOE determined with the static method.

Tests of spruce wood (35 x 70 x 2700 mm) were carried out by Posta (Posta et al. 2016). In this study, the values of dynamic modulus of elasticity determined with the use of Timber Grader MTG, Sylvatest and Fakopp, were compared to the values obtained with bending methods. The researchers obtained high coefficients of determination for the modulus of elasticity determined with Sylvatest and the modulus of elasticity obtained with the static method in bending

$R^2 = 0.94$. Similarly, the coefficient of determination obtained for the modulus of elasticity with the Fakopp device amounted to $R^2 = 0.95$, and for MTG $R^2 = 0.97$.

A comparison of properties of Douglas fir wood and spruce from forest lands and post-agricultural lands was presented by Zeidler for wood from the Czech Republic (Zeidler and Borůvka 2017). The density was similar (spruce $460 \text{ kg}\cdot\text{m}^{-3}$, Douglas fir $570 \text{ kg}\cdot\text{m}^{-3}$), spruce wood from permanent forest land had a slightly higher MOE than wood from forested agricultural land (7541 MPa / 7744 MPa), and the difference was higher for Douglas fir (9783 MPa / 8940 MPa). A comparative study of pine wood from forest and post-agricultural lands was conducted by Jelonek et al. (2009). For wood from a fresh coniferous stand growing in a forest area, the density of wood amounted to $452 \text{ kg}\cdot\text{m}^{-3}$, and in post-agricultural lands it amounted to $470 \text{ kg}\cdot\text{m}^{-3}$.

Another important matter is knowledge related to the usability of different kinds of logs (butt, middle and top) for the production of structural timber. Studies aimed at verifying the influence of log type on the mechanical properties of structural timber obtained from them were carried out in various countries. Glos et al. 1999, tested spruce wood from two different habitats in Bavaria. The timber was strength graded with a visual method and with a machine method, taking into account the place of origin of timber from different logs. The highest efficiency of the strength grade S13 (DIN 4074-1): 79%, was achieved for butt logs; while in case of middle logs the efficiency reached 40%. As a result of machine strength grading of the same timber batch, the efficiency of the MS13 class (DIN 4074-4) amounted to 81% for butt logs and 71% for middle logs.

In Austria, within the framework of the XXL-Wood project (Teischinger and Patzelt 2006), an extensive study of spruce was conducted, taking into account the origin of wood, the conditions of growth, the quality class and the type of logs (butt, middle, top) from which the tested timber was obtained. The timber obtained from the logs was strength graded with the machine method, the dynamic modulus of elasticity was determined by measuring the frequency of own vibrations, and afterwards, the modulus of elasticity in stretching, the average width of growth rings, density and fibre twist were tested. The test results permitted to conclude that the mechanical properties of wood remain stable up to the height of 12-15 m.

Stód et al. (2016) conducted research related to the determination of MOE and MOR for pine wood from Finnish forests. The tested wood from different regions, with quite diverse density between $474 \text{ kg}\cdot\text{m}^{-3}$ and $546 \text{ kg}\cdot\text{m}^{-3}$, and mechanical properties: MOR (42.7 MPa, 65.8 MPa), MOE (11.4 GPa, 14.9 GPa). Moreover, they tested the properties of wood from the first and second thinning, as well as the final logging, and also the influence of the log part (butt, middle or top) on the properties of timber acquired from them. The results of that research revealed most of the timber that was classified within the highest resistance grades (C30 and C35) was acquired during the 2nd thinning. For structural timber obtained from the final logging, it turned out that there is no statistically significant difference between the main density of timber obtained from middle and top logs. The MOR of timber obtained from butt, middle and top logs amounted to, respectively: 56.1 MPa, 39.7 MPa and 36.4 MPa; and the MOE values: 13.5 GPa, 11.7 GPa and 10.2 GPa.

Ranta-Maunus et al. (2009, 2011) prepared extensive reports from research conducted on timber from Europe and Russia. The timber was tested using non-destructive methods, with the use of various devices that are used in Europe (GoldenEye 706, Escan, MTG, Combiscan, Triomatic) and also with a destructive method, in line with EN 408. This research did not take into account the type of log that timber was obtained from. According to the report, non-destructive methods used to determine the modulus of elasticity tend to give higher values than the modulus of elasticity determined with the destructive method.

MATERIAL AND METHODS

Material

The material investigated within the research described in the hereby paper originated from the Silesian Region. The timber was obtained from a mixed, young forest located in the Regional National Forest Directorate of Katowice (Nadleśnictwo Olesno, Leśnictwo Sternalice department 14d, geographical coordinates: 50.898629, 18.423915). The boards used in the research came from three types of logs: butt, middle and top.

Tree trunks were cut into 3 logs, each 3.5 m long: first, 1 m adjacent to the ground was cut off to remove the root deformations. Later, the butt log was obtained. A section for small samples, 0.5 m long, was cut between the butt log and the middle log. Later, the middle log was cut. The top log was obtained as follows: the diameter of $d = 14$ cm was found in the top part of the trunk (diameter on the thinner end, according to PN 93-D-02002) and 3.5 m were measured from that point (Fig.1).

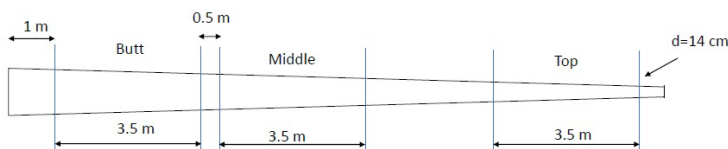


Fig. 1: Diagram presenting divisions of the trunk into logs.

Subsequently, 70 board pieces were sawn from each kind of logs (butt, middle and top). The boards were dried in an industrial drier until reaching the moisture content of ca. 12%, and then they were planed on four sides. The nominal cross sections of the boards had the dimensions 40 x 138 mm, and the length of 3500 mm.

Methods

The moisture content of wood, before testing its mechanical properties, was determined with the help of a resistance moisture meter Tanel, model HIT5, with measurement precision of 0.1%. During the moisture content measurements, the nominal density of pine wood as well as the temperature of the air-conditioned room, where the tests took place, were both taken into account. The density of each board was determined with the stereometric method.

The dynamic modulus of elasticity of individual boards (MOE_dyn) and their strength grade C, were specified with the help of a Mobile Timber Grader (MTG) by the Brookhuis MicroElectronics Company (Brookhuis Applied Technologies, Enschede, The Netherlands). In case of boards with low modulus of elasticity and high amount of defects, the MTG rejected such piece of timber. In case of roughly cut board ends, the MTG device displayed the error message, informing that the strength grading (determination of modulus of elasticity and strength grade C) for this piece of wood was not possible.

The global modulus of elasticity (MOE_EN-408) and modulus of rupture (MOR) were determined during a bending test with four points of support, using a universal testing machine - the TIRA Test 2300, in line with the EN 408 standard Timber structures – Structural timber and glued laminated timber – Determination of some physical and mechanical properties. The crosshead speed in the test amounted to $3 \text{ mm}\cdot\text{min}^{-1}$. The degree of bending of the boards was measured with an inductive sensor of the Novotechnik company, type TRS 75,

with the precision of 0.01 mm. During the test, the value of the bending strength and the degree of bending were recorded.

To determine the significance of differences between the average values, the t-Student (with a confidence level of 0.95) Statistica v.13.3 software was used.

RESULTS AND DISCUSSION

The results of moisture content and density tests for the structural timber sawn from butt, middle and top logs, have been presented in Tab. 1. If we assume an average density of boards sawn from butt logs at the level of $592 \text{ kg}\cdot\text{m}^{-3}$ to be 100%, then the average density of boards from middle logs would amount to 92%, and from top logs: 85% of the reference density. The differences in density between timber from different kinds of logs are statistically significant. The average density value for all timber pieces amounted to $547 \text{ kg}\cdot\text{m}^{-3}$, and moisture content to 11.6%.

Tab. 1: Characteristics of the tested structural timber (boards). Moisture content (MC), density, strength class (from C18 to C40) graded with the help of an MTG device.

	Boards cut from		
	butt logs	middle logs	top logs
Number of boards	70	70	70
Average MC (%)	12.4	11.3	11.0
SD (%)	1	1	1
COV (%)	9	12	11
Average density ($\text{kg}\cdot\text{m}^{-3}$)	592	545	503
SD ($\text{kg}\cdot\text{m}^{-3}$)	55	52	43
COV	9	10	9
Number of boards C18 class	2	4	9
Number of boards C24 class	2	21	40
Number of boards C30 class	18	23	17
Number of boards C35 class	28	16	3
Number of boards C40 class	16	5	0
Reject	1	1	1
Error	3	0	0
Average density in failure zone ($\text{kg}\cdot\text{m}^{-3}$)	583	527	483
SD ($\text{kg}\cdot\text{m}^{-3}$)	65	60	45
COV	11	11	9
Width of annual rings (mm)	1.7	1.8	1.9

The density differences between boards sawn from different kinds of logs (butt, middle and top) translate into different shares of the highest quality grades (C40 and C35) in each of the three timber groups. The number of timber pieces classified in the grades C40 or C35 for butt, middle and top log timber groups, amounted to, respectively: 44, 21 and 3 pieces. In case of the lowest quality grade - C18 - the number of timber pieces in each of the groups (butt, middle and top logs) amounted to 2, 4 and 9, respectively. A lower density, and as a result, lower values of other mechanical properties of wood from the top logs, can be caused by a lower share

of heartwood in this section of wood, and also by the presence of juvenile wood.

Three pieces from the butt log group could not be strength graded, because the non-destructive strength grading device displayed the ERROR message. Visual inspection of those pieces revealed strongly twisted fibres in two of them, exceeding the permitted value for the lowest strength grade according to the visual strength grading method. The third board had a low modulus of elasticity during bending.

As a consequence of the significant differences in density of boards sawn from butt, middle and top logs, the wood elasticity moduli determined with the non-destructive MOE_dyn and destructive MOE_EN-408 methods were very diverse. The differences were statistically significant. If we assume that the average value of MOE_dyn at the level of 15039 MPa for butt logs corresponds to 100%, then the MOE_dyn of boards from middle logs would amount to 86%, and top logs, 76%. In case of the global modulus of elasticity MOE_EN-408, butt logs had a modulus of elasticity of 13740 MPa, which would correspond to 100%, while for middle and top logs it amounted to 85% and 75% of the reference modulus, respectively. All of the tested log groups (butt, middle and top) had higher values of MOE_dyn than MOE_EN-408 (Fig. 2).

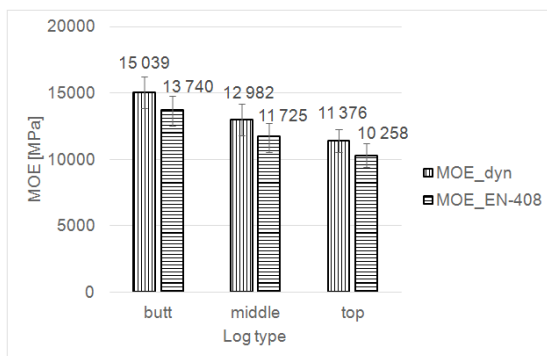


Fig. 2: Modulus of elasticity of boards made of butt, middle and top logs determined using the Mobile Timber Grader (MOE_dyn) and according to EN 408 (MOE_EN-408).

In case of all the three sets of timber under research, the ratio between MOE_dyn and MOE_EN-408 was similar, around 1.1. Therefore, the values of MOE_dyn were by about 10% higher than the values of MOE_EN-408 for the tested timber sets. The correlation between those two moduli (Fig. 3) is very high (coefficient of determination R^2 between 0.84 and 0.89), and it has the highest value for butt logs - $R^2=0.89$. A similarly high correlation $R = 0.92$ ($R^2 = 0.85$) was quoted by Krzosek (2009) in his research.

Correlations between the dynamic and static moduli of elasticity for small control samples of pine wood without defects were also specified by Rautkari et al. (2014). They obtained coefficient of determination values at the level of 0.80. The dynamic and static moduli of elasticity for pine sapwood, whose density amounted to ca. $490 \text{ kg}\cdot\text{m}^{-3}$, were 17.0 GPa and 16.3 GPa, respectively. These results of modulus of elasticity were much higher due to the fact that the wood under research had no defects. Polish-grown pine timber for construction applications, originating from five different forestry regions, was tested by Krzosek et al. (2008) and Krzosek (2009).

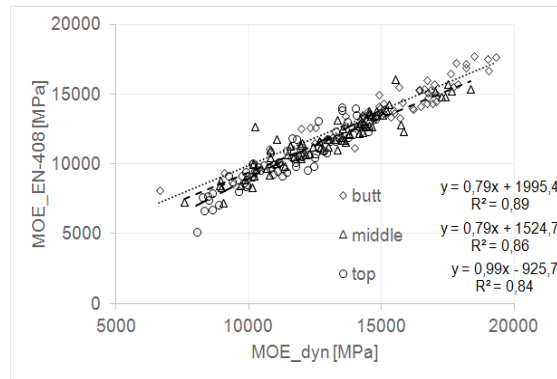


Fig. 3: Correlations between the modulus of elasticity of boards made of butt, middle and top logs determined using the Mobile Timber Grader (MOE_{dyn}) and according to EN 408 (MOE_{EN-408}).

His research revealed that wood from the regions of Pomerania and Kujawy-Pomerania had an average density of $525 \text{ kg}\cdot\text{m}^{-3}$ and $522 \text{ kg}\cdot\text{m}^{-3}$ - similarly to the density of wood from middle logs, while the values of global modulus of elasticity during bending, that is MOE_{EN-408} , amounted to 11183 MPa and 11683 MPa, and were similar to the modulus of elasticity values for middle logs. Moreover, we can find data about Polish-grown pine timber in the work of Stapel et al. (2014). Timber with the density of $515 \text{ kg}\cdot\text{m}^{-3}$, has a bending strength at the level of 39.0 MPa and MOE_{dyn} : 12500 MPa. The wood density values determined with the stereometric method near the failure zone of a piece of timber during the destructive test were lower than for the entire board. This phenomenon results from the lack of knots in small samples. The growth ring width (annual growth) in butt, middle and top logs was quite similar and amounted to 1.7 mm, 1.8 mm and 1.9 mm, respectively (Tab. 1). The performed tests revealed a high correlation between the values of global modulus of elasticity (MOE_{EN-408}) and density ($R^2 = 0.55$) for all the timber pieces under research from the groups of butt, middle and top logs (Fig. 4).

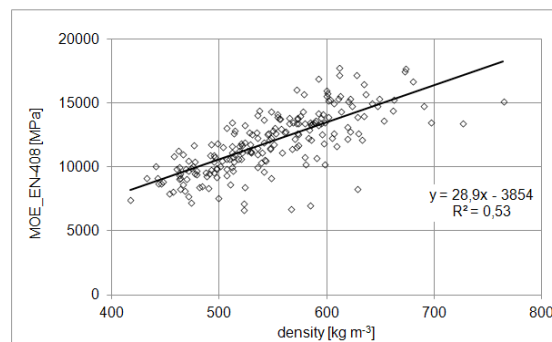


Fig. 4: Correlations between the global modulus of elasticity and density of all boards made of butt, middle and top logs determined according to EN 408 (MOE_{EN-408}).

The analysis of correlations of the global modulus of elasticity and density of individual groups of timber (from butt, middle and top logs) revealed weaker correlations (Fig. 5)

($R^2 = 0.36$; $R^2 = 0.42$; $R^2 = 0.30$, for timber cut from butt, middle and top logs, respectively). Higher correlations in similar kind of research (not taking into account the location of wood within the trunk) were obtained for pine wood $R^2 = 0.72$ (Baltrušaitis and Mišeikytė 2011).

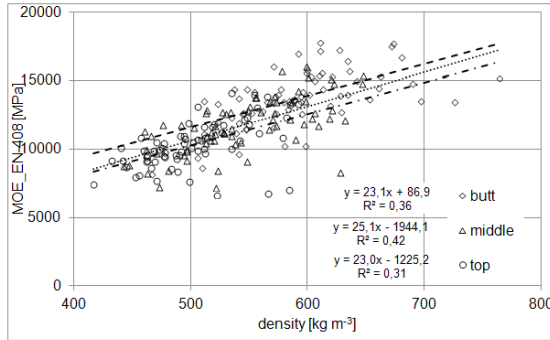


Fig. 5: Correlations between the global modulus of elasticity and density of separate board sets made of butt, middle and top logs, determined according to EN 408 (MOE_EN-408).

The analysis of results of the timber bending strength test (MOR) for timber sets made of butt, middle and top logs (Fig. 6) show that the highest average value was obtained for butt logs (61 MPa). If we assume that this value corresponds to 100%, then the resistance of timber made of middle logs would amount to 69%, and top logs only 61% of the strength measured for boards cut from butt logs. The differences between the average values calculated for each of the timber groups are statistically significant, according to the t Student programme. A comparison of these strength values with the differences observed for the global modulus of elasticity during bending, we can see that they are higher in case of the bending strength..

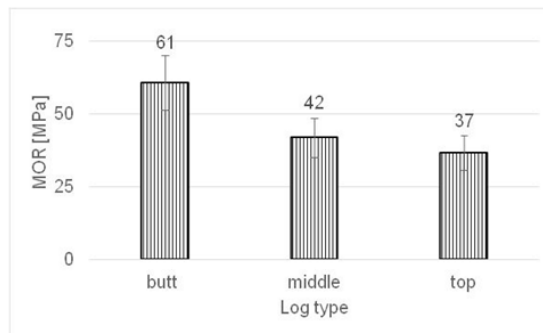


Fig. 6: Modulus of rupture (MOR) for boards made of butt, middle and top logs determined according to EN 408.

Polish-grown pine timber for construction applications, originating from the forestry regions of Pomerania and Kujawy-Pomerania was studied by Krzosek et al. (2008); and the obtained results of average density were 525 kg·m⁻³ and 522 kg·m⁻³, similar to the density of middle logs; MOR values received by them amounted to 42 MPa and 45 MPa, which also indicates

mechanical properties similar to the value for middle logs. The results obtained for a larger set of pine timber obtained from five different Polish forestry regions (Krzosek 2009), were as follows: average timber density $510 \text{ kg}\cdot\text{m}^{-3}$ and average bending strength 36 MPa .

The results of tests described in the hereby paper indicate a lower correlation between the modulus of rupture (MOR) and wood density (Fig. 7) for all the structural timber pieces made of butt, middle and top logs (coefficient of determination, $R^2 = 0.23$) than for the modulus of elasticity during bending (MOE_EN_408)

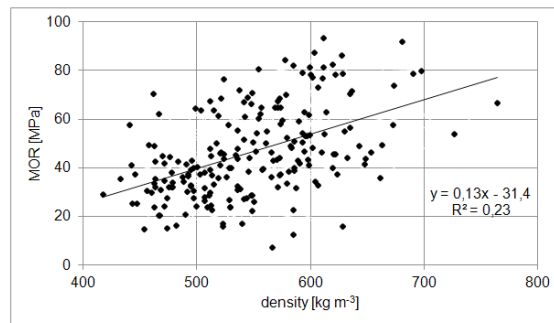


Fig. 7: Correlations between MOR and density for all tested boards made of butt, middle and top logs, determined according to EN 408.

For individual sets of structural timber made of butt, middle and top logs, MOR - density correlations are weaker and the coefficients of determination amount to $R^2 = 0.15$; $R^2 = 0.02$ and $R^2 = 0.01$, respectively. The highest correlation between MOR and density was determined for butt logs (Fig. 8).

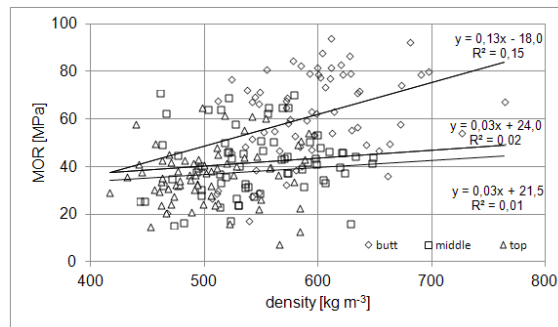


Fig. 8: Correlations between MOR and density of separate board sets made of butt, middle and top logs, determined according to EN 408.

CONCLUSIONS

(1) The MOE_dyn, MOE_EN-408, and MOR for pine timber acquired from butt logs are higher than those for middle and top logs. We observed greater differences between the timber made of top and butt logs in case of MOR than MOE_dyn and MOE_EN-408. (2) MOE_dyn was by 10% higher than MOE_EN-408 for all the groups of timber: butt, middle and top. (3) The correlations between the global modulus of elasticity (MOE_EN-408) and wood density are stronger than the correlations between bending strength (MOR) and density. The above is true for all the sets of timber: butt, middle and top.

ACKNOWLEDGMENTS

The authors are grateful for the support of the National Centre for Research and Development, Poland, under "Environment, agriculture and forestry" – BIOSTRATEG strategic R&D programme, agreement No BIOSTRATEG3/344303/14/NCBR/2018.

REFERENCES

1. Baltrušaitis, A., Mišeikytė, S., 2011: Strength and stiffness properties of the Lithuanian grown Scots pine (*Pinus Sylvestris* L.): Non-destructive testing methods vs. static. Wood Research 56(2): 157-168.
2. Bucur, V., 2003: Nondestructive characterization and imaging of wood. Springer Berlin, 214 pp.
3. DIN 4074-1, 2008: Strength grading of wood - part 1: Coniferous sawn timber.
4. DIN 4074-4, 2008. Strength grading of wood - Part 4: Certificate of suitability for devices supporting visual grading of sawn timber.
5. Denzler, J.K., Diebold, R., Glos, P., 2005: Machine strength grading – commercially used grading machines – current developments. Proceedings of the 14th International Symposium on Nondestructive Testing of Wood. University of Applied Science, Eberswalde, May 2-4, Pp 11- 16.
6. EN 338, 2004: Structural timber. Strength classes.
7. Glos, P., 1982: Die maschinelle Sortierung von Schnittholz. Stand der Technik – Vergleich der Verfahren. Holz-Zentralblatt 13: 153-155.
8. Glos, P., Diebold, R., Schleifer, A., 2000: Höherwertige Nutzung von Bauholz aus einheimischen Laub- und Nadelhölzern durch maschinelle Sortierverfahren. Institut Für Holzforschung, München, Abschlußbericht 98511, 195 pp.
9. Glos, P., Henrici, D., Lederem, B., 1999: Verbesserung der Wettbewerbsfähigkeit der Sägeindustrie durch Erhöhung der Schnittholzqualität. Bericht Nr. 96507. Institut für Holzforschung der Universität München. 85 pp.
10. Jelonek, T., Pazdrowski, W., Tomczak, A., 2009: Właściwości drewna sosny zwyczajnej (*Pinus silvestris* L.) na gruntach porolnych w północnej Polsce (Selected properties of wood in Scots pine (*Pinus silvestris* L.) growing on post-agricultural land in northern Poland). Leśne Prace Badawcze (Forest Research Papers) 70(3): 277-286.
11. Karlsson, M., 2009: Maschinelle Festigkeitssortierung mit dem Precigrader. Internationale Kongress der Säge und Holzindustrie. 16 – 17 Februar, Rosenheim, Pp 290-296.

12. Krzosek, S., 1995: Maszynowe sortowanie tarcicy w Niemczech. (Strength grading of sawn timber in Germany) *Przemysł Drzewny* 2: 10-12.
13. Krzosek, S., 2009: Wytrzymałościowe sortowanie polskiej sosnowej tarcicy konstrukcyjnej różnymi metodami. (Strength grading of Polish structural pine timber with various methods). Wydawnictwo SGGW, Warszawa, 127 p.
14. Krzosek, S, Bacher, M., 2011: Aktueller Stand der maschinellen Festigkeitssortierung von Schnittholz in Polen und in Europa. *Annals of Warsaw University of Life Science – SGGW. Forestry and Wood Technology* 74: 254-259.
15. Krzosek, S., Grześkiewicz, M., 2008: Strength grading Polish-grown *Pinus Sylvestris* L. structural timber using Timber Grader MTG and Visual method. *Annals of Warsaw University of Life Science – SGGW. Forestry and Wood Technology* 66: 26–31.
16. Krzosek, S., Grześkiewicz, M., Bacher, M., 2008: Mechanical properties of Polish-grown *Pinus silvestris* L. structural sawn timber. Conference COST E53, 29-30 October, Delft, The Netherlands, Pp. 253-260.
17. Mišeikyte, S., Baltrušaitis, A., Kudakas, L., 2008: Strength and stiffness properties of the Lithuanian grown Scots pine (*Pinus sylvestris*): Comparison of various testing methods. Proceedings of the 4th meeting of the Nordic Baltic network in wood material science and engineering (WSE), Latvian State Institute of Wood Chemistry, Pp 101-107 .
18. Noskowiak, A., 2017: Mechaniczne właściwości świerkowej tarcicy konstrukcyjnej pochodzącej z wybranych krain przyrodniczo-leśnych Polski. (Mechanical properties of spruce structural timber from selected Polish forestry regions. PhD thesis (in Polish). Warszawa, 110 pp.
19. Oberhofnerová, E., Arnetová, K., Holeček, T., Borůvka, V. Bomba, J., 2016: Determination of correlation between destructive and nondestructive methods applied on modified wood exposed to natural weathering test. *BioResources* 11(2): 5155-5168.
20. PN-D-94021, 2013: Structural sawn timber visual strength grade.
21. PN-EN 408: 2010 + A1, 2012: Timber structures. Structural timber and glued laminated timber. Determination of some physical and mechanical properties.
22. PN 93/D-02002, 1993: Surowiec drzewny – Podział, terminologia i symbole (Round wood. Classification, terminology and symbols).
23. Pošta, J., Ptáček, P., Jára, R., Terebesyová, M., Kuklík, P., Dolejš, J., 2016: Correlations and differences between methods for non-destructive evaluation of timber elements. *Wood Research* 61(1): 129-140.
24. Ranta-Maunus, A., 2009: Strength of European timber. Part 1. Analysis of growth areas based on existing test results. VTT Publications 706, 174 pp.
25. Ranta-Maunus, A., Denzler, J.K., Stapel, D., 2011: Strength of European timber. Part 2. Properties of spruce and pine tested in Gradewood project. VTT Working Papers 179, 67 pp.
26. Rautkari, L., Honkanen, J., Hill, C.A.S., Ridley-Ellis, D., Hughes, M., 2014: Mechanical and physical properties of thermally modified Scots pine wood in high pressure reactor under saturated steam at 120, 150 and 180. *European Journal of Wood and Wood Product* 72: 33–41.
27. Stapel, P., van de Kuilen, J.-W. G., 2014: Efficiency of visual strength grading of timber with respect to origin, species, cross section, and grading rules: A critical evaluation of the common standards. *Holzforschung* 68(2): 203–216.
28. Stod, R., Verkasalo, E., Heinonen, J., 2016: Quality and bending properties of sawn timber from commercial thinnings of Scots pine (*Pinus sylvestris* L.). *Baltic Forestry* 22 (1): 148-162.

29. Teischinger, A., Patzelt, M., 2006: XXL-Wood. Materialkenngrößen als Grundlage für innovative Verarbeitungstechnologien und Produkte zur wirtschaftlichen nachhaltigen Nutzung der Österreichischen Nadelstarkholzreserven. Universität für Bodenkultur Wien. Berichte aus Energie- und Umweltforschung 27/2006, 137 pp.
30. Zeidler, A., Boruvka, V., Schönfelder, O., 2018: Comparison of wood quality of Douglas fir and spruce from afforested agricultural land and permanent forest land in the Czech Republic. Forests 9(1): 13.

SŁAWOMIR KRZOSEK, MAREK GRZEŚKIEWICZ*,
IZABELA BURAWSKA-KUPNIEWSKA, PIOTR MAŃKOWSKI
WARSAW UNIVERSITY OF LIFE SCIENCES – SGGW
INSTITUTE OF WOOD SCIENCES AND FURNITURE
159 NOWOURSYNOWSKA
02-776 WARSAW
POLAND

*Corresponding author: marek_grzeskiewicz@sggw.edu.pl

MAREK WIERUSZEWSKI
POZNAŃ UNIVERSITY OF LIFE SCIENCES
FACULTY OF FORESTRY AND WOOD TECHNOLOGY
38/42 WOJSKA POLSKIEGO
60-637 POZNAŃ
POLAND

CHANGES IN GROSS CALORIFIC VALUE OF THERMALLY TREATED SCOTS PINE (*PINUS SYLVESTRIS* L.) AND SESSILE OAK (*QUERCUS PETRAEA* L.) WOOD AND THEIR EXPLANATION USING FTIR SPECTROSCOPY

EMÍLIA ORÉMUSOVÁ, EVA VÝBOHOVÁ
TECHNICAL UNIVERSITY IN ZVOLEN
SLOVAKIA

(RECEIVED MAY 2020)

ABSTRACT

Scots pine (*Pinus sylvestris* L.) and Sessile oak (*Quercus petraea* L.) wood were thermally treated in an oven at the temperatures of 160°C, and 200°C under atmospheric pressure in the presence of air for 3 and 9 hrs. The mass loss and gross calorific value were determined. Non-treated wood samples achieved a gross calorific value of 22 193 J·g⁻¹ for pine wood and 19 277 J·g⁻¹ for oak wood. Whereas the calorific value of pine wood with increasing severity of treatment decreased, in the case of oak it increased. The mass loss increased with increasing treatment severity by both wood species. Mentioned differences in pine and oak wood behaviour using ATR-FTIR spectroscopy were explained. In the case of pine wood with increasing temperature and time of exposure a decrease of resin acids was observed. This may be contributed to decrease in GCV. In the case of oak wood, mainly at temperature of 200°C the degradation of hemicelluloses was observed that results in relative increasing in the lignin content with followed increase in the GCV.

KEYWORDS: Gross calorific value, mass loss, pine, oak, thermal treatment, FTIR.

INTRODUCTION

Thermal treatment is a very effective way of improving the most important properties of wood. As a result of thermally induced chemical changes in the macromolecular constituents, the physical and biological properties of the wood are altered. Its ability to absorb water will be greatly reduced therefore it is particularly suitable for the production of wooden items that are used in humid environments. Moreover, its dimensional stability and the resistance to microbiological attack will be enhanced. Thermally treated wood does not need any coating or chemical preservatives. During treatment it becomes discolored to darker shades similar

to tropical woods. Thanks to its improved properties it is increasingly used in a wide variety of areas (Hill 2006, Výboňová et al. 2018, Kúdela and Andor 2018, Esteves and Pereira 2009, Candelier 2016, Cademartori 2015, Dzurenda 2018, Dubey et al. 2012, Martinka et al. 2013). Various thermal treatment processes have been used on the present, which differences in the process conditions (temperature, duration, open or closed system, oxygen or nitrogen atmosphere, wet or dry process, use of oils, etc.) (Militz 2002, Bazyar 2012).

The heat treatment causes chemical changes in the wood. The changes due to heating depend on the duration and temperature of the treatment. Hemicelluloses are the most thermally labile of the wood polymeric components. At the beginning of treatment their depolymerization occurs whereby oligosaccharides and monosaccharides are formed. During their degradation methanol, acetic acid and various volatile heterocyclic compounds are produced. Because the presence of acetyl groups is a significant factor in the thermal degradation of hemicelluloses, hardwoods are less thermally stable than softwoods. Cellulose degradation occurs at a higher temperature than degradation of hemicelluloses, and begins in its amorphous regions. First, its degree of polymerization decreases, and subsequently carbonyl and carboxylic groups due to oxidation of the cellulosic -OH groups are produced. The degradation of polysaccharides results in an increase in the lignin content (Výboňová et al. 2018, Čabalová et al. 2018). It is generally accepted that lignin is the most thermally stable component of the cell wall. Nevertheless, some degradation of lignin can occur at relatively low temperatures. The cleavage of β -O-4 linkages and a decrease in methoxyl content leads to auto-condensation of lignin to a more condensed structure (Hill 2006, Esteves and Pereira 2009, Wikberg and Maunu 2004, Chen et al. 2012, Brebu and Vasile 2010). As regards extractives, the most volatile compounds leave the wood, while others are degraded. Nevertheless, some authors (Výboňová et al. 2018, Esteves et al. 2011, Wang et al. 2015, Severo 2016) found, that the content of extractives due to heating increased. That can be caused by the release of degradation products of lignin and saccharides in the extraction mixture, or by their condensation reactions with the extractives originally present in untreated wood.

Gross calorific value (GCV) is the absolute value of the specific energy combustion, in joules for unit mass of a solid fuel burned in oxygen in a calorimetric bomb under specified conditions. It can be defined as the total heat liberated by the complete combustion of the fuel. GCV assumes that the water of combustion is entirely condensed. Value of GCV depends on the chemical composition of materials (Dietenberger and Hasburgh 2016). GCV is an important characteristic not only from energetic but also fire protection and safety (Majlingová et al. 2019). Based on this value, the net calorific value is calculated, which serves as a parameter to calculate the fire loading when planning the fire protection of buildings.

The content of wood components and their elemental composition play an important role for its calorific value. Lignin is richer in carbon and hydrogen than polysaccharides. Because these elements produce heat by burning, the calorific value of lignin is higher than of carbohydrates that are richer in oxygen. Moreover, in hardwood lignins is due to higher amount of methoxyl groups higher oxygen content than that in softwood lignins, therefore their calorific values are lower (Hill 2006, Fengel and Wegener 1984, Hon and Shiraishi 2001, Santos et al. 2012). Although the extractives are a minor component of wood, they raise its calorific values. Out of all wood constituents, for extractives have been determined the highest GCV values (Dietenberger and Hasburgh 2016). Inorganic elements present in wood play also certain role. These elements will remain after burning as ash, whose content in wood ranges between 0.08 to 2.30%. High content of inorganic elements in the fuel generally reduces its calorific value (Telmo and Lousada 2011, Dzurenda and Pňakovič 2016, Dzurenda et al. 2013).

Several authors (Kúdela and Andor 2018, Čabalová et al. 2018, Wang et al. 2015, Andor and Lagaña 2018, Bubeníková et al. 2018, Esteves et al. 2013, Barčík et al. 2015, Percin et al. 2016) studied the effect of thermal treatment on color, biological resistance, chemical and mechanical properties of wood. However, it can be assumed that changes in the ratio of main wood components caused by heating affected also the calorific value of thermally treated wood. Nevertheless, these features of thermally treated wood have seldom been studied.

In our research effect of thermal treatment under various process conditions (temperature and time) on the gross calorific value of treated wood was studied. Softwood and hardwood, Scots pine (*Pinus sylvestris* L.) and Sessile oak (*Quercus petraea* L.), were examined. Both wood species are an important raw material in building and wood processing industry (Klement et al. 2010). GCV using oxygen bomb calorimeter was determined. Chemical changes in wood due to thermal treatment using Fourier transform infrared (FTIR) spectroscopy were studied.

MATERIAL AND METHODS

Materials

In the experiments the samples of softwood (*Pinus sylvestris* L.) and hardwood (*Quercus petraea* L.) were used. Both trees were logged from altitude of 300 m above sea level, in Kremenny Jarok locality in the Slovak Republic. The timber logging activities were performed in summer period. The average stand age was 110 years. The stem breast height diameter of the Scots pine was of 36 cm, timber moisture content of 30%. The stem breast height diameter of the Sessile oak was of 45 cm and timber moisture content of 30%, too. For Scots pine $654 \text{ kg}\cdot\text{m}^{-3}$ and for Sessile oak wood $695 \text{ kg}\cdot\text{m}^{-3}$ density at 0% moisture content was determined.

The samples were cut from the core part of the stem in longitudinal sections to dimensions of $10 \times 1 \times 2$ cm and oven dried at temperature of $103 \pm 2^\circ\text{C}$ until the weight of the samples was not stabilized and they reached 0% moisture content. Further, the samples were modified by the thermal treatment in the oven (Memmert UFP 500) at atmospheric pressure in the presence of air at temperatures of 160°C and 200°C for 3 hours and 9 hours. The treated samples were placed in a desiccator to eliminate the effect of moisture. Introduction of the test samples is shown in Tab. 1 and in Fig. 1.

Tab. 1: Data on the test samples.

Tree species	Latin name	Identifications of the sample	Thermal treatment
		P	no thermal treatment
Scots pine	<i>Pinus sylvestris</i> L.	P160/3	160°C , 3 hrs.
		P160/9	160°C , 9 hrs.
		P200/3	200°C , 3 hrs.
		P200/9	200°C , 9 hrs.
		O	no thermal treatment
Sessile oak	<i>Quercus petraea</i> L.	O160/3	160°C , 3 hrs.
		O160/9	160°C , 9 hrs.
		O200/3	200°C , 3 hrs.
		O200/9	200°C , 9 hrs.



Fig. 1: Samples of Scots pine (*Pinus sylvestris* L.) and Sessile oak (*Quercus petraea* L.) wood before and after thermal treatment.

In the research, we first investigated the difference in weight of pine and oak samples after thermal treatment at temperatures of 160 and 200°C, taking into consideration the duration of thermal treatment (3 and 9 hrs). The mass loss was determined gravimetrically on the basis of the sample weights before and after the thermal treatment.

The gross calorific value was determined using a fully automatic calorimeter IKA C 5000 control (IKA-WERKE GMBH) under adiabatic conditions, in a setting without titration. Calculations correspond to the applicable standards ISO 1928 for gross calorific value determination.

The principle of the determination of the GCV consists of the complete combustion of the sample in oxygen at a pressure of 3 MPa in a calorimetric pressure vessel, in measuring the temperature rise in the calorimetric vessel and the determination of heat corrections. The weight of the samples was about 0.80 g. The samples were tested at 0% moisture content. From each set of samples, the GCV was determined by min 3 measurements. The GCV values for pre-defined samples moisture content of 8% were calculated according to the ISO 1928 standard.

Fourier transform-infrared (FTIR) spectra of the wood samples were recorded using the Nicolet iS10 FTIR spectrometer equipped with Smart iTR attenuated total reflectance (ATR) sampling accessory with diamond crystal (Thermo Fisher Scientific, Madison, WI, USA). Wood samples were disintegrated into sawdust and the average samples were analyzed. Spectra were measured in the wavenumber range from 4000 to 650 cm^{-1} . A resolution of 4 cm^{-1} and 32 scans per sample were used. Measurements were performed on four replicates per sample and average spectra were created and evaluated. The OMNIC 8.0 software (Thermo Fisher Scientific, Madison, WI, USA) was used to evaluate the spectra.

RESULTS AND DISCUSSION

Mass loss

When wood is modified by thermal treatment, there is a significant change in the color of the wood, in the chemical composition of wood and also mass loss. The change in mass loss is one of the most important features in the thermal treatment of wood, and is commonly referred to as an indicator of quality (Esteves and Pereira 2009). The results of mass loss due to sample thermal treatment are shown in Fig. 2. From the Fig. 2, we can see substantial changes in mass loss of samples. In both species, the mass loss increased with increasing temperature and thermal treatment duration, although

at temperature of 160°C the mass loss was higher for Scots pine wood, while at temperature of 200°C the mass loss was higher for Sessile oak wood regardless of the treatment duration. Different behaviour of Scots pine and Sessile oak wood is caused by different chemical composition of investigated wood species. Scots pine wood is characterized by a high proportion of volatile extractives, which are largely released from wood at a lower thermal treatment temperature (Ekeberg 2006, Traoré 2018).

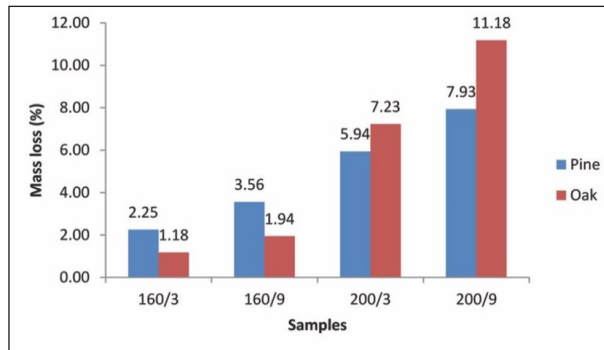


Fig. 2: Mass loss of samples after thermal treatment.

Another significant factor is the different content and composition of hemicelluloses in Scots pine and Sessile oak wood. In comparison to Scots pine, Sessile oak wood contains higher proportion of hemicelluloses, higher proportion of pentosanes and more acetyl groups in hemicellulose polysaccharides. At a temperature near 200°C, glycosidic linkages are ruptured as well as some C-C bonds of pyranose rings (Fengel and Wegener 1984). Also Výbohá et al. (2018) found that the degradation of hardwood hemicelluloses is more pronounced at 200°C than at 160°C. That is why we observed higher mass loss at temperature 200°C in the case of Sessile oak wood compared to Scots pine wood.

The mass loss during the thermal treatment depends on the wood species, biotope, the temperature and the duration of the thermal treatment (Luptáková and Kačík 2018). However, it is sometimes difficult to compare data published by different authors, as individual experiments often differ in thermal treatment conditions. In the literature (Gonzalez-Pena and Curling 2009) there are published changes in Scots pine wood during thermal modification at temperatures ranging from 190°C to 245°C using different exposure duration, i.e. 0.33 hour, 1 hour, 4 hours, 8 hours and 16 hours. In the case of Scots pine wood, the mass loss was of 0.6% (exposure duration of 0.33 hour) and 4.5% (exposure duration of 16 hours) at temperature of 190°C. At temperature of 245°C, it ranged between 5.6% (exposure duration of 0.33 hour) and 21.5% (exposure of 16 hours). The authors conclude that the mass loss of wood is more affected by the temperature of exposure than the duration of exposure and wood species. Mazela et al. (2003) treated Scots pine wood at temperatures of 160°C, 190°C, and 220°C during 6 hours and 24 hours in both air and water vapor. They found that in both environments the mass loss was similar when exposed to thermal treatment for 6 hours. But when exposed to thermal treatment for 24 hours, the mass loss was higher in air, especially at treatment temperatures of 190°C and 220°C.

Gross calorific value

The GCV values of the test samples of thermally treated Scots pine wood and Sessile oak wood compared to the non-treated samples are shown in Fig. 3. The results of the determination of the GCV show different values between the non-treated samples of both wood species as well as the effect of duration and temperature of the thermal treatment. Higher GCV value was obtained for non-treated sample of Scots pine wood compared to Sessile oak wood. The difference between these values was of $2916 \text{ J}\cdot\text{g}^{-1}$ and it was caused by a different chemical composition of investigated wood species. It was found that energy content of different wood components varied depending on its elemental composition (Dietenberger and Hasburgh 2016, Geffertová 2009, Tillman 1978, White 1986). Lignin that is rich in carbon and hydrogen has a gross calorific value about $23.2 - 27.4 \text{ MJ}\cdot\text{kg}^{-1}$. For holocellulose that has higher oxygen content the GCV in the range $17.5 - 18.8 \text{ MJ}\cdot\text{kg}^{-1}$ was found. The highest GCV values (about $32 - 37 \text{ MJ}\cdot\text{kg}^{-1}$) were found in extractives. In general, hardwoods contain more hemicelluloses than softwoods but less lignin (Baeza and Freer 2001). Therefore the GCV of Sessile oak wood might be lower than Scots pine wood. In addition, Scots pine wood is characterized by a high resin content, which also increases its GCV. Other authors reported GCV values for Sessile oak of $19685 \text{ J}\cdot\text{g}^{-1}$ and Scots pine of $22360 \text{ J}\cdot\text{g}^{-1}$ (Nosek and Holubčík 2016, Alakangas 2005).

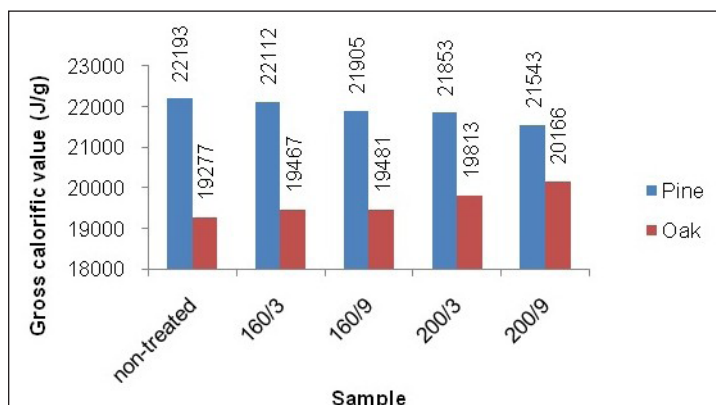


Fig. 3: Gross calorific value of Scots pine and Sessile oak wood.

Changes in GCV of Scots pine and Sessile oak wood caused by thermal treatment have an opposite trend. During the thermal treatment of the Scots pine wood a downward trend in GCV values with increasing temperature and treatment duration was observed. For sample P160/3, the GCV decreased by 0.35%, for sample P160/9 by 1.30%, for sample P200/3 by 1.53%, and for sample P200/9 by 2.93%, compared to non-treated Scots pine sample. On other hand, the GCV values increase with increasing temperature and thermal treatment duration in the case of Sessile oak wood. The GCV increase by 0.95% for sample O160/3, by 1.06% for sample O160/9, by 2.78% for sample O200/3 and by 4.61% for sample O200/9, compared to non-treated Sessile oak wood.

The GCV values shown in Fig. 3 were determined at 0% moisture content. We chose these conditions to make the results comparable to each other and not to be affected by the moisture content factor. This is the worst scenario in terms of fire protection. In general, the GCV values decrease with increasing moisture content. In practice, each wood product has a certain moisture

content, which also applies to thermo-wood, but in the case of thermally treated wood, there can be found the decrease in its equilibrium moisture content and consequently also decrease in its swelling and drying. Compared to non-treated wood, thermally treated wood absorbs significantly less moisture in the form of water vapor. The hygroscopic equilibrium moisture of thermally treated wood is about 30-50% lower than any of other wood, including impregnated wood. At a temperature of about 20°C, when the relative humidity of the air is about 60-70%, the equilibrium moisture content of the thermally treated wood is about 6-7%. If the air relative humidity rises to 80%, the equilibrium wood moisture content is about 8%. Thus, the moisture content of thermally treated wood is about 6-8% (Reinprecht and Vidholdová 2011). Tab. 2 shows the values of gross calorific value calculated to 8% moisture content.

Tab. 2 Resulting GCV at 8 % moisture content.

Sample	Gross calorific value (J·g ⁻¹)
P	20 418 ± 80.21
P160/3	20 344 ± 93.83
P160/9	20 153 ± 46.20
P200/3	20 105 ± 85.54
P200/9	19 820 ± 73.65
O	17 735 ± 42.57
O160/3	17 910 ± 52.72
O160/9	17 928 ± 18.66
O200/3	18 228 ± 91.10
O200/9	18 553 ± 28.38

It is known that chemical composition of wood varied due to its thermal treatment. In our experiments chemical changes using ATR-FTIR spectroscopy were studied (see Fig. 4 and Fig. 5).

In the Scots pine wood spectra, a decrease in the intensity of the typical absorption band for resin acids at 1693 cm⁻¹ can be observed with increasing temperature and treatment duration. Also, a decrease in peak intensity in the range of 3000-2800 cm⁻¹, which is attributed to the stretch vibrations of -CH in the -CH₂ and -CH₃ groups, may also be caused by the release of resin acids from wood. Many authors (Ekeberg 2006, Traoré 2018) found that resin acids are notable components in pine wood extractives. Furthermore, at the temperature of 200°C and treatment time 9 h the decrease in intensity of characteristic peaks for aromatic skeletal vibrations at wavenumber 1510 cm⁻¹ can be observed. This might be caused by degradation of lignin and aromatic extractives. Although lignin is considered to be the most thermally stable component of wood, some thermal degradation of lignin can occur at relatively low temperatures (Hill 2006, Brebu and Vasile 2010). From aromatic extractives pine wood contains mainly phenolic compounds, which cause darkening of wood in the light and have been implicated in the decay resistance of pine wood and also stilbenes, especially pinosylvin (Fengel and Wegener 1984, Ekeberg et al. 2006). The decomposition of extractives due to thermal treatment contributes to the mass loss. Because extractives have a highest GCV values from all wood components, their decomposition and release from wood decreases the calorific value of thermally treated wood

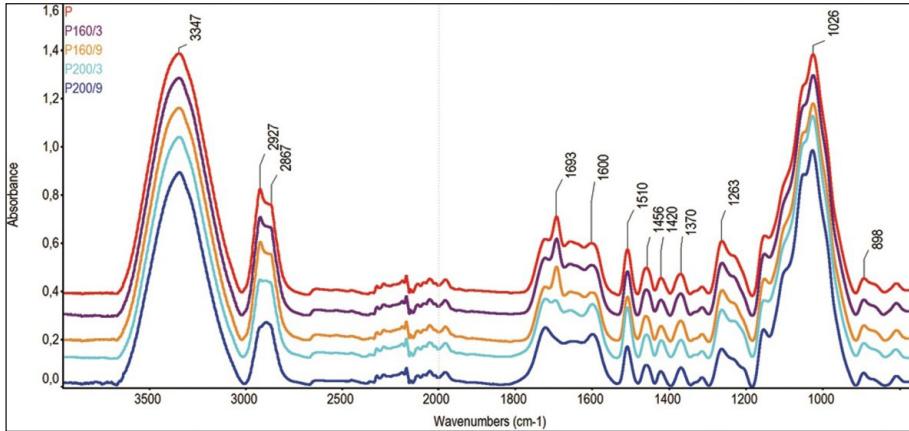


Fig. 4: FTIR spectra of non-treated and thermally treated Scots pine (*Pinus sylvestris* L.) wood.

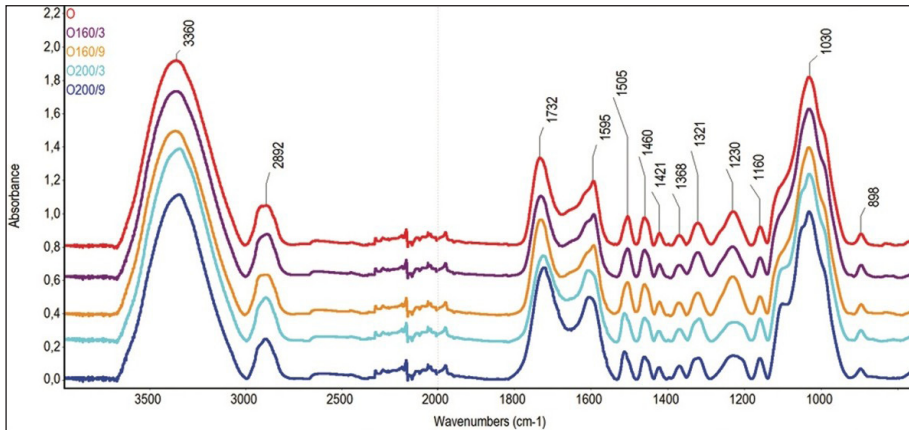


Fig. 5: FTIR spectra of non-treated and thermally treated Sessile oak (*Quercus petraea* L.) wood.

In the FTIR spectra of oak wood, the carbonyl peak at 1732 cm⁻¹ initially at the temperature of 160°C and the time 3 hrs mildly decreased. The decrease at the beginning of the heat treatment might be due to the breaking of acetyl or acetoxy groups in xylan. However, at longer treatment time and at the temperature of 200°C it markedly increased. Heating in air causes oxidation of the hydroxyl groups resulting in an increase of carbonyl and subsequently of carboxyl groups (Fengel and Wegener 1984). Furthermore, with increasing treatment severity, the shift in a maximum from 1732 cm⁻¹ to 1720 cm⁻¹ was observed. This appearance also suggested that in the wood components new carbonyl or carboxyl groups are formed (Esteves et al. 2013).

In the non-treated Sessile oak wood spectra the characteristic peak for aromatic ring at 1505 cm⁻¹ can be observed. The maximum of mentioned peak shifts to 1514 cm⁻¹ with increasing temperature and treatment duration. A similar trend was observed also by Geffert et al. (2019) in the case of oak wood steaming. According to Faix (1991), this band

has maximum at about 1505 cm^{-1} for hardwood lignin and at about 1510 cm^{-1} for softwood lignin. Shifting the maximum of this peak to higher wavenumber can be due to the decrease of the methoxyl groups in lignin which would lead to a lignin more similar to softwood or to the loss of syringyl units. Syringyl monomers are generally less condensed by C-C bonds than guaiacyl monomers and are more liable to be released by a thermal degradation (Faix et al. 1990).

The decrease in the intensity of absorption band at 1243 cm^{-1} in spectra of oak wood suggests that mainly at the temperature of 200°C the degradation of more labile hemicelluloses occurred. The process begins with the partial degradation of long hemicellulose chains into shorter ones and then follows with their decomposition through monosaccharides to volatile products (Hill 2006). In accordance with the findings of other authors (Výbohá et al. 2018, Čabalová et al. 2018) it can be assumed that the earlier degradation of hemicelluloses increases the proportion of lignin in Sessile oak wood relatively. According to Sun et al. (2019) increase of the relative content of lignin and extractives after degradation of hemicelluloses by thermovacuum treatment of eucalyptus wood results in decrease in O/C ratio. Because hemicelluloses have a low calorific value and lignin, on the other hand, a high calorific value, GCV values of Sessile oak wood increase due to degradation of hemicelluloses with increasing temperature and time of thermal treatment.

CONCLUSIONS

The effect of thermal treatment under various process conditions (at temperatures of 160 and 200°C , duration of 3 and 9 hrs) on the gross calorific value of Scots pine (*Pinus sylvestris* L.) and Sessile oak (*Quercus petraea* L.) wood were studied. The value of GCV of untreated Scots pine wood was higher than in the case of Sessile oak wood. It is because softwoods contain more lignin and resins than hardwoods and just these components increase the calorific value of wood. The different composition of Scots pine and Sessile oak wood also influences their behaviour during thermal treatment. With increasing temperature and thermal treatment duration, the mass loss of both tree species increased but at 160°C the mass loss was higher for Scots pine samples, while at 200°C for Sessile oak samples. Whereas the calorific value of Scots pine wood with increased severity of treatment decreased, in the case of Sessile oak it increased. Mentioned differences in Scots pine and Sessile oak wood behaviour using ATR-FTIR spectroscopy were explained. In the case of Scots pine wood with increasing temperature and time of exposure a decrease of resin acids was observed. The decomposition of these compounds contributes to decrease in GCV. In the case of Sessile oak wood, mainly at temperature of 200°C the degradation of hemicelluloses was observed that results in higher mass loss at this temperature. Reducing the hemicelluloses content of the wood, the lignin content increases relatively, resulting in an increase in the GCV.

ACKNOWLEDGMENT

This work was supported by Slovak Research and Development Agency under the contract No. APVV-17-0005 (50%) and project VEGA V-1/0493/18 (50%).

REFERENCES

1. Alakangas, E., 2005: Properties of wood fuels used in Finland. Technical research centre of Finland. Jyväskylä, 90 pp.
2. Andor, T., Lagaňa, R., 2018: Selected properties of thermally treated ash wood. *Acta Facultatis Xylogologiae Zvolen* 60(1): 51-60.
3. Baeza, J., Freer, J., 2001: Chemical characterization of wood and its components. In: *Wood and Cellulosic Chemistry* (ed. Hon DNS., Shiraishi N.), Marcel Dekker Inc. New York, Pp 275-384.
4. Barčík, Š., Gašparík, M., Razumov, E. Y., 2015: Effect of temperature on the color changes of wood during thermal modification. *Cellulose Chemistry and Technology* 49(9-10): 789-798.
5. Bazzyar, B., 2012: Decay resistance and physical properties of oil heat treated aspen wood. *BioResources* 7(1): 696-705.
6. Bubeniková, T., Luptáková, J., Kačíková, D., Kačík, F., 2018: Characterization of macromolecular traits of lignin from heat treated spruce wood by size exclusion chromatography. *Acta Facultatis Xylogologiae Zvolen* 60(2): 33-42.
7. Brebu, M., Vasile, C., 2010: Thermal degradation of lignin – A review. *Cellulose Chemistry and Technology* 44(9): 353-363.
8. Čabalová, I., Kačík, F., Lagaňa, R., Výboňová, E., Bubeniková, T., Čaňová, I., Ďurkovič, J., 2018: Effect of thermal treatment on the chemical, physical, and mechanical properties of pedunculate oak (*Quercus robur* L.) wood. *BioResources* 13(1): 157-170.
9. Cademartori, P.H.G., Missio, A.L., Mattos B.D., Gatto D.A., 2015: Effect of thermal treatments on technological properties of wood from two *Eucalyptus* species. *Anais da Academia Brasileira de Ciências* 87(1): 471-481.
10. Candelier, K., Thevenon, M.F., Petrissans, A., Dumarcay, S., Gerardin, P., Petrissans, M., 2016: Control of wood thermal treatment and its effects on decay resistance: a review. *Annals of Forest Science* 73: 571-583.
11. Chen, Y., Gao, J., Fan, Y., Tshabalala, M.A., Stark, N.M., 2012: Heat-induced chemical and color changes of extractive-free Black Locust (*Robinia pseudoacacia*) wood. *BioResources* 7(2): 2236-2248
12. Dietenberger, M.A., Hasburgh, L.E., 2016: Wood products: Thermal degradation and fire. Pp 9712-9716, USDA Forest Products Laboratory, Madison.
13. Dubey, M.K., Pang, S., Walker, J., 2012: Changes in chemistry, color, dimensional stability and fungal resistance of *Pinus radiata* D. Don wood with oil heat-treatment. *Holzforschung* 66(1): 49-57.
14. Dzurenda, L., 2018: The shades of color of *Quercus robur* L. wood obtained through the processes of thermal treatment with saturated water vapor. *BioResources* 13(1): 1525-1533.
15. Dzurenda, L., Pňakovič, L., 2016: Influence of the burning temperature of the non-volatile combustible content of wood and bark of plantation-grown, fast-growing tree species upon ash production, and its properties in terms of fusibility. *BioResources* 11(3): 6464-6476.
16. Dzurenda, L., Ridzik, L., Dzurenda, M., 2013: Popolnatosť biopaliva – energetickej štiepky z dendromasy porastov plantážnický pestovaných vrb a topoľov (Ash of biofuels – green wood chips made of dendromass from willows and poplars grown on plantations). *Acta Facultatis Xylogologiae Zvolen* 55(1): 111-118.

17. Ekeberg, D., Flåte, P.O., Eikenes, M., Fongen, M., Naess-Andresen, C.F., 2006: Qualitative and quantitative determination of extractives in heartwood of Scots pine (*Pinus sylvestris* L.) by gas chromatography. *Journal of Chromatography A* 1109(2): 267-272
18. Esteves, B.M., Pereira, H.M., 2009: Wood modification by heat treatment: A review. *BioResources* 4(1): 370-404.
19. Esteves, B., Velez Marques, A., Domingos, I., Pereira, H., 2013: Chemical changes of heat treated pine and eucalypt wood monitored by FTIR. *Maderas. Ciencia y tecnología* 15(2): 245-258.
20. Esteves, B., Videira, R., Pereira, H., 2011: Chemistry and ecotoxicity of heat-treated pine wood extractives. *Wood Science and Technology* 45: 661-676.
21. Faix, O., 1991: Classification of lignins from different botanical origins by FT-IR spectroscopy. *Holzforschung* 45(s1): 21-27.
22. Faix, O., Meier, D., Fortmann, I. 1990: Thermal degradation products of wood. *Holz als Roh-und Werkstoff* 48: 351-354.
23. Fengel, D., Wegener, G., 1984: *Wood - Chemistry, ultrastructure, reactions*. Walter de Gruyter. Berlin and New York, 613 pp.
24. Geffert, A., Výbohá, E., Geffertová, J., 2019: Changes in the chemical composition of oak wood due to steaming. *Acta Facultatis Xylogiae Zvolen* 61(1): 19-29.
25. Geffertová, J., 2009: Heating value of hydrolysed birch wood. *Acta Facultatis Xylogiae Zvolen* 51(2): 63-69.
26. Gonzalez-Pena, M.M., Curling, S.F., 2009: On the effect of heat on the chemical composition and dimensions of thermally-modified wood. *Polymer Degradation and Stability* 94(12): 2184-2193.
27. Hill, C.A.S., 2006: *Wood Modification. Chemical, thermal, and other processes*. John Wiley & Sons. Chichester, 239 pp.
28. Hon, D.N.S, Shiraishi, N., 2001: *Wood and cellulosic chemistry*. Marcel Dekker, New York, 914 pp.
29. ISO 1928, 2009: Solid mineral fuels. Determination of gross calorific value by the bomb calorimetric method and calculation of net calorific value.
30. Klement, I., Réh, R., Detvaj, J., 2010: Základné charakteristiky lesných drevín drevín (Basic characteristics of forest trees). *NLC Zvolen*, 82 pp.
31. Kúdela, J., Andor, T., 2018: Beech wood discoloration induced with specific modes of thermal treatment. *Annals of Warsaw University of Life Sciences – SGGW, Forestry and Wood Technology* 103: 64-69.
32. Luptáková, J., Kačík, F., 2018: The influence of thermal modification on selected wood properties. *Delta: Fire Protection & Safety Scientific Journal* 12(1): 33-43.
33. Majlingova, A., Lieskovsky, M., Zachar, M., 2019: Fire and energetic properties of selected fast-growing tree species and energy crop species. *Technical University in Zvolen*, 178 pp.
34. Martinka, J., Hroncová, E., Chrebet, T., Balog, K., 2013: Fire risk assessment of thermally modified spruce wood. *Acta Facultatis Xylogiae Zvolen* 55(2): 117-128.
35. Mazela, B., Zakrzewski, R., Grzeskowiak, W., Cofta, G., Bartkowiak, M., 2003: Resistance of thermally modified wood to basidiomycetes. *Electronic journal of Polish agricultural universities* 7(1): #3 (published online), 7pp.
36. Miltz, H., 2002: Heat treatment technologies in Europe: Scientific background and technological state-of-art. In: *Enhancing the durability of lumber and engineered wood product.*, Forest Products Society. Madison, Pp 239-249.
37. Nosek, R., Holubčík, M., 2016: Energy properties of air dry firewood. *Acta Facultatis Xylogiae Zvolen* 58(1): 105-112.

38. Percin, O., Peker, H., Atilgan, A., 2016: The effect of heat treatment on the some physical and mechanical properties of beech (*Fagus orientalis* Lipsky) wood. Wood Research 61(3): 443-456.
39. Reinprecht, L., Vidholdová, Z., 2011: Termodrevo. Thermowood. Šmíra – Print s.r.o, Česká republika, 89 pp.
40. Santos, R.B., Capanema, E.A., Balakshin, M.Y., Chang, H., Jameel, H., 2012: Lignin structural variation in hardwood species. Journal of Agricultural and Food Chemistry 60(19): 4923-4930.
41. Severo, E.T.D., Calonego, F.W., Sansígolo, C.A., Bond, B., 2016: Changes in the Chemical composition and decay resistance of thermally-modified *Hevea brasiliensis* wood. PLOS One 11(3): e0151353.
42. Sun, B., Wang, Z., Liu, J., 2019: Study on color and surface chemical properties of *Eucalyptus pellita* wood subjected to thermos-vacuum treatment. Wood Research 64(1): 01-12.
43. Telmo, C., Lousada, J., 2011: The explained variation by lignin and extractive contents on higher heating value of wood. Biomass and bioenergy 35(5): 1663-1667.
44. Tillman, D. A., 1978: Wood as an Energy Resource. New York: Academic Press, 252 pp.
45. White, R., 1986: Effect of lignin content and extractives on the higher heating value of wood. Wood and Fiber Science 19(4): 446-452.
46. Traoré, M., Kaal, J., Cortizas, A.M., 2018: Differentiation between pine woods according to species and growing location using FTIR-ATR. Wood Science and Technology 52: 487-504.
47. Výbohová, E., Kučerová, V., Andor, T., Balážová, Ž., Velková, V., 2018: The effect of heat treatment on the chemical composition of ash wood. BioResources 13(4): 8394-8408.
48. Wang, X., Wu, Z., Fang, L., Wei, P., Fei, B., Liu, J., 2015: Changes of chemical composition, crystallinity, and Fourier transform infrared spectra of *Eucalypt pellita* wood under different vacuum heat treatment temperatures. Forest Products Journal 65(7-8): 346-351.
49. Wikberg, H., Maunu, S.L., 2004: Characterization of thermally modified hard- and softwoods by ¹³C CPMAS NMR. Carbohydrate Polymers 58(4): 461-466.

EMÍLIA ORÉMUSOVÁ
TECHNICAL UNIVERSITY IN ZVOLEN
FACULTY OF WOOD SCIENCES AND TECHNOLOGY
DEPARTMENT OF FIRE PROTECTION
T. G. MASARYKA 24
96001 ZVOLEN
SLOVAK REPUBLIC

EVA VÝBOHOVÁ*
TECHNICAL UNIVERSITY IN ZVOLEN
FACULTY OF WOOD SCIENCES AND TECHNOLOGY
DEPARTMENT OF CHEMISTRY AND CHEMICAL TECHNOLOGIES
T. G. MASARYKA 24
96001 ZVOLEN
SLOVAK REPUBLIC

*Corresponding author: eva.vybohova@tuzvo.sk

EFFECTS OF DIFFERENT FLAME RETARDANT TREATMENTS ON THE COMBUSTIBILITY OF BAMBOO FILAMENT

CHUNYAN LI, XINJIE ZHOU, CHANGHAO YANG, LILI YU
TIANJIN UNIVERSITY OF SCIENCE AND TECHNOLOGY
CHINA

HUI LI
¹HUBEI ACADEMY OF FORESTRY
²NATIONAL POSITIONING OBSERVATION AND RESEARCH STATION OF BAMBOO FOREST
ECOSYSTEM IN MUFU MOUNTAIN
CHINA

BENHUA FEI
INTERNATIONAL CENTER FOR BAMBOO AND RATTAN
CHINA

(RECEIVED MAY 2020)

ABSTRACT

Bamboo filaments were treated with boric acid and borax (the mass ratio of 1:1, the concentration of 20%) with four different treatment methods including atmospheric immersion, cold and hot bath immersion, vacuum impregnation and vacuum-pressure impregnation. The different treatment methods on the boron loading were analyzed and the corresponding flame resistance of bamboo filaments were evaluated by the cone analysis. The results showed that suitable treatment method with optimized processing indexes, such as hot and cold bath immersion in the condition of 100°C/2 h and 20°C/2 h with 3 cycles, was more credible to accelerate the percentages of boron loading in the bamboo filaments, and the lowest result was found in the samples with vacuum impregnation. Compared to the untreated samples, the heat and smoke release would be decreased significantly, especially for the samples with the promising hot and cold treatment, and promising pressure treatment, attributed to the more stable boron fixed in the bamboo filaments.

KEYWORDS: Bamboo, flame resistance, boron loading, flame-retardant treatment, combustibility.

INTRODUCTION

As one of the most important substitutes for wood, bamboo has been widely used in the fields of decoration, furniture and building materials due to its excellent mechanical properties, short growth cycle, strong regeneration ability, longer fiber length, good elasticity and superior carbon fixation ability (Verma et al. 2012, Subekti et al. 2018, Zhu et al. 2019).

However, as one of the flammable substances, the combustibility of bamboo has become the major obstacle for its utilization (Du et al. 2014, Zhou et al. 2018), for examples, once the bamboo was ignited, the flame and toxic gases would fill in the whole room within 5 to 10 minutes (Zheng et al. 2019). As the result, it is critical to perform suitable flame-retardant treatment to guarantee the application safety of bamboo-based materials (Zheng et al. 2016, Li et al. 2018, Fang et al. 2020). However, the permeability of bamboo is very poor, which is attributed to the vertical penetration mainly depending on the tube and screen (Kučerová 2012, Yu et al. 2016), as the result, it is difficult to be treated with the flame retardants to reach the suitable retention (Yong et al. 2013, Wen 2017). Many researches involving in the sample pre-treatments and the flame-retardant treatment methods have been performed to improve the retention in bamboo. The pre-treatments such as reducing the thickness of the samples, selecting the suitable indexes of the flame retardants including the active ingredients, pH, concentration, have obtained some promising results in some researches (Shu 2010, Li et al. 2011). Additionally, some other researchers have paid more attentions to modify the permeability of bamboo by many physical and chemical measures, such as microwave treatment, pressure treatment, freeze-drying treatment, extraction, etc. (Guan et al. 2013, Haase et al. 2018). Xu et al. (2018) found that vacuum freeze-drying increased the porosity of bamboo to 73%, and it had no obvious effect on the mechanical properties of bamboo. The ultrasonic treatment of bleached and carbonized bamboo increased the surface free energy and improved the wettability and permeability of bamboo (Huang 2017). In addition, hydrochloric acid (2%) hydrolysis and ethanol extraction could also effectively improve the permeability of bamboo (Rao et al. 2013).

The direct and effective means to increase the flame-retardant retention are to perform suitable flame-retardant treatment methods with appropriate processing indexes. Recently, the widely used flame retardant treatment methods of bamboo in the industry could be summarized as immersion and surface coating. The most commonly used immersion methods include atmospheric immersion, hot and cold bath immersion and vacuum/and pressure impregnation (Du et al. 2016, Yu et al. 2017). Surface coating is another convenient method for bamboo flame retardant treatment. The flame retardant or flame-retardant coating is directly sprayed or painted on the surface of bamboo materials or bamboo products to form a thinner film, which can effectively obstruct the heat and oxygen from bamboo. However, the coating film was so thin that the active flame-retardant gradients were limited, and it was vulnerable to be damaged by mechanical force (Jin et al. 2015, Li et al. 2018).

In order to clarify the difference in the flame resistance of bamboo performed with different treatment methods, four frequently used flame retardant treatment methods including atmospheric immersion, cold and hot bath immersion, vacuum impregnation and vacuum-pressure immersion were performed in this research, and based on the results, it was conducted to determine the correlation between boron loading and flame resistance with different treatment conditions as well as to obtain the suitable processing indexes with the promising treatment method.

MATERIAL AND METHODS

Samples

Moso bamboo (*Phyllostachys edulis* (Carr.) H.de Lehaie) was taken from Hubei Province, China. After air-drying, the moso bamboo was cut along the direction of the fiber to obtain the bamboo splits, then to cut into the bamboo filaments. The filaments were stuck together with non-woven fabric by a polyvinyl acetate adhesive and cut into small pieces with dimensions of

100 mm (tangential) × 100 mm (longitudinal) × 1.5 mm (radial). Bamboo filaments with similar weights were selected as the test samples. The mass fraction of boric acid and borax fire retardant was 20%, and the ratio between boric acid and borax was 1:1.

Flame retardant treatments

Bamboo filaments were dried to constant weight in a drying oven at 60°C. Then bamboo filaments were taken out and cooled to weight and recorded. Bamboo filaments were treated with four different flame-retardant treatments including atmospheric immersion, cold and hot bath immersion, vacuum impregnation and vacuum-pressure impregnation with different processing indexes as showed in Tab. 1, and six repeated specimens were set in each treatment. In the atmospheric immersion treatments, the bamboo filaments were immersed into the flame retardant at 20, 60, and 100°C, respectively. In the cold and hot bath immersion treatments, the bamboo filaments were first immersed in hot flame retardant at 100°C for 0.5, 1, and 2 h, respectively, and then replaced them into the cold flame retardant for 0.5, 1, and 2 h, respectively. In the vacuum impregnation, the bamboo filaments were put into a beaker and the flame retardant was introduced into the beaker to immerse the samples at room temperature by the vacuum pressure (-0.1 MPa). In the vacuum-pressure impregnation, the bamboo filaments were put in a closed vacuum pressurized tank, which was vacuumed to -0.1 MPa for 30 min, and introduced the flame retardant to the tank, then pressurized to 0.8 MPa for 1 h. After different flame-retardant treatments, then bamboo filaments were dried to constant weight in a drying oven at 60°C. The specimens would be treated with the same recycle for 1 to 4 cycles.

Tab. 1: Fire retardant immersion conditions for bamboo filament.

Treatment method	Temperature (°C)	Treatment duration (h)	Vacuum (MPa)	Pressure (MPa)	Treatment cycles
Atmospheric immersion	20, 60, 100	2			
Cold and hot bath immersion	20, 100	0.5, 1, 2			1, 2, 3, 4
Vacuum impregnation	20	1	-0.1		
Vacuum-pressure impregnation	20	1	-0.1	0.8	

Percentages of boron loading (BL) in the samples were calculated using Eq. 1:

$$BL = \frac{W_2 - W_1}{W_1} \times 100\% \quad (1)$$

where: W1 and W2 are the weights of each specimen before and after the flame-retardant treatment.

Combustibility by cone calorimeter

After different flame-retardant treatments, the bamboo filaments were dried to constant weight in a drying oven at 60°C. The combustibility of the samples with the highest boron loading in each flame-retardant treatment method were selected and evaluated by a cone calorimeter according to ISO 5660 (2002). Six specimens with the same treatment condition were prepared with dimensions of 100 × 100 × 1.5 mm, and placed horizontally under a cone heater with a heat flux of 50 kW·m⁻². A stainless-steel cover with an opening of 0.0088 m² on the upper part was attached. The data was recorded by a computer on a second basis.

RESULTS AND DISCUSSION

Effects of different treatment methods on boron loading*Atmospheric immersion*

As showed in Fig. 1, the immersion temperature played a significant effect on the percentages of boron loading in the bamboo filament. At ambient temperature (about 20°C), the percentages of boron loading were less than 8%, however, when the temperature was up to 100°C, it could reach more than 14% in all the samples with different treatment cycles.

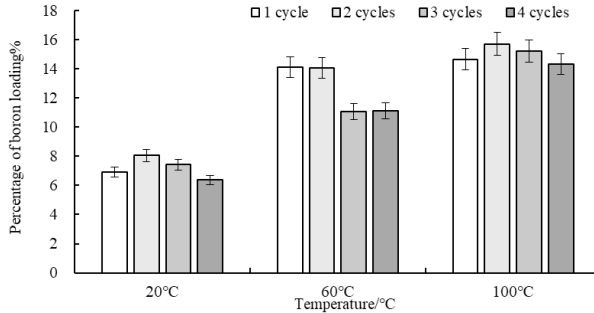


Fig. 1: Effect of different atmospheric immersion treatments on the boron loading of bamboo filaments.

Additionally, the treatment cycles of the flame-retardant treatments also had a certain effect on the boron loading. However, it was not the more, the better, and the maximum boron loading was observed in the samples with 2 cycles of immersion treatments, which was attributed to that too many treatments would increase the leaching risk of the flame retardants during treatment. In the atmospheric immersion, the maximum percentage of boron loading was observed in the samples treated at 100°C for 2 h with 2 cycles of treatments, and it could reach 15.72%.

Hot and cold bath immersion

As showed in Fig. 2, hot and cold bath immersion was more favorable to increase the boron loading of bamboo filaments than atmospheric immersion, and the percentages of boron loading of all the samples were above 14%. In the hot and cold bath immersion, the processing duration and the cycles of cold and hot bath immersion played significant effects on the boron loading of bamboo filaments. The similar results could be observed that the increase of treatment cycles was not always conducive to improve the boron loading of bamboo filament, and the boron loading in all the samples with four cycles of treatments began to decrease. In cold and hot bath treatment, the better results were observed in the samples treated with twice or three cycles of treatments. The maximum percentages of boron loading in the same treatment condition with different treatment cycles were showed in Tab. 2. It could be seen that the duration of hot bath immersion was not as obvious as cold bath immersion on the boron loading of bamboo filaments, and the percentages of boron loading changed slightly as the hot bath immersion increased in the same cold bath immersion. The results indicated that the extension of cold bath immersion was the key factor to increase the boron loading of bamboo filaments in the cold and hot bath immersion, because during the hot bath immersion, the thinner bamboo filaments could remove the internal air in a very short time to achieve the vacuum state, as the result, the samples could quickly become saturated with the flame retardant. The boron loading of bamboo filament increased obviously with the extension of the cold bath immersion, which was due to the slow absorption rate of the cold flame-retardant immersion.

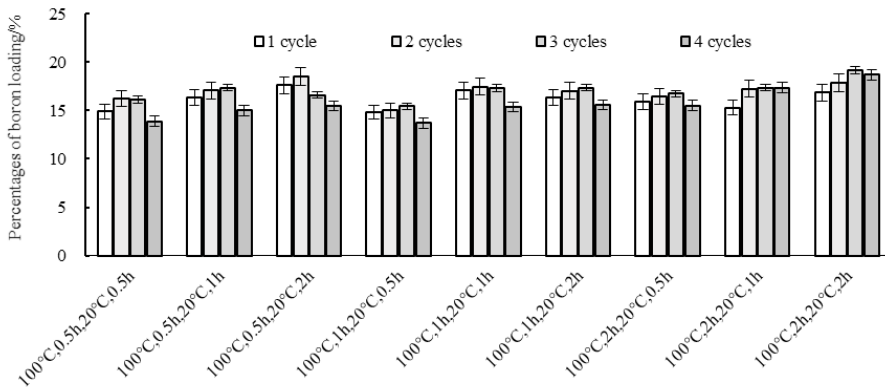


Fig. 2: Effect of different cold and hot bath immersion treatments on the boron loading of bamboo filaments.

The maximum percentages of boron loading in the same treatment condition with different treatment cycles were showed in Tab. 2. It could be seen that the duration of hot bath immersion was not as obvious as cold bath immersion on the boron loading of bamboo filaments, and the percentages of boron loading changed slightly as the hot bath immersion increased in the same cold bath immersion. The results indicated that the extension of cold bath immersion was the key factor to increase the boron loading of bamboo filaments in the cold and hot bath immersion, because during the hot bath immersion, the thinner bamboo filaments could remove the internal air in a very short time to achieve the vacuum state, as the result, the samples could quickly become saturated with the flame retardant. The boron loading of bamboo filament increased obviously with the extension of the cold bath immersion, which was due to the slow absorption rate of the cold flame-retardant immersion.

Tab. 2: Effects of different cold and hot bath immersion treatments on the maximum boron loading of the bamboo filaments.

Treatment conditions	20°C			
	0.5 h	1 h	2 h	
100°C	0.5h	16.21 (0.95)	17.35 (0.72)	18.55 (1.29)
	1h	15.45 (1.02)	17.45 (1.99)	17.36 (1.27)
	2h	16.73 (1.53)	17.37 (1.27)	19.16 (0.78)

Vacuum impregnation

Percentages of boron loading in the bamboo filaments with vacuum impregnation were showed in Fig. 3. It can be seen that the treatment cycles played an obvious role in the vacuum impregnation. The percentage of boron loading of bamboo filaments with two cycles were the highest and it could reach 10.54%, which was significantly lower than those with cold and hot bath immersions. The reason was mainly caused by the lower negative pressure generated by the vacuum.

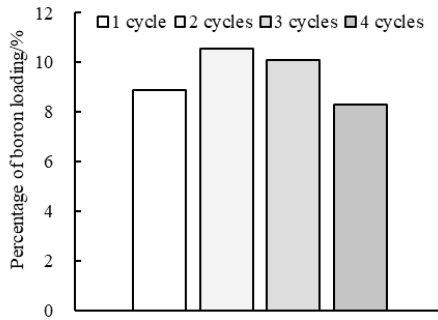


Fig. 3: Effect of different vacuum impregnation cycles on the boron loading of bamboo filaments.

Pressure impregnation

Due to the limitation of pressure equipment, only the effect of different flame-retardant impregnation cycles on the boron loading of bamboo filaments were investigated in this study. As shown in Fig. 4, the percentages of boron loading were increased insignificantly with the flame-retardant cycles increased, and it could be up to 15.52% in the samples with 4 cycles of pressure impregnation. The result demonstrated that the flame retardant could have more opportunities to penetrated into bamboo filaments with the favor of higher pressure.

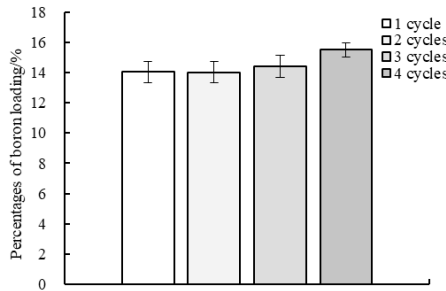


Fig. 4: Effect of different pressure impregnation cycles on the boron loading of bamboo filaments.

Combustibility analysis

Heat release analysis

The heat release rates (HRR) and the total amounts of heat release (THR) for the bamboo filaments with different flame-retardant treatments are shown in Figs. 5a,b.

Compared with untreated samples, different flame-retardant treatments could effectively reduce the HRR during the whole combustion process, which indicated that boric acid/borax could effectively block heat and oxygen by the thin layer of melting primevally to reduce the rate of heat release during combustion process, which was similar with other research that boron based complexes had excellent flame retardant performance (Li et al. 2018). However, the difference in the samples treated with these four flame retardant treatment methods respectively were very obvious. At 0-35 s, the HRR of bamboo filaments treated by cold and hot bath were the lowest among all the samples, while at 35-45 s, the HRR of bamboo filaments treated by pressure decreased sharply. The results that the samples with higher boron loading

or/and suitable treatment were both important to reduce the heat release during combustion process, which was also proved by the results observed in the whole process of combustion that the samples with the vacuum treatment had the worst flame retardance, while the HRR in the samples with hot and cold bath immersion and pressure impregnation were decreased significantly.

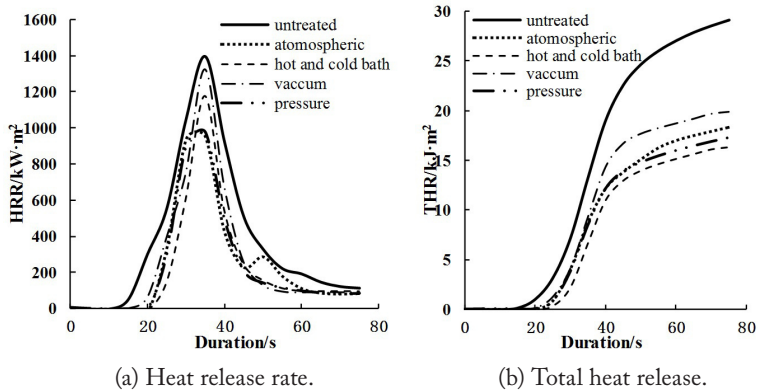


Fig. 5: HRR curves of bamboo filaments with different treatments.

As observed from Fig. 5b, the process of bamboo filament combustion can be divided into three stages according to the change of heat release: early stage of combustion (0-25 s), middle stage of combustion (25-45 s) and final stage of combustion (45-75 s). In the early stage, the THR of all the treated samples were lower than those in the untreated samples, but the difference in THR among different flame-retardant treatments could be negligible. In the middle stage, the flame-retardant treatments had a significant different effect on the THR of bamboo filaments, which seemed that the best flame resistance were observed in the samples with hot and cold immersion, followed by pressure impregnation. At the final stage, the THR of all the bamboo filaments increased gently. From the whole combustion process, the bamboo filament treated by immersion, cold and hot bath, vacuum and pressure flame retardant decreased by 36.94%, 44.01%, 31.67% and 40.65%, respectively, which also demonstrated that cold and hot bath immersion and pressure impregnation were suitable treatment methods for bamboo filaments.

Smoke release analysis

The total smoke release (TSP) of bamboo filaments treated with different flame-retardant treatments was showed in Fig. 6. It can be seen that the TSP in all the treated bamboo filaments was significantly reduced. Compared to the untreated samples, TSP in the bamboo filaments treated with immersion, cold and hot bath, vacuum and pressure flame retardant could decreased by 91.30%, 89.49%, 83.93% and 89.67%, respectively. Except for the slightly higher smoke emission of vacuum treated bamboo filaments, the other flame-retardant treated bamboo filaments had excellent smoke inhibition, while the difference among different treatment methods were very slight. This result further proved that the reasonable flame retardant was essential to reduce the smoke emission caused by the combustion of bamboo.

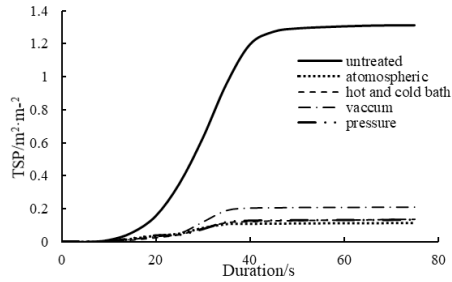


Fig. 6: TSP-time curves of bamboo filament with different treatments.

The average amount of smoke release from per mass (ASEA) and the toxic gases of CO and CO₂ yield in the bamboo filaments during the combustion process were showed in Tab. 3. As observed, compared to the untreated samples, different flame-retardant treatments could significantly reduce the ASEA value of all the treated samples. Bamboo filaments treated by immersion, cold and hot bath, vacuum and pressure flame retardant would decrease by 86.90%, 73.66%, 65.68% and 77.21%, respectively. The results indicated different flame retardants would change the thermal decomposition process of bamboo filaments and affect the visible smoke production of bamboo filaments, and just as other researchers showed the smoke release were changed to some flame-retardant gases such as NH₃ and CO₂ (Wang et al. 2004, Zhang et al. 2018).

Tab. 3: Smoke production parameters with different flame-retardant treatments.

Smoke emission parameter	Untreated	Atmospheric immersion	Cold and hot bath	Vacuum impregnation	Pressure immersion
ASEA/ (m ² •kg ⁻¹)	85.84	11.25	22.61	29.46	19.57
Average CO yield / (kg•kg ⁻¹)	0.1455	0.0527	0.0715	0.0667	0.0669
Average CO ₂ yield / (kg•kg ⁻¹)	3.6101	2.0914	1.9516	1.6827	2.2654

As Tab. 3 showed, compared to the untreated samples, bamboo filaments treated with different flame-retardant treatments had significantly reduced the CO and CO₂ production rates, which was mainly due to the fact that during the dehydration reaction, the volatile products during the combustion contained less CO₂ and more water. It seemed that different flame-retardant treatment methods had slight effect on the CO and CO₂ yield compared with the value of ASEA.

CONCLUSIONS

Because of the poor permeability of bamboo, it is essential to perform some modifications to improve the flame retardant of bamboo. Different flame-retardant treatments including atmospheric immersion, cold and hot bath immersion, vacuum impregnation and vacuum-pressure impregnation had obvious difference in the boron loading of bamboo filaments attributed to the permeability modification difference. Suitable treatment method with optimized processing indexes including treatment duration, temperature and cycles was more

propitious to increase the percentages of boron loading in the bamboo filaments, which was also demonstrated the reasonable conditions for improving the permeability of bamboo. Compared to the untreated samples, the indexes of heat and smoke were reduced dramatically in all the boron-treated bamboo filaments during the combustion process, and would be affected by the flame treatment methods. These improvements were attributed to the permeability of the flame retardants into bamboo. Generally, the samples with the vacuum treatment had the worst heat suppressibility, while the samples with hot and cold bath immersion and pressure impregnation had better performance, which was also attributed to the significant permeability difference of flame retardants into bamboo. The similar results were also observed in the ASEA values, however the effects of different treatment methods on the CO and CO₂ yield were not obvious.

ACKNOWLEDGMENT

The authors are grateful for the financial support of the Subjects of National Natural Science Foundation of China (NSFC No. 31400499), the National College Students Innovation and entrepreneurship training program (201910057047), and the Science and Technology of Tianjin University College Students Innovation and entrepreneurship training program (202110057013).

REFERENCES

1. Verma, C.S., Chariar, V.M., 2012: Development of layered laminate bamboo composite and their mechanical properties. *Composites Part B: Engineering* 43(3): 1063-1069.
2. Subekti, N., Widiyaningrum, P., Yoshimura, T., Fibriana, F., 2018: The strength and termite resistance characteristics of fiberboards produced from the renewable bamboo biomass. *Wood Research* 63(3): 409-418.
3. Zhu, Z.Z., Zhu, S.L., Zhang, T.T., Guo, Y., Liu, S.Q., Liu, H.R., Chen, Y.X., 2019: A brief analysis on the design of detachable furniture made of bamboo oriented strand board (BOSB). *Journal of Bamboo Research* 38(2): 70-74.
4. Du, C.G., Song, J.G., Chen, Y.X., 2014: The effect of applying methods of fire retardant on physical and mechanical properties of bamboo scrimber. *Advanced Materials Research* 1048: 465-468.
5. Zhou, Z.X., Yao, X.L., Du, C.H., Yu, H.L., Huang, Q.L., Liu, H.Z., 2018: Effect of hygroscopicity of fire retardant on hygroscopicity of fire retardant bamboo chips. *Wood Research* 63(3): 373-382.
6. Zheng, M.H., Wang, K., Wu, Q., Zhang, W.B., Zhang, X.C., Li, C.B., Zhou, Z.C., Zhang, S.H., 2016: The performances of bamboo treated with three flame retardants. *Journal of Bamboo Research* 35(4): 8-13.
7. Fang, L., Lu, X.Z., Zeng, J., Chen, Y.Y., Tang, Q.H., 2020: Investigation of the flame-retardant and mechanical properties of bamboo fiber-reinforced polypropylene composites with melamine pyrophosphate and aluminum hypophosphite addition. *Materials* 13(2): 479-491.
8. Li, H., Chen, M.L., Lv H.F., Yang, F., Yu, L.L., Fei, B.H., Ma, X.X., 2018: Effects of guanidurea phosphate treatment on the performance of decorative bamboo filament. *Bioresources* 13(2): 3487-3499.
9. Kučerová, I., 2012: Methods to measure the penetration of consolidant solutions into 'dry' wood. *Journal of Cultural Heritage* 13(3): 191-195.

10. Wen, X.W., 2017: Study on preservative penetration of bamboo and its influencing factors. Master's thesis. Pp 25-32, Chinese Academy of Forestry, Beijing, China.
11. Yong, C., Zhou, M.M., Guan, M.J., 2013: Effect of ultrasonic cavitation on microscopic structure and starch granule of bamboo. *China Forestry Science and Technology* 27(3): 99-102.
12. Li, Y.F., Liu, Y.X., Wang, F.H., Gang, G.J., 2011: Controlling factors of wood permeability and its improving measures. *Scientia Silvae Sinicae* 47(5):131-139.
13. Shu, T.T., 2010: The research of moso-bamboo dye solution permeability. Master's thesis. Pp 31-35, Zhejiang A&F University, Zhejiang, China.
14. Haase, J., Leung, L., Evans, P., 2018: Plasma pre-treatments to improve the weather resistance of polyurethane coatings on black spruce wood. *Coatings* 9(8): 1-14.
15. Guan, M.J., Yong, C., Wang, L., 2013: Shear strain and microscopic characterization of a bamboo bonding interface with poly(vinyl alcohol) modified phenol-formaldehyde resin. *Journal of Applied Polymer Science* 130(2): 1345-1350.
16. Xu, J., He, S., Li, J., Yu, H., Zhao, S., Chen, Y., Ma, L., 2018: Effect of vacuum freeze-drying on enhancing liquid permeability of moso bamboo. *BioResources* 13(2): 4159-4174.
17. Huang, Z.W., 2017: Effects of ultrasonic treatment on surface characteristics and bonding interface properties of bamboo laminated lumber. Pp 12-24, Nanjing Forestry University, Nanjing, China.
18. Rao, S., Yu, L.P., 2013: Effect of pretreatment on fluid permeability of moso bamboo. *Forestry Machinery&Woodworking Equipment* 41(8): 26-29.
19. Du, C.G., Wei, J.G., Jin, C.D., 2016: Fire retardant treatment process of bamboo scrimber. *Journal of Forestry Engineering* 1(1): 55-54.
20. Yu, L.L., Cai, J., Lu, F., Qin, D.C., Fei, B.H., 2017: Combustibility of boron-containing fire retardant treated bamboo filament. *Wood and Fiber Science* 49(2): 125-133.
21. Jin, C.D., Li, J.P., Yao, Q.F., 2015: A novel electrically conductive material derived from in situ synthesis of silver nanoparticles on the surface of bamboo timer. *Wood Research* 60(4): 617-621.
22. Li, H., Yang, Z.B., Yang, F., Gu, Z.C., Yu, L.L., Ma X.X., Fei B.H., 2018: Influence of four coatings on the mold-resistance and combustion performance of decorative bamboo curtain. *Wood and Fiber Science* 50(4): 447-457.
23. Li, H., Chen, M.L., Lv, H.F., Fei, B.H., 2018: Effect of flame retardant treatments on the antimold and combustion properties of decorative bamboo filament. *Journal of Central South University of Forestry & Technology* 38(7): 110-116.
24. Wang, Q.W., Li, J., Winandy, J.E., 2004: Chemical mechanism of fire retardance of boric acid on wood. *Wood Science and Technology* 38: 375-389
25. Zhang, Y.H., Cai, J.W., Li, Z. 2018: Research on improving mechanical and flame retardant properties of bamboo. *Chemical Research* 29(2): 197-201.

CHUNYAN LI, XINJIE ZHOU, CHANGHAO YANG, LILI YU*
TIANJIN UNIVERSITY OF SCIENCE AND TECHNOLOGY
FACULTY OF LIGHT INDUSTRY SCIENCE AND ENGINEERING
DAGU SOUTHROAD 1038, HEXI DISTRICT, P. O. BOX 546
300222 TIANJIN
P. R. CHINA

*Corresponding author: yulilucky@tust.edu.cn

HUI LI*
¹HUBEI ACADEMY OF FORESTRY
WUHAN 430075, HUBEI
P. R. CHINA
²NATIONAL POSITIONING OBSERVATION AND RESEARCH STATION
OF BAMBOO FOREST ECOSYSTEM IN MUFU MOUNTAIN
XIANNING 437100, HUBEI
P. R. CHINA

BENHUA FEI*
INTERNATIONAL CENTER FOR BAMBOO AND RATTAN
FUTONG EASTROAD 8, CHAOYANG DISTRICT
100102 BEIJING
P. R. CHINA

**PHYSICAL AND MECHANICAL CHARACTERIZATION
OF *PLANCHONELLA PACHYCARPA* WOOD SPECIES FOR
USE IN STRUCTURAL PURPOSE**

VINICIUS BORGES DE MOURA AQUINO, MARCUS VINICIUS PEREIRA DE FREITAS,
CLAUDIA QUEIROZ DE VASCONCELOS
FEDERAL UNIVERSITY OF SOUTHERN AND SOUTHEASTERN PARÁ
BRAZIL

JOÃO PAULO BOFF ALMEIDA, FELIPE NASCIMENTO ARROYO,
EDSON FERNANDO CASTANHEIRA RODRIGUES, ANDRÉ LUIS CHRISTOFORO
FEDERAL UNIVERSITY OF SÃO CARLOS
BRAZIL

DIEGO HENRIQUE DE ALMEIDA
FEDERAL UNIVERSITY OF RONDONIA
BRAZIL

SERGIO AUGUSTO MELLO SILVA
SÃO PAULO STATE UNIVERSITY
BRAZIL

DIOGO APARECIDO LOPES SILVA
FEDERAL UNIVERSITY OF SÃO CARLOS
BRAZIL

ROBERTO VASCONCELOS PINHEIRO
MATO GROSSO STATE UNIVERSITY
BRAZIL

FRANCISCO ANTONIO ROCCO LAHR
UNIVERSITY OF SÃO PAULO
BRAZIL

(RECEIVED APRIL 2020)

ABSTRACT

This research aimed to characterize the wood species Goiabão (*Planchonella pachycarpa*), following the precepts set forth in the Brazilian standard ABNT NBR 7190, as well as to evaluate the possibility of estimating physical and mechanical properties, using the analysis of variance (ANOVA) as a function of apparent density, and also to estimate the stiffness properties as a function of the respective strength property. The physical and mechanical properties were considered adequate for the use of this wood for structural purposes, being classified in class C40. According to the results of the regression models, it is possible to estimate the tensile strength parallel to the fibers as a function of the apparent density. It was also possible to estimate the longitudinal elastic modulus in the compression parallel to the fibers as a function of the compressive strength parallel to the fibers.

KEYWORDS: *Planchonella pachycarpa*, apparent density, regression models, analysis of variance (ANOVA).

INTRODUCTION

Considering that wood is a natural material, subject to different edaphoclimatic conditions (Lahr et al. 2016c, Silva et al. 2018, Morando et al. 2019) and that Brazil is the country with the largest number of tree species (Beech et al. 2017, Steege et al. 2016, ter Steege et al. 2019). The characterization of new species of wood must also be carried out so that there is no predatory use of known species, which can lead them to extinction (Cardoso et al. 2012, Couto et al. 2018, Nogueira et al. 2019). Thus, the species *Planchonella pachycarpa* can be an alternative for use with structural purposes. This species is present in the Brazilian states of Pará, Mato Grosso, Amazonas (Lorenzi 1998).

In Brazil, the characterization of wood species for structural use, as well as the requirements for dimensioning and classification of wood are recommended by the Brazilian standard ABNT NBR 7190 (ABNT 1997), on specimens with no defects. The characterization tests are analogous to those recommended in the international standard ISO 13061 (2017). An alternative to estimate physical and mechanical properties in a simple and effective way with the use of mathematical methods is to use the apparent density, defined as the ratio between mass and apparent volume at 12% moisture content, a property of easy experimental determination (Christoforo et al. 2017, Couto et al. 2018, Dias and Lahr 2004, Lahr et al. 2016c, Lobão et al. 2004).

In the design of wooden structures, such as bridges, roofs, walkways and residences, rigidity properties are used, as well as strength properties. How obtaining those properties requires a higher level of complexity in the equipment compared to obtaining the strength properties (Dadzie and Amoah 2015, Komariah et al. 2015, Logsdon et al. 2005, Machado et al. 2014, Ruelle et al. 2011), it is important to evaluate the possibility of estimating the stiffness properties as a function of the respective strength property.

Thus, this work aimed to present the physical and mechanical characterization of the wood species *Planchonella pachycarpa*, a wood species in which there are no studies in the literature. In addition to characterizing, this study aimed to evaluate the possibility of estimating physical and mechanical properties as a function of apparent density, rigidity properties as a function of the respective strength property, as well as evaluating the relationships between the strength properties and comparing with the arranged relationships in the Brazilian standard ABNT NBR 7190 (ABNT 1997).

MATERIAL AND METHODS

The samples of *Planchonella pachycarpa* wood were properly stored, which resulted in equilibrium moisture content close to 12% according to ABNT NBR 7190 (1997). The tests were performed at the Laboratory of Wood and Wood Structures (LaMEM), Department of Structural Engineering (SET), São Carlos School of Engineering (EESC), University of São Paulo (USP). The physical and mechanical properties were obtained in accordance with the requirements of the Brazilian standard ABNT NBR 7190 (1997), set out in its Annex B, determining the following physical and mechanical properties: apparent density ($\rho_{ap,12\%}$), total radial shrinkage (TRR), total tangential shrinkage (TTR), compressive strength parallel to the grain (f_{c0}), tensile strength parallel to fibers (f_{t0}), tensile strength normal to the grain (f_{t90}), shear strength parallel to the grain (f_{v0}), splitting strength (f_{s0}), conventional strength on static bending test (f_m), modulus of elasticity in parallel directions to the grain (E_{c0}), modulus of elasticity in tension parallel to the grain (E_{t0}), conventional modulus of elasticity on static bending test (E_m), hardness parallel to the grain (f_{H0}), hardness normal to the grain (f_{H90}) and toughness (W). On Fig. 1, it is described the dimensions of wood specimens.

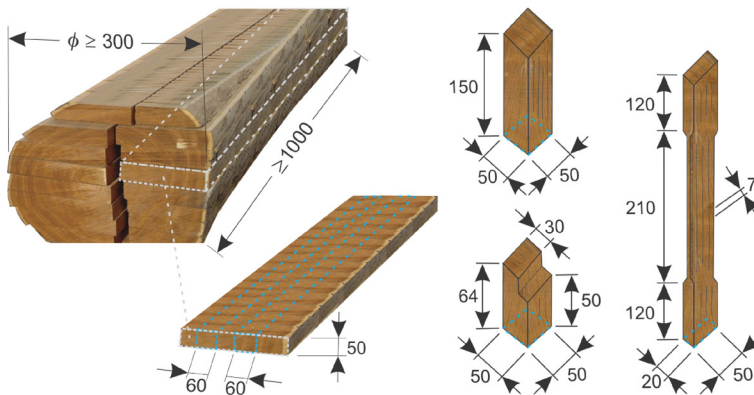


Fig. 1: Dimension of wood specimens and description of their extraction on timber (Dimension in mm). Source: Morando et al. (2019).

It should be noted that 15 values for each one of its physical (3) and mechanical properties (12) were investigated, resulting in 225 experimental values obtained. *Planchonella pachycarpa* wood was classified in the appropriate strength class (ABNT 1997) according to the characteristic value of the compressive strength parallel to the fibers ($f_{c0,k}$).

The classification of *Peltophorum vogelianum* wood in the strength classes for wood of the dicotyledon group was made using Eq. 1, where f_k is the characteristic strength value and n is the number of test pieces used. It should be noted from Eq. 1 that the results of strength should be placed in ascending order $f_1 \leq f_2 \leq \dots \leq f_n$, ignoring the highest value if the number of specimens is odd, and not taking f_k below f_1 nor 0.70 of the average value:

$$f_{c0,k} = \left(2 \cdot \frac{f_1 + f_2 + f_3 + \dots + f_{(n/2)-1}}{(n/2)-1} - f_{n/2} \right) \cdot 1.10 \quad (1)$$

Regression models (Eqs. 2-5) based on analysis of variance (ANOVA) were used to estimate the strength and stiffness properties as a function of the apparent density of the wood and also the stiffness as a function of strength, with Y being the estimated property (variable dependent), X the independent variable and b and the parameters adjusted by the Least squares method:

$$Y = a + b \cdot X \quad [\text{Lin} - \text{linear}] \quad (2)$$

$$Y = a \cdot e^{b \cdot X} \quad [\text{Exp} - \text{exponential}] \quad (3)$$

$$Y = a + b \cdot \text{Ln}(X) \quad [\text{Log} - \text{logarithmic}] \quad (4)$$

$$Y = a \cdot X^b \quad [\text{Geo} - \text{geometric}] \quad (5)$$

By the ANOVA of the regression models, it is considered at the level of 5% of significance (α), the null hypothesis formulated consisted of the non-representativeness of the tested models ($H_0: \beta = 0$) and in the representativeness as an alternative hypothesis. P-value higher than the significance level implies the acceptance of H_0 (the model is not representative - the variations of the independent variable are not able to explain the variations in the estimated properties), refuting it otherwise (the tested model is representative). The determination coefficient (R^2) was used to assess the quality of the adjustments obtained, making it possible to choose the best precision for each evaluated relationship. It should be noted that 56 regression models were used for density as an estimator of the fourteen other variables (including physical properties TRR and TTR), and 16 other models for strength properties as estimators of stiffness, which resulted in 72 equations in all.

RESULTS AND DISCUSSION

Tab. 1 presents the average values (X_m), coefficients of variation (C_v), maximum values (Max) and minimum values (Min), the confidence interval of the mean (CI - 95% reliability) of the physical and mechanical properties of the wood of Goiabão wood species, as well as the characteristic values of the mechanical properties.

Tab. 1: Descriptive statistics of experimentally obtained values for wood species *Planchonella pachycarpa*.

Property	X_m	Min	Max	CV (%)	CI	f_{wk}
$\rho_{ap,12\%}(\text{g}\cdot\text{cm}^{-3})$	0.93	7.00	0.80	7.00	0.88; 0.97	-
TRR (%)	8.90	15.00	6.90	15.00	8.08; 9.71	-
TTR (%)	18.84	9.00	15.60	9.00	17.81; 19.86	-
f_{c0} (MPa)	48.40	12.00	41.00	12.00	44.58; 52.21	43.10
f_{t0} (MPa)	119.33	30.00	66.00	30.00	97.10; 141.57	70.13
f_{t90} (MPa)	8.70	22.00	5.20	22.00	7.49; 9.91	5.79
f_{v0} (MPa)	14.00	15.00	11.00	15.00	12.72; 15.27	12.14
f_{s0} (MPa)	1.16	26.00	0.90	26.00	0.97; 1.35	1.01
f_M (MPa)	106.50	12.00	84.00	12.00	99.14; 113.85	91.12
E_{c0} (MPa)	18716	15.00	13501	15.00	16982; 20449	-
E_{t0} (MPa)	18267	17.00	11468	17.00	16294; 20240	-

E_M (MPa)	18367	16.00	14361	16.00	16488; 20245	-
f_{H0} (MPa)	109.67	6.00	93.00	6.00	105.86; 113.48	114.56
f_{H90} (MPa)	100.00	8.00	81.00	8.00	94.91; 105.09	104.04
W (N-m)	21.09	20.00	12.90	20.00	18.48; 23.69	-

Considering the characteristic value of the compressive strength parallel to the $f_{c0,k}$ (43 MPa) fibers of *Planchonella pachycarpa* wood, this wood is classified as C40 of dicotyledons, the same class of wood species *Erismia uncinatum* (Almeida et al. 2019), *Vataireopsis araroba* (Almeida et al. 2016), *Vatairea sp.* (Lahr et al. 2016a), *Mimosa caesalpiniaefolia* (Nascimento et al. 2018) and *Copaifera sp.* (Aquino et al. 2018a), wood species used for structural purposes (ABNT 1997). Considering the data in the literature, and the value of compressive strength parallel to Goiabão fibers is close to that found by Dias and Lahr (49 MPa) (Dias and Lahr 2004), a value close to that found in the present work. The Goiabão wood species can be considered very heavy ($\rho_{ap,12\%} = 0.92 \text{ g}\cdot\text{cm}^{-3}$) (Dias and Lahr 2004), with density similar to the species *Manilkara huberi* and *Mezilaurus itauba* (Silveira et al. 2013).

Evaluating the values of the coefficients of variation, the Brazilian standard ABNT NBR 7190 (ABNT 1997) establishes that the maximum value of the coefficient of variation for the characterization if considered adequate, that is, to have statistical significance without further analysis, must be 18% for normal efforts and 28% for tangential efforts. The tensile strength parallel to the grain (f_{t0}) property presented a value above that allowed by norm. This may occur due to the inherent variability in the tensile strength test parallel to the fibers (Christoforo et al. 2020, Pertuzzatti et al. 2018), as well as the shape of the rupture, in which it is fragile, as well as the rupture plane in the tested specimen, which can be explained by internal anatomical structure, which demands more studies on such a rupture (Morando et al. 2019). Tab. 2 presents the best adjustments obtained using regression models for the apparent density in the estimation of the other properties, underlining the models considered significant by ANOVA (5% significance).

Tab. 2: Regression models based on apparent density as an estimator of the other properties.

Property	Regression model (ANOVA)	P-value	a	b	R ² (%)
TRR	Logarithmic	0.4200	8.61	- 4.35	6.60
TTR	Linear	0.7518	21.03	- 2.34	1.05
f_{c0}	Exponential	0.2584	26.80	0.62	12.55
f_{t0}	Exponential	<u>0.0001</u>	2.83	3.93	81.21
f_{i90}	Logarithmic	0.3558	9.18	7.20	8.57
f_{v0}	Geometric	0.3696	13.31	- 0.59	8.11
f_{s0}	Linear	0.2681	-0.24	1.49	12.09
f_M	Geometric	0.2604	109.91	0.58	12.46
f_{H0}	Linear	0.8716	105.29	4.65	0.27
f_{H90}	Geometric	0.6216	98.50	- 0.18	2.53
W	Exponential	0.3653	46.49	- 0.86	8.25
E_{c0}	Geometric	0.2345	19459.84	0.74	13.80
E_{t0}	Geometric	<u>0.0136</u>	20118.27	1.68	47.14
E_M	Geometric	0.0801	19453.19	1.02	27.48

The apparent density was considered significant only in the estimate of the tensile strength

parallel to the fibers (f_{t0}) ($R^2 = 81.21\%$) and longitudinal elastic modulus in the tensile parallel to the fibers (E_{t0}) ($R^2 = 47.14\%$), with the exponential and geometric models of best fit for these properties, respectively. Fig. 2 illustrates the two regression models considered significant.

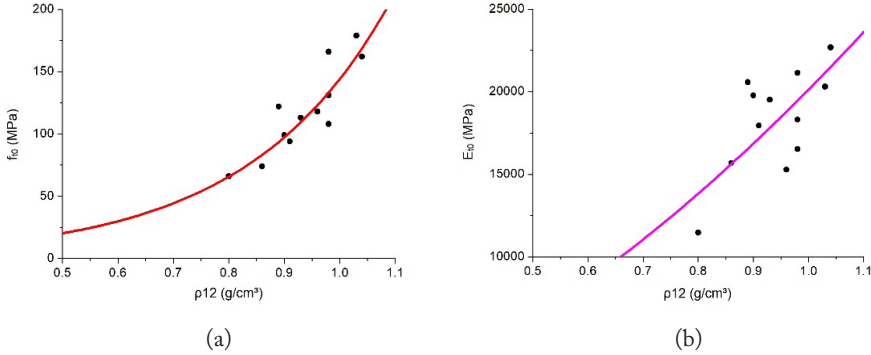


Fig. 2: Graph of the density models as an estimation of the tensile strength (a) and of the longitudinal elastic modulus in the tension (b).

Observing the adjustments considered significant shown in Tab. 3, it can be considered that it is possible to use the apparent density as an estimator of the tensile strength parallel to the fibers due to the high value of the coefficient of determination, with good quality in the adjustment ($R^2 > 70\%$). However, for the tensile modulus it is not possible due to the poor quality of the fit. In several works in the literature it was not possible to find significant relationships between physical and mechanical density and property (Aquino et al. 2018b, Christoforo et al. 2019, Lahr et al. 2016b, Montgomery 2012, Morando et al. 2019, Nogueira et al. 2019).

Tab. 3 illustrates the best adjustments obtained in the estimation of the stiffness properties as a function of the respective strength property.

Tab. 3: Regression models for estimating stiffness properties as a function of strength properties.

Property	Regression model (ANOVA)	P-value	a	b	Expression	R ² (%)
E_{c0}	Logarithmic	<u>0.0001</u>	-57362	19644	$E_{c0} = a + b \cdot \ln(f_{c0})$	79.13
E_{t0}	Geometric	<u>0.0179</u>	2638	0.40	$E_{t0} = a \cdot f_{t0}^b$	44.41
E_M	Logarithmic	0.6964	4600	2954	$E_M = a + b \cdot \ln(f_m)$	1.59

Considering the data in Tab. 3, it appears that the models using the modules of longitudinal elasticity to parallel compression and parallel traction were significant. Based on the quality of the fit, the resistance to parallel compression can be used to estimate the elasticity module to compression parallel to the fibers ($R^2 > 70\%$). As for the longitudinal elastic modulus in traction, this is not possible due to the poor quality of the fit. In the literature, Guarucaia wood specie did not present significant models for estimating the rigidity property as a function of the respective strength (Christoforo et al. 2019). Fig. 3 shows the models considered significant.

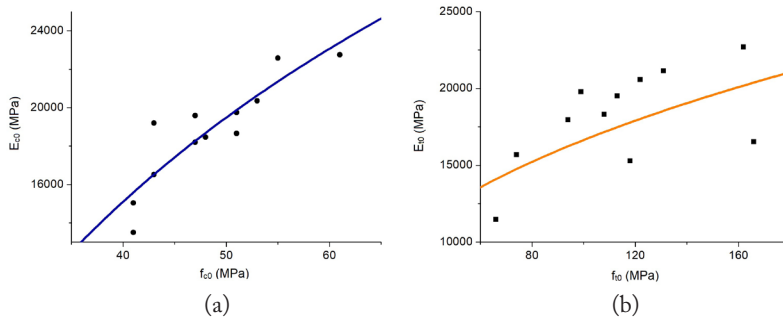


Fig. 3: Graph of the strength (compression and tension parallel to the grain) models as an estimation of the longitudinal elastic modulus on compression (a) and of the longitudinal elastic modulus in the tension (b).

CONCLUSIONS

Based on the results presented in the present research, it is concluded that the characterization of the species *Planchonella pachycarpa* was adequate, following the precepts presented in the Brazilian standard ABNT NBR 7190. The Goiabão species was classified in class C40 of the hardwoods, based on the characteristic value of the compressive strength parallel to the fibers (ABNT 1997). This classification indicates the possibility of using Goiabão wood species for structural purposes. Evaluating the significant regression models, the apparent density can be used to estimate the tensile strength parallel to the fibers as well as to estimate the longitudinal elasticity module to the compression parallel to the fibers as a function of the compressive strength parallel to the fibers. The models showed good quality in the fit, which shows the possibility of use.

ACKNOWLEDGMENT

For all the support provided during the production of this research, the authors thank the Coordination for the Improvement of Higher Education (CAPES) and the National Council for Scientific and Technological Development (CNPq).

REFERENCES

1. ABNT, 1997: Projeto de estruturas de madeira ABNT- Técnicas NBR 7190 (Timber structures design).
2. Almeida, A.S., Criscuolo, G., Almeida, T.H., Christoforo, A.L., Chahud, E., Branco, L.A.M.N., Pinheiro, R.V., Lahr, F.A.R., 2019: Influence of CCA-A Preservative on physical-mechanical properties of Brazilian tropical woods. *BioResources* 14(2): 3030–3041.
3. Almeida, T.H. De, Almeida, D.H., Christoforo, A.L., Chahud, E., Branco, L.A.M.N., Lahr, F.A.R., 2016: Density as estimator of strength in compression parallel to the grain in wood. *International Journal of Materials Engineering* 6(3): 67–71.

4. Aquino, V.B. de M., Almeida, J.P.B., Almeida, D.H., Almeida, T.H., Panzera, T.H., Christoforo, A.L., Lahr, F.A.R., 2018a: Physical and mechanical characterization of *Copaifera* sp. wood specie. *International Journal of Materials Engineering* 8(3): 55–58.
5. Aquino, V.B. de M., Panzera, T.H., Magalhães, L.N., Christoforo, A.L., Lahr, F.A.R., 2018b: Physical and mechanical characterization of *Ocotea* sp. wood specie. *Construindo* 10(2): 31–40.
6. Beech, E., Rivers, M., Oldfield, S., Smith, P.P., 2017: Global tree search: The first complete global database of tree species and country distributions. *Journal of Sustainable Forestry* 36(5): 454–489.
7. Cardoso, C.C., Moutinho, V.H.P., Melo, L. de O., Sousa, L.K.V. dos S., de Souza, M.R., 2012: Caracterização físico-mecânica de madeiras amazônicas com aptidão tecnológica para comercialização (Physical-mechanical characterization of Amazonic woods with technological fitness for commercialization). *Revista de Ciências Agrárias* 55(3): 176–183.
8. Christoforo, A.L., Aftimus, B.H.C., Panzera, T.H., Machado, G. de O., Lahr, F.A.R., 2017: Physico-mechanical characterization of the *Anadenanthera colubrina* wood specie. *Engenharia Agrícola* 37(2): 376–384.
9. Christoforo, A.L., Aquino, V.B.D.M., Wolenski, A.R.V, Araujo, V.A., Lahr, F.A.R., 2019: Evaluation of the *Peltophorum vogelianum* Benth. wood species for structural use. *Engenharia Agrícola* 39(6): 763–768.
10. Christoforo, A.L., Couto, N.G., Almeida, J.P.B., Aquino, V.B.M., Lahr, F.A.R., 2020: Apparent density as an estimator of wood properties obtained in tests where failure is fragile. *Engenharia Agrícola* 40(1): 105–112.
11. Couto, N.G., Aquino, V.B. de M., Almeida, J.P.B., Almeida, D.H. de, Christoforo, A.L., Lahr, F.A.R., 2018: Determination of physical and mechanical properties of wood specie *Dinizia excelsa* Ducke. *International Journal of Materials Engineering* 8(6): 158–161.
12. Dadzie, P.K., Amoah, M., 2015: Density, some anatomical properties and natural durability of stem and branch wood of two tropical hardwood species for ground applications. *European Journal of Wood and Wood Products* 73(6): 759–773.
13. Dias, F.M., Lahr, F.A.R., 2004: Estimativa de propriedades de resistência e rigidez da madeira através da densidade aparente (Estimation of strength and stiffness properties of wood through apparent density). *Scientia Forestalis* (65): 102–113.
14. ISO 13061, 2017: Physical and mechanical properties of wood. Test methods for small clear wood specimens.
15. Komariah, R.N., Hadi, Y.S., Massijaya, M.Y., Suryana, J., 2015: Physical-mechanical properties of glued laminated timber made from tropical small-diameter logs grown in Indonesia. *Journal of the Korean Wood Science and Technology* 43(2): 156–167.
16. Lahr, F.A.R., Aftimus, B.H.C., Arroyo, F.N., Almeida, D.H., Christoforo, A.L., Chahud, E., Branco, L.A.M.N., 2016a: Full characterization of *Vatairea* sp. wood specie. *International Journal of Materials Engineering* 6(3): 92–96.
17. Lahr, F.A.R., Arroyo, F.N., Almeida, T.H., Almeida Filho, F.M., Mendes, I.S., Christoforo, A.L., 2016b: Full characterization of *Erisma uncinatum* Warm wood specie. *International Journal of Materials Engineering* 6(5): 147–150.
18. Lahr, F.A.R., Christoforo, A.L., da Silva, C.E.G., Andrade, J.R., Pinheiro, R.V., 2016c: Evaluation of physical and mechanical properties of Jatobá (*Hymenaea stilbocarpa* Hayne) wood with different levels of moisture content and different regions of extractions. *Revista Arvore* 40(1): 147–154.

19. Lobão, M.S., Lúcia, R.M. Della, Moreira, M.S.S., Gomes, A., 2004: Caracterização das propriedades físico-mecânicas da madeira de eucalipto com diferentes densidades (Characterization of the physico-mechanical properties of eucalyptus wood with different densities). *Sociedade de Investigações Florestais* 28(6): 889–894.
20. Logsdon, N.B., Finger, Z., Estevão, J.G., 2005: Descrição dendrológica e caracterização físico-mecânica da madeira de Amescla-Aroeira, *Protium heptaphyllum* (Aubl.) March. (Burseraceae) (Dendrological description and physical-mechanical characterization of Amescla-Aroeira, *Protium heptaphyllum* (Aubl.) March. (Burseraceae)). *Revista Madeira Arquitetura e Engenharia* 6(17).
21. Lorenzi, H., 1998: Árvores Brasileiras: Manual de identificação de plantas arbóreas nativas do Brasil (Brazilian Trees: Identification Manual of Brazilian Trees). Plantarum, Nova Odessa – SP, Brazil, 352 pp.
22. Machado, J.S., Louzada, J.L., Santos, A.J.A., Nunes, L., Anjos, O., Rodrigues, J., Simões, R.M.S., Pereira, H., 2014: Variation of wood density and mechanical properties of blackwood (*Acacia melanoxylon* R. Br.). *Materials and Design* 56: 975–980.
23. Montgomery, D.C., 2012: Design and analysis of experiments. Wiley, New York, USA, 752 pp.
24. Morando, T.C., Christoforo, A.L., Aquino, V.B. de M., Lahr, F.A.R., Rezende, G.B.M., Ferreira, R.T.L., 2019: Characterization of the wood species *Qualea albiflora* for structural purposes. *Wood Research* 64(5): 769–776.
25. Nascimento, M.F., Almeida, D.H., Almeida, T.H., Christoforo, A., Lahr, F.A.R., 2018: Physical and mechanical properties of sabiá wood (*Mimosa caesalpiniaefolia* Benth.). *Current Journal of Applied Science and Technology* 25(4): 1–5.
26. Nogueira, M.C. de J.A., Almeida, D.H., Araujo, V.A. de, Vasconcelos, J.S., Christoforo, A.L., Almeida, T.H., Lahr, F.A.R., 2019: Physical and mechanical properties of *Eucalyptus saligna* wood for timber structures. *Ambiente Construído* 19(2): 233–239.
27. Pertuzzatti, A., Missio, A.L., de Cademartori, P.H.G., Santini, E.J., Haselein, C.R., Berger, C., Gatto, D.A., Tondi, G., 2018: Effect of process parameters in the thermomechanical densification of *Pinus elliottii* and *Eucalyptus grandis* fast-growing wood. *BioResources* 13(1): 1576–1590.
28. Ruelle, J., Beauchêne, J., Yamamoto, H., Thibaut, B., 2011: Variations in physical and mechanical properties between tension and opposite wood from three tropical rainforest species. *Wood Science and Technology* 45(2): 339–357.
29. Silva, C.E.G., De Almeida, D.H., De Almeida, T.H., Chahud, E., Branco, L.A.M.N., Campos, C.I., Lahr, F.A.R., Christoforo, A.L., 2018: Influence of the procurement site on physical and mechanical properties of *Cupiúba* wood species. *BioResources* 13(2): 4118–4131.
30. Silveira, L.H.C., Rezende, A.V., Vale, A.T. Do., 2013: Teor de umidade e densidade básica da madeira de nove espécies comerciais amazônicas (Moisture content and basic wood density of nine commercial Amazonian tree species). *Acta Amazonica* 43(2): 179–184.
31. ter Steege, H., Mota de Oliveira, S., Pitman, N.C.A., Sabatier, D., Antonelli, A., Guevara Andino, J.E., Aymard, G.A., Salomão, R.P., 2019: Towards a dynamic list of Amazonian tree species. *Scientific Reports* 9(1): 3501.
32. Steege, H. Ter, Vaessen, R.W., Cárdenas-López, D., Sabatier, D., Antonelli, A., Oliveira, S.M., Pitman, N.C.A., Jørgensen, P.M., Salomão, R.P., 2016: The discovery of the Amazonian tree flora with an updated checklist of all known tree taxa. *Scientific Reports* 6: article number 29549.

VINICIUS BORGES DE MOURA AQUINO*, MARCUS VINICIUS PEREIRA DE FREITAS,
CLAUDIA QUEIROZ DE VASCONCELOS
FEDERAL UNIVERSITY OF SOUTHERN AND SOUTHEASTERN PARÁ
TECHNOLOGY FACULTY
SANTANA DO ARAGUAIA, PARÁ, BRAZIL
*Corresponding author: aquino.vini@hotmail.com

JOÃO PAULO BOFF ALMEIDA, FELIPE NASCIMENTO ARROYO,
EDSON FERNANDO CASTANHEIRA RODRIGUES, ANDRÉ LUIS CHRISTOFORO
FEDERAL UNIVERSITY OF SÃO CARLOS
DEPARTMENT OF CIVIL ENGINEERING
SÃO CARLOS, SÃO PAULO, BRAZIL

DIEGO HENRIQUE DE ALMEIDA
FEDERAL UNIVERSITY OF RONDONIA
DEPARTMENT OF CIVIL ENGINEERING
PORTO VELHO, RONDONIA, BRAZIL

SERGIO AUGUSTO MELLO SILVA
SÃO PAULO STATE UNIVERSITY
DEPARTMENT OF CIVIL ENGINEERING
ILHA SOLTEIRA, SÃO PAULO, BRAZIL

DIOGO APARECIDO LOPES SILVA
FEDERAL UNIVERSITY OF SÃO CARLOS
DEPARTMENT OF PRODUCTION ENGINEERING
SOROCABA, SÃO PAULO, BRAZIL

ROBERTO VASCONCELOS PINHEIRO
MATO GROSSO STATE UNIVERSITY
DEPARTMENT OF CIVIL ENGINEERING
SINOP, MATO GROSSO, BRAZIL

FRANCISCO ANTONIO ROCCO LAHR
UNIVERSITY OF SÃO PAULO
DEPARTMENT OF STRUCTURAL ENGINEERING
SÃO CARLOS, SÃO PAULO, BRAZIL

POROSITY AND PORE SIZE DISTRIBUTION OF RECENT AND ANCIENT BURIED *PHOEBE ZHENNAN* WOOD DETERMINED BY MERCURY INTRUSION POROSIMETRY

JIALIN ZHANG, HUI XIAO, YUZHU CHEN, JINQIU QI, JIULONG XIE
XINGYAN HUANG, YONGZE JIANG
¹SICHUAN AGRICULTURAL UNIVERSITY
CHINA

²KEY LABORATORY OF WOOD INDUSTRY AND FURNITURE ENGINEERING
OF SICHUAN PROVINCIAL COLLEGES AND UNIVERSITIES
CHINA

(RECEIVED MARCH 2020)

ABSTRACT

The porosity and pore size distribution of recent and ancient buried *Phoebe zhennan* are studied in this paper by means of mercury intrusion porosimetry. The results show that the micropore and mesopore diameters of recent and buried wood are mainly distributed in range of 40.3 nm and 183.1 nm respectively, while the macropore in 45276.6 nm and 3503.9 nm separately. For both samples, the pores with diameters below 349.9 nm account for about 60% of the total intrusion volume, and contribute more than 98% of the surface area. The cumulative pore area of recent wood is slightly greater and the pore diameter ranges from 50.3 nm to 349.9 nm. While the cumulative pore area of buried wood is significantly larger than and the pore diameter ranges until 50.3 nm. These results can provide information for further investigations on the sorption behaviour and the liquid permeability of ancient buried wood.

KEYWORDS: Porosity, pore structure, *Phoebe zhennan*, ancient buried wood, mercury intrusion porosimetry.

INTRODUCTION

Buried wood refers to dead wood that is more than 50% buried by soil, garbage or ground vegetation through natural disasters such as landslides and river deposits or through excessive growth of ground vegetation (Jianyi et al. 2019, Moroni et al. 2015). The buried wood often persists many centuries (Boutelje and Bravery1968, Kim 1987, 1990) or even thousands of years (Hedges et al. 1985, Hoffmann et al. 1986, Liyama et al. 1988, Meyers et al. 1980).

The process of wood burial appears to occur mainly through two mechanisms (Moroni 2015), rapid burial through catastrophic events such as landslides and fluvial deposition (Eden 1967) or gradual burial of downed deadwood through litter deposition and overgrowth by ground vegetation (Dynesius et al. 2010, Hagemann et al. 2010a, Moroni et al. 2010). Buried wood has different physical and chemical property from that of recently cut wood. The effect of time on the buried wood caused hemicelluloses degradation and a decrease in the crystallinity index and the crystallite length, resulting in an increase in the proportion of amorphous zones (Esteban et al. 2006). Because of this, the equilibrium moisture contents of the buried wood are higher than of the recent wood, both in adsorption and desorption (Esteban et al. 2008). In terms of the thermodynamic properties, the heat involved is greater in the buried wood than in the recent wood (Esteban et al. 2009).

Buried *Phoebe zhenan* (family: Lauraceae, category: *Phoebe*) wood is precious for its beautiful color and pattern, light fragrance, and is widely used in costly furniture manufacturing, handicraft carving and other fields. However, the ancient buried *P. zhenan* wood is hard to dry and easy to crack, which affects its processing and utilization. The deformation and drying characteristics of buried wood are related to its internal structural characteristics, especially the porosity and pore size distribution. At present, the researches on pore size distribution of wood and wood-based products by mercury intrusion porosimetry are studied (Zauer et al. 2014, Pfriend et al. 2009, Plötze and Niemz 2011, Gigac et al. 2017). But the study on the pore characteristics of ancient buried wood is rarely reported. The aim of this research is to study porosity and pore size distribution of recent and ancient buried *P. zhenan*, which can provide useful information, particularly on the liquid permeability, and supply technological characteristics in its industrial processing.

MATERIAL AND METHODS

Recent and ancient buried *P. zhenan* were both provided by a wood company located in Chengdu, Sichuan Province, China. The samples were obtained from an 80-year old *P. zhenan* tree that had been buried for approximately 1500 years, dating by means of conventional radiocarbon, Carbon-14 (14C), radiocarbon dating. Recent samples were obtained from an 86-year old living tree. Both wood samples were placed in room temperature about 20°C conditions for air drying.

Mercury intrusion porosimetry

Porosity and pore size distribution of wood were tested by mercury injection apparatus (AutoPore IV 9500). The samples, with dimensions of 20 × 10 × 10 mm (longitudinal × tangential × radial), were cut by scroll saw from both woods.

Samples were immersed in non-wetting mercury, and measurements were then conducted by two processes of low and high pressure to increase the pressure steadily from 0 to 400 MPa. Mercury progressively intruded into smaller voids under the increased pressure. The pore volume could then be derived from the quantity of the intruded mercury. The pore size distribution can be determined according to Eq. 1 (Washburn 1921):

$$d = - \frac{4\gamma\cos\theta}{p} \quad (1)$$

where: d - pore diameter, p - pressure, γ - surface tension of mercury (0.48 N.m-1), θ - wetting angle of mercury (141°) (Junghans et al. 2005).

RESULTS AND DISCUSSION

The results of the mercury intrusion porosimetry measurements for recent and ancient buried *P. zbennan* samples are showed in Tab. 1.

Tab. 1: Mercury intrusion porosimetry test results of recent and ancient buried *P. zbennan* samples.

<i>Phoebe zbennan</i>	Total intrusion volume (mL·g ⁻¹)	Total pore area (m ² ·g ⁻¹)	Median pore diameter (volume) (nm)	Median pore diameter (area) (nm)	Average pore diameter (4V/A) (nm)	Bulk density at 0.43 psia (g·cm ⁻³)	Porosity (%)
Ancient buried <i>P. zbennan</i>	1.0909	65.44	113.7	34.7	66.7	0.521	56.812
Recent <i>P. zbennan</i>	0.9678	25.95	255.2	55.2	149.2	0.577	55.841

The bulk density (at 0.43 psia) of the buried wood is lower than that of the recent, which may be due to the degradation of cellulose and hemicellulose, so the porosity and total intrusion volume of buried wood are larger (Schniewind 1990). However, the median pore diameter (volume), median pore diameter (area), average pore diameter (4 V/A) of the buried wood are significant lower, indicating that most of the pore in the buried wood is smaller, which caused the total pore area of buried wood is more than 2.5 times larger than that of the recent wood.

Log differential intrusion versus pore diameter of recent and ancient buried *P. zbennan* are showed in Fig. 1. According to the pore size distribution, four pore size classes could be distinguished: macropores (58 μm - 0.5 μm), mesopores (500 nm - 80 nm), and micropores (80 nm - 1.8 nm) (Plötze and Niemz 2011). There are two obvious peaks of recent *P. zbennan*, and the corresponding pore diameter of the two peaks are 45376.6 nm and 183.1 nm. The pore structure of vary structural in hardwoods are showed in Tab. 2 (Butterfield 2006, Stamm 1972, Stamm 1967). It can be seen from the data in the Tab. 2, the pore with diameter of 45376.6 nm is mainly from vessels, while the pore with diameter of 183.1 nm are mainly from pit membranes of bordered pits. Compared with recent *P. zbennan*, the peak of ancient buried *P. zbennan* moves in the direction of small pore diameter and the corresponding pore diameter of vessels are 3503.9 nm and 7244.9 nm, which due to the cell wall of buried wood were obviously compressed and more natural mineral deposits were deposited inside the vessels cavities of the buried wood (Jianyi et al. 2019). The pore diameter of ancient buried *P. zbennan* microcapillary (vessels, cavities of fibers, pit chamber apertures, pit apertures) are smaller than that of the recent *P. zbennan*, which reduces the gas and liquid permeability of the ancient buried *P. zbennan*, and results in water movement, adhesive penetration in ancient buried *P. zbennan* wood difficult. The corresponding pore diameter of pit membranes is 40.3 nm, which due to pit membranes were blocked by natural mineral deposits adhered in cell wall of the buried wood.

Tab. 2: Pore structure in hardwoods.

Structural elements	Diameter	Pore shape
Vessels	20 ~ 400 μm	Tubular
Cavities of fibers	10 ~ 15 μm	Tubular
Pit chamber apertures of bordered pits	4 ~ 30 μm	Ink bottle-like
Pit apertures of bordered pits	400 nm ~ 6 μm	Tubular
Pit membranes of bordered pits	10 nm ~ 8 μm	Polygonous spaces
Cell wall (dried)	2 ~ 100 nm	Slite-like, cylindric, slite-like and cylindric

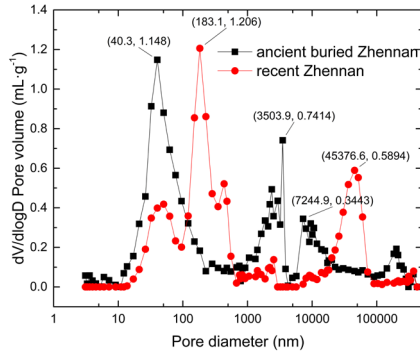


Fig. 1: Log differential intrusion versus pore diameter of recent and ancient buried *P. zhennan*.

Fig. 2 and Fig. 3 show the cumulative pore volume (CPV) and percentage of intrusion volume (PIV) versus pore diameter of recent and ancient buried *P. zhennan*. Fig. 2 indicates that the CPV and PIV of recent *P. zhennan* is greater than that of ancient buried *P. zhennan* in the pore diameter range from 3224.5 nm to 60385.8 nm, which are mainly from vessels, cavities of fibers, pit chamber apertures, pit apertures from the data shown in Tab. 1, and it shows a similar phenomenon in Fig. 3 for the increase of percentage of intrusion volume.

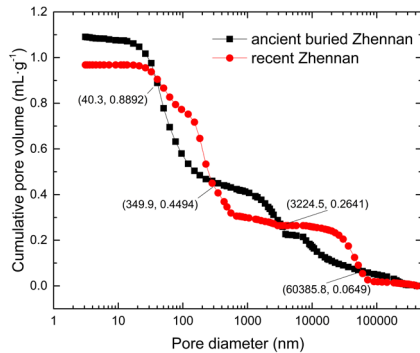


Fig. 2: Cumulative pore volume versus pore diameter of recent and ancient buried *P. zhennan*.

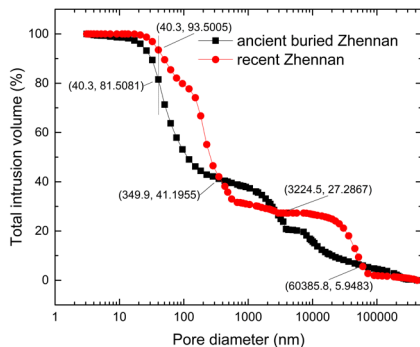


Fig. 3: Percentage of intrusion volume versus pore diameter of recent and ancient buried *P. zhennan*.

The reason is the cell wall of buried wood were obviously compressed and more natural mineral deposits were deposited inside the vessels and fibers cavities of the buried wood, blocking the vessels, cavities of fibers, pit chamber apertures and pit apertures (Jianyi et al. 2019). The compression of cell wall and deposition of the natural mineral lead to the pore diameter range from 349.9 nm to 3224.5 nm of ancient buried *P. zhennan* is more than that of the recent *P. zhennan*, so the CPV and PIV of recent *P. zhennan* is less than that of ancient buried *P. zhennan* in the pore diameter range from 349.9 nm to 3224.5 nm. The pore diameters range from 40.3 nm to 349.9 nm are mainly from pit membranes, the pit membranes of ancient buried *P. zhennan* were blocked by natural mineral deposits, so the CPV and PIV of ancient buried *P. zhennan* in this pore diameter range is less than that of recent *P. zhennan*. The pore diameters less than 40.3 nm are micropores in cell wall, the CPV and PIV of recent *P. zhennan* is more than that of ancient buried *P. zhennan* in this pore diameter range. This due to the microstructure of buried wood is destroyed after the transformation of the natural environment, causing a small amount of cellulose or hemicellulose to be degraded, which leads to the micropores in the cell wall of buried wood is more than that of the recent one (Jianyi et al. 2019).

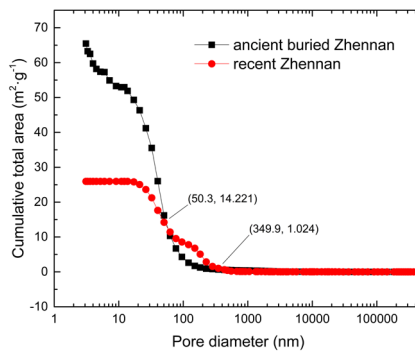


Fig. 4: Cumulative pore area versus pore diameter of recent and ancient buried *P. zhennan*.

Fig. 4 shows the cumulative pore area versus pore diameter of recent and ancient buried *P. zhennan*. It can be known from Fig. 3 and Fig. 4, for both recent ancient buried *P. zhennan* samples, the pores with diameters below 349.9 nm account for about 60% of the total intrusion volume, and contribute more than 98% of the surface area, while the pores with diameters above 349.9 nm account for about 40% of the total intrusion volume, and contribute less than 2% of the surface area. This can be explained by the surface area of micropores is much larger than that of macropores with the same volume. According to the log differential intrusion versus pore diameter of recent and ancient buried *P. zhennan* in Fig. 1, the micropore diameter of recent and ancient buried *P. zhennan* are distributed in 40.3 nm and 183.1 nm respectively, so the cumulative pore area of recent *P. zhennan* is slightly greater than that of ancient buried *P. zhennan* in the pore diameter range from 50.3 nm to 349.9 nm, while the cumulative pore area of ancient buried *P. zhennan* is significantly larger than that of recent *P. zhennan* in the pore diameter range below 50.3 nm, which proved that the degradation of cellulose or hemicellulose leading to the micropores in the cell wall of buried wood is more than that of the recent one.

CONCLUSIONS

The bulk density (at 0.43 psia) of the ancient buried *Phoebe zhenan* is slightly lower than that of the recent *P. zhenan*, while the porosity and total intrusion volume of ancient buried *P. zhenan* are a little larger. However, the median pore diameter (volume), median pore diameter (area), average pore diameter (4V/A) of the ancient buried *P. zhenan* are significantly lower than that of the recent *P. zhenan*, which caused the total pore area of ancient buried *P. zhenan* is more than 2.5 times than that of the recent *P. zhenan*. The micropore diameter of recent and ancient buried *P. zhenan* are main distributed in 40.3 nm and 183.1 nm respectively, while the macropore are main distributed in 45276.6 nm and 3503.9 nm separately. The pore diameter of ancient buried *P. zhenan* macrocapillary is smaller than the that of the recent *P. zhenan*, while pore diameter of ancient buried *P. zhenan* microcapillary is bigger than that of the recent *P. zhenan*. For both recent and ancient buried *P. zhenan* samples, the pores with diameters below 349.9 nm account for about 60% of the total intrusion volume, and contribute more than 98% of the surface area. The cumulative pore area of recent *P. zhenan* is slightly greater than that of ancient buried *P. zhenan* in the pore diameter range from 50.3 nm to 349.9 nm, while the cumulative pore area of ancient buried *P. zhenan* is significantly larger than that of recent *P. zhenan* in the pore diameter range below 50.3 nm.

ACKNOWLEDGEMENTS

The authors gratefully acknowledge the support of Education Fund of Sichuan Provincial Department (16ZB0049) and the Innovative experimental program for College Students of China (04054633).

REFERENCES

1. Boutelje, J.B., Bravery A.F., 1968: Observations on the bacterial attack of piles supporting a Stockholm building. *Journal of the Institute of Wood Science* 20: 47-57.
2. Butterfield, B., 2006: The structure of wood: form and function. Pp 1-22, Primary wood processing, Springer, Dordrecht, Pp.1-22.
3. Dynesius, M., Gibb, H., Hjältén, J., 2010: Surface covering of downed logs: drivers of a neglected process in dead wood ecology. *Plos One* 5(10): e13237.
4. Eden, W.J., 1967: Buried soil profile under apron of an earth flow. *Geological Society of America Bulletin* 78(9): 1183.
5. Esteban, L.G., Fernandez, F.G., Guindeo, C.A., De Palacios, P., Gril, J., 2006: Comparison of the hygroscopic behaviour of 205-year-old and recently cut juvenile wood from *Pinus sylvestris* L. *Annals of Forest Science* 63(3): 309-317.
6. Esteban, L.G., De Palacios, P., Fernandez, F.G., Guindeo, C.A., Cano, N.N., 2008: Sorption and thermodynamic properties of old and new *Pinus sylvestris* wood. *Wood and Fiber Science* 40(1): 111-121.
7. Esteban, L.G., De Palacios, P., Fernandez, F.G., Martín, J.A., Génova, M., Fernández Golfín, J.I., 2009: Sorption and thermodynamic properties of buried juvenile *Pinus sylvestris* L. wood aged 1,170 ± 40 BP. *Wood Science and Technology* 43(7-8): 679-690.
8. Gigac, J., Stankovska, M., Fiserova, M., 2017: Comparison of capillary flow porosimetry and mercury intrusion porosimetry in determination pore size distribution of papers. *Wood Research* 62(4): 587-596.

9. Hagemann, U., Moroni, M.T., Gleißner, J., Makeschin, F., 2010: Accumulation and preservation of dead wood upon burial by bryophytes. *Ecosystems* 13(4): 600–611.
10. Hedges, J.I., Cowie, G.L., Ertel, J.R., Barbour, J.R., Hatcher, P.G., 1985: Degradation of carbohydrates and lignins in buried woods. *Geochimica et Cosmochimica Acta* 49(3): 701–711.
11. Hoffmann, P., Peek, R.D., Puls, J., Schwab, E., 1986: Das Holz der Archäologen. *Holz Als Roh- Und Werkstoff* 44(7): 241–247.
12. Jianyi, J., Zhenzhong, G., Xianfeng, H., Yuanhua, S., Shuqi, C., Jin, S., 2019: Study on thermogravimetric, flammability properties and micromorphology of buried wood. *Materials Research Express* 6(10): 105106.
13. Junghans, K., Niemz, P., Bächle, F., 2005: Untersuchungen zum Einfluss der thermischen Vergütung auf die Porosität von Fichtenholz. *Holz als Roh- und Werkstoff* (63): 243–244.
14. Kim, Y.S., 1990: Chemical characteristics of water-logged archaeological wood. *Holzforschung* 44(3): 169–172.
15. Liyama, K., Kasuya, N., Tuyet, L.T.B., Nakano, J., Sakaguchi, H., 1988: Chemical Characterization of ancient buried wood. *Holzforschung* 42(1): 5–10.
16. Meyers, P.A., Leenheer, M.J., Erstfeld, K.M., Bourbonniere, R.A., 1980: Changes in spruce composition following burial in lake sediments for 10,000 yr. *Nature* 287(5782), Pp 534–536.
17. Moroni, M.T., Morris, D.M., Shaw, C., Stokland, J.N., Harmon, M.E., Fenton, N.J., Merganičová, K., Merganič, J., Okabe, K., Hagemann, U., 2015: Buried wood: A common yet poorly documented form of deadwood. *Ecosystems* 18(4): 605–628.
18. Moroni, M.T., Hagemann, U., Beilman, D.W., 2010: Dead wood is buried and preserved in a Labrador boreal forest. *Ecosystems* 13(3): 452–458.
19. Pfriem, A., Zauer, M., Wagenführ, A., 2009: Alteration of the pore structure of spruce (*Picea abies* (L.) Karst.) and maple (*Acer pseudoplatanus* L.) due to thermal treatment as determined by helium pycnometry and mercury intrusion porosimetry. *Holzforschung* 63(1): 94–98.
20. Plötze, M., Niemz, P., 2011: Porosity and pore size distribution of different wood types as determined by mercury intrusion porosimetry. *European Journal of Wood and Wood Produce* (69): 649–657.
21. Schniewind A.P., 1990: Physical and mechanical properties of archaeological wood. In: Rowell, R.M., Barbour, R.J. (eds): *Archaeological wood: properties, chemistry and preservation, advances in chemistry series 225*. Pp 87–109, American Chemical Society, Washington.
22. Stamm, A.J., 1972: Maximum effective vessel diameters of hardwoods. *Wood Science and Technology* 6(4): 263–271.
23. Stamm, A.J., 1967: Movement of fluids in wood. Part I: Flow of fluids in wood. *Wood Science and Technology* 1(2): 122–141.
24. Washburn, E.W., 1921: Note on a method of determining the distribution of pore sizes in a porous material. *Proceedings of the National Academy of Sciences of the United States of America* 7(4): 115–116.
25. Xie, J.L., Qi, J.Q., Huang, X.Y., Zhou, N., Hu, Y., 2015: Comparative analysis of modern and ancient buried *Phoebe zhenan* wood: surface color, chemical components, infrared spectroscopy, and essential oil composition. *Journal of Forestry Research* 26(2): 501–507.
26. Zauer, M., Hempel, S., Pfriem, A., Mechtcherine, V., Wagenführ, A., 2014: Investigations of the pore-size distribution of wood in the dry and wet state by means of mercury intrusion porosimetry. *Wood Science and Technology* 48(6): 1229–1240.

JIALIN ZHANG, HUI XIAO*, YUZHU CHEN, JINQIU QI, JIULONG XIE,
XINGYAN HUANG, YONGZE JIANG

¹SICHUAN AGRICULTURAL UNIVERSITY
COLLEGE OF FORESTRY

²KEY LABORATORY OF WOOD INDUSTRY AND FURNITURE ENGINEERING
OF SICHUAN PROVINCIAL COLLEGES AND UNIVERSITIES
NO.211, HUIMING ROAD, WENJIANG DISTRICT
CHENGDU CITY, SICHUAN PROVINCE, 611130
CHINA

*Corresponding author: shawwe@126.com

INFLUENCE OF KRAFT LIGNIN ON THE PROPERTIES OF RUBBER COMPOSITES

MATSHIDISO MAKHALEMA¹, PERCY HLANGOTHI¹, SETUMO VICTOR MOTLOUNG^{2,3}
LEHLOHONOLO FORTUNE KOAO⁴, TSHWAFO ELIAS MOTAUNG^{3,5}

¹NELSON MANDELA UNIVERSITY, SOUTH AFRICA

²WALTER SISULU UNIVERSITY

³SEFAKO MAKGATHO HEALTH SCIENCES UNIVERSITY, SOUTH AFRICA

⁴UNIVERSITY OF THE FREE STATE, SOUTH AFRICA

⁵UNIVERSITY OF SOUTH AFRICA, SOUTH AFRICA

(RECEIVED JUNE 2020)

ABSTRACT

The influence of lignin content on reclaimed rubber (RR)/natural rubber (NR) blend composite properties has successfully been studied. Scanning electron microscopy (SEM) were used to understand morphology. Fourier-transform infrared spectroscopy (FTIR) for the possible chemical interaction, whereas thermogravimetric analysis (TGA) and tensile tester were used to predict strength and elongation for possible practical applications. The results indicated that the presence of lignin forms cavities which seemed to arise from complex interactions of the blend with the lignin. Those cavities dominated tensile fractured surface and the increase in lignin indicated inconsistencies of interfacial interactions. Lignin RR/NR blend composites revealed a drop in tensile strength and shift in glass transition temperature, except for the highest lignin containing blend composite. More active interactive constituent of the blend appeared to be NR. The interaction has not favored the thermal stability and crosslinking density.

KEYWORDS: Blend composites, polymer composites, lignin, biomass, lignin-polymer composites.

INTRODUCTION

Recently, there has been renewed interests in the utilization of lignocellulosic components such as cellulose lignin and hemicellulose to advance green applications of materials (Mohomane et al. 2017, Sibiyi et al. 2018). Some researchers compared modified characteristics of celluloses from different sources (Linganiso et al. 2019), whereas some tested potential of the modified surfaces in different polymeric matrices (Sibiyi et al. 2018). Of more interest

is the employment of lignin, a complex, amorphous-thermoplastic material as a filler, modifier and reinforce in polymeric materials such as rubbers and plastics. Due to its abundance and versatility compared to inorganic fillers, lignin has gained a lot of attention (Datta et al. 2017, Frigerio et al. 2014, Yu et al. 2015, Liu et al. 2015, Botros et al. 2005, Barana et al. 2016, Sen et al. 2015). Lignin has been reported to have interesting properties which include flame retardant abilities, antioxidative characteristics, biodegradability, antimicrobial behaviour and adhesive capabilities. Furthermore, the structure of lignin contains a variety of chemical functional groups that positively influence its reactivity, making it able to meet the needs of most rubber industries (Sen et al. 2015, Setua et al. 2000, Jiang et al. 2014, Košíková et al. 2007, Košíková et al. 2005, Gregorová et al. 2006, Kumaran et al. 1978).

A lot of research has been done on the incorporation cellulose to formulate composites that could be applied industrially. For instance, Che et al. (2018) utilized a water-soluble copolymer for wood modification, while Furuno et al. (2004), Klüppel and Mai (2013), Yu et al. (2011) small molecular sizes, low molecular weight urea formaldehyde and phenol formaldehyde resins. Those materials can effectively penetrate through wood micropores and grafting and/or crosslinking with wood cells to enhance the dimensional stability and other properties of wood. Lignin is one component of lignocellulosic material which also received fair attention as a filler in polymer blends. For instance, as a filler in natural rubber (NR) Yu et al. (2015), Setua et al. (2000), Jiang et al. (2014) and Košíková et al. (2005, 2007) studied NR composites filled with sulphur-free lignin under sulphur vulcanization. The addition of lignin up to 30 phr into the NR rubber composites resulted in improved physico-mechanical properties such as 100% increment in modulus, elongation at break and tensile strength. It was also reported that lignin influenced the cure characteristics (increased scorch time and decreased optimum cure time) of the NR compounds. They further demonstrated that the significant improvement in the study was observed when the NR was filled with 20 phr lignin. This observed positive effect on the mechanical properties of NR vulcanizates was attributed to the relatively low molecular mass and polydispersity of the lignin which allowed for a good lignin-NR miscibility. Similar results were observed by Gregorová et al. (2006). They argued that the lignin influences the retention of physico-mechanical properties of non-aged natural rubber system in the small concentrations. Setua et al. (2000) also showed that reinforcing nitrile rubber with modified lignin resulted in better thermal stability when compared against phenolic resins or carbon black. It was shown that lignin is a more capable replacement to the costlier petroleum derived carbon black and phenolics subsequently imparting on the lignin-rubber composite superior oil resistance. Košíková et al. (2007) has demonstrated through SEM micrographs, the morphological properties of NR vulcanizates with and without lignin which showed that lignin enhanced the dispersion of other compounding ingredients in the mix.

There is little or/and no information regarding the influence of lignin on the blend of reclaimed rubber (RR)/ natural rubber (NR). The novelty of this study is based on systematic incorporation of lignin in the blend. The blend composites were analyzed by scanning electron microscopy (SEM), Fourier transform infrared spectroscopy (FTIR) thermogravimetric analysis (TGA) and tensile tester.

MATERIAL AND METHODS

Materials

Kraft (alkali) lignin in the form of brown powder, was obtained from Sigma Aldrich, South Africa. It has average molecular weight of about 10 000. Reclaimed rubber was obtained

from EnvanDe Rubber, Pietermaritzburg, South Africa. It has specific gravity of 1.15, tensile strength of and elongation at break of natural rubber (SMR 20) was obtained from S&N Rubber, Port Elizabeth, South Africa.

Preparation of blends and composites

All samples were prepared by twin roll mill at room temperature for 15 min before hydraulic pressing into sheets. The blend homogeneity was achieved at about 15 min prior lignin addition, at which the time counting of mixing blend composites was started. Preliminary results recommend 90:10 ratio due to homogeneity as confirmed in literature (Sen et al. 2015, Kumaran et al. 1978, Tibenham et al. 1954). A mixture design was used to formulate the different blend composites as shown in Tab. 1 below.

Tab. 1: Formulations used in preparation of lignin-rubber blends and composites by mixed design.

Abbreviations	Reclaimed rubber (g)	Natural rubber(g)	Lignin (%)
RR/NR blend	90	10	0
10 ppfr	90	10	10
20 ppfr o	90	10	20
30 ppfr	90	10	30

Scanning electron microscopy (SEM)

Morphological analysis of the composites was characterised by SEM. The micrographs were taken using an FEI Quanta 200 (FEI Co., Eindhoven, the Netherlands) electron microscope operated at an accelerating voltage of 15 kV. All samples were fractured in liquid nitrogen, sputter-coated with gold and allowed to dry before taking images.

Fourier-transform infrared spectroscopy (FTIR)

The FTIR spectra were collected by using a Perkin Elmer FTIR spectrometer in the diffuse reflectance mode. The samples were analysed in the spectral region between 4000 and 400 cm^{-1} with a 4 cm^{-1} resolution.

Thermogravimetric analysis (TGA)

Thermogravimetric analyses were performed using TGA analyser unit (Perkin Elmer), under flowing nitrogen atmosphere at flow rate of 20 $\text{ml}\cdot\text{min}^{-1}$. Approximately 10-15 mg of sample was heated from 30°C to 700°C at a heating rate of 10°C min^{-1} .

Dynamic mechanical analysis (DMA)

The dynamic mechanical analysis (DMA) Q800 of the PP and composites were investigated from 40 to 180°C by 3-point bending mode with 15 mm sample size at a heating rate of 5°C $\cdot\text{min}^{-1}$ and a frequency of 1 Hz.

Tensile testing

Measurements of tensile strength were carried out on three dumb-bell shaped samples, width of 1 mm using a Universal Testing Machine QC 505 with a crosshead speed of 500 $\text{mm}\cdot\text{min}^{-1}$ and a 500 N load cell. Median values of at least 5 samples per test were used for data analysis

Swelling experiments

Swelling was studied in toluene according to ASTM D 471-79. A sorption-desorption

method was used to determine the swelling behavior of the rubber samples; this being demonstrated as the mole percent uptake of toluene by a gram of rubber at room temperature. The rubber sample was cut into 20 x 20 mm for measuring and calculation of swelling percentage.

RESULTS AND DISCUSSION

Scanning electron microscopy (SEM)

SEM micrographs of the tensile fractured surface of lignin RR/NR blend composites are shown in Fig. 1. The 10 pphr (Fig. 1a) of lignin in the blend composite generally showed smaller pore sizes, compared to 20 pphr (Fig. 1b) and 30 pphr (Fig. 1c), ranging from approximately 50 to 173 μm . Whereas 20 pphr lignin indicated pore sizes ranging from approximately 70 to 400 μm . Surprisingly the pores generally seemed to reduce (most are smaller from 50 to 294 μm) in sizes for the 30 pphr blend composites and the surface appeared rougher. In fact, there are clear potholes or pits in Figs. 1b,c which maybe an indication of a departure of a material during fracturing. There is a limited information on a study involving lignin blend with reclaimed rubber, however Ramarad et al. (2015) studied lignin reinforced rubber composites. Formation of pits, large cavities and grooves were dominating their tensile fractured surface. They related the observation to the interaction of alcohol and phenolic groups in lignin with mostly unvulcanised part of the rubber. The same explanation is highly possible in the current study, however the natural rubber seemed to be more interactive with lignin than the reclaimed rubber. In fact, this is logical because reclaiming rubber is known for reducing molecular weight and promotes a partial degradation that limit pendent groups for more interactions (Barana et al. 2016, Gregorová et al. 2006, Asrul et al. 2014). Therefore, some of pores may have resulted from an escape of natural rubber when interacting with the lignin.

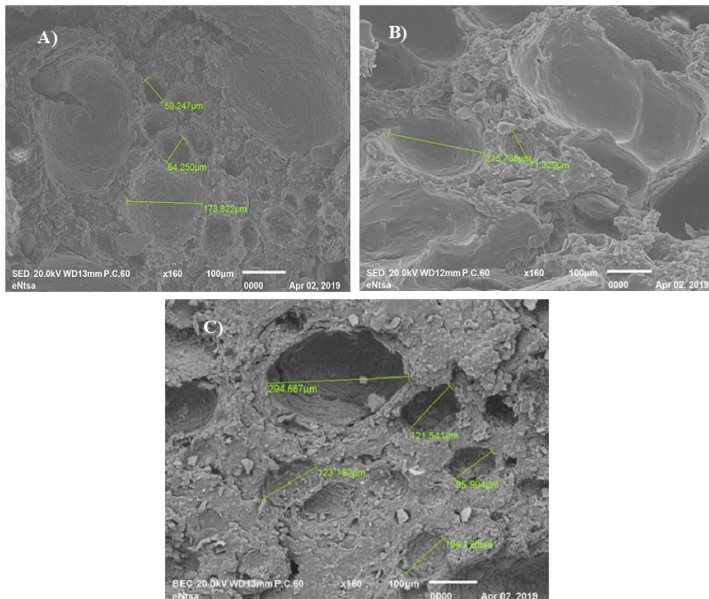


Fig. 1: SEM image of lignin RR/NR blend composites containing: a) 10 pphr, b) 20 pphr, and c) 30 pphr of lignin.

Fourier-transform infrared spectroscopy (FTIR)

FTIR spectra of RR/NR blend and blend composites are presented in Fig. 2. The blend exhibited peaks at $3100\text{--}3000\text{ cm}^{-1}$, $1596\text{--}1680\text{ cm}^{-1}$, and $1384\text{--}1000\text{ cm}^{-1}$ and a hump at 3400 cm^{-1} which are known for CH, C=C, C-C and N-H vibrations respectively (Ramarad et al. 2015, Yu et al. 2015, Liu et al. 2010, Botros et al. 2005). The peaks are typical in literature for a blend of the two rubbers (Ismail et al. 2002). The presence of lignin in the blend generally led to inconsistent effect. For instance, 10 pphr exhibited a suppression of C=C vibrations that seemed to resurrect at highest lignin content. In fact, there are virtually double peaks at approximately 1384 cm^{-1} for all except for 10 pphr containing blend composite. Nonetheless it could be convincing to consider the inconsistencies as the elements of interfacial interaction that promoted pores as seen from SEM.

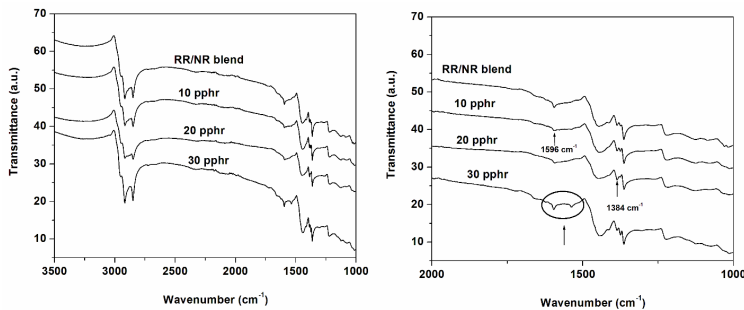


Fig. 2: FTIR spectra of RR/NR blend and lignin RR/NR blend composites.

Thermal gravimetric analysis (TGA)

Fig. 3 shows the TGA and DTG graphs of lignin RR/NR blend composites. The presence of lignin generally decreased the thermal stability of the composites.

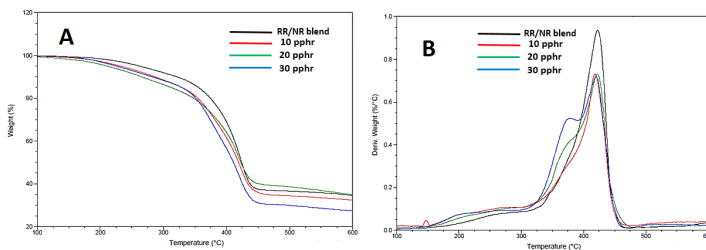


Fig. 3: TGA(A) and DTG (B) graphs of the lignin RR/NR blend composites.

This observation is not extraordinary in literature as a presence of lignin in natural fibres is known for diminishing thermal stability of the fibres. In most cases researchers centralised the rational to phenolic content, low molecular weight and the origin of lignin thereof (Datta et al. 2017, Frigerio et al. 2014, Yu et al. 2015, Liu et al. 2010, Botros et al. 2005, Barana et al. 2016). But in our case, the interfacial interaction appeared to be promoted by compatibility of the lignin and the major phase (see SEM results Fig. 1b,c). That could account for the observed drop in thermal stability. There seems to be no clear order of the lignin content against thermal stability of the blend composites, nonetheless the 30 pphr lignin RR/NR blend composite has

shown lowest thermal stability and char content than the rest. It is worth noting that lignin has a potential to increase char content of the blend composites to almost equal that of the pure blend. In fact, irregular pore sizes and complex interfacial interaction of lignin and reclaimed rubber as confirmed by SEM and FTIR could account for the lack of order in both thermal stability and residual content.

Mechanical properties

The mechanical properties of the blend composites such as tensile strength, elongation at break and modulus were investigated. Fig. 4 shows that with increasing amount of lignin RR/NR blend composites revealed a drop in tensile strength, except for the highest lignin containing blend composite which has shown increased tensile strength that is even higher than of the pure blend composite by almost 40%.

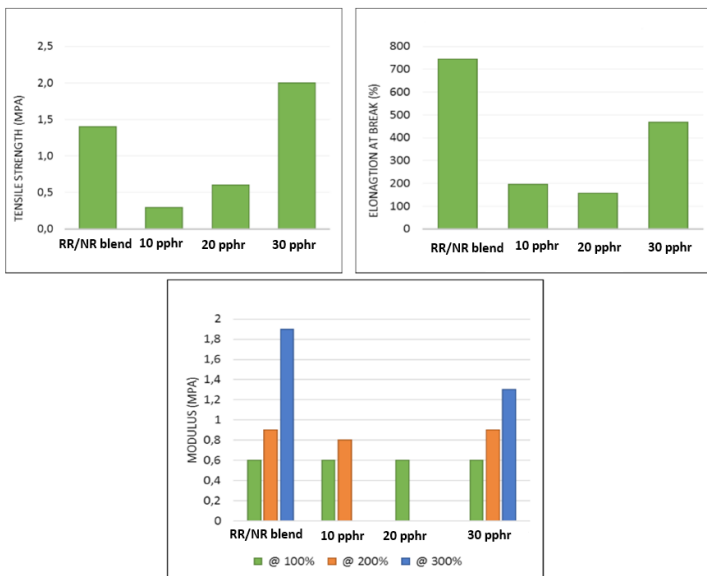


Fig. 4: Mechanical properties of the lignin RR/NR blend composites.

Almost the similar trend was also observed in the case of elongation at break, nonetheless in opposite direction for each content. For instance, the elongation at break of the clean blend composite decreased by more than 50% compared to 10 and 20 pphr and almost 45% for 30 pphr lignin containing blend composites. Moduli were measured at 100%, 200%, and 300% elongation. There was no much changes in modulus at 100% elongation, but at 300% elongation there was a surprise decrease in modulus of 30 pphr blend composites compared to the clean blend. This could be the results of inconsistencies as the elements of interfacial interaction and formation of pores as confirmed by SEM and FTIR. In fact, such defects are known for promoting lowering molecular weight of NR to shorter segments for a reduced tensile strength in RR/NR blend composites (Premachandra et al. 2011, Datta et al. 2017, Frigerio et al. 2014, Yu et al. 2015, Liu et al. 2010). Therefore, it may be virtually fair in this study to regard lignin as a contributing agent that lowered molecular weight of NR to render reduced

mechanical properties of the blend composites. Furthermore, SEM suggested the formation of the pores which are known for lowering a load transfer within the rubber matrix. In fact, Kumaran et al. (1978) explain it as a reduced elastic behavior of the elastomer by the addition of lignin.

Dynamic mechanical analysis (DMA)

The DMA analysis was used to characterize the dynamic mechanical behaviour of the prepared lignin rubber composites. The variation of tangent delta ($\tan \delta$) and storage modulus (E') as a function of temperature are reported in Fig. 5.

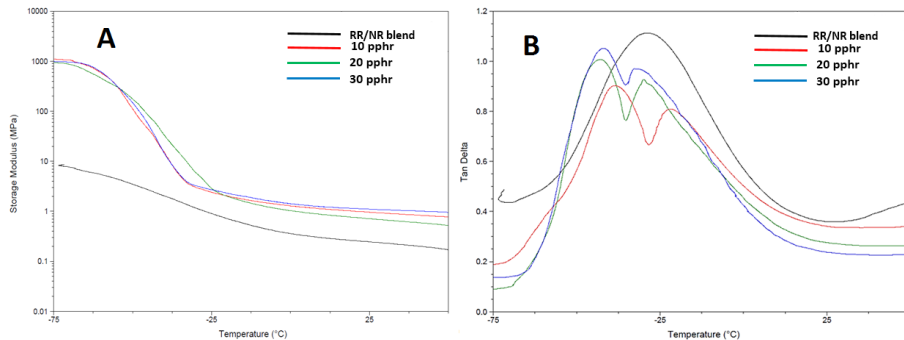


Fig. 5: Storage modulus and $\tan \delta$ curves of RR-NR-LG composites.

The figure shows the influence of lignin on the storage modulus and damping of RR-NR blends. The addition of lignin resulted in the increase in storage modulus and that can be explained by reduced chain mobility due to the lignin addition. This is in agreement with the mechanical properties particularly the highest containing lignin composite that indicated increased storage modulus. As shown in Fig. 4, the $\tan \delta$ curves revealed that the RR-NR-LG composites exhibit two glass transition temperatures. One occurring at low temperatures is associated to RR-NR blends and the second at high temperatures corresponds to the lignin. Both the T_g s slightly shifted to higher temperatures with increasing lignin loading. Furthermore, it can be observed that the $\tan \delta$ peak values decreased each by approximately 10% with the increase in lignin content, suggesting a continuous decrease in rubber chain mobility and this is due to the strong interaction between the lignin and RR-NR matrix.

Crosslink density

Fig. 6 represents blend and lignin blend composites. The presence of lignin generally increased the crosslinking density except for the highest lignin containing blend composite.

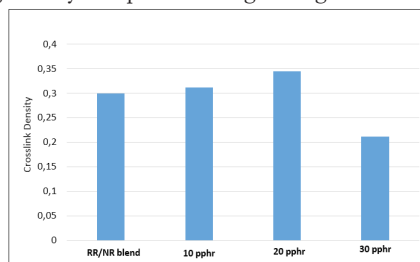


Fig. 6: Crosslinking density of the lignin RR/NR blend composites.

There was no much change in crosslinking density, nonetheless 30pphr blend composite revealed a decrease in the density by almost 40%. For 20 pphr, the observed slight increase in crosslinking density could have emanated from the complex interaction of lignin with the crosslinking sites. This is could be confirmed by suppression of C=C vibrations that seemed to revive at highest lignin content and disappearance of a peak observed from FTIR and/or cavities from SEM. It is recorded in literature that a material with a higher crosslinking density could have high thermal stability apparently due to crosslinking sites which delay a chain mobility (Ismail et al. 2002, Rattanasom et al. 2005, Yahya et al. 2011, Košíková et al. 2007). The explanation clarifies somehow TGA results in this study because it has the similar trend to crosslinking density. By the way modulus also has shown decline at 30 pphr. Perhaps lowering molecular weight of NR to shorter segments also confirms the loss of crosslinking site which rendered lower density ultimately.

CONCLUSIONS

The effect of the lignin on properties of reclaimed rubber/natural rubber blend composites were successfully prepared and investigated. SEM revealed clear pores which varied in sizes which according to FTIR emanated from the presence of the symmetric aromatic skeletal vibration by lignin macromolecules. Of course, the pores resulted into the general decrease in mechanical properties to almost 50% and crosslinking density of reclaimed rubber/natural rubber blend composites. On the other hand, the observation is a resilient proposal that the lignin could be a potential foam agent in the blend without a blowing agent. The presence of lignin has also resulted in a general decrease in thermal stability. In fact, is worth noting that lignin has a potential to increase char content of the blend composites significantly. The observed char content trend provokes some applications for flame retardants material.

REFERENCES

1. Brinchi, L., Cotana, F., Fortunati, E., Kenny, J.M., 2013: Production of nano-crystalline cellulose from lignocellulosic biomass: Technology and applications. *Carbohydrates Polymers* 94: 145-169.
2. Ramarad, S., Khalid, M., Ratnam, C.T., Chuah, A.L., Rashmi, W., 2015: Waste tire rubber in polymer blends: A review on the evolution, properties and future. *Progress in Materials Science* 72: 100-40.
1. Ismail, H., Nordin, R., Noor, A.M., 2002: Cure characteristics, tensile properties and swelling behaviour of recycled rubber powder-filled natural rubber compounds. *Polymer Testing* 21(5): 565-9.
2. Ismail, H., Nordin, R., Noor, A.M., 2003: The effects of recycle rubber powder content and various vulcanization systems on curing characteristics and mechanical properties of natural rubber/recycle rubber powder blend. *Iranian Polymer Journal* 12: 373-380.
3. Rattanasom, N., Poonsuk, A., Makmoon, T., 2005: Effect of curing system on the mechanical properties and heat aging resistance of natural rubber/tire tread reclaimed rubber blends. *Polymer Testing* 24(6): 728-32.
4. Hassan, M.M., Mahmoud, G.A., El-Nahas, H.H., Medhat, M., Ghada, A., Hussien, H., El-Sayed, A., Hegazy, H.A., 2007: Reinforced material from reclaimed rubber/natural rubber, using electron beam and thermal treatment. *Journal of Applied Polymer Science* 104(4): 2569-78.

5. Premachandra, J.K., Edirisinghe, D.G., De Silva, M.I., 2011: A novel reclaiming agent for ground rubber tyre (GRT). Part 1: Property evaluation of virgin natural rubber (NR)/novel reclaimed GRT blend compounds. *Progress in Rubber, Plastic and Recycling Technology* 27(1): 31-48.
6. Sombatsompop, N., Kumnuantip, C., 2003: Rheology, cure characteristics, physical and mechanical properties of tire tread reclaimed rubber/natural rubber compounds. *Journal of Applied Polymer Science* 87(10): 1723-31.
7. Sreeja, T.D., Kutty, S.K., 2000: Cure characteristics and mechanical properties of natural rubber/reclaimed rubber blends. *Polymer-Plastics Technology and Engineering* 39(3): 501-12.
8. Farahani, T.D., Bakhshandeh, G.R., Abtahi, M., 2006: Mechanical and viscoelastic properties of natural rubber/reclaimed rubber blends. *Polymer Bulletin* 56(4-5): 495-505.
9. Yahya, Y.R., Azura, A.R., Ahmad, Z., 2011: Effect of curing systems on thermal degradation behaviour of natural rubber (SMR CV 60). *Journal of Physical Science* 22(2): 1-4.
10. Valášek, P., Müller, M., Ružbarský, J., 2014: Using recycled rubber particles as filler of polymers. *Applied Mechanics and Materials* 616: 260-267.
11. Datta, J., Parcheta, P., Surówka, J., 2017: Softwood-lignin/natural rubber composites containing novel plasticizing agent: Preparation and characterization. *Industrial Crops and Products* 95: 675-85.
12. Frigerio, P., Zoia, L., Orlandi, M., Hanel, T., Castellani, L., 2014: Application of sulphur-free lignins as a filler for elastomers: effect of hexamethylenetetramine treatment. *Bioresource Technology* 9(1): 1387-400.
13. Yu, P., He, H., Jiang, C., Wang, D., Jia, Y., Zhou, L., Jia, D.M., 2015: Reinforcing styrene butadiene rubber with lignin-novolac epoxy resin networks. *Express Polymer letters* 9(1).
14. Liu, S., Cheng, X., 2010: Application of lignin as antioxidant in styrene butadiene rubber composite. *AIP Conference Proceedings* 1: 344-347.
15. Botros, S.H., Eid, M.A., Nageeb, Z.A., 2005: Thermal stability and dielectric relaxation of NR/soda lignin and NR/thiolignin composites. *Egyptian Journal of Solids* 28(1):1-67.
16. Barana, D., Ali, S.D., Salanti, A., Orlandi, M., Castellani, L., Hanel, T., Zoia, L., 2016: Influence of lignin features on thermal stability and mechanical properties of natural rubber compounds. *ACS Sustainable Chemistry and Engineering* 4(10): 5258-67.
17. Sen, S., Patil, S., Argyropoulos, D.S., 2015: Thermal properties of lignin in copolymers, blends, and composites: a review. *Green Chemistry* 17(11): 4862-87.
18. Setua, D.K., Shukla, M.K., Nigam, V., 2000: Lignin reinforced rubber composites. *Polymer Composites* 21(6): 988-995.
19. Jiang, C., He, H., Yao, X., Yu, P., Zhou, L., Jia, D., 2014: Self-crosslinkable lignin/epoxidized natural rubber composites. *Journal of Applied Polymer Science* 131(23).
20. Košíková, B., Gregorová, A., Osvald, A., Krajčovičová, J., 2005: Role of lignin filler in stabilization of natural rubber-based composites. *Journal of Applied Polymer Science* 103(2): 1226-31.
21. Košíková, B., Gregorová, A., 2005: Sulfur-free lignin as reinforcing component of styrene-butadiene rubber. *Journal of Applied Polymer Science* 97(3): 924-9.
22. Gregorová, A., Košíková, B., Moravčík, R., 2006: Stabilization effect of lignin in natural rubber. *Polymer Degradation and Stability* 91(2): 229-33.
23. Kumaran, M.G., De, S.K., 1978: Utilization of lignins in rubber compounding. *Journal of Applied Science* 22(7): 1885-93.

24. Asrul, M., Othman, M., Zakaria, M., Nazir A.K., 2014: Morphology, tensile strength and oil resistance of gum rubber sheets prepared from lignin modified natural rubber. *EDP Sciences Journals* 13: 1-6.
25. Tibenham, F.J., Grace, N.S., 1954: Compounding natural rubber with lignin and humic acid. *industrial and engineering chemistry* 46(4): 824-8.
26. Chigondo, F., Shoko, P., Nyamunda, B.C., Guyo, U., Moyo, M., 2013: Maize stalk as reinforcement in natural rubber composites. *International Journal of Scientific and Technology Research* 2(6): 263-71.
27. Barana, D., Ali, S.D., Salanti, A., Orlandi, M., Castellani, L., Hanel T., Zoia, L., 2016: Influence of lignin features on thermal stability and mechanical properties of natural rubber compounds. *ACS Sustainable Chemistry and Engineering* 4(10): 5258-67.
28. Yu, P., He, H., Jia, Y., Tian, S., Chen, J., Jia, D., Luo, Y., 2016: A comprehensive study on lignin as a green alternative of silica in natural rubber composites. *Polymer Testing* 54: 176-85.
29. Tanasi, P., Santana, M.H., Carretero-González, J., López-Manchado, M.A., 2019: Thermo-reversible crosslinked natural rubber: A Diels-Alder route for reuse and self-healing properties in elastomers. *Polymer* 175: 15-24.
30. De, D., Panda, P.K., Roy, M., Bhunia, S., 2013: Reinforcing effect of reclaim rubber on natural rubber/polybutadiene rubber blends. *Materials and Design* 46: 142-50.
31. Che, W., Xiao, Z., Han, G., Zheng, Z., Xie, Y., 2018: Radiata pine wood treatment with a dispersion of aqueous styrene/acrylic acid copolymer. *Holzforschung* 72(5): 387-396.
32. Furuno, T., Imamura, Y., Kajita, H., 2004: The modification of wood by treatment with low molecular weight phenol-formaldehyde resin: a properties enhancement with neutralized phenolic-resin and resin penetration into wood cell walls. *Wood Science and Technology* 37(5): 349-361.
33. Yu, X., Sun, D., Li, X., 2011: Preparation and characterization of urea-formaldehyde resinsodium montmorillonite intercalation-modified poplar. *Journal of Wood Science* 57(6): 501-506.
34. Klüppel, A., Mai, C., 2013: The influence of curing conditions on the chemical distribution in wood modified with thermosetting resins. *Wood Science and Technology* 47(3): 643-658.
35. Mohomane, S.M., Linganiso, L.Z., Buthelezi, T., Motaung, T.E., 2017: Effect of extraction period on properties of sugarcane bagasse and softwood chips cellulose. *Wood Research* 62: 931-938.
36. Sibiya, N.N., Mochane, M.J., Motaung, T.E., Linganiso, L.Z., Hlangothi, S.P., 2018: Morphology and properties of sugarcane bagasse cellulose- natural rubber composites. *Wood Research* 63: 821-832.
37. Linganiso, L.Z., Buthelezi, T., Motaung, T.E., 2019: A comparative study of sugarcane bagasse and soft wood. *Wood Research* 64: 273-28.

MATSHIDISO MAKHALEMA, PERCY HLANGOTHI
NELSON MANDELA METROPOLITAN UNIVERSITY
DEPARTMENT OF CHEMISTRY
P.O. BOX 77000
PORT ELIZABETH 6031
SOUTH AFRICA

SETUMO V. MOTLOUNG
SEFAKO MAKGATHO HEALTH SCIENCES UNIVERSITY
DEPARTMENT OF PHYSICS
P.O. BOX 94, MEDUNSA 0204
SOUTH AFRICA
WALTER SISULU UNIVERSITY
DEPARTMENT OF CHEMICAL AND PHYSICAL SCIENCES
PRIVATE BAG XI, MTHATHA CAMPUS, UNITRA 5117
SOUTH AFRICA

LEHLOHONOLO KOAO
UNIVERSITY OF THE FREE STATE (QWAQWA CAMPUS)
DEPARTMENT OF PHYSICS
PRIVATE BAG XI3, PHUTHADITJHABA 9866
SOUTH AFRICA

TSHWAFO E. MOTAUNG*
UNIVERSITY OF SOUTH AFRICA
DEPARTMENT OF CHEMISTRY
SCHOOL OF SCIENCE IN THE COLLEGE OF SCIENCE
ENGINEERING AND TECHNOLOGY
UNIVERSITY OF SOUTH AFRICA
PRELLER STREET, MUCKLENEUK RIDGE, CITY OF TSHWANE
P.O. BOX 392, UNISA 0003
SOUTH AFRICA
SEFAKO MAKGATHO HEALTH SCIENCES UNIVERSITY
DEPARTMENT OF CHEMISTRY
P.O. BOX 94, MEDUNSA 0204
SOUTH AFRICA

*Corresponding author: motaungte@live.com

INTERNAL CAUSE ANALYSIS OF DAMAGE OF WOODEN COMPONENTS IN DANXIA TEMPLE ANCIENT ARCHITECTURES: TREE SPECIES

YAN YANG

NANYANG INSTITUTE OF TECHNOLOGY
CHINA

HE SUN

SOUTHWEST FORESTRY UNIVERSITY
CHINA

SHUANG YANG

HENAN UNIVERSITY MINSHENG COLLEGE
CHINAAIFENG WANG, RUI ZHAO, WEI WANG, YIMING HE, BIN LI
BINXIN ZHANG, QIAN WU
NANYANG INSTITUTE OF TECHNOLOGY
CHINA

(RECEIVED MAY 2020)

ABSTRACT

In the study, part of degraded wooden components of Danxia Temple ancient architectures in China were identified through the bright field microscope, and chemical compositions in cell walls were observed using polarized and fluorescence lights, respectively. The results showed that samples were belonged to *Quercus* spp., *Ulmus* spp., *Salix* spp., and *Populus* spp., respectively. Cellulose composition in *Quercus* spp. was seriously consumed by brown decay fungi, cellulose and lignin compositions in *Ulmus* spp. were consumed by white decay fungi under polarized and fluorescence light observations. All of these four kind of tree species themselves were easily vulnerable to be attacked by insects.

KEYWORDS: Danxia Temple ancient architectures, wooden components, wood identification, analysis of damage by fungi and insects, polarized light, fluorescence.

INTRODUCTION

Danxia Temple, founded in AD 824 and located at Liushan town, Nanzhao county, Nanyang city, Henan province, China, is listed as the national key cultural relic conservation unit. At present, part of the wooden components have been damaged by fungi and insects. Normally, the damage of harmful organisms would cause changes of anatomical structure (Wilcox 1970, Highley et al. 1987, Koyani et al. 2014, Wang et al. 2017, Bari et al. 2019), and degradations of chemical composition (Ferraz et al. 1995, Arias et al. 2010, Witomski et al. 2012, Witomski et al. 2013, Karami et al. 2013, Bari et al. 2019), thereby decrease the quality of its physical and mechanical properties (Ferraz et al. 1995, Choi et al. 2006, Arias et al. 2010, Koyani et al. 2014, Wang et al. 2017, Bari et al. 2019, Li et al. 2019, Brischke et al. 2019, Gao et al. 2019, Chang et al. 2020). These changes eventually decrease the residual mechanical strength of wooden components and affect the quality and life span of ancient architectures. Studying on wood identification and analysis of damage reasons can provide reference and guidance for the future maintenance and reinforcement of the degraded wooden components of the Danxia Temple.

In the present study, the microscopic structures of the wooden components in the Danxia Temple ancient architectures were observed through a bright field microscope to identify the tree species. The extent of damage of these wooden components were observed using polarized light and fluorescence microscopes, respectively. In general, the higher the brightness of the crystalline cellulose birefringence is, the higher the cellulose content is (Zhai et al. 2014, Kanbayashi 2016, Cui et al. 2016b, Yang et al. 2020), and the greater the brightness of green fluorescence intensity is, the higher the lignin density and concentration is (Xu et al. 2009, Yoshizawa et al. 2000, Ma et al. 2011, Wang et al. 2012, Nakagawa et al. 2012, Ma et al. 2013, Cui et al. 2016a,b, Liu et al. 2017a,b, Kiyoto et al. 2018, Yang et al. 2020). Such observations of cellulose and lignin contents and their distributions in the cell walls would provide important data support and theoretical basis for cause analysis of damage, and the maintenance and reinforcement of the Danxia Temple ancient architectures in the future.

MATERIAL AND METHODS

Materials

The samples were collected from the wooden components of the Danxia Temple ancient architectures in Nanzhao County, Nanyang City, Henan Province, China. All the wooden component samples, Nos. 3-1, to 3-12, were obtained from the surface of twelve wooden column' roots, respectively. Due to the dark black color of these wooden components, detailed observations of the macroscopic structural characteristics was not possible. Therefore, only the microscopic structural characteristics could be observed and described in detail.

Treatment of the sample

For air exhausting the small samples were placed into the vacuum dryer to drain the air within the wood samples. For infiltration the samples were immersed into 20%, 40%, 60%, 80%, and 100% polyethylene glycol (PEG) aqueous solution successively (molecular weight = 2000). The process was conducted in an oven at 60°C for 48 h every gradient, in which 100% PEG aqueous solution was infiltrated twice. For PEG embedding the samples were placed at the bottom of the embedding mold. Then, 100% PEG aqueous solution was added to the samples, and the set-up was covered with a plastic embedding box. The embedding box was placed inside the freezer for about 10 min.

Sample slicing

The embedded samples were sliced with microtome (SM2000R, Laika company). Each slice was about 10 μm in thickness and included the transverse, radial, and tangential sections. The slices were placed inside a baking machine at 60°C for about 60 min in order to remove the extra water. The slices were dehydrated in 50%, 75%, 95%, and 100% ethanol solution; each concentration treatment lasted for 10 min. Then the slices were defatted in dimethylbenzene solution for 3 min and neutral gum was used to seal the slices after all the treatments. To avoid the effect of dye on polarized light and fluorescence, all slices were not dyed with red O dye.

Observations via bright-field microscopy

The prepared slices were observed and photographed under a biological digital microscope (ECLIPSE 80i, Nikon Company). To complete the identification of these wood components, their microscopic characteristics were recorded according to the *Chinese Timber Records* (Cheng et al. 1992) and the *IAWA list of microscopic features for hardwood identification* (IAWA Committee 1989).

Observation via polarized light and fluorescence microscopy

The prepared slices were observed and photographed under a polarizing and fluorescent microscope (ECLIPSE 80i, Nikon Company). The cell wall deformations of these wood components was analyzed using a bright-field light microscope. Meanwhile, the cellulose distribution and content in the wooden components were analyzed using a polarized light microscope. The lignin distribution and content in wood components were analyzed using a fluorescence microscope (the blue light excitation with 515 nm to 560 nm) to determine the degree of decay of the wooden components (Cui et al. 2016b).

RESULTS AND DISCUSSION

Wood identification and analysis of damage of samples Nos. 3-1, 3-2, and 3-6

Fig. 1 shows the microstructures of sample Nos. 3-1, 3-2, and 3-6. Based on these microstructures, the distribution of vessels with circular and oval circles on the transverse section was that of ring-porous wood, the arrangement of late wood vessels was stream-shape radial pattern, and the combination was mainly exclusively solitary (90% or more). There were almost no or few of tyloses and gums in vessels. The type of perforations was simple perforation plate, and the type of intervessel pits was alternate. No helical thickening of vessels was found throughout the body of vessel elements. Vasicentric tracheids were abundant. An abundance of apotracheal axial parenchymas consisted of diffuse, diffuse-in-aggregates, and narrow bands or lines up to three cells wide with prismatic crystals of more than 15 cells were found. The cell walls of the wood fibers, which were fibrous tracheid with distinctly bordered pits, ranged from thin to thick. Wood rays were non-storied and had rays of two distinct sizes. These rays consisted exclusively of uniseriate rays and larger rays commonly > 10-seriate, the height of which could exceed the range of slices. All ray cells were procumbent cells, and no special cells were found in ray cells. Moreover, no axial and radial intercellular canals was found in these woods. These findings were in good agreement with the microstructures of red oak presented by Yang et al. (2020).

On the basis of the microstructure observations (Figs. 1a,b,c), we concluded that sample Nos. 3-1, 3-2, and 3-6 belonged to red oak wood (*Quercus* spp.) (Fagaceae) (Cheng et al. 1992).

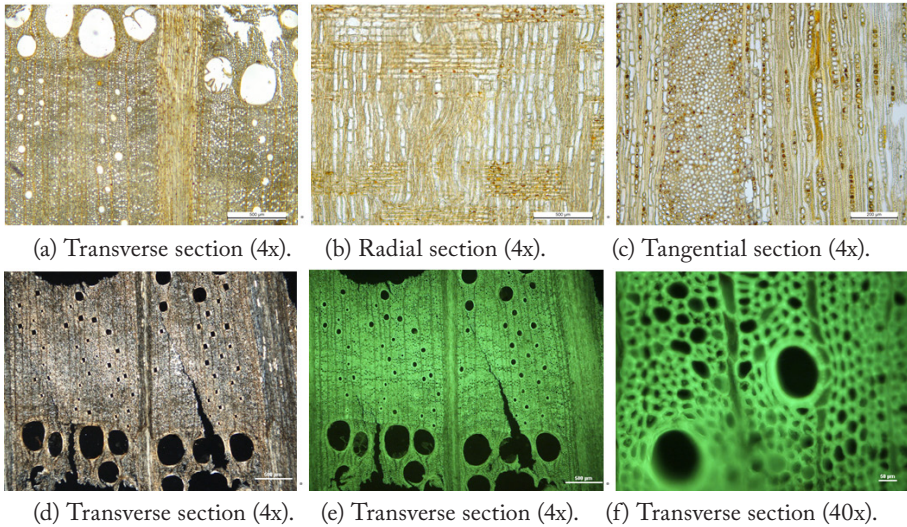


Fig. 1: Microstructures of sample Nos. 3-1, 3-2 and 3-6: (a),(b),(c) under bright-field light, (d) under polarized light, (e) and (f) under fluorescence light.

Red oak woods have many excellent characteristics, such as, straight grain, heavy basic density (about 0.70 g.cm^{-3}), high hard, strength and impact toughness, but contain high shrinkage, and low resistance to decay fungi compared to white oak wood (Cheng et al. 1992). Under polarized light (Fig. 1d), the brightness of crystalline cellulose birefringence of vessel and wood fiber cell walls was almost not observed both in the early wood and the late wood, indicating that the cellulose composition was severely consumed by decay fungi. Under fluorescence light (Figs. 1e,f), the brightness of fluorescence of vessel and wood fiber cell walls was evident both in early wood and late wood, indicating an abundant amount of lignin composition retained in vessels and wood fibers. Moreover, the fluorescence in the micro-area distribution of lignins was still stronger in the cell corner layer (CC layer) than that in the compound middle lamellar layer (CML layer) and the secondary wall layer (S layer) of fiber cell walls (Fig. 1f). This finding is consistent with the micro-area distribution of lignin in other researches (Yoshizawa et al. 2000, Xu et al. 2009, Ma et al. 2011, Nakagawa et al. 2012, Wang et al. 2012, Ma et al. 2013, Cui et al. 2016a, Liu et al. 2017a, Liu et al. 2017b, Kiyoto et al. 2018). According to the observations, we speculated that cellulose composition was seriously consumed by brown decay fungi which they preferred to assume cellulose composition and retain lignin composition (Guo et al. 2015).

One of the important reasons for the serious decay of red oak wooden components is closely related to the lack of protection of tyloses in vessels. Due to the existence of an abundant of tyloses in white oak woods, these woods have excellent anti-decay, anti-insect, and water resistance properties (Cheng et al. 1992) and are often used as red wine barrel, architecture, and furniture materials. In comparison, red oak woods are not used in these aspects. In addition to vulnerability to decay fungi, red oak woods are especially vulnerable to be attacked by insects, such as domestic longhorn beetles (*Stromatium longicorne*) (Cerambycidae) and powder-pest beetle (*Minthea rugicollis*) (Lyctidae) etc. (Cheng et al. 1992). However, almost no difference has been found in their macro-and micro-structures except for tylose between red oak and white

oak woods. Thus, the ancient architects of Nanyang could not provide an accurate distinction when selecting materials to be used in Danxia Temple ancient architectures, thus leading to the serious decay and damage by insects several years later.

Wood identification and analysis of damage of samples Nos. 3-4, and 3-9

Fig. 2 shows the microstructures of sample Nos. 3-4, and 3-9 of the wooden components. As shown in these microstructures, the distribution of vessels was that of ring-porous wood. Early vessels with one to three cells of width were circular, oval circle, and orbicular-ovate on the transverse section, and tyloses were contained in many vessels. The arrangement of late vessels was tangential wavy bands, and the combinations were mainly clusters common, and a few of exclusively solitary and radial multiples. The type of perforations was simple perforation plate, and the type of intervessel pits was alternate. Helical thickening of late vessels was found throughout the body of vessel elements. Many paratracheal axial parenchymas were found, and these were vascentric, diffuse-in-aggregates, and wavy banded parenchyma that were more than three cells of width. Wood rays with 2-6 cells of width were non-storied, All ray cells were procumbent cells, and no special cells were found in ray cells. Moreover, no axial and radial intercellular canals was found in these woods.

On the basis of the microstructure observations (Figs. 2a,b,c), we concluded that sample Nos. 3-4, and 3-9 belonged to elm wood (*Ulmus* spp.) (Ulmaceae) (Cheng et al. 1992).

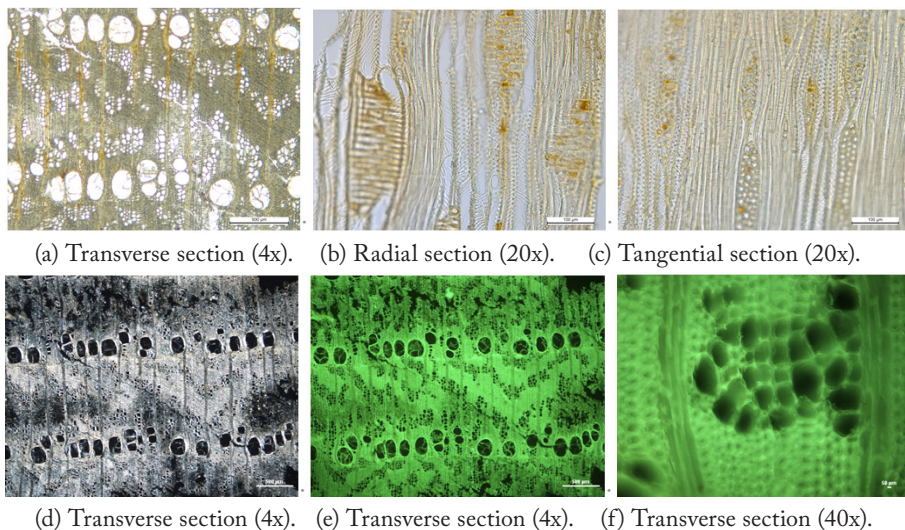


Fig. 2: Microstructures of sample No. 3-4, and 3-9: (a),(b),(c) under bright-field light, (d) under polarized light, (e) and (f) under fluorescence light.

Elm woods have many excellent characteristics, such as, straight grain, medium structure, medium shrinkage, beautiful pattern, but contain low basic density (about $0.45 \text{ g}\cdot\text{cm}^{-3}$), low strength, easy to crack, and low resistance to decay fungi and insects (Cheng et al. 1992). Under polarized light (Fig. 2d), the brightness of crystalline cellulose birefringence of vessel and wood fiber cell walls was evidently observed except for that in part of late wood fibers, indicating that part of cellulose composition were consumed by decay fungi. Under fluorescence light (Figs. 2e,f), the brightness of fluorescence in part of wood fiber cell walls was also not evident, indicating that part of lignin composition was consumed. Moreover, the fluorescence

in the micro-area distribution of lignins was still stronger in the CC layer than that in the CML layer and the S layer of fiber cell walls (Fig. 2f). This finding is consistent with the micro-area distribution of lignin in red oak wood in this research and in other researches (Yoshizawa et al. 2000, Xu et al. 2009, Ma et al. 2011, Nakagawa et al. 2012, Wang et al. 2012, Ma et al. 2013, Cui et al. 2016 a, Liu et al. 2017 a, Liu et al. 2017b, Kiyoto et al. 2018). According to the observations, we speculated that cellulose and lignin compositions were consumed by white decay fungi which they consumed not only cellulose and hemicellulose compositions but also lignin composition (Guo et al. 2015).

Elm woods are suitable for furniture due to beautiful pattern. Because elms are native tree species, taking into account the principle of proximity, they were widely used in ancient architectures by ancient architects of Nanyang city. The property of low resistance to decay fungi and insects led to the serious damage after several years later

Wood identification and analysis of damage of samples Nos. 3-3, 3-7, 3-8, and 3-12

Fig. 3 shows the microstructures of sample Nos. 3-3, 3-7, 3-8, and 3-12 of the wooden components. As shown in these microstructures, the distribution of vessels with orbicular-ovate and oval circle on the transverse section was that of diffuse-porous wood, whereas the arrangement of vessels was diffuse. Furthermore, the combinations of vessels were mainly exclusively solitary and a few of radial multiples of two to four cells. No tyloses and gums were found in the vessels. No helical thickening of vessels was found throughout the body of vessel elements. The type of perforation was simple perforation plate. The type of intervessel pits was alternate. A few of marginal and diffuse-in-aggregates axial parenchymas were found. The cell walls of wood fibers with distinctly simple pits were thin. Wood rays were non-storied, ray cells with one cell of width was upright and procumbent. No special cells and gums were found in the ray cells. No axial and radial intercellular canal was found in these woods.

On the basis of the microstructure observations (Figs. 3a,b,c), we concluded that sample Nos. 3-3, 3-7, 3-8, and 3-12 belonged to willow wood (*Salix* spp.) (*Salicaceae*) (Cheng et al. 1992).

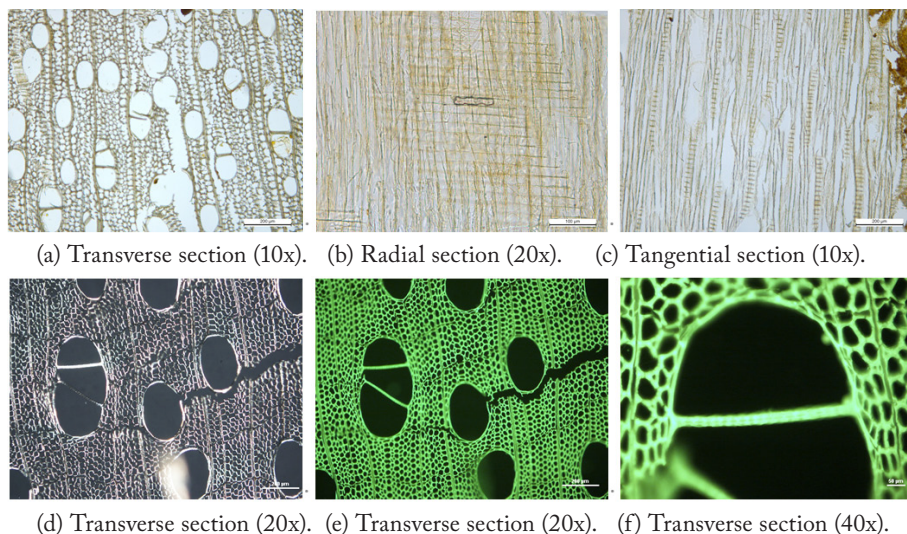


Fig. 3: Microstructures of sample No. 3-3, 3-7, 3-8, and 3-12: (a),(b),(c) under bright-field light, (d) under polarized light, (e) and (f) under fluorescence light.

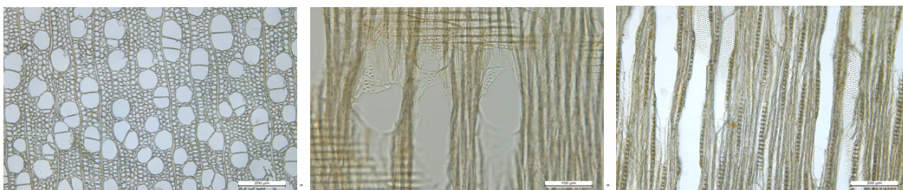
Willows grow fast, and are highly absorbent. The living standing willows are not resistant to decay fungi and insects, so hollow phenomenon occur common. The willow woods have many excellent characteristics, such as, straight grain, fine and smooth structure, low shrinkage, but contain low basic density (about $0.40 \text{ g}\cdot\text{cm}^{-3}$) and strength, low resistance to decay fungi and insects (Cheng et al. 1992). Under polarized light (Fig. 3d), the brightness of crystalline cellulose birefringence of vessel and wood fiber cell walls was evidently observed, indicating that the cellulose composition still retained in vessels and wood fibers. Under fluorescence light (Figs. 3e,f), the brightness of fluorescence of the cell walls of vessels and wood fibers was also evident, indicating that an abundant of lignin composition existed in vessels and wood fibers. Moreover, the fluorescence in the micro-area distribution of lignins was still stronger in the CC layer than that in the CML layer and the S layer of fiber cell walls. This finding is consistent with the micro-area distribution of lignin in red oak and elm woods in this research and in other researches (Yoshizawa et al. 2000, Xu et al. 2009, Ma et al. 2011, Nakagawa et al. 2012, Wang et al. 2012, Ma et al. 2013, Cui et al. 2016a, Liu et al. 2017a,b, Kiyoto et al. 2018). According to the observation, we speculated that cellulose and lignin compositions were not consumed by decay fungi.

Because willows are native tree species, taking into account the principle of proximity, they were widely used in ancient architectures by the ancient architects of Nanyang city. The property of low resistance to insects was an important internal cause of serious damage.

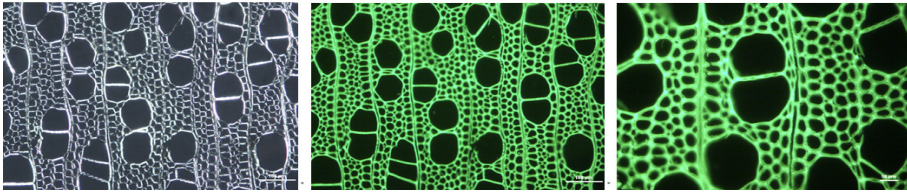
Wood identification and analysis of damage of samples Nos. 3-5, 3-10, and 3-11

Fig. 4 shows the microstructures of sample Nos. 3-5, 3-10, and 3-11 of the wooden components. As shown in these microstructures, the distribution of vessels with orbicular-ovate and oval circle on the transverse section was that of diffuse-porous wood or semi-ring-porous, whereas the arrangement of vessels was radial pattern. Furthermore, the combinations of vessels were mainly radial multiples of two to four cells and a few of solitary. No tyloses and gums were found in the vessels. No helical thickening of vessels was found throughout the body of vessel elements. The type of perforation was simple perforation plate. The type of intervessel pits was alternate. A few of marginal and diffuse-in-aggregates axial parenchymas were found. The cell walls of wood fibers with distinctly simple pits was thin. Wood rays were non-storied, all ray cells was procumbent and one cell of width. No special cells and gums were found in the ray cells. No axial and radial intercellular canal was found in these woods.

On the basis of the microstructure observations (Figs. 4 a,b,c), we concluded that sample Nos. 3-5, 3-10, and 3-11 belonged to poplar wood (*Populus* spp.) (*Salicaceae*) (Cheng et al. 1992).



a) Transverse section (10x). (b) Radial section (20x). (c) Tangential section (10x).



d) Transverse section (20x). (e) Transverse section (20x). (f) Transverse section (40x).

Fig. 4: Microstructures of sample No. 3-5, 3-10, and 3-11: (a),(b),(c) under bright-field light, (d) under polarized light, (e) and (f) under fluorescence light.

Poplars grow fast, the moisture content of raw woods are quite high, the wet heartwood phenomena are especially obvious almost in all poplar trees. And the living standing poplars are not resistant to decay fungi and insects. Especially in spring, we can always hear woodpeckers pecking at insects on poplar trees. The poplar woods have many excellent characteristics, such as, straight grain, fine and smooth structure, low shrinkage, but contain low basic density (about $0.35 \text{ g}\cdot\text{cm}^{-3}$), low strength and impact toughness, and low resistance to decay fungi and insects (Cheng et al. 1992). Under polarized light (Fig. 4d), the brightness of crystalline cellulose birefringence of vessel and wood fiber cell walls was evidently observed, indicating that the cellulose composition still retained in vessels and wood fibers. Under fluorescence light (Figs. 4e,f), the brightness of fluorescence of vessel and wood fiber the cell walls of was also evident, indicating that an abundant of lignin composition existed in vessels and wood fibers. Moreover, the fluorescence in the micro-area distribution of lignins was still stronger in the CC layer than that in the CML layer and the S layer of fiber cell walls. This finding is consistent with the micro-area distribution of lignin in red oak, elm and willow woods in this research and in other researches (Yoshizawa et al. 2000, Xu et al. 2009, Ma et al. 2011, Nakagawa et al. 2012, Wang et al. 2012, Ma et al. 2013, Cui et al. 2016a, Liu et al. 2017a,b, Kiyoto et al. 2018). According to the observation, we speculated that cellulose and lignin compositions were not consumed by decay fungi. Poplar woods are suitable for pulp, fibreboard, particleboard, packing box, toothpick and so on, but not suitable for buildings. Because poplars are native tree species, taking into account the principle of proximity, they were widely used in ancient buildings by the ancient architects of Nanyang city. The property of low resistance to insects resulted in the serious damage after several years later.

Different tree species have different ability to resist decay, some have high ability to resist decay such as, white oak woods, softwoods, etc.; others are low, such as, red oak, elm, willow, poplar woods in this paper. In addition to vulnerability to decay fungi and insects themselves, an important reason might be that these wooden components did not be treated with preservative and insect-resist agents prior to use, thus leading to the serious decay and damage by insects several years later.

CONCLUSIONS

Sample Nos. 1-12 from the wood components of the Danxia Temple ancient architecture were identified and the reason of damage by fungi and insects were analysed. The conclusions are as follows: (1) On the basis of the microstructure observations, we concluded that sample Nos. 3-1, 3-2, and 3-6 belonged to *Quercus* spp. According to the observations under polarized

light and fluorescence light, we speculated that the cellulose composition was seriously consumed by brown decay fungi. In additional, red oak woods themselves are easily vulnerable to be attacked by insects. (2) On the basis of the microstructure observations, we concluded that sample Nos. 3-4, and 3-9 belonged to *Ulmus* spp. According to the observations under polarized light and fluorescence light, we speculated that cellulose and lignin compositions were consumed by white decay fungi. In additional, elm woods themselves are easily vulnerable to be attacked by insects. (3) On the basis of the microstructure observations, we concluded that sample Nos. 3-3, 3-7, 3-8, and 3-12 belonged to *Salix* spp. According to the observations under polarized light and fluorescence light, we speculated that cellulose and lignin compositions were not consumed by decay fungi, but were attacked by insects due to its themselves vulnerability to insects. (4) On the basis of the microstructure observations, we concluded that sample Nos. 3-5, 3-10, and 3-11 belonged to *Populus* spp. According to the observations under polarized light and fluorescence light, we speculated that cellulose and lignin compositions were not consumed by decay fungi, but were attacked by insects due to Willow woods themselves are easily vulnerable to be attacked by insects due to its themselves vulnerability to insects

ACKNOWLEDGMENT

The authors gratefully acknowledge financial supports from Natural National Science Foundation of China (31700481), Cross-science Research Project of Nanyang Institute of Technology, Scientific Research Start-up Projects of Nanyang Institute of Technology, and Humanities and Social Sciences Research Project of Henan Province (2021-ZZJH-252).

REFERENCES

1. Arias, M.E., Rodríguez, J., Pérez, M.I., Hernández, M., Polvillo, O., González-Pérez, J.A., González-Vila, F.J., 2010: Analysis of chemical changes in *Picea abies* wood decayed by different *Streptomyces* strains showing evidence for biopulping procedures. *Wood Science and Technology* 44(2): 179-188.
2. Bari, E., Daryaei, M.G., Karim, M., Bahmani, M., Schmidt, O., Woodward, S., Ghanbary, M.A.T., Sistani, A., 2019: Decay of *Carpinus betulus* wood by *Trametes versicolor* - An anatomical and chemical study. *International Biodeterioration and Biodegradation* 137: 68-77.
3. Brischke, C., Stricker, S., Meyer-Veltrup, L., Emmerich, L., 2019: Changes in sorption and electrical properties of wood caused by fungal decay. *Holzforschung* 73(5): 445-455.
4. Chang, L., Rong, B.M., Xu, G., Meng, Q., Wang, L., 2020: Mechanical properties, components and decay resistance of *Populus davidiana* bioincised by *Coriolus versicolor*. *Journal of Forestry Research* 31: 2023-2029.
5. Cheng, J.Q., Yang, J.J., Liu, P., 1992., China Forestry Publishing House. Chinese timber records. Pp 295, 577, 583, and 688.
6. Choi, J.W., Choi, D.H., Ahn, S.H., Lee, S.S., Kim, M.K., Meier, D., Faix, O., Scott, G.M., 2006: Characterization of trembling aspen wood (*Populus tremuloides* L.) degraded with the white rot fungus *Ceriporiopsis subvermispora* and MWLs isolated thereof. *Holz als Roh- und Werkstoff* 64(5): 415-422.
7. Cui, H.S., Yang, S.M., Liu, X.E., Ma, J.F., Tian, G.L., 2016a: Chemical composition and lignin distribution of *Salix integra*. *Chemistry and Industry of Forest Products* 36(5): 120-126.
8. Cui, X.J., Qiu, J., Gao, J.R., 2016b: Evaluation of the decay level and reinforcement of

- ancient wood by fluorescence and polarizing technology. *Sciences Of Conservation And Archaeology* 28(4): 48-53.
9. Ferraz, A., Durán, N., 1995: Lignin degradation during softwood decaying by the ascomycete *Chrysonilia sitophila*. *Biodegradation* 6(4): 265-274.
 10. Gao, S., Yue, X.Q., Wang, L.H., 2019: Effect of the degree of decay on the electrical resistance of wood degraded by brown-rot fungi. *Canadian Journal of Forest Research* 49: 145-153.
 11. Guo, M.L., Lan, H.F., Qiu, J., 2015: Wood deterioration and preservation. China Metrology Publishing House. Beijing, Pp 167-168.
 12. Highley, T.L., Murmanis, L.L., 1987: Micromorphology of degradation in Western hemlock and sweetgum by the white-rot fungus *Corioliolus versicolor*. *Holzforschung* 41(2): 67-71.
 13. IAWA Committee. 1989: IAWA list of microscopic features for hardwood identification. IAWA Bull. Leiden, 226 pp.
 14. Kanbayashi, T., Miyafuji, H., 2016: Effect of ionic liquid treatment on the ultrastructural and topochemical features of compression wood in Japanese cedar (*Cryptomeria japonica*). *Scientific Reports* 6: 1-8.
 15. Karami, L., Schmidt, O., Fromm, J., Klinberg, A., Schmitt, U., 2013: Wood decay characterization of a naturally-infected oak wood bridge using PY-GC/MS. *Wood Research* 58(4): 591-598.
 16. Kiyoto, S., Yoshinaga, A., Fernandez-Tendero, E., Day, A., Chabbert, B., Takabe, K., 2018: Distribution of lignin, hemicellulose, and arabinogalactan protein in hemp phloem fibers. *Microscopical Society of Canada* 24(4): 442-452.
 17. Koyani, R.D., Rajput, K.S., 2014: Light microscopic analysis of *Tectona grandis* L.f. wood inoculated with *Irpex lacteus* and *Phanerochaete chrysosporium*. *European Journal of Wood and Wood Products* 72(2): 157-164.
 18. Li, S., Gao, Y., Brunetti, M., Macchioni, N., Nocetti, M., Palanti, S., 2019: Mechanical and physical properties of *Cunninghamia lanceolata* wood decayed by brown rot. *Forest* 12: 317-322.
 19. Liu, C.W., Su, M.L., Zhou, X.W., Zhao, R.J., Lu, J.X., Wang, Y.R., 2017a: Analysis of content and distribution of lignin in cell wall of transgenic poplar with fourier infrared spectrun (FTIR) and confocal laser scanning microscopy (CLSM). *Spectroscopy and Spectral Analysis* 37(11): 3404-3408.
 20. Liu, X.E., Jin, K.X., Cui, H.S., Ma, J.F., 2017b: The lignin topochemistry of *Daemonorops margaritae* (Hance) Becc. by molecular spectroscopic imaging. *Spectroscopy and Spectral Analysis* 37(10): 3138-3144.
 21. Ma, J.F., Ji, Z., Zhou, X., Zhang, Z.H., Xu, F., 2013: Transmission electron microscopy, fluorescence microscopy, and confocal raman microscopic analysis of ultrastructural and compositional heterogeneity of *Cornus alba* L, wood cell wall. *Microscopy and Microanalysis* 19(1): 243-253.
 22. Ma, J.F., Yang, G.H., Mao, J.Z., Xu, F., 2011: Characterization of anatomy, ultrastructure and lignin microdistribution in *Forsythia suspensa*. *Industrial Crops and Products* 33(2): 358-363.
 23. Nakagawa, K., Yoshinaga, A., Takabe, K., 2012: Anatomy and lignin distribution in reaction phloem fibres of several Japanese hardwoods. *Annals of Botany* 110(4): 897-904.
 24. Wang, D., Peng, L.M., Fu, F., Song, B.Q., Liu, M.H., 2017: Changes of microscopic structures and sound absorption properties of decayed wood. *Wood Research* 62(4): 529-538.
 25. Wang, Y.R., Xing, X.T., Ren, H.Q., Yu, Y., Fei, B.H., 2012: Distribution of lignin

- in Chinese fir branches determined microspectrometer ultraviolet. Spectroscopy and Spectral Analysis 32(6): 1685-1688.
26. Wilcox, W.W., 1970: Anatomical changes in wood cell walls attacked by fungi and bacteria. Botanical Review 36(1): 1-28.
 27. Witomski, P., Radomski, A., Zawadzki, J., Tomaszewski, W., 2013: Variation in cellulose properties in the common pine (*Pinus sylvestris* L.) wood during white- and brown-rot decay induced by *Coniophora puteana* and *Trametes versicolor* fungi. Wood Research 58(2): 165-172.
 28. Witomski, P., Zawadzki J., Radomski A., 2012: Changes of the pine wood (*Pinus sylvestris* L.) chemical composition during white- and brown-rot decay originated from chosenfungi species. Wood Research 57(3): 463-468.
 29. Xu, F., Mao, J.Z., Jones, G.L., Sun, R.C., 2009: Ultrastructure and lignin distribution in fiber cell walls of *Caragana korshinskii* normal wood and tension wood. Transactions of china pulp and paper 24(4): 15-18.
 30. Yang, Y., Sun, H., Li, B., Han, L., Wang, A.F., Wang, W., He, Y.M., Zhao, R. 2020: Study on the identification and the extent of decay of the wooden components in the Xichuan Guild Hall ancient architectures. International Journal of Architectural Heritage 6: 1-10.
 31. Yang, Y., He, Y.M., Han, L., Wang, A.F., Wang, W., Zhao, R., Li, B., 2020: Application of histochemical stains for rapid qualitative analysis of the lignin content in multiple wood species. BioResources 15(2): 3524-3533.
 32. Yoshizawa, N., Inami, A., Miyake, S., Ishiguri, F., Yokota, S., 2000: Anatomy and lignin distribution of reaction wood in two Magnolia species. Wood Science and Technology 34(3): 183-196.
 33. Zhai, S.C., Horikawa, Y., Imai, T., Sugiyama, J., 2014: Cell wall ultrastructure of palm leaf fibers. IAWA Journal 35(2): 127-137.

YAN YANG*

NANYANG INSTITUTE OF TECHNOLOGY

¹SCHOOL OF ARCHITECTURE

²HENAN KEY LABORATORY OF ZHANG ZHONGJING FORMULAE

AND HERBS FOR IMMUNOREGULATION

CHANGJIANG ROAD 80#, WANCHENG DISTRICT

NANYANG

CHINA

*Corresponding author: yangyanrainy@163.com

HE SUN

SOUTHWEST FORESTRY UNIVERSITY

COLLEGE OF MATERIAL SCIENCE

AND ENGINEERING

BAILONG ROAD 300#, PANGLONG DISTRICT

KUNMING

CHINA

SHUANG YANG
HENAN UNIVERSITY MINSHENG COLLEGE
SCHOOL OF ECONOMICS
JINMIN STREET, LONGTING DISTRICT
KAIFENG
CHINA

AIFENG WANG, RUI ZHAO, WEI WANG, YIMING HE, BIN LI,
BINXIN ZHANG, QIAN WU
NANYANG INSTITUTE OF TECHNOLOGY
SCHOOL OF ARCHITECTURE
CHANGJIANG ROAD 80#, WANCHENG DISTRICT
NANYANG
CHINA

BENDING CHARACTERISTICS OF LAMINATED WOOD COMPOSITES CONSTRUCTED WITH BLACK PINE WOOD AND ARAMID FIBER REINFORCED FABRIC

ABDURRAHMAN KARAMAN
USAK UNIVERSITY
TURKEY

MEHMET NURI YILDIRIM
KARABUK UNIVERSITY
TURKEY

ONDER TOR
KASTAMONU UNIVERSITY
TURKEY

(RECEIVED APRIL 2020)

ABSTRACT

The aim of this study was to determine the 4-point bending strength and modulus of elasticity in bending of Black pine wood laminated materials reinforced with aramid fiber was bonded using epoxy or polyurethane glues separately. The samples were prepared in accordance with the TS 5497 EN 408 (2006). The results of the study determined that the highest value for static bending strength was found in the laminated wood samples ($83.94 \text{ N}\cdot\text{mm}^{-2}$) that were prepared using inter-layer aramid fiber reinforced polymer (AFRP) and epoxy glue. The highest value of modulus of elasticity in bending was found in the samples prepared with inter-layer epoxy and AFRP ($10311.62 \text{ N}\cdot\text{mm}^{-2}$). It was observed that the samples parallel to the glue line of the laminated material showed higher performance compared to those perpendicular to the glue line. The data obtained as a result of this study demonstrated that aramid fiber reinforced Black pine wood laminated materials can be used in the building industry as building materials.

KEYWORDS: Wood laminate, bending strength, modulus of elasticity, aramid fiber fabric, Black pine wood.

INTRODUCTION

Wood as a natural material is vulnerable to attack by biotic agents, such as fungi or insects, and abiotic agents such as fire. The damage caused by these conditions, or new load or design alternations, can require an increase in the load-carrying capacity of the structure (Arriaga et al. 2002) which weaken its mechanical properties. To overcome the inferior mechanical properties of wood elements, fiber reinforced polymer (FRP) composite can be one of the solutions (Johns et al. 2000). Recently, FRP applications have started to be used in strengthening wooden structures, as in strengthening steel and reinforced concrete structures. In wooden structures, the element is sized according to the type of joining. The advantage of using high performance jointing systems is to use less volume of material with the same durability. Over time, wooden structures need to be strengthened due to reasons such as eliminating the damage caused by external factors and earthquakes, increasing the load bearing capacity of the building by restoration, preventing the early fatigue and breaks that may occur as a result of design mistakes (Alsheghri et al. 2019).

There are various strengthening methods applied during the production of laminated wood material. Metal materials as well as synthetic fibers are also used for strengthening purposes. According to Laufenberg et al. (1984), the first trials on strengthening wood or wood-based composite materials were conducted in the 1960s. Strengthening wood with synthetic fibers was first carried out by Wangaard (1964) and Biblis (1965). Among the studies in the literature regarding strengthening the majority have been conducted on polymer composites reinforced with glass fibers, carbon fibers and aramid fibers of wood materials.

The commonly utilized FRP composites as reinforcement for wood beams are carbon fiber reinforced polymer (CFRP), E-glass reinforced polymer (GFRP) and aramid fiber reinforced polymer (AFRP) (Tautanji 1999, Johns et al. 2000, Fiorelli et al. 2003, Lopez et al. 2003, Fiorelli et al. 2006, Dempsey et al. 2006, Fiorelli et al. 2011, Yahyaei et al. 2011, Alshurafa et al. 2012, Abu-Talib 2012, Osmannezhad et al. 2014, Yerlikaya 2014, Morales et al. 2015, Glisovic et al. 2016, Song et al. 2017, Yerlikaya 2019). Various experimental studies have shown that the reinforcement of wood material provides a wide range of improvement of load bearing capacity, elasticity and ductility (Amy et al. 2004, Buell et al. 2005, Li et al. 2009, Fiorelli et al. 2011, Komán et al. 2013, Nowak et al. 2013, Kánnár et al. 2014, Fedyukov et al. 2017, Essert et al. 2018, Krisztián et al. 2020).

Recently, the appearance on the market of new products such as carbon fiber or aramid and basalt fibers have increased the number of researches works on their implementation as reinforcement materials in timber elements (Romani et al. 2001, Borri et al. 2005). Aramid fiber is a well-known synthetic organic polymer fibre with the lowest specific gravity and highest tensile strength - to weight ratio of all reinforcing fibres. As such, aramid fibres are widely used in industry, especially in military and aerospace applications (Mallick 1993). Aramid fiber is one of the common fiber types used to hybridize carbon/epoxy composite due to its low density, high stiffness, high deformability, and high resistance to impact damage (Yayun et al. 2017). Aramid fibers have also been used to hybridize glass fiber and carbon fiber-reinforced epoxy composites for maintaining or improving stiffness and impact damage resistance (Gustin et al. 2005, Valenca et al. 2015, Priyanka et al. 2017).

The current research was outlined to address the creep response of solid wood and AFRP composites under constant load and environmental conditions, individually and in a combined mode (Plevris et al. 1995). A study by Yahyaei-Moayyed and Taheri (2011), defined the elasticity performance of Southern Scots pine and Douglas fir lumber beams strengthened with one-sided aramid fiber-reinforced polymer (AFRP) boards with short-term experimental and numerical

research. The effect of the strengthening on the resistance of elasticity for the strengthened beams was also explained. An increase in AFRP-strengthened wood beams increased both the resistance and the hardness and effectively decreased the elastic deterioration of wooden beams (Yahyaei-Moayyed and Taheri 2011). Zhou et al. (2020), studied bond integrity of aramid, basalt and carbon fiber reinforced polymer bonded wood composites at elevated temperature. Cheon et al. (2020) studied on the stab resistance mechanism and performance of the carbon, glass and aramid fiber reinforced polymer and hybrid composites.

In the present study, aramid fiber reinforced polymer (AFRP), which is used to strengthen hose plastic and ballistic materials, was used in hydraulic systems that showed resistance under the influence of external forces. This study aimed to determine the four-point bending strength of Black pine (*Pinus nigra*) laminated wood materials reinforced with AFRP and the modulus of elasticity in bending. The utilization of AFRP in strengthening the Black pine laminated wood material constitutes to the originality of this study.

MATERIAL AND METHODS

The Black pine wood (*Pinus nigra*) used to prepare the test samples, was obtained randomly from timber enterprises in the Karabuk, Turkey. Careful attention was paid to the fact that the wood material used in experimental studies was not subjected to physical damage, mechanical impacts or biological harm.

Aramid fiber reinforced polymer (AFRP) was purchased from a private manufacturer (Dost Chemistry Tuzla, Istanbul) in Turkey. The aramid fibers are a class of heat-resistant and strong synthetic fibers and used in aerospace and military applications, for ballistic-rated body armor fabric and ballistic composites, marine hull reinforcement, and as an asbestos substitute. Aramid fibers possess a unique combination of high strength and modulus with low density and high elongation that results in improved impact resistance of the respective composites. Aramid fibers are the dominant reinforcement in fiber-reinforced polymers (FRP) for demanding applications in aerospace industry where excellent mechanical properties per unit weight are required (Denchev and Dencheva 2012). The density of the AFRP, which is a material that has high resistance to abrasion, impact, fracture, increased temperatures and low density, was $1.4 \text{ g}\cdot\text{cm}^{-3}$ (Dost Chemistry Tuzla, Istanbul)

Romabond polyurethane adhesive (Starwood Building Market, Usak, Turkey) was used. This polyurethane adhesive is a one component, fast curing, polyurethane based wood adhesive. Easy to apply, low viscosity and high bonding strength, water resistant. The technical properties of the glue are as follows: density $1.1 \pm 0.02 \text{ g}\cdot\text{cm}^{-3}$, viscosity (25°C) $4500 \pm 500 \text{ cp}$, pH value 3, gluing time 20°C , 30 min in 65% relative humidity conditions (Romabond, 2018). Epoxy glue (L160/H160) is a two-component adhesive that provides great adhesion to wood materials and is an epoxide that reaches the desired mechanical strength extremely quickly. The technical properties of the glue are as follows: density $0.96\text{-}1.0 \text{ g}\cdot\text{cm}^{-3}$, viscosity (25°C) $10\text{-}50 \text{ MPa}$, refractor index 1.520, gluing time 25°C , 45 min in 65% relative humidity conditions, as recommended by the manufacturer (Dost Chemistry, Tuzla, Istanbul) in Turkey.

Preparation of the test samples

5 x 70 x 1000 mm slats were acquired from Black pine timber using the mowing method in a circular saw machine. After being stacked, the slats were kept in an air-conditioned room of $20 \pm 2^\circ\text{C}$ temperatures and $65 \pm 5\%$ relative humidity conditions until they reached 12% humidity. The test samples were prepared in accordance with the TS 5497 EN 408 (2006).

For the preparation of the sample's polyurethane (PU-D4) and epoxy resin (L160/H160) were used. AFRP was placed between the slats. To produce the control samples without reinforcement, the glue was applied to both surfaces of the wood slats in amount of 180-200 g·m⁻². To create the AFRP reinforced test samples, the glue solution was applied to the solid bonding surfaces with a brush in amount of 180-200 g·m⁻². The surfaces were glued and left to rest for 5-6 min (open time) and then pressed at 1.2 N·mm⁻² for 8 hours (closed time). For the cold press lamination process the materials were cold pressed in a press machine with a pressure gauge suitable for both hot and cold press at 1.2 N·mm⁻². The laminated wood material obtained after the pressing process was prepared with a wood processing machines in accordance with the dimensions specified in the standard (Fig. 1).

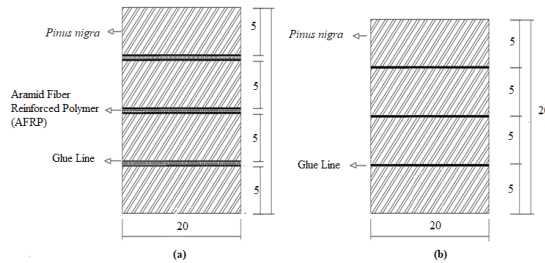


Fig. 1: General configuration of laminated wood material with (a) AFRP reinforced laminated wood (b) glue laminated wood (dimension mm).

In total 80 samples were prepared, 10 replicates for each parameter. Prior to testing, all specimens were stored in a conditioning room maintained at 20 ± 2°C and 65% RH until moisture equilibrium was achieved.

The four-point bending strength test

The universal test device with a capacity of 50 kN was applied to the prepared samples with static load parallel and perpendicular to the glue line. Static loading was determined with the four-point bending apparatus (Fig. 2).



Fig. 2: Configuration of a four-point bending strength test (dimension mm).

In this study, the TS 5497 EN 408 (2006) was taken into consideration. The test machine had a loading speed of 5 mm·min⁻¹. The four-point bending strength, modulus of elasticity in bending and load bearing capacity were determined for the samples placed in such a way that the fulcrum point span was 360 mm. The bending strength and modulus of elasticity were calculated according to the following equations:

$$\text{Bending strength (N.mm}^{-2}\text{)} = \frac{F_{max} \cdot L}{bh^2} \tag{1}$$

$$\text{Modulus of elasticity (N.mm}^{-2}\text{)} = \frac{\lambda^3 (F_2 - F_1)}{b_1 h_1^3 (W_2 - W_1)} \left[\left(\frac{3a}{4\lambda} \right) - \left(\frac{a}{\lambda} \right)^3 \right] \tag{2}$$

where: F_{max} is the maximum force at the time of rupture (N), L is the span between supports (mm), b is the width of the specimens (mm), and d is the thickness of the specimens (mm), λ - measured length for determination of elasticity modulus (mm), $b1$ - sample width (cm) (tangent measure), $b1$ - sample height (cm) (radial measure), a - distance between loading point and nearest bearing (mm), $F2 - F1$ - increase of the load ratio on the straight line of the load deflection curve (N), Difference in deformation corresponding to $W2 - W1 = F2 - F1$ (mm).

The statistical results, namely the arithmetic mean and standard deviation were calculated from the data acquired from the experiments. To determine the results of the experiments, multiple analysis of variance (ANOVA) was used to determine the effects of the factors on the values obtained for all the sample groups. Duncan's test was used to indicate the degree of significance if the interaction of the mutual strength of the factors was significant with a margin of error of ($p < 0.05$) 5%.

RESULTS AND DISCUSSION

Bending strength

Tab. 1 shows the statistical evaluation of the bending strength of both the control samples and the Black pine laminated wood. Tab. 2 and Tab. 3 show the results of the mean comparisons.

Tab. 1: Summary of mean bending strength values of laminated wood.

	Bending strength (N.mm ⁻²)							
	Parallel to the glue line				Perpendicular to the glue line			
	Adhesive type							
	Epoxy		Polyurethane		Epoxy		Polyurethane	
	Mean	Std.	Mean	Std.	Mean.	Std.	Mean	Std.
Control sample	79.06	3.6	75.92	3.4	75.02	2.2	73.03	1.7
Reinforced sample	88.21	3.7	79.66	6.7	76.86	3.2	75.73	2.5

When the bending strength values of the samples parallel to the glue line were examined it was found that the bending strength of the samples produced using epoxy glue without reinforcement was 79.06 N·mm⁻², while the bending strength of the AFRP reinforced samples was 88.21 N·mm⁻². On the other hand, it was observed that the bending strength of the samples produced using polyurethane glue without using the reinforcement was 75.92 N·mm⁻², while the bending strength of the samples reinforced with AFRP was 79.66 N·mm⁻². The evaluation of the bending strength values of the samples perpendicular to the glue line determined that the bending strength of the samples produced using epoxy glue without reinforcement was 75.02 N·mm⁻² while the bending strength of the AFRP reinforced samples was 76.86 N·mm⁻². It was determined that the bending strength of the samples produced using polyurethane glue without reinforcement was 73.03 N·mm⁻² and the bending strength of AFRP reinforced samples was 75.73 N·mm⁻². According to Tab. 2, the applied load differed depending on the position of the laminated wood material. It was found that the bending strength values of the samples parallel to the glue line were higher than those perpendicular to the glue line.

Tab. 2: Mean comparison of bending strength values in laminated wood materials.

	Bending strength (N.mm ⁻²)	
	Parallel to the glue line	Perpendicular to the glue line
Reinforced sample	(83.94) A	(76.29) A
Control sample	(77.49) B	(74.03) B

According to Tab. 3, the lowest bending strength value was obtained from the laminated wood samples produced without using the supporting material, and the highest bending strength value was obtained from the AFRP samples.

Tab. 3: Mean comparison of bending strength values of adhesive type in laminated wood materials.

Adhesive type	Bending strength (N.mm ⁻²)	
	Parallel to the glue line	Perpendicular to the glue line
Epoxy glue	(82.54) A	(75.94) A
PU-D4	(77.04) B	(74.38) B

Various experimental studies show that the reinforcement of timber structures yields the improvement of load-bearing capacity, stiffness, and ductility, in a wide range, most likely owing to the organic nature of wood. Most studies report an increase of capacity 20% to 50% (Gentile et al. 2002, Triantafillou et al. 1992) or sometimes higher (Li et al. 2009, Borri et al. 2005, Nowak et al. 2013), a negligible increase of stiffness (Amy et al. 2004, Buell et al 2005) or occasionally much higher (Borri et al. 2005, Fiorelli et al. 2011), and a general improvement of ductility.

AFRP reinforcement was successfully used for flexural strengthening of timbers; (II) the maximum load-carrying capacity of reinforced timber was dominant with the shear capacity of the AFRP layer/wood bond interface; (III) the flexural strength of southern yellow pine (SYP) and Douglas-fir (DF) wood species were improved by an average amount of 74% and 31% (Yahyaei-Moayyed and Taheri 2011).

Modulus of elasticity in bending

The statistical evaluation of the results on modulus of elasticity in bending of the laminated wood materials, laminated stratified composite materials and solid wood materials are given in Tab. 4 and the results of the mean comparisons are given in Tab. 5 and Tab. 6. According to Tab. 4, when the modulus of elasticity in bending parallel to the glue line values are compared, it can be seen that the samples created using epoxy glue and AFRP gave maximum value, while those that used polyurethane glue and no reinforcement gave minimum value. It was observed that the elasticity values in bending perpendicular to the glue line were similar in the direction of the support with the reinforcement and AFRP.

Tab. 4: Summary of mean modulus of elasticity in bending values of laminated wood materials.

	Modulus of elasticity in bending strength (N.mm ⁻²)							
	Parallel to the glue line				Perpendicular to the glue line			
	Adhesive type							
	Epoxy glue		PU-D4		Epoxy glue		PU-D4	
	Mean	Std.	Mean.	Std.	Mean.	Std.	Mean.	Std.
Control sample	9101	197.2	8761	433.6	8604	224.6	8303	210.9
Reinforced sample	10311	532.6	9116	723.1	9201	527.3	8756	606.1

The difference between the groups in terms of the effects of variance sources on the elasticity modulus parallel and perpendicular to the glue line was found to be statistically significant in terms of material type ($p < 0.05$). While glue variety was effective on the elasticity modulus of the samples parallel to the glue line, it was observed that there was no difference

on the elasticity modulus of the samples perpendicular to the glue line. Furthermore, it was found that the binary interaction of material type and glue type, both perpendicular and parallel to the glue line, did not differ on the modulus of elasticity in bending. The results of the Duncan's test applied to determine the difference between the groups are given in Tab. 5 according to supporting material type and in Tab. 6 according to glue type.

Tab. 5: Mean comparison of modulus of elasticity in bending of supporting material type in laminated wood materials.

	Modulus of elasticity in bending strength (N.mm ⁻²)	
	Parallel to the glue line	Perpendicular to the glue line
Reinforced sample	(9714) A	(8979) A
Control sample	(8931) B	(8454) B

The results of the comparative Duncan's homogeneity test (Tab. 5), which was conducted to determine the significance of the type of supporting material on the modulus of elasticity in bending of the reinforced laminated wooden construction elements parallel and perpendicular to the glue line, the lowest value of the modulus of elasticity in bending both parallel to the glue line and perpendicular to the glue line was found in the laminated wooden construction elements produced without the reinforcement and the highest value in the samples in which AFRP was used. The homogeneity test results showed that the highest modulus of elasticity value in bending for samples parallel and perpendicular to the glue line was obtained in the laminated wood construction elements produced with epoxy glue, while the lowest value was found in the laminated wood construction elements produced with polyurethane glue (Tab. 6).

Consequently, several researchers considered the use of FRP an effective reinforcing agent for wood structural components. Wangard (1964) and Biblis (1965) studied the effect of bonding unidirectional fiberglass/epoxy-reinforced plastic to the compression and tension faces of wood cores of various species. Increases in modulus of elasticity (MOE) ranging from 20% to 50% using only 10% reinforcement by volume were reported. Osmannezhad et al. (2014) studied the behavior of glued laminated timbers and swan timbers for two different species (beech and poplar) was investigated under three-point bending. The results of MOR and MOE in three-point bending test, of the reinforced glulams with GFRP layers showed a slightly higher bending and shear capacities than the non-reinforced glue-laminated and sawn timbers. The best results were for reinforced glulam with four GFRP layers. It was expected increasing layers of GFRP layers improve mechanical properties.

Tab. 6: Mean comparison of modulus of elasticity in bending of adhesive type in laminated wood materials.

Adhesive type	Modulus of elasticity in bending strength (N.mm ⁻²)	
	Parallel to the glue line	Perpendicular to the glue line
Epoxy glue	(9707) A	(8903) A
PU-D4	(89379) B	(8530) B

Fracture types

The use of supporting materials between the layers of the produced reinforced laminated wood construction elements increased the bending strength both parallel to the glue line and perpendicular to the glue line. It can be said that using AFRP between layers as a supporting material reduced the brittleness between the layers due to glue, which in turn resulted in a more ductile structure, thus damping some of the energy that was generated as a result of loading. Furthermore, as shown in Fig. 3, it was determined that AFRP prevented the layers from separating from each other. As a result of the loading applied perpendicular to the glue line, the beginning of a breakage occurred in the wood material, and deformation developed in the glue layer and AFRP, and these deformations occurred between the layers. In the parallel applications to the glue line, deformations developed with the wood material glue layer and AFRP material and the fractures were in the form of zigzags. It was seen that the deformation zone formed in the loading perpendicular to the glue line covered more space in the loading parallel to the glue line. Fig. 4 shows the fractures caused by the loading parallel to the glue line.

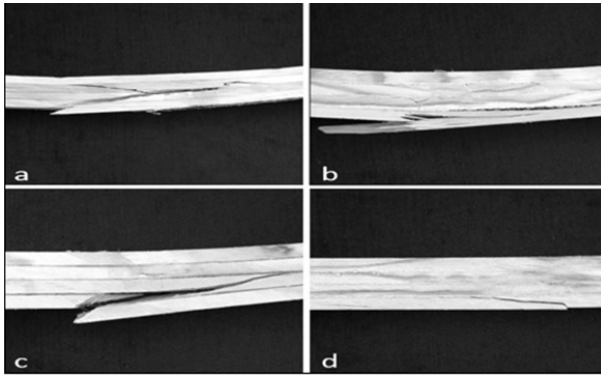


Fig. 3: Fracture types for bending test to perpendicular to the glue line; (a) Epoxy glue+No SMT, Epoxy+AFRP (b), PU-D4+ No SMT and (c) PU-D4+AFRP.

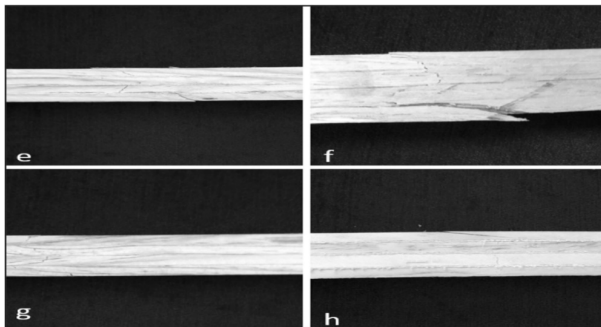


Fig. 4: Fracture types for bending test to parallel to the glue line; (e) Epoxy glue+No SMT Epoxy+AFRP (f), PU-D4 glue+No SMT and (h) PU-D4+AFRP.

CONCLUSIONS

This study investigated, the modulus of elasticity in bending and four-point bending of wood laminated material reinforced by AFRP. Within this scope, AFRP was placed between four layers of slat prepared from Black pine (*Pinus nigra*) wood, which is extensively used in the manufacturing of furniture and building materials in Turkey, and epoxy and polyurethane glues were used to glue the layers. The control samples and samples supported with AFRP were statistically evaluated according to support material type, glue type and load application type. In terms of glue type, the highest bending strength value parallel to the glue line and perpendicular to the glue line was obtained from the epoxy glue, while the lowest bending strength value was obtained from the polyurethane glue. Additionally, the highest modulus of elasticity in bending value parallel to the glue line and perpendicular to the glue line was determined in the epoxy glue and the lowest in the polyurethane glue.

According to the evaluations made in terms of glue type, it was determined that using epoxy glue influenced increasing bending strength perpendicular to the glue line and parallel to the glue line. This could be explained by the fact that epoxy glue has a stronger chemical bond between wood lamellae than polyurethane glue. In spite of this, for the best results in terms of bending strength in applications parallel to the glue line and perpendicular to the glue line, it was determined that the laminated elements produced using epoxy glue reinforced with AFRP showed an increase in bending strength compared to the laminated elements produced without the reinforcement. The highest bending strength value parallel to the glue line and perpendicular to the glue line in terms of support material type was obtained from the AFRP support material, while the lowest bending strength value was obtained from the laminated elements produced without the reinforcement. In terms of glue line, the highest modulus of elasticity in bending value parallel and perpendicular to the glue line was determined in the AFRP material and the lowest value was determined in the laminated elements produced without the reinforcement. The reinforcement between the layers of the produced reinforced laminated wood construction elements increased the bending strength parallel and perpendicular to the glue line. It can be said that using AFRP between the layers reduced the brittleness caused by the glue between the layers, resulting in a more ductile structure, thus damping some of the energy that emerged as a result of the loading. This damping was found to be more in the applications perpendicular to the glue line. According to the experimental results in bending strength and modulus of elasticity in bending the AFRP supporting material increased strength of laminated wood material. As there were significant increases in the resistance properties of the material used as the intermediate filling material in the laminated wood materials, it is suggested that furniture and construction materials should have high strength properties.

REFERENCES

1. Abu-Talib, A.R., Ramadhan, A.A., Mohd Rafie, A.S., Zahari, R., 2013: Influence of cut-out hole on multi-layer Kevlar-29/epoxy composite laminated plates. *Materials and Design* 43: 89-98.
2. Alsheghri, A., Akgul, T., 2019: Investigation of used of carbon fiber reinforced polymer sheets in joints of wooden structures. *Academic Platform Journal of Engineering and Science* 7(3): 406-413.
3. Alshurafa, S., Alhayek, H., Taheri, F., 2012: An investigation into the response of GFRP-reinforced glue-laminated tudor arches. *Hindawi Publishing Corporation Advances in Civil Engineering* Vol. 2012, Article ID 357346, 11 pp.

4. Amy, K., Svecova, D., 2004: Strengthening of dapped timber beams using glass fibre reinforced polymer bars. *Canadian Journal of Civil Engineering* 31: 943–55.
5. Arriaga, F., Peraza, F., Esteban, M., Bobadilla, I., García, F., 2002: Intervención en estructuras de Madera (Intervention in wooden structures). AITIM, 464 pp.
6. Biblis, E.J., 1965: Analysis of wood-fiberglass composite beams within and beyond the elastic region. *Forest Product Journal* 15(2): 81–89.
7. Borri, A., Corradi, M., Grazini, A., 2005: A method for flexural reinforcement of old wood beams with CFRP materials. *Composite Part B* 36(2): 143–153.
8. Buell, T.W., Saadatmanesh, H., 2005: Strengthening timber bridge beams using carbon fibre. *Journal of Structural Engineering* 131(1): 173–187.
9. Cheon, J., Lee, M., Kim, M., 2020: Study on the stab resistance mechanism and performance of the carbon, glass and aramid fiber reinforced polymer and hybrid composites. *Composite Structures* 234: 111690.
10. Dempsey, D.D., Scott, D.W., 2006: Wood members strengthened with mechanically fastened FRP strips. *Journal of Composites for Construction* 10(5): 392–398.
11. Denchev, Z.Z., Dencheva, N.V., 2012: Manufacturing and properties of aramid reinforced polymer composites. In: *Synthetic polymer-polymer* (ed. Bhattacharyya, D., Fakirov, S.), Munich, Germany Pp 251–280, Hanser Publishers.
12. Essert, S., Rede, V., Svagej, Z., 2018: The bending modulus of elasticity of subfossil elm wood. *Wood Research* 63(2): 239–248.
13. Fedyukov, V., Saldaeva, E., Chernova, M., 2017: Different ways of elastic modulus comparative study to predict resonant properties of standing spruce wood. *Wood Research* 62(4): 607–614.
14. Fiorelli, J., Dias, A.A., 2003: Analysis of the strength and stiffness of timber beams reinforced with carbon fiber and glass fiber. *Materials Research* 6(2): 193–202.
15. Fiorelli, J., Dias, A.A., 2006: Fiberglass-reinforced glulam beams: mechanical properties and theoretical model. *Materials Research* 9(3): 263–269.
16. Fiorelli, J., Dias, A.A., 2011: Glulam beams reinforced with FRP externally bonded: theoretical and experimental evaluation. *Materials and Structures* 44(8): 1431–1440.
17. Glišović, I., Stevanović, B., Todorović, M., Stevanović, T., 2016: Glulam beams externally reinforced with CFRP plates. *Wood Research* 61(1): 141–154.
18. Gustin, J., Joneson, A., Mahinfalah, M., Stone, J., 2005: Low velocity impact of combination Kevlar/carbon fiber sandwich composites. *Composite Structures* 69(4): 396–406.
19. Hillermeier, K., 1984: Prospects of aramid as a substitute for asbestos. *Textile Research Journal* 54 (9): 575–580.
20. Johns, K.C., Lacroix, S., 2000: Composite reinforcement of timber in bending. *Canadian Journal of Civil Engineering* 27(5): 899–906.
21. Kánnár, A., 2014: Evaluation of glulam beams' performance in special environmental conditions. *Wood Research* 59(5): 803–812.
22. Komán, S., Fehér, S., Ábrahám, J., Taschner, R., 2013: Effect of knots on the bending strength and the modulus of elasticity of wood. *Wood Research* 58(4): 617–626.
23. Krisztián, A., Bertalan, B., 2020: Analysis of modulus of elasticity of spruce beams under bending with and without fibre reinforcement. *Wood Research* 65(1): 101–110.
24. Laufenberg, T.L., Rowlands, R.E., Krueger, G.P., 1984. Economic feasibility of synthetic fiber reinforced laminated slat lumber (LVL). *Forest Product Journal* 34(4): 15–22.
25. Li, Y.F., Xie, Y.M., Tsai, M.J., 2009: Enhancement of the flexural performance of retrofitted wood beams using CFRP composite sheets. *Construction and Building Materials* 23(1): 411–422.

26. Lopez-Anido, R., Michael, A.P, Sandford, T.C., 2003: Experimental characterization of FRP composite-wood pile structural response by bending tests. *Marine Structures* 16: 257–274.
27. Mallick, P.K., 1993: *Fiber-reinforced composites: materials, manufacturing, and design*. 2nd edition, New York, USA: Marcel Dekker Inc, 74 pp.
28. Morales-Conde, M.J., Rodríguez-Liñán, C., Rubio-de Hita, P., 2015: Bending and shear reinforcements for timber beams using GFRP plates. *Construction and Building Materials* 96: 461–472.
29. Nowak, T.P., Jasienko J., Czepizak, D., 2013: Experimental tests and numerical analysis of historic bent timber elements reinforced with CFRP strips. *Construction and Building Materials* 40: 197–206.
30. Osmannezhad, S., Faezipour, M., Ebrahimi, G., 2014: Effects of GFRP on bending strength of glulam made of poplar (*Populus deltoids*) and beech (*Fagus orientalis*). *Construction and Building Materials* 51: 34–39.
31. Plevris, N., Triantafillou, T.C., 1995: Creep behaviour of FRP-reinforced wood members. *Journal of Structural Engineering* 121: 174–86.
32. Priyanka, P., Dixit, A., Mali, H.S., 2017: High-strength hybrid textile composites with carbon, kevlar and e-glass fibers for impact-resistant structures. a review. *Mechanics of Composite Materials* 53(5): 685–704.
33. Romani, M., Blab, H.J., 2001: Design model for FRP reinforced glulam beams, in: *Proceedings of the International Council for Research and Innovation in Building and Construction (CIB). Working Commission W18 Timber Structures, Meeting Vol. 34*, 10 pp.
34. Song, Y., Hong, S., Suh, J., Park, S., 2017: Strength performance evaluation of moment resistance for cylindrical-LVL column using GFRP reinforced wooden pin. *Wood Research* 62(3): 417–426.
35. Valenca, S.L., Griza, S., De-Oliveira, V.G., Sussuchi, E.M., De-Cunha, F.G.C., 2015: Evaluation of the mechanical behavior of epoxy composite reinforced with Kevlar plain fabric and glass/Kevlar hybrid fabric. *Composites: Part B* 70: 1–8.
36. Toutanji, H., Saafi, M., 1999: Performance of concrete beams prestressed with aramid fiber-reinforced polymer tendons. *Composite Structures* 44: 63–70.
37. TS 5497 EN 408, 2006: *Timber structures. Structural timber and glue laminated timber. Determination of some physical and mechanical properties*.
38. Wangaard, F.F., 1964: Elastic deflection of wood–fiberglass composite beams. *Forest Product Journal* 13(6): 256–260.
39. Yahyaei-Moayyed, M., Taheri, F., 2011: Experimental and computational investigations into creep response of AFRP reinforced timber beams. *Composite Structures* 93: 616–628.
40. Yayun, Z., Yuxin, S., Ruiyu, L., Qiran, S., Jiangtuo, F., 2017: Response of aramid honeycomb sandwich panels subjected to intense impulse loading by Mylar flyer. *International Journal of Impact Engineering* 104: 75–84.
41. Yerlikaya, N.C., 2014: Investigation of optimum dowel spacing for corner joints, which are reinforced with glass-fiber fabric in case-type furniture. *Wood Research* 59(1): 91–200.
42. Yerlikaya, N.C., 2019: Investigation of the differences between the glass-fiber fabric band and the edge bands in case-type furniture. *Wood Research* 64(6): 1087–1100.
43. Zhou, A., Oin, R., Chow, L.C., Lau, D., 2020: Bond integrity of aramid, basalt and carbon fiber reinforced polymer bonded wood composites at elevated temperature. *Composite Structures* 245: 112342.

ABDURRAHMAN KARAMAN*
USAK UNIVERSITY
BANAZ VOCATIONAL SCHOOL
64500 USAK
TURKEY

*Corresponding author: abdurrahman.karaman@usak.edu.tr

MEHMET NURI YILDIRIM
KARABUK UNIVERSITY
SAFRANBOLU VOCATIONAL SCHOOL
78600 KARABUK
TURKEY

ONDER TOR
KASTAMONU UNIVERSITY
FORESTRY FACULTY
37100 KASTAMONU
TURKEY

NUMERICAL STUDY ON EFFECTS OF TENON SIZES ON WITHDRAWAL LOAD CAPACITY OF MORTISE AND TENON JOINT

TIANXING ZHANG
WUYI UNIVERSITY
CHINA

WENGANG HU
NANJING FORESTRY UNIVERSITY
CHINA

(RECEIVED JUNE 2020)

ABSTRACT

The effect of tenon length and tenon width on withdrawal load capacity of mortise and tenon (M-T) joint was studied based on the finite element method (FEM), and the relationship of withdrawal load capacity relating to tenon length and tenon width was regressed using response surface method. The results showed that the tenon length and tenon width had remarkable effects on withdrawal load capacity of M-T joint T-shaped sample. The effect of tenon length on withdrawal load capacity was greater than tenon width. The regression equation used to predict the withdrawal load capacity was capable of optimizing the tenon sizes of M-T joint with R-square of 0.926. Using FEM can get more knowledge of M-T joint visually, and reduce the costs of materials and time of experiments.

KEYWORDS: Withdrawal load capacity, finite element method, tenon size effect, mortise and tenon joint.

INTRODUCTION

Mortise and tenon (M-T) is a traditional joint type commonly used in wood structures and wood products, which dominates the strength of the whole framework. Withdrawal load capacity is a common load type imposed on M-T joint. Many studies have investigated the factors influencing the withdrawal resistance of M-T joint, such as wood species, adhesive type, tenon geometry etc. (Záborský et al. 2017, Zhao et al. 2019). Diler et al. (2017) studied the withdrawal resistance of T-shaped joint made from heat-treated pine (*Pinus sibirica*) and common ash (*Fraxinus excelsior*) and iroko (*Chlorophora excelsa*) wood. The results showed

that the withdrawal resistances of joints constructed from common ash and iroko wood were higher than the joint made from heat-treated wood. Heat-treated wood reduced the withdrawal resistance of joint by 25%. Renbutsu and Koizumi (2018) used greenwood shrinkage as a clamping pressure to increase the withdrawal resistance. The results showed that proposed shrink-fitted glued round M-T joint exhibited sufficient withdrawal strength, and after applying four humidity cycles to simulate seasonal variations in moisture content, withdrawal strength did not decrease significantly. In addition, Eckelman et al. (2004) studied the withdrawal resistance of pinned and unpinned round M-T joint. The results showed that cross-pined round M-T joints enhanced the withdrawal resistance, which would be usable in the construction of furniture where adhesives were unobtainable. Derikvand et al. (2013) studied the effect of wood species and loose tenon length on the withdrawal force capacity of M-T joint T-shaped sample. The results showed that the gluing in length of the tenon exerted a significant influence on the withdrawal force capacity of the joints. Tenon sizes, length and width, are basic parameters of M-T joint, which affect the strength of M-T joint directly. A huge amount of experimental tests were conducted to investigate the tenon sizes on bending moment strength of M-T joint (Wilczyński and Warmbier 2003, Edirl et al. 2005, Likos et al. 2012, Oktae et al. 2014, Kasal et al. 2016), and tenon shoulder on strength of M-T joint (Eckelman and Haviarova 2006, Džinčić 2016). However, the effect of tenon sizes on withdrawal load capacity of M-T joint was rarely studied.

Finite element method (FEM) has been confirmed as an effective method commonly used in wood engineering (Zhou et al. 2017, Liu et al. 2018, Hu et al. 2019, Xi et al. 2020). Previous studies also proved that the FEM can be used to analyse the M-T joint (Smardzewski 2008, Silvana and Smardzewski 2010, Çolakoglu and Apay 2012, Zhou 2018, Kilic et al. 2018, Chen 2019). Therefore, in this study, the effect of tenon sizes (length and width) on withdrawal load capacity of M-T joint was investigated numerically based on FEM, and the relationship of withdrawal load capacity relating to tenon length and tenon width was regressed using response surface method. This study will contribute to reduce the costs of experiments through using FEM and response surface method.

MATERIAL AND METHODS

Material properties of wood

The wood used to prepare the T-shaped specimens was beech (*Fagus orientalis* Lipsky) (Nanjing Wood Lumber, Nanjing, China). The physical and mechanical properties of beech wood were measured in the authors' previous study (Hu and Guan 2017a). The specific gravity of beech averaged 0.69, and the moisture content was 10.8%. Tab. 1 shows the mechanical properties of beech wood which are basic parameters used in the finite element model, including elastic moduli, Poisson's ratios, shear moduli, yield strengths and ultimate strengths.

Tab. 1: Mechanical properties of beech wood (Hu and Guan 2017a).

Modulus of elasticity (MPa)			Poisson's ratio					
E_L^*	E_R	E_T	ν_{LR}	ν_{LT}	ν_{RT}	ν_{TR}	ν_{TL}	ν_{RL}
12205	1858	774	0.502	0.705	0.526	0.373	0.038	0.078
Shear modulus (MPa)			Yield strength (MPa)			Ultimate strength (MPa)		
G_{LR}	G_{LT}	G_{RT}	L	R	T	L	R	T
899	595	195	53.62	12	6.23	59.20	48.88	23.82

Note: * E is elastic modulus (MPa); ν is Poisson's ratio; G is shear modulus (MPa); L, R, and T refer to the longitudinal, radial, and tangential directions of beech wood, respectively.

Dimensions of M-T joint specimens

Fig. 1 shows the configurations of T-shaped specimen evaluated in this study. The dimensions of the post leg were $200 \times 40 \times 40$ mm (length \times width \times thickness). The stretcher measured 160 mm long \times 30 mm wide \times 30 mm thick. The dimensions of tenon length and tenon width were variables studied in this study, while the tenon thickness was a constant. The fit between tenon width and mortise height was 0.2 interference fit, and 0.2 mm clearance fit was applied between tenon thickness and mortise width according to common wood M-T joint technique. The polyvinyl acetate (PVA) was used to connect mortise and tenon, and the bonding strengths of M-T joint were shown in Tab. 2.

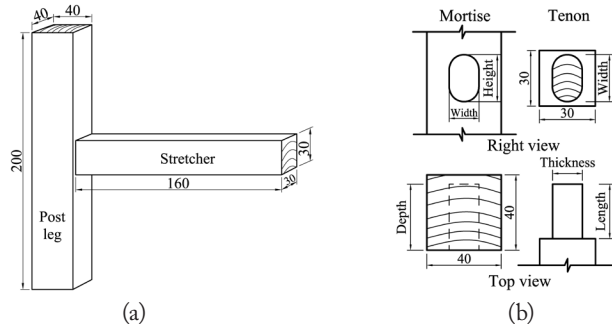


Fig. 1: Dimensions of specimen: (a) T-shaped sample, (b) mortise and tenon joint (unit mm).

Tab. 2: Bonding strength of mortise and tenon joint (Hu and Guan 2019).

Bonding strength (MPa)		
Shear strength G_I	Shear strength G_{II}	Internal bonding strength
3.49	2.45	1.23

Finite element model

Fig. 2 shows the finite element model of the M-T joint T-shaped sample subjected to withdrawal load established using finite element software (ABAQUS 6.14-1, Dassult, Providence, RI, USA). The model considered the orthotropic properties of wood. The mechanical properties used in this model were shown in Tab. 1. In this study, ductile damage was used in the finite element model to judge the failure of elements with the parameters of fracture strain 0.00833, stress triaxiality 0.33, strain rate 0.01 and displacement at failure 0.6452 mm. Local coordinates were used to define the grain orientations of the leg and the stretcher, *i.e.*, x, y, and z corresponded to the longitudinal, radial, and tangential directions, respectively. The oval M-T joint model was regarded as a semi-rigid joint. The interactions of the mortise and tenon were surface-to-surface contact. For the curve contact surfaces of the M-T joint, the penalty friction formulation was specified with a friction coefficient of 0.54 (Hu and Guan 2017b) to simulate the friction behaviour between the mortise and tenon with a 0.2 mm interference fit. For the flat contact surfaces of the M-T joint, Traction-Separation law was used as criterion to simulate the cohesive bonding behaviour, and the parameters needed in ABAQUS were bonding strengths of glue joint in different directions shown in Tab. 2. The loading conditions were that a displacement load applied at the loading point at the end of the stretcher to get the force (F) shown in Fig. 2. The mesh of the model is also shown in Fig. 2, and the sizes of most elements

were approximately 5 mm. For contact parts, the sizes of elements were about 2 mm. The element type was C3D8, an 8-node linear brick element that was assigned to the T-shaped sample.

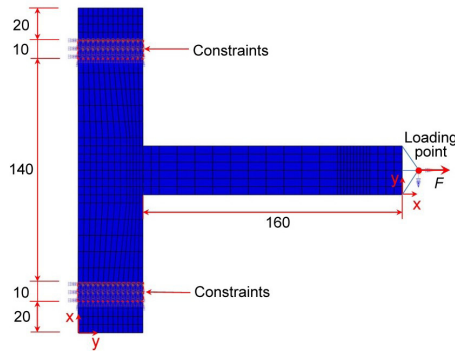


Fig. 2: Finite element models of T-shaped mortise and tenon joint subjected to withdrawal load.

Tab. 3: Combinations of tenon width and tenon length evaluated in this study.

Tenon size (mm)	Width (W)		
	15	20	25
Length (L)			
10	L10-W15	L10-W20	L10-W25
20	L20-W15	L20-W20	L20-W25
30	L30-W15	L30-W20	L30-W25
40	L40-W15	L40-W20	L40-W25

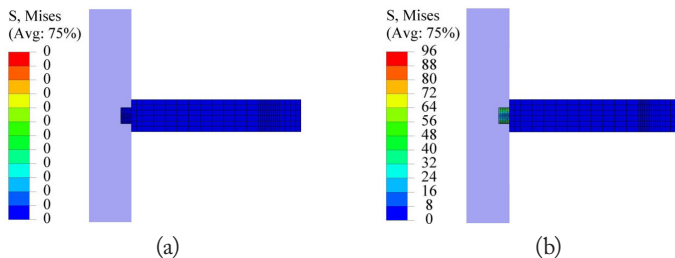
Statistical analysis

All data were analyzed by Design expert (Version 8.06, Stat-Ease, Inc. Minneapolis, MN, USA) using the response surface method, and the model terms were statistically analyzed by analysis of variance (ANOVA).

RESULTS AND DISCUSSION

Stress distributions of M-T joint

Fig. 3 shows stress distributions of a typical T-shaped M-T joint (L10-W15) during withdrawal process. Most simulation results were in the same trend. Figs. 3a-d suggested the initial state, interference fit, half-tenon withdrawal and complete withdrawal states, respectively.



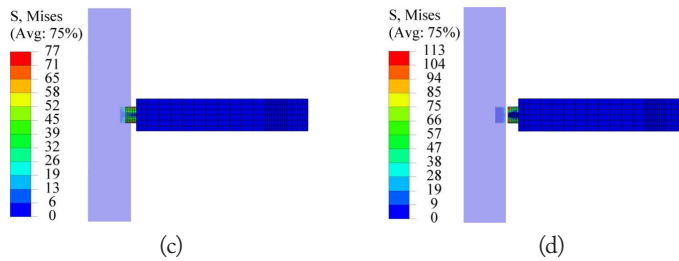


Fig. 3: Stress distributions of M-T joint T-shaped specimen subjected to withdrawal load: (a) initial state, (b) interference fit state, (c) half-tenon withdrawal state and (d) complete withdrawal state.

Withdrawal load capacity of M-T joints

Fig. 4 shows the withdrawal load and displacement curves of all M-T joint T-shaped finite element models. Most curves were in the same trend that the withdrawal load increased linearly until reaching the peak value, and then dropped linearly until the tenon completely pulled out. These curves reflected the process of tenon pulled out the mortise smoothly and the most materials of tenon were in elastic stage. However, the curves of L30-W15, L40-W15 and L40-W20 had different trends at the dropped stage of curves, which caused by different failure modes of M-T joint.

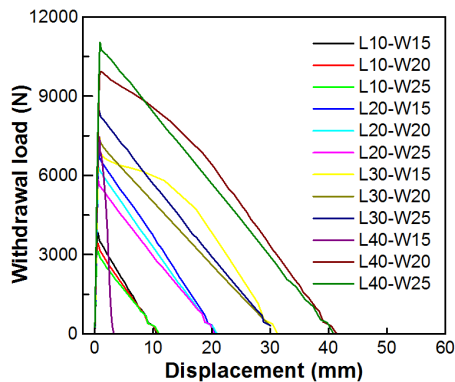


Fig. 4: Withdrawal load-displacement curves of T-shaped specimens with different tenon sizes.

Fig. 5a-c show the failure modes of M-T joint with the tenon sizes of L30-W15, L40-W15 and L40-W20, respectively. In case of Fig. 5b, the tenon damaged before pulled out, so the withdrawal load decreased once reaching the peak value. In case of Fig. 5a and 5c, in the dropped stage of curves, the withdrawal load decreased nonlinearly, since most materials of tenon were in plastic stage, especially for M-T joint with tenon sizes of L30-W15. It can be inferred that when the tenon length is twice bigger than or equal to tenon width, the materials of tenon have the risk of suffering plasticity or fracture. Therefore, it is recommended that the tenon length is greater than tenon width and smaller than twice tenon width in designing the tenon sizes of M-T joint of wood products especially subjected to withdrawal load.

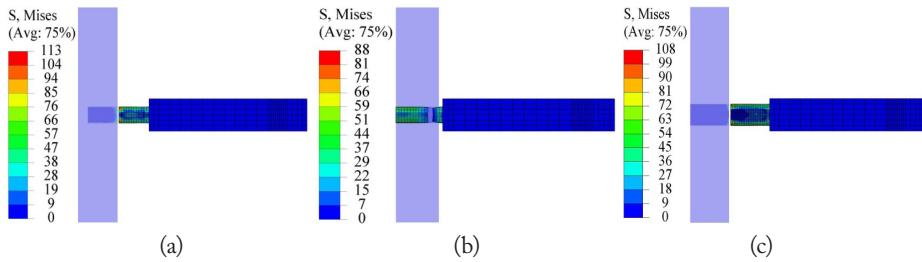


Fig. 5: Stress distributions and failure modes of T-shaped specimens subjected to withdrawal load: (a) 30-mm tenon length by 15-mm tenon width (L30-W15), (b) 40-mm tenon length by 15-mm tenon width (L40-W15) and (c) 40-mm tenon length by 20-mm tenon width (unit MPa).

Fig. 6 shows the simulation results of withdrawal load capacities of M-T joint with different tenon sizes. Apart from the tenon sizes of L40-W15, when the tenon width is fixed at a certain value, the withdrawal load capacities increased remarkably with increase of tenon length (Derikvand et al. 2013). However, when the tenon length kept at a certain constant, the withdrawal load increased or decreased slightly with the tenon width increasing. All of above results indicated that the tenon length affected the withdrawal load capacity greater than tenon width.

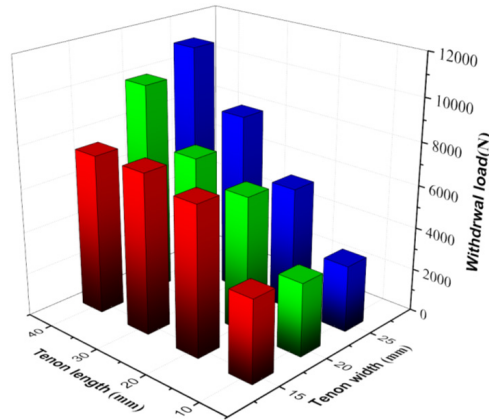


Fig. 6: Withdrawal load capacities of mortise and tenon joint with different tenon sizes.

Modelling of withdrawal load capacity

In this model, the result of M-T joint with dimensions of L40-W15 was eliminated from the data for its failure mode (Fig. 5b) different from others. Therefore, the response surface model was regressed based on 11 runs. Fig. 7 shows the 3D surface of the model, and the corresponding response surface model equation was shown in Eq. 1:

$$F = 4720.9 + 834.5 \times A - 650.8 \times B + 8.8 \times AB - 34.2 \times A^2 + 11.1 \times B^2 + 0.44 \times A^3 \tag{1}$$

where: F is withdrawal load capacity (N);
 A and B are tenon length and tenon width (mm), respectively.

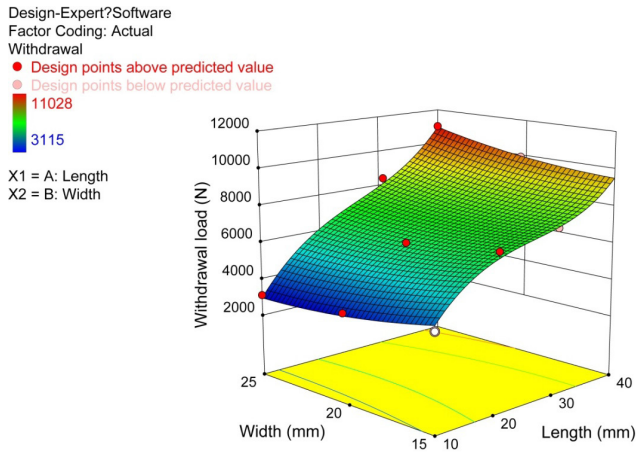


Fig. 7: 3D surface of response surface model of withdrawal capacity of mortise and tenon joint relating to tenon length and tenon width.

Tab. 4 shows that analysis of variation (ANOVA) of the response surface reduced cubic model. The *F*-value of 61.29 implies the model is significant. There is only a 0.07% chance that a *F*-Value this large could occur due to noise. The *F*-value of length was much bigger than the one of width indicating that the effect of tenon length on withdrawal load capacity was greater than tenon width, which was consistent with the results of simulation (Fig. 6).

Tab. 4: ANOVA of response surface reduced cubic model.

Source	F-value	p-value
Model	61.29	0.0007
Length (A)	10.33	0.0325
Width (B)	0.15	0.7165
AB	6.03	0.0700
A ²	0.80	0.4219
B ²	1.01	0.3720
A ³	5.56	0.0779

The *p*-values less than 0.05 indicate model terms are significant. The *p*-values greater than 0.1 indicate the model terms are not significant. The *p*-values between 0.05 and 0.1 are moderately significant. Therefore, *A* is significant model terms, *AB* and *A³* are moderately significant, and *B*, *A²* and *B²* are not significant. In addition, the "Pred R-Squared" of 0.9261 is in reasonable agreement with the "Adj R-Squared" of 0.9731. Therefore, this model can be used to predict the withdrawal capacity of M-T joint.

CONCLUSIONS

In this study, the effects of tenon sizes, length and width, on withdrawal load capacity of M-T joint were studied numerically using FEM combining with response surface model. Following conclusions were drawn: (1) The tenon sizes have remarkable effect on withdrawal load capacity of M-T joint. (2) The effect of tenon length on withdrawal load capacity of M-T joint is greater than the one of tenon width. (3) It is recommended that the tenon length is greater than tenon width and smaller than twice tenon width in designing the tenon sizes of M-T joint especially subjected to withdrawal load. (4) The method of combining FEM and response surface method is an efficient way to optimize the tenon sizes, which can help researchers and engineers, know more about the details of wood structures visually and reduce the costs of time and materials used to conduct experiments.

Further studies can focus on numerically and experimentally optimizing the tenon sizes of M-T joint considering the tenon length, tenon width and tenon thickness together when subjected to bending and withdrawal loads.

ACKNOWLEDGMENTS

This work was supported by a Scientific Research Foundation of Wuyi University for Doctor (BSQD1901), Scientific Research Foundation of Metasequoia teacher (163104060) and Project from International Cooperation Joint Laboratory for Production, Education, Research and Application of Ecological Health Care on Home Furnishing.

REFERENCES

1. Chen Y.S., Zhu J., 2019: Study on bending characteristics of fast growing eucalyptus bookcase shelves by using Burgers model. *Wood Research* 64(1): 137-144.
2. Çolakoglu, M.H., Apay, A.C., 2012: Finite element analysis of wooden chair strength in free drop. *International Journal of Physical Sciences* 7(7): 1105-1114.
3. Derikvand, M., Smardzewski, J., Ebrahimi, G., Dalvand, M., Maleki, S., 2013: Withdrawal force capacity of mortise and loose tenon T-type furniture joints. *Turkish Journal of Agriculture and Forestry* 37: 377-384.
4. Diler, H., Acar, M., Balıkcı, E., Demirci, S., Erdil, Y.Z., 2017: Withdrawal force resistance of T-type furniture joints constructed from various heat-treated wood species. *BioResources* 12(4): 7466-7478.
5. Džinčić, I., Nestorović, B., Dacić, V., 2016: The effect of shoulder on the strength of the oval tenon–mortis. *Glasnik Sumarskog fakulteta* 113: 35–46.
6. Eckelman, C.A., Haviarova, E., 2006: Effect of shoulders on bending moment capacity of round mortise and tenon joints. *Forest Products Journal* 56: 82–86.
7. Eckelman, C.A., Haviarova, E., Tankut, A., Denizli, N., Akcay, H., Erdil, Y., 2004: Withdrawal capacity of pinned and unpinned round mortise and tenon furniture joints. *Forest Products Journal* 54(12): 185-191.
8. Erdil, Y.Z., Kasal, A., Eckelman, C.A., 2005: Bending moment capacity of rectangular mortise and tenon furniture joints. *Forest Products Journal* 55(12): 209-213.
9. Hu, W.G., Guan, H.Y., 2017a: Study on elastic constants of beech in different stress states. *Journal of Forestry Engineering* 2(6): 31-36.

10. Hu, W.G., Guan, H.Y., 2017b: Investigation on withdrawal force of mortise and tenon joint based on friction properties. *Journal of Forestry Engineering* 2(4): 158-162.
11. Hu, W.G., Guan, H.Y., 2019: A finite element model of semi-rigid mortise-and-tenon joint considering glue line and friction coefficient. *Journal of Wood Science* 65: 14.
12. Hu, W.G., Wan, H., Guan, H.Y., 2019: Size effect on the elastic mechanical properties of beech and its application in finite element analysis of wood structures. *Forests* 10(9): 783 ,13 pp.
13. Kasal, A., Smardzewski, J., Kuşkun, T., Erdil, Y.Z., 2016: Numerical analyses of various sizes of mortise and tenon furniture joints. *BioResources* 11: 6836–6853.
14. Kilic, K., Kasal, A., Kuskun, T., Acar, M., Edil, Y.Z., 2018: Effect of tenon size on static front to back loading performance of wooden chairs in comparison with acceptable design loads. *BioResources* 13(1): 256-271.
15. Likos, E., Haviarova, E., Eckelman, C.A., Erdil, Y.Z., Özcifci, A., 2012: Effect of tenon geometry, grain orientation, and shoulder on bending moment capacity and moment rotation characteristics of mortise and tenon joints. *Wood and Fiber Science* 44(4): 462-469.
16. Liu, J.X., Zhou, W., Li, C., 2018: Stress wave vibration characterization of cross section of log using finite element method. *Journal of Forestry Engineering* 3(6): 19-24.
17. Oktae, J., Ebrahimi G., Layeghi, M., Ghofrani, M., Eckelman C.A., 2014: Bending moment capacity of simple and haunched mortise and tenon furniture joints under tension and compression loads. *Turkish Journal of Agriculture and Forestry* 38(2): 291-297.
18. Renbutsu, T., Koizumi, A., 2018: Withdrawal properties of glued, round, mortise and tenon joints using greenwood shrinkage as a clamping pressure. *Mokuzai Gakkaishi* 64(5): 187-194.
19. Silvana, P., Smardzewski, J., 2010: Effect of glue line shape on strength of mortise and tenon joint. *Drvna Industrija* 61(4): 223-228.
20. Smardzewski, J., 2008: Effect of wood species and glue type on contact stresses in a mortise and tenon joint. *ARCHIVE Proceedings of the Institution of Mechanical Engineers Part C Journal of Mechanical Engineering Science* 222(12): 2293-2299.
21. Wilczyński, A., Warmbier, K., 2003: Effect of joint dimensions on strength and stiffness of tenon joints. *Folia Forestalia Polonica* 34: 53-66.
22. Xi, X., Yang, Y., Zhang, Z.F., 2020: Pull-out force and finite element analysis of T-type components of *Vitex negundo* L. scrimber with different node forms. *Journal of Forestry Engineering* 5(1): 182-187.
23. Záborský, V., Borůvka, V., Kašičková, V., Ruman, D., 2017: Effect of wood species, adhesive type and annual ring directions on the stiffness of rail to leg mortise and tenon furniture joints. *BioResources* 12: 7016-7031.
24. Zhao, Z., Sakai, S., Wu, D., Chen, Z., Zhu, N., Huang, C., Sun, S., Zhang, M., Umemura, K., Yong, Q., 2019: Further exploration of sucrose–citric acid adhesive: investigation of optimal hot-pressing conditions for plywood and curing behavior. *Polymers* 11: 1996.
25. Zhou, C.M., Yu, M.N., Zhou, T., 2018: Experimental study on three-dimensional shape mapping of complex furniture. *EURASIP Journal on Image and Video Processing* 9: 89.
26. Chen, Y., Yang, Y., Zhang, Z., 2019: Study on small-diameter wood scrimber and furniture design. *Journal of Forestry Engineering* 4(1): 155-159.

TIANXING ZHANG
WUYI UNIVERSITY
SCHOOL OF ART AND DESIGN
JIANGMEN 529020
CHINA

WENGANG HU*
NANJING FORESTRY UNIVERSITY
CO-INNOVATION CENTER OF EFFICIENT PROCESSING AND UTILIZATION OF FOREST
RESOURCES,
COLLEGE OF FURNISHINGS AND INDUSTRIAL DESIGN
NANJING 210037
CHINA

*Corresponding author: hwg@njfu.edu.cn